

Reconstruction of volcano-tectonic processes in interplay with sedimentary deposition in the Gulf of Naples (Italy) using a seismoacoustic dataset

Dissertation

Zur Erlangung des Doktorgrades der Naturwissenschaften
am Fachbereich Geowissenschaften
der Universität Bremen

vorgelegt von

Lena Steinmann

Bremen, Juni 2016

Gutachter:

Prof. Dr. Volkhard Spiess

Prof. Dr. Sebastian Krastel

Contents

List of Figures.....	iv
List of Tables.....	vii
Abbreviations	viii
Preface.....	ix
Thesis Abstract	1
Zusammenfassung.....	3
Chapter 1.....	5
Introduction.....	5
1.1 Motivation and objectives.....	5
1.2 Caldera volcanism.....	10
1.2.1 Caldera architecture	10
1.2.2 Collapse-caldera formation and resurgence.....	12
1.2.3 Pyroclastic density currents (PDCs) and ignimbrite deposits	14
1.3 Regional Setting.....	16
1.3.1 Formation of the Tyrrhenian Sea	16
1.3.2 The Campanian Margin.....	18
1.3.3 Volcanism in the Campanian Plain	19
1.3.4 Existing data from the Campi Flegrei caldera.....	24
1.4 Thesis outline.....	26
1.5 Declaration of co-author contributions	27
Chapter 2.....	29
Data and Methods.....	29
2.1 CAFE-7/3 – GeoB08.....	29
2.2 CAFE_2015 – GeoB16	31
2.3 Multichannel seismic data processing.....	33
2.3.1 Pre-Processing	34
2.3.2 Geometry set-up and CMP sorting.....	37
2.3.3 Trace editing	37
2.3.4 Normal moveout (NMO) and statics correction	38
2.3.5 Multiple suppression and spherical divergence	40
2.3.6 CMP stacking.....	41
2.3.7 Post-stack noise attenuation.....	41
2.3.8 Time migration.....	42
Chapter 3.....	45
Tectono-sedimentary evolution of the Gulf of Naples half-graben basin (Italy)	
in interaction with volcanism during the last one million years	45
Abstract.....	45
3.1 Introduction	46
3.2 Regional setting	47

3.3	Materials and methods	50
3.4	Results.....	52
3.4.1	Seismic analysis.....	52
3.5	Discussion.....	60
3.5.1	Stratigraphic framework.....	60
3.5.2	Volcano-tectonic implications	62
3.5.3	Tectono-sedimentary evolution	64
3.6	Conclusions.....	66
3.7	Acknowledgements	67
Chapter 4	69
The Campi Flegrei caldera (Italy): formation and evolution in interplay with sea-level variations since the Campanian Ignimbrite eruption at 39 ka.....		69
Abstract	69
4.1	Introduction.....	70
4.2	Regional setting.....	71
4.3	Materials and methods	73
4.4	Results.....	74
4.4.1	Seismic analysis.....	74
4.5	Discussion.....	81
4.5.1	Stratigraphic context	81
4.5.2	Caldera formation and evolution.....	85
4.6	Conclusions.....	91
4.7	Acknowledgements	92
Chapter 5	93
Post-collapse evolution of the Campi Flegrei caldera since the Neapolitan Yellow Tuff eruption at 15 ka: Insights from a 2.5D multichannel seismic survey		93
Abstract	93
5.1	Introduction.....	94
5.2	Regional setting.....	95
5.3	Materials and methods	97
5.4	Results.....	98
5.4.1	Seismic analysis.....	99
5.5	Discussion.....	106
5.5.1	Seismostratigraphic framework	106
5.5.2	Shallow hydrothermal gases and/or fluids	109
5.5.3	3D evolutionary model.....	111
5.6	Conclusions.....	114
5.7	Acknowledgements	115
Chapter 6	117
Conclusions and Outlook		117

6.1	Tectono-sedimentary processes in the Gulf of Naples	118
6.2	The origin of the Campi Flegrei caldera	118
6.3	Post-collapse processes and deposition at the Campi Flegrei caldera	119
6.4	Hydrothermalism at the Campi Flegrei caldera	120
6.5	Outlook	121
Acknowledgements		123
References.....		124

List of Figures

Fig. 1.1: Worldwide distribution of collapse calderas	6
Fig. 1.2: Histogram showing erupted volume of important historic and geological caldera eruptions	6
Fig. 1.3: Caldera end-member models illustrating alternative subsidence geometries	11
Fig. 1.4: Relative size of some selected calderas compared to the Campi Flegrei.	12
Fig. 1.5: Simplified sketch illustrating a caldera-forming eruption in five stages	13
Fig. 1.6: Overview map of the Tyrrhenian Sea and southern Italy	17
Fig. 1.7: Paleo-tectonic reconstruction of the Tyrrhenian Sea back-arc basin evolution..	18
Fig. 1.8: Overview map of the Campania Margin, southern Italy	19
Fig. 1.9: Summary of the Quaternary eruption history in the Campanian Plain.....	20
Fig. 1.10: Bathymetric and topographic map of the Campi Flegrei caldera.....	21
Fig. 1.11: Geophysical evidence for the offshore location of the Campi Flegrei caldera margin.....	24
Fig. 2.1: Overview map of the working area in the Gulf of Naples and the acquired multichannel seismic datasets as utilized in this thesis.....	30
Fig. 2.2: Illustration of the acquisition geometry of the 96-channel streamer during the CAFE_2015 expedition	32
Fig. 2.3: General seismic data processing as applied to the four utilized datasets.	34
Fig. 2.4: Exemplary illustration of the recording scheme during CAFE-7/3 cruise.....	35
Fig. 2.5: Shot gather of shot 5693 of profile GeoB08-050 (CAFE-7/3), illustrating the incorrect channel recording	36
Fig. 2.6: Illustration of (A) shot gather and (B) CMP gather.	37
Fig. 2.7: Receiver gather (channel 21) of profile GeoB08-050, illustrating the effect of the irregular vertical shift on the data.....	39
Fig. 2.8: Illustration of the hyperbolic two-way traveltime (TWT) difference (normal moveout) with increasing offset.....	40
Fig. 2.9: Processing result of the predictive deconvolution	41
Fig. 2.10: Processing result of the post-stack noise attenuation.....	43
Fig. 2.11: Processing result of the time migration.....	44
Fig. 3.1: Overview map of the Gulf of Naples and Campanian Plain illustrating the main fault pattern.....	48
Fig. 3.2: Overview map of the multichannel seismic profiles utilized in Chapter 3.....	51
Fig. 3.3: Composed NE-SW-trending multichannel seismic line consisting of profile GeoB16-259 and GeoB08-062.....	53
Fig. 3.4: Multichannel reflection seismic profile GeoB16-254	54

Fig. 3.5: Gridded horizon maps of the four main unconformities U1-U4 in the Gulf of Naples	55
Fig. 3.6: Thickness maps illustrating the spatial distribution of the individual seismic units SU1-5 in the Gulf of Naples	56
Fig. 3.7: Thickness maps of the CI and the NYT deposits.....	58
Fig. 3.8: Stratigraphic column in correlation to sea-level variations during the past 1 Ma	61
Fig. 3.9: 3D tectono-sedimentary model outlining the evolution of the Gulf of Naples over the past 1 Ma.	65
Fig. 4.1: Topography and bathymetry of the Campi Flegrei volcanic area and the Gulf of Naples with location of the presented multichannel seismic profiles.	73
Fig. 4.2: N-S trending multichannel seismic profile GeoB08-050	75
Fig. 4.3: N-S trending multichannel seismic profile GeoB08-032	77
Fig. 4.4: ENE-WSW trending multichannel seismic profile GeoB08-070.....	78
Fig. 4.5: E-W trending multichannel seismic profile GeoB08-065.....	80
Fig. 4.6: Stratigraphic column and volcanic activity in correlation with sea level variations during the past 39 ka.....	84
Fig. 4.7: Conceptual 2-dimensional reconstruction of the caldera formation and evolution since ~39 ka based on GeoB08-065	88
Fig. 4.8: Close-up of GeoB08-065 to illustrate the mathematical relationship between total uplift of the western margin, sediment thickness on the uplifted block and sediment thickness in the basin.....	90
Fig. 5.1: Location of the semi-3D high-resolution multichannel seismic profiles acquired during the CAFE7-3 cruise in 2008.....	96
Fig. 5.2: N-S trending multichannel seismic profile GeoB08-044	99
Fig. 5.3: N-S trending multichannel seismic profile GeoB08-036	101
Fig. 5.4: Topography of unconformity U1 with major structural, volcanological and erosive features being indicated.	102
Fig. 5.5: E-W trending multichannel seismic profile GeoB08-026.....	103
Fig. 5.6: N-S trending profile GeoB08-029	104
Fig. 5.7: Thickness maps of the main seismic units (M1-M4) illustrating centres of deposition and non-deposition in the Campi Flegrei caldera.....	105
Fig. 5.8: Graphical summary of main post-caldera stratigraphic markers and depositional units in correlation with sea-level rise	107
Fig. 5.9: Location of gas and NYT caldera fault as inferred from multichannel seismic data	110

Fig. 5.10: Close-up of GeoB08-044 illustrating the escape of gas along the NYT caldera fault	111
Fig. 5.11: Post-caldera spatial evolutionary model illustrating the depositional environment in interplay with volcano-tectonic processes and sea-level rise....	112
Fig. 6.1: Overview map of all the GeoB16 profiles acquired in the Gulf of Naples.	122

List of Tables

Table 2.1: Commonly used trigger scheme during CAFE-7/3 expedition.....	30
Table 2.2: Commonly used trigger scheme during CAFE_2015.....	32
Table 3.1: Summary of the specifications of the utilized multichannel seismic datasets...	51
Table 3.2: Seismic facies description and associated geological interpretation of the main seismic units in the Gulf of Naples	51
Table 4.1: Seismic facies description and associated geological interpretation of the main seismic units in the offshore sector of the Campi Flegrei caldera.....	82
Table 5.1: Volume calculations for identified post-caldera volcanic units.....	109

Abbreviations

CI	Campanian Ignimbrite
CFc	Campi Flegrei caldera
CVZ	Campi Flegrei Volcanic Zone
DRE	Dense-Rock Equivalent
LGM	Last Glacial Maximum
mbpsl	meters below present sea level
NYT	Neapolitan Yellow Tuff
PDC	Pyroclastic density currents

Preface

This thesis was submitted for the degree of Doctor of Natural Sciences (Dr. rer. nat.) at the Department of Geosciences, University of Bremen. The majority of the research was conducted at the University of Bremen in the research group *Marine Technology – Environmental Research* under the supervision of Prof. Dr. Volkhard Spiess. The second thesis reviewer is Prof. Dr. Sebastian Krastel. The doctoral project was carried out in close cooperation with our Italian partners, in particular Marco Sacchi from the *Institute for Coastal Marine Environment, Italian Research Council (IAMC-CNR)*.

Data processing and analysis was funded through the German Research Foundation (DFG) within the ICDP priority programme (Grant Nos. SP296/34-1; SP296/34-2). Funding for data acquisition was provided by the Italian Research Council through the CNR Shiptime Programme and the DFG's ICDP and IODP priority programmes (Grant Nos. SP296/30-1, SP293/37-1). Additional financial support was provided by the *Bremen International Graduate School for Marine Sciences* (GLOMAR) for conducting a research stay at the IAMC-CNR in September/October 2014 as well as international conference participations.

This thesis was written in the cumulative format and thus consists of a collection of in total three standalone research manuscripts which have been submitted or will be submitted as joint-author articles to international peer-reviewed journals. A general introduction outlining the project background and context, objectives and aims as well as the utilized methods precedes the three research manuscripts. The last chapter synthesizes the main conclusions of this thesis and illustrates prospects for future research opportunities in the researched field.

Lena Steinmann
Bremen, June 2016

This page is intentionally left blank

Thesis Abstract

The formation of large collapse calderas is associated with highly destructive explosive volcanic eruptions, which have the potential to trigger a global catastrophe in the same order of magnitude as a giant meteorite impact. Understanding caldera-forming eruption mechanisms and dynamics is of paramount importance in order to reliably assess volcanic hazards and risks of future eruptions.

The present thesis aims at contributing to the overall knowledge of caldera volcanism by examining (1) the interplay between tectonism and volcanic activity, (2) the caldera architecture and collapse mechanisms, and (3) post-caldera volcano-tectonic processes at the most active caldera on Earth, the Campi Flegrei caldera located in southern Italy. Due to its history of large-scale explosive eruptions, its ongoing episodes of unrest, and its high population density with nearly 2.5 million people living in the close vicinity, the Campi Flegrei caldera represents one of the world's maximum volcanic risk areas. As a future eruption could have significant impact on regional as well as global scale, comprehending its genesis and evolution is a matter of global relevance.

The current thesis is based on high-resolution multichannel reflection seismic data acquired in the offshore sector of the Campi Flegrei caldera and the greater vicinity of the Gulf of Naples. Within the context of this thesis, the first semi-3D multichannel seismic investigation of a large collapse caldera is presented, providing novel insights on the shallow structures of the Campi Flegrei caldera.

For the first time, high-resolution multichannel seismic data show evidence for the existence of a nested-caldera system formed during two collapses associated with the Campanian Ignimbrite (CI) eruption at 39 ka and the more recent Neapolitan Yellow Tuff (NYT) eruption at 15 ka. An arc-shaped inner caldera ring-fault separating the caldera margin from the subsided caldera depression could clearly be imaged and spatially mapped. At the Eastern and Western caldera margin, this fault was already activated during the CI eruption. However, at the southern section of the caldera margin, it seems to be associated with only the NYT collapse, while the CI fracture zone is assumed to lie further south and at greater depth. The NYT caldera probably formed during an asymmetrical, piecemeal-like collapse with a maximum subsidence of ~75 m in the offshore portion. The vertical displacement related to the CI caldera collapse may be significantly larger.

In the post-caldera phase, the NYT caldera depression acted as significant accommodation space and was rapidly filled with an on average 61-m thick sequence of marine and reworked volcanoclastic sediments deposited between 15 and 8.6 ka. Since 8.6 ka, the accommodation space was limited as a result of resurgence-related uplift in the caldera centre. Furthermore, the 3D aspect of the seismic dataset allows for the

assessment of post-caldera eruption volumes. Specifically, the erupted volumes of the Nisida Bank, Nisida Island and Capo Miseno post-caldera eruptions are estimated to be at least 0.14 km³, 0.10 km³ and 0.08 km³, respectively. These values are significantly higher than previous estimates because the deposits in the offshore portion have previously not been considered.

Moreover, the effect of hydrothermalism on the offshore sector of the Campi Flegrei caldera is investigated in order to contribute to the understanding of the hypothesised shallow (<2 km) hydrothermal system, which is supposedly strongly linked to the recent unrest episodes. The findings from the current thesis reveal that the fractured caldera margin acts as pathway for the ascent of hydrothermal gases/fluids potentially originating from the hypothesised shallow hydrothermal system.

The multichannel seismic data from the Gulf of Naples are analysed in order to examine the interaction between fault activity, volcanism and sedimentary deposition with respect to the regional tectonic setting. Two tectonically active phases leading to the subsidence of the Gulf of Naples half-graben basin are recognized (1) between 1 and 0.40 Ma and (2) between 0.14 to 0.02 Ma. Time periods between 0.40 and 0.14 Ma and from 0.02 Ma onwards seem to have been tectonically stable. The onset of increased subsidence at 0.14 Ma was approximately coeval with the initiation of severe volcanic activity in the Campi Flegrei Volcanic Zone (CVZ) and at the adjacent Somma-Vesuvius. Hence, a close linkage between tectonism and volcanism is suggested, probably related to the reactivation of major NE-SW and NW-SE-trending normal faults. Therefore, it can be hypothesised that the large-scale CI eruption at 39 ka was triggered by regional tectonism. In contrast, the NYT eruption at 15 ka occurred during a phase of tectonic stability, which may either indicate that the tectonic control on eruptions played only a minor role from 0.02 Ma onwards, or that the presented seismic data were not able to resolve subsidence during that relatively short time interval.

The main outcomes of the current thesis are presented in three novel and comprehensive evolutionary models addressing (1) a 3D reconstruction of the tectono-sedimentary variability in the Gulf of Naples half-graben with respect to volcanism during the past one million years, (2) the conceptual formation of the Campi Flegrei nested-caldera complex, and (3) the 3D post-caldera evolution of the Campi Flegrei caldera. In summary, the findings from the current thesis represent a significant advancement towards understanding the genesis and evolution of the Campi Flegrei caldera as well as the tectonic formation of the Gulf of Naples half-graben basin and its influence on volcanism. The suitability of multichannel reflection seismic data to investigate (partly) submerged collapse calderas was underlined and may also be applicable to other calderas.

Zusammenfassung

Die Entstehung von großen kollabierten Calderen steht im Zusammenhang mit äußerst zerstörerischen Vulkanausbrüchen, welche das Potential haben eine globale Katastrophe in der Größenordnung eines riesigen Meteoriteneinschlags, auszulösen. Um die Gefahren und Risiken einer solchen zukünftigen Eruption besser abschätzen zu können, ist es von höchster Wichtigkeit ihre Eruptionsmechanismen und -dynamik zu verstehen.

Das Ziel dieser Doktorarbeit ist es, einen signifikanten Beitrag zum Allgemeinwissen über Calderavulkanismus zu leisten und dieses auszubauen. Dafür werden (1) das Zusammenspiel zwischen Tektonik und Vulkanismus, (2) der Aufbau einer Caldera und Kollapsmechanismen sowie (3) post-caldera vulkanisch-tektonische Prozesse exemplarisch an der aktivsten Caldera der Welt untersucht: der Campi Flegrei Caldera (Süditalien). Auf Grund ihrer langen Geschichte von gigantischen Vulkanausbrüchen, andauernden Unruhephasen sowie ihrer hohen Populationsdichte mit nahezu 2.5 Mio. Anwohnern in nächster Nähe, stellt die Campi Flegrei Caldera eine der gefährdesten vulkanischen Gegenden der Welt dar.

Diese Arbeit basiert auf hochauflösenden mehrkanalseismischen Daten aus dem marinen Teil der Campi Flegrei Caldera und der Umgebung im Golf von Neapel. Im Rahmen dieser Doktorarbeit wird der erste semi-3D mehrkanalseismische Datensatz von einer großen Kollaps-caldera präsentiert.

Zum ersten Mal haben hochauflösende mehrkanalseismische Daten Beweise für die Existenz eines sogenannten *nested-caldera* Systems bestehend aus zwei verschachtelten Calderen in der Campi Flegrei Caldera geliefert. Gebildet wurde dieses durch zwei gigantische Vulkanausbrüche zum Einen der *Campanian Ignimbrite* (CI) Eruption vor 39.000 Jahren und zum Anderen der *Neapolitan Yellow Tuff* (NYT) Eruption vor 15.000 Jahren. Eine bogenförmige Verwerfung, welche die Calderadepression von dem Calderarand trennt, wird abgebildet und auskartiert. Am östlichen und westlichen Calderarand war diese Störung bereits zur Zeit des CI Ausbruchs aktiv. Im südlichen Calderateil hingegen ist diese Störung nur mit der NYT Eruption assoziiert, wohingegen die CI Störungszone vermutlich weiter südlich und in größeren Tiefen liegt. Die NYT Eruption führte vermutlich zu einem asymmetrischen, sogenannten *piecemeal* (stückweise) Kollaps mit einer maximalen Subsidenz von 75 m im marinen Teil. Im Vergleich dazu war der CI-Kollaps vermutlich signifikant größer, mit Subsidenz von hunderten bis tausenden Metern.

Während der Post-Caldera Phase, im Zeitraum zwischen 15.000 und 8.000 Jahren, fungierte die NYT Calderadepression als Hauptablagerungsraum und wurde rasch mit einer 61 m mächtigen Sequenz an marinen und vulkanisch-klastischen Sedimenten gefüllt. Vermutlich durch eine erneute Füllung der Magmakammer wurde der zentrale Bereich

der Calderadepression seit 8.600 Jahren stetig angehoben, was zu einer Begrenzung des Ablagerungsraumes führte. Der 3D Aspekt der seismischen Daten erlaubt eine neue Volumenabschätzung einiger Post-Caldera Eruptionen durchzuführen: *Nisida Bank* (0,14 km³), *Nisida Island* (0,10 km³) und *Capo Miseno* (0,08 km³). Die ermittelten Werte sind signifikant höher als zuvor in der Literatur postulierte Volumen, da diese die marinen Ablagerungen vernachlässigt haben.

Des Weiteren wird der Effekt von Hydrothermalismus auf den marinen Teil der Campi Flegrei Caldera untersucht um weitere Einblicke in die mögliche Existenz eines relativ flachen hydrothermalen Systems (<2 km) zu erhalten, welches womöglich in direktem Zusammenhang mit den andauernden Unruhephasen steht. Die Ergebnisse dieser Arbeit zeigen, dass der gestörte Calderarand als Aufstiegszone für hydrothermale Gase/Fluide dient, welche vermutlich aus dem postulierten Hydrothermalsystem stammen.

Die mehrkanalseismischen Profile aus dem Golf von Neapel erlauben einen Einblick in die regionale Tektonik. Im Detail wurde das Zusammenspiel zwischen tektonischen Störungen, Vulkanismus und sedimentärer Ablagerung beleuchtet. Zwei tektonisch aktive Phasen wurden zwischen (1) 1 und 0,40 Mio. Jahren und (2) zwischen 0,14 und 0,02 Mio. Jahren identifiziert. Die Zeiträume zwischen 0,40 und 0,14 Mio. Jahren und seit 0,02 Mio. Jahren scheinen hingegen tektonisch stabil gewesen zu sein. Die zweite tektonisch aktive Phasen beginnt zeitgleich mit intensivem Vulkanismus in the *Campi Flegrei Volcanic Zone* (CVZ) und am *Somma-Vesuvius*. Daher wird eine enge Verbindung beider Prozesse postuliert, die vermutlich im Zusammenhang mit der Reaktivierung von regionalen NO-SW und NW-SO Störungen steht. Dementsprechend kann davon ausgegangen werden, dass auch die gigantische CI Eruption vor 39.000 Jahren signifikant durch Tektonik beeinflusst wurde. Für die NYT Eruption vor 15.000 Jahren kann ein solcher Zusammenhang allerdings nicht hergestellt werden, da diese anscheinend während einer Phase tektonischer Stabilität statt fand.

Die wichtigsten Ergebnisse dieser Doktorarbeit werden in drei neuartigen und umfassenden Modellen wie folgt zusammengefasst (1) eine 3D Rekonstruktion der tektonisch-sedimentären Prozesse im Golf von Neapel im Zusammenspiel mit Vulkanismus über die letzten 1 Mio. Jahre, (2) die konzeptionelle Entstehung des Campi Flegrei nested-caldera Systems und (3) die Post-Caldera Evolution der Campi Flegrei Caldera in 3D im Hinblick auf Post-Caldera Vulkanismus, sedimentäre Ablagerung und Meeresspiegelschwankungen. Diese Arbeit stellt einen signifikanten Beitrag zum Wissen über die Entstehung und Evolution der Campi Flegrei Caldera im Zusammenspiel mit regionaler Tektonik dar. Die Tauglichkeit von Mehrkanal-Reflektionsseismik zur Erforschung von (teilweise) submarinen großen Kollapsalderen wurde unter Beweis gestellt und eignet sich auch für die Anwendung an ähnlichen Calderen.

Chapter 1

1 Introduction

1.1 Motivation and objectives

Caldera-forming explosive eruptions are among the most catastrophic natural events to affect the Earth's surface and human society. As they are capable of triggering global catastrophes in the same order of magnitude as giant meteorite impacts, they have attracted particular attention in scientific communities and governmental institutions worldwide. Hazardous products of caldera-forming eruptions include (1) highly-destructive pyroclastic density currents (PDCs) depositing large-volume ignimbrites, (2) extensive ashfall deposits covering continent-size areas, and (3) the release of noxious gases into the atmosphere and significantly affect the global climate. Important aspects on caldera dynamics and structure still remain uncertain and controversial and, as demonstrated by ample volcanological research in the last decades, they may be very different from those characterizing the more commonly studied stratovolcanoes and shield volcanoes. However, since large collapse calderas occur on all continents in various tectonic settings and also often in densely populated areas (Fig. 1.1), understanding their eruption mechanisms in order to assess volcanic hazards and risks is a matter of global relevance.

Famous historic examples of highly-destructive caldera-forming eruptions include the eruption of Mount Vesuvius in AD 79 during which the cities Pompeii and Herculaneum were buried by several PDCs (Cioni et al., 1999), the 1815 Tambora eruption causing the death of 90,000 people and a 2-year global cooling event (Self et al., 1984), and the 1883 eruption of Krakatau which generated tsunamis claiming ~36,000 lives and led to a 2-year episode of cooling in the Northern Hemisphere (Fig. 1.2) (Rampino and Self, 1982; Sigurdsson et al., 1991). On a geological timescale, significantly larger and more devastating caldera-forming eruptions, with much more severe and long-lasting impact on the global climate, have been recognized (Self, 2015). Such eruptions include the 73 ka Toba eruption (Williams et al., 2009), the 600 ka Yellowstone eruption (Mastin et al., 2014), the 760 ka Long Valley eruption (Bailey et al., 1976), the 26.5 ka Taupo eruption (Wilson, 2001), and the 39 ka Campi Flegrei eruption (Fitzsimmons et al., 2013) (Fig. 1.2).

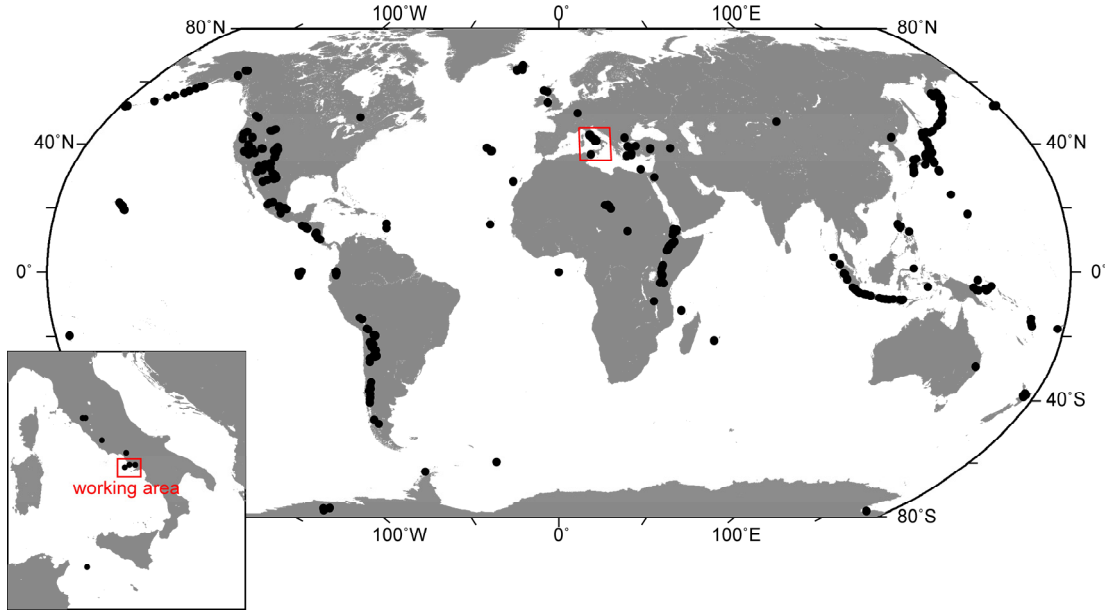


Fig. 1.1: Worldwide distribution of collapse calderas (black dots) with close-up of Italy. Caldera locations were taken from the *Large Collapse Caldera Database* (Geyer and Martí, 2008). Red square in world map indicates the location of the inset map showing the Italian Peninsula and the Gulf of Naples (Fig. 1.6). Please refer to Figures 1.6 and 1.8 for a more detailed map of the working area.

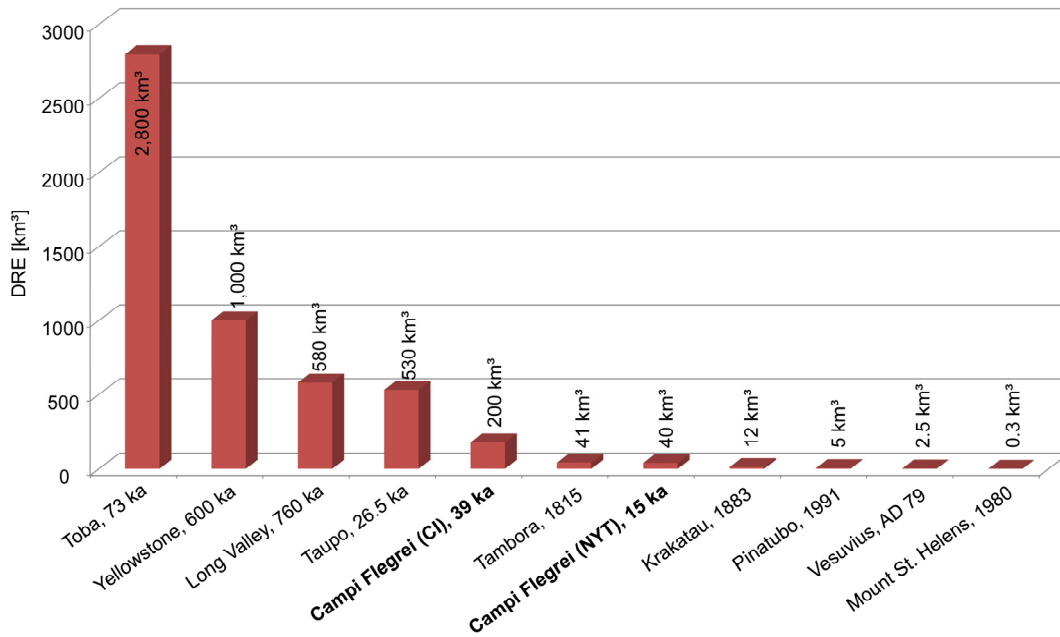


Fig. 1.2: Histogram illustrating the Dense-Rock Equivalent (DRE) volume of selected historical and geological eruptions. The two major eruptions associated with the Campi Flegrei caldera (CFc) are highlighted in bold. Volumetric values were taken from Crosweller et al. (2012).

In addition to the societal and scientific aspects, calderas are also of economic value as they commonly host hydrothermal systems which are associated with the formation of scarce ore deposits and constitute a valuable geothermal energy resource.

Traditionally, calderas have been analysed based on geological field studies and borehole observations, which mainly allowed for selective and spatially limited information on complex caldera systems. More recently, analogue modelling has provided additional insights into the formation and development of collapse calderas. However, this method is limited by the simplification of the processes related to caldera volcanism. Geophysical studies such as seismic refraction tomography, gravity or magnetic measurements have proven to be useful for the identification of the overall caldera structure (i.e. distinguish margin from collapsed area). Even though such geophysical methods provide good spatial coverage, they are limited by their low resolution. In submerged caldera settings, marine reflection seismic imaging has emerged as powerful tool to understand the stratigraphic architecture and structure of calderas as well as the dispersal of PDCs.

This thesis represents a caldera case study, focusing on the most active caldera on Earth: the Campi Flegrei caldera (CFc) situated in the Campanian Plain in southern Italy (Fig. 1.1) (De Natale et al., 2006). As approximately half of the caldera structure is located offshore, the CFc provides an ideal opportunity to study a complete stratigraphic record in the marine portion, thereby avoiding challenges posed on land by subsequent destruction or burial of earlier features as well as urbanization. The CFc is located in a densely populated region with the city of Naples at its eastern border and the town of Pozzuoli in its centre. This area is considered as one of the maximum volcanic risk areas worldwide as a future caldera-forming eruption could expose more nearly 2.5 million people to direct volcanic hazards. Hence, the CFc has received significant scientific and societal interest during the last decades. In that context, the CFc has also become subject to a joint approach for scientific drilling in the ICDP and IODP programmes. In order to support the drilling projects, two joint Italian-German research expeditions were carried out in 2008 and 2016, covering the offshore sector of the CFc as well as the greater vicinity of the Gulf of Naples. Funding for data acquisition was provided by the Italian Research Council through the CNR Shiptime Programme and the DFG's ICDP and IODP priority programmes. During these cruises, high-resolution multichannel reflection seismic profiles were acquired, building the foundation of this thesis. In particular, a semi-3D grid of high-resolution multichannel seismic lines provides a unique opportunity to analyse caldera-related processes in interplay with sedimentation in space and time. Data processing and interpretation were carried out in the framework of a DFG project funded within the ICDP Priority Programme namely "*Shallow structures of the marine Campi Flegrei Caldera and the volcanoclastic and sedimentary deposits in the Gulf of Naples*".

The main scientific objectives of this thesis are the following:

- (1) Providing new insights on the link between regional tectonics and volcanism by examining the tectono-sedimentary evolution of the Gulf of Naples half graben

The Gulf of Naples represents a Plio-Quaternary half-graben basin formed in the course of NW-SE and NE-SW faulting. The volcanic activity in the CVZ and at the Somma-Vesuvius seems to have been strongly controlled by these regional fault systems (e.g. Acocella and Funicello, 2006; Turco et al., 2006; Milia et al., 2013). In order to understand the linkage between tectonism and volcanism, the regional tectono-sedimentary setting requires detailed examination. So far, the stratigraphic understanding of the Gulf of Naples is based either on low-frequency multichannel seismic data with limited vertical and horizontal resolution (e.g. Fusi et al., 1991; Milia and Torrente, 1999; Milia et al., 2003; Milia et al., 2006; Milia and Torrente, 2007), or on very high-resolution single-channel seismic data with limited penetration (Milia et al., 1998; Aiello et al., 2005; Passaro et al., 2014). The multi-frequency approach utilized in this thesis offers the ideal combination of resolution and penetration and is thus suitable for refining and extending the previously proposed stratigraphic framework as well as providing novel insights on the link between tectonism and volcanism (Chapter 3).

- (2) Re-evaluating the Campi Flegrei caldera collapse history in order to ascertain whether it was formed by only one or two large-scale ignimbritic eruptions

Despite ample research, the genesis of the CFc is still controversial. Traditionally, it has been regarded as a nested-caldera system, formed by two major ignimbritic eruptions namely the Campanian Ignimbrite (CI) eruption (39 ka) and the subsequent Neapolitan Yellow Tuff (NYT) eruption (15 ka) (e.g. Rosi et al., 1983; Barberi et al., 1991; Orsi et al., 1996; Deino et al., 2004; Acocella, 2008). On the other hand, it has been proposed that the CFc was formed only by the NYT eruption, while the CI eruption was assumed to have occurred along fissure-type vents without leading to a collapse (e.g. Di Girolamo et al., 1984; Florio et al., 1999; De Vivo et al., 2001). Some authors have even questioned the existence of a caldera in Campi Flegrei entirely (Bellucci et al., 2006; Milia et al., 2006; Milia and Torrente, 2007). The mapping of the caldera ring-fault as well as major stratigraphic units (including sedimentary and volcanoclastic deposits) allows for a novel and comprehensive reconstruction of the CFc genesis (Chapter 4).

(3) Understanding the post-collapse evolution of the Campi Flegrei caldera by carrying out a 3D analysis of the shallow architecture, fault system and sedimentary fill

In the post-caldera phase, the CFc has been modified by various processes including sea-level variations, caldera resurgence, and post-caldera eruptions. However, a detailed spatial and temporal analysis of the combined effects on the caldera evolution and its depositional environment is lacking in the current literature. For instance, the post-caldera eruptions are well constrained onshore, however, only limited knowledge exists about their impact on the offshore portion of the caldera. The 3D-investigative effort presented in this thesis allows for a comprehensive analysis of the caldera's structure and the post-caldera depositional environment as well as for a reassessment of post-caldera eruption volumes, thereby significantly advancing the current knowledge of the post-caldera evolution of the CFc (Chapter 5).

(4) Assessing the influence of hydrothermalism on the offshore sector of the Campi Flegrei caldera

Since the 1960s, the caldera centre has been characterized by short-term episodes of unrest involving ground deformation, shallow earthquakes and increased temperature at the fumaroles (De Natale et al., 2006). Recent studies suggested that such short-term uplift phases may be associated with fluid migration related to a hypothesized hydrothermal system (Lima et al., 2009; Chiodini et al., 2015). The high-resolution multichannel seismic dataset allows for the identification of zones of hydrothermal activity (e.g. trapped fluids/gases) based on amplitude anomalies, as well as the mapping of potential fluid pathways (e.g. faults). The location of amplitude anomalies may provide further insights into the existence of the hypothesised hydrothermal system and potential escape pathways. This objective is directly related to one of the main goals of the ongoing ICDP campaign namely the unravelling of the interplay between the magmatic and hydrothermal systems in order to understand the unrest mechanism at the CFc (Chapter 4, 5).

1.2 Caldera volcanism

Calderas are often referred to as so-called *super-volcanoes*. However, this term should be used with care as it actually only refers to those calderas that were formed by exceptionally large eruptions, which, on average, occur every 100,000 years (Self, 2015). In order to be termed a *super-eruption*, more than 450 km³ of magma needs to be erupted, which is roughly equivalent to ~1,000 km³ of ash deposits, and corresponds to an 8-9 on the Volcanic Explosivity Index (VEI), a measure of the explosive magnitude of an eruption (Newhall and Self, 1982). Human civilisation has experienced many devastating large-scale eruptions; however, the last super-eruptions occurred far before our existence, 26,500 years ago at the Taupo caldera (Fig. 1.2). Nonetheless, as proven by historic eruptions, even “non-super” caldera-forming events have the potential to significantly affect humanity and the global climate for a long time. In any case, all calderas are associated with similar underlying eruption mechanisms, which will be explained in detail in the current section.

1.2.1 Caldera architecture

In general, calderas are sub-circular topographic depressions originating from a collapse or subsidence into the top of a partly drained magma chamber during or immediately after an explosive volcanic eruption (Cole et al., 2005). A simplified “end-member” classification of collapse calderas was established to allow for a better systematic understanding of caldera subsidence geometries. In that context, four structural types were defined including plate (piston), piecemeal, trap-door, and downsag calderas (Fig. 1.3) (Lipman, 1997; Cole et al., 2005). However, in reality, several of these end-members may coexist at a single caldera rather than defining the overall architecture of a single structure. Hence, they should rather be considered as common attributes that may develop coevally (Branney and Acocella, 2015). The amount of subsidence may be variable, ranging from a few meters to a few kilometres depending on the style and geometry of collapse (Acocella, 2007).

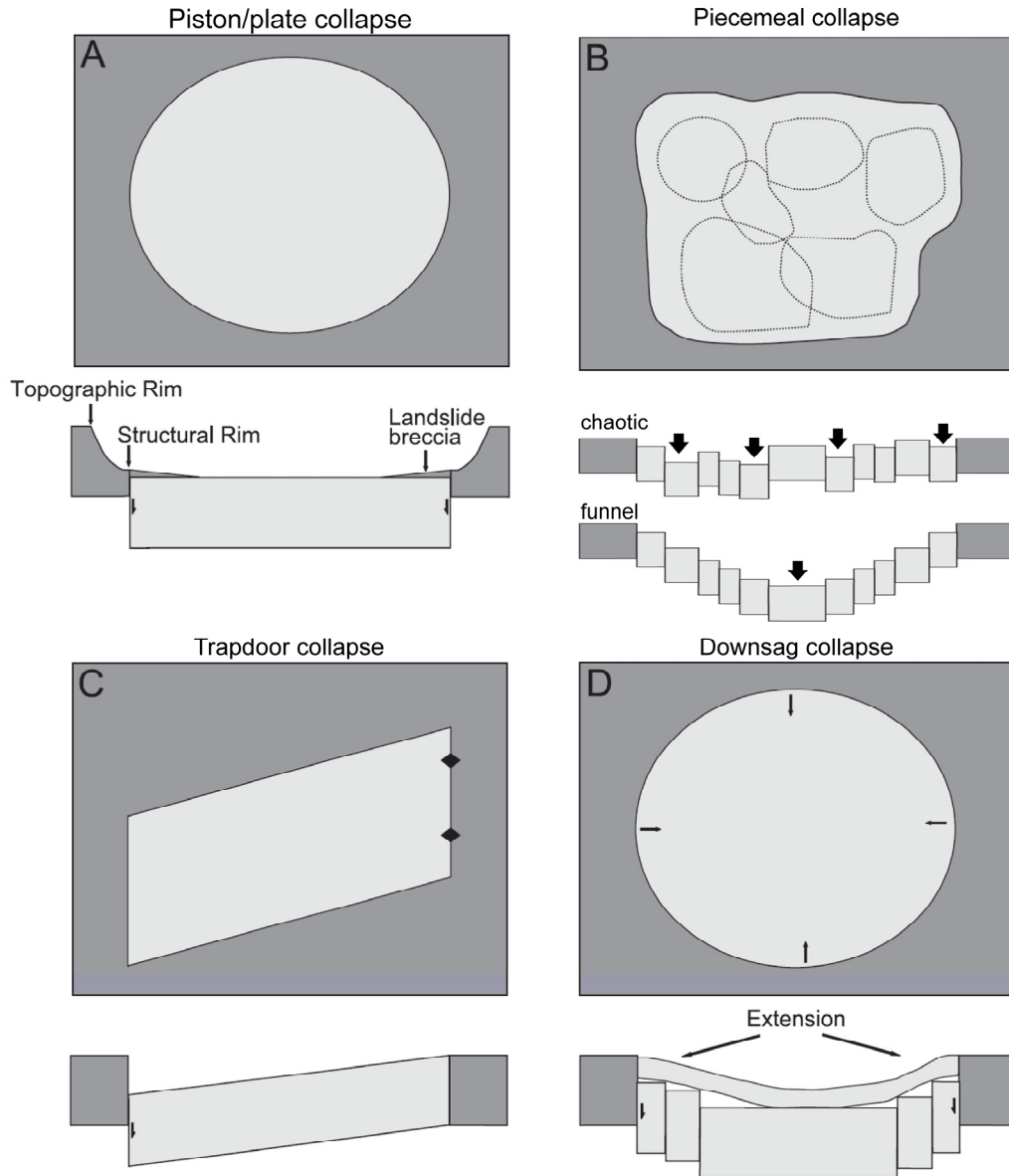


Fig. 1.3: Caldera end-member models illustrating alternative subsidence geometries (modified from Cole et al., 2005).

The shape and size of caldera depressions varies (Fig. 1.4) and is closely linked to the tectonic setting and the geometry of the underlying magma chamber. Pre-existing structural faults may act as pathways for the ascent of magma from a deeper reservoir, thereby controlling eruptive fissures (Acocella and Funicello, 2006; Aizawa et al., 2006). Generally, it is assumed that the overall caldera width is similar to that of the magma reservoir (Aizawa et al., 2006). If a caldera is formed by more than one eruption (i.e. undergoes multiple collapses), it is referred to as a *nested-caldera complex*.

The intra-caldera region (i.e. subsided area within a caldera) is separated from the extra-caldera region (i.e. area unaffected by caldera formation) by a complex caldera margin. The marginal area is characterized by intense deformation often accompanied by a ring-

fracture zone, hydrothermal alteration, occurrence of magmatic intrusions, and topographical instability (Branney and Acocella, 2015).

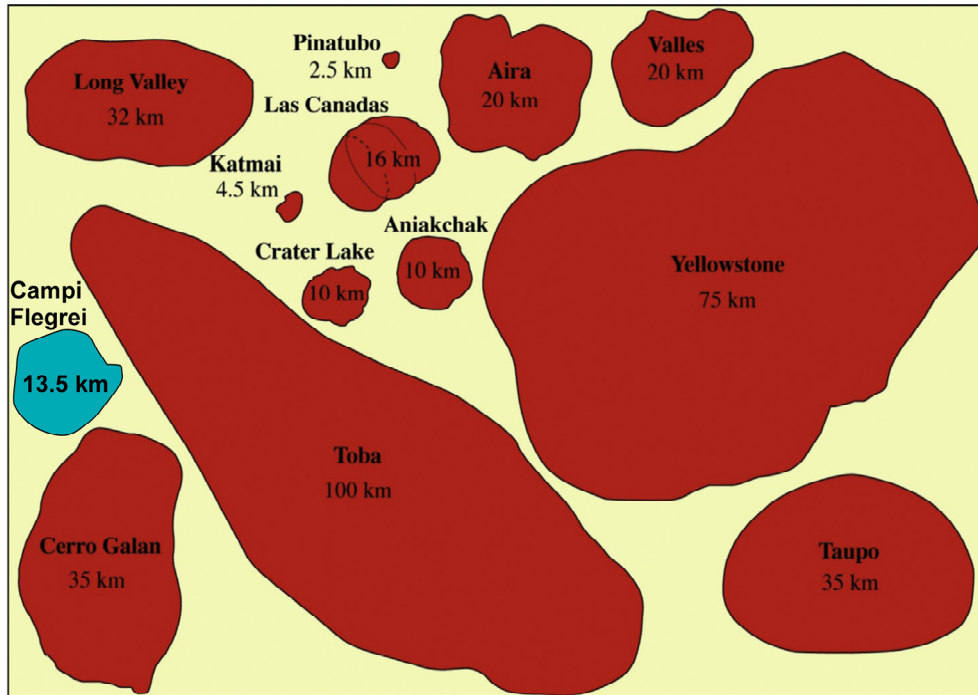


Fig. 1.4: Relative size of some selected calderas compared to the Campi Flegrei (modified from de Silva and Lindsay (2015)).

1.2.2 Collapse-caldera formation and resurgence

Typically, large collapse-calderas form during highly-explosive (i.e. pyroclastic-dominated) andesitic-dacitic and rhyolitic eruptions emplacing high-volume ignimbrites. An entire explosive caldera-forming eruption can take place in only a few days, erupting hundreds to thousands of cubic kilometre of magma (de Silva and Lindsay, 2015). In contrast, there are also examples of relatively quiet, effusive (i.e. lava-dominated) caldera-forming eruptions mainly associated with basaltic calderas as for instance those on Hawaii or Galapagos. Such effusive calderas are related to significantly smaller eruption volumes ($<1 \text{ km}^3$) and may be generated during a longer timespan of days to months (Cole et al., 2005; Branney and Acocella, 2015). This section will focus in the generation of calderas related to explosive volcanic activity.

Prior to a caldera-forming eruption, tumescence (i.e. uplift due to an inflation of the magma chamber) and small-scale eruptions commonly occur (Fig. 1.5-A). Tumescence is generally regarded as a sign for an increase in volume and pressure of the magma in the underlying reservoir (Aizawa et al., 2006). The magma chamber of most calderas is located within the upper crust and can be as shallow as a few kilometres. As geophysical data have shown, the depth of the magma reservoir is usually smaller than the diameter of the caldera at the surface (Aizawa et al., 2006).

The caldera-forming eruption itself may start as a Plinian, central-vent eruption during which a huge eruption column is generated, transporting large amounts of ash to high altitude, and producing PDCs when collapsing (Fig. 1.5-B) (see section 1.2.3) (Cioni et al., 2015). Eventually, the eruption proceeds to a large-scale ignimbritic eruption along

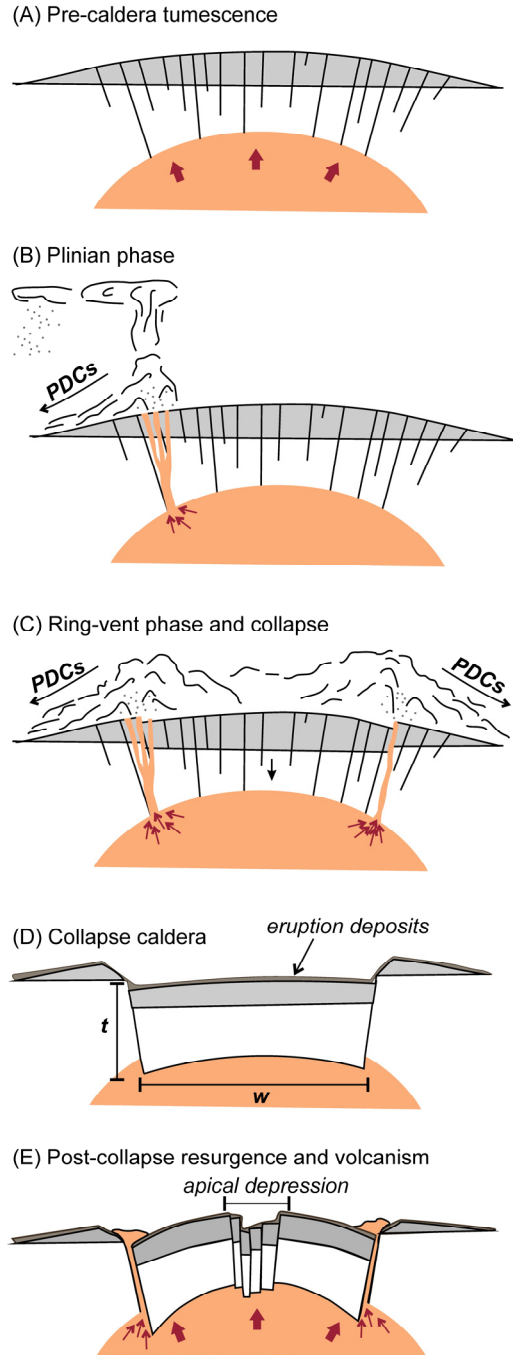


Fig. 1.5: Simplified sketch illustrating a caldera-forming eruption in five stages (compiled from Smith and Bailey (1968) Acocella et al. (2001)). In (D) t = thickness of overburden, w = caldera width.

the caldera ring-fault coincident with caldera collapse. During the ring-vent phase, large amounts of magma are being withdrawn in a short time and extensive PDCs are being produced, depositing massive ignimbrites (Fig. 1.5-C) (Cole et al., 2005). Consequently, the magma chamber is quickly being emptied, resulting in an under-pressure within. This ultimately leads to a (coeval) subsidence of the overburden (i.e. magma chamber roof) and, thus, to the formation of the caldera depression and associated ring-fault system (Fig. 1.5-D) (Acocella et al., 2000; Cole et al., 2005; Aizawa et al., 2006).

In the post-collapse phase, calderas are typically associated with short-term episodes of unrest and eruptions. Furthermore, many calderas are characterized by post-collapse resurgence (i.e., renewed inflation of the magma chamber), resulting in long-term uplift of the intra-caldera area (Fig. 1.5-E) (Smith and Bailey, 1968; Acocella et al., 2000; Kennedy et al., 2012). At the top of the resurgent dome, extensional normal faults develop, leading to the formation of an apical depression. The architecture of the resurgent dome depends on the aspect ratio (thickness/width) of the magma chamber roof (Fig. 1.5-D) (Acocella et al., 2001). Aspect ratios of ~ 1 favour the development of a resurgent block, as for instance present on Ischia Island (Acocella and Funiciello, 1999), while aspect ratios of ~ 0.4 are associated with the formation of a resurgent dome as observed

at the CFc (Acocella et al., 2001). Resurgent calderas in particular are associated with vent eruptions along the ring-fracture zone (Lipman, 1984) and, as analogue models have shown, with extrusion along radial fractures occurring on the crest of the resurgent dome (Acocella et al., 2001). Such post-caldera volcanism can involve the formation of lavas, domes, tuff or cinder cones, maars and tuff rings.

Besides the widely accepted concept that large-scale caldera-forming eruptions have a severe effect on the global climate (e.g. Bray, 1977; Robock, 2000; Williams et al., 2009; Fitzsimmons et al., 2013), it has also frequently been suggested that climatic changes such as sea-level and ice-load variations may initiate explosive volcanic eruptions (e.g. Rampino et al., 1979; Hall, 1982; McGuire et al., 1997; Mason et al., 2004; Albino et al., 2010).

1.2.3 Pyroclastic density currents (PDCs) and ignimbrite deposits

Caldera-forming eruptions are generally accompanied by PDCs, which are considered to be the most devastating and hazardous products of caldera eruptions. These hot, high-velocity (>200 m/s), ground-hugging flows can travel distances of >100 km, covering large areas of up to $20,000$ km² (Druitt, 1998). Their associated deposits are referred to as ignimbrites, which may have a volume of several thousands of cubic kilometres and emplace at a temperature of ~ 200 - 600°C (Brown and Andrews, 2015; Neri et al., 2015b).

Essentially, PDCs are gravity-driven flows containing a hot mixture of a fluid phase (gas) and pyroclastic particles such as ash, lapilli, and blocks (Druitt and Sparks, 1984). PDCs consist of a dense underflow that moves in direct contact with the ground and a buoyant so-called co-ignimbrite ash plume. The term PDC encompasses two end-members: (1) dilute suspension currents called *pyroclastic surges* and (2) highly concentrated *pyroclastic flows* (Burgisser and Bergantz, 2002). During explosive caldera-forming eruptions, PDCs are generated when the bulk density of the pyroclastic jet exiting the vent exceeds that of the atmosphere, leading to a collapse of the eruption column (Fig. 1.5-B, C) (Brown and Andrews, 2015). Smaller-volume PDCs can be generated by other eruption processes such as lateral explosions of hot material, dome collapse, and so-called boiling-over eruptions (i.e. low column collapse) (Dufek et al., 2015).

The flow direction of PDCs is strongly influenced by the underlying topography. Preferentially, they move along valleys and fill topographic depressions. However, large-scale, high-velocity PDCs can pass over topographic highs and may also travel large distances over water (Cas and Wright, 1991; Brown and Andrews, 2015). The thickness of the associated ignimbrite deposits is generally highest in depressions (up to hundreds of meters) and thins towards elevated areas (only a few centimetres). The thick, valley-filling ignimbrites are often massive, poorly-sorted deposits, while the coeval thinner

deposits tend to be stratified better-sorted (Branney and Kokelaar, 2001; Brown and Andrews, 2015).

Submarine ignimbrites

The behaviour of PDCs when entering the sea, for instance in the case of an eruption close to the shoreline, is still poorly understood (Cas and Wright, 1991; Legros and Druitt, 2000). In historical times, several observations of PDCs entering the sea and travelling several kilometres under water have been made for instance during the Montagne Pelée eruption in 1902, the Montserrat eruption in 1996 and also during the Krakatau eruption in 1883 (Legros and Druitt, 2000 and references therein). However, in total only about 30 cases of submarine PDCs are known, implying that only few PDCs make it to shore, that a large portion is being eroded on shallow submarine environment, or that many cases have not yet been documented (Cas and Wright, 1991). Generally, it has been assumed that PDCs transform into secondary water-supported mass-flows upon entering a marine environment. According to this assumption, most submarine PDC deposits are by definition no ignimbrites but rather mass-wasting deposits consisting of pyroclastic material. Primary PDC deposits, meaning that they were emplaced in a hot state, are assumed to only occur in shallow marine environments (Cas and Wright, 1991). However, numerical models have shown that PDCs exceeding a volume of 10 km³ are capable of pushing back the shoreline by a few kilometres and potentially even more in areas of extensive shallow water, thereby causing instantaneous regression and allowing for a hot emplacement of the ignimbrite. Hence, large-scale submarine PDC deposits in shallow water environment may represent (primary) ignimbrite deposits (Legros and Druitt, 2000).

1.3 Regional Setting

The Campanian Plain is a structural depression situated along the Campania Margin in southern Italy (Figs. 1.6, 1.8). It developed within the overall context of back-arc extensional tectonism related to retreating subduction within the Africa–European convergence zone. It is bounded to the East by the Apenninic Mountain range and to the West by the Tyrrhenian Sea, the youngest of the Mediterranean basins (Fig. 1.6). Two active volcanic complexes are located in the Neapolitan area in the Campanian Plain. One of them being the Somma-Vesuvius stratovolcano, consisting of an older volcano, the Mt. Somma, and a recent cone, the Vesuvius, and the other one being the Campi Flegrei Volcanic Zone (CVZ), which includes the volcanic fields of the Campi Flegrei (also termed *Phlegraean Fields*), Procida and Ischia islands, as well as a number of submerged vents located in the Gulf of Naples and Gulf of Pozzuoli (Fig. 1.8).

1.3.1 Formation of the Tyrrhenian Sea

The Tyrrhenian Sea has undergone lithospheric stretching and crustal thinning since the Late Miocene (~10 Ma) and is commonly regarded as a back-arc basin (Fig. 1.7) (Malinverno and Ryan, 1986; Kastens et al., 1988; Dewey et al., 1989; Gueguen et al., 1998). A widely accepted explanation for the formation of the Tyrrhenian Sea implies that the hinge of the subducting African Plate migrates away from the overriding Eurasian Plate due to the fact that the motion in the overriding plate does not compensate for the retreat of the subduction zone (Malinverno and Ryan, 1986). This results in a SE rollback of the Apennine thrust front and, thus, in a counter-clockwise rotation of the Italian peninsula, which eventually led to the opening of the Tyrrhenian Sea (Fig. 1.7) (Malinverno and Ryan, 1986; Lavecchia, 1988; Malinverno, 2012). Consequently, extension occurs in the Eurasian Plate (Tyrrhenian Sea domain) while, simultaneously, the Apennine domain in the East undergoes compressional deformation. Due to a larger retreat of the subducted hinge in the South compared to the North, the southern part of the Tyrrhenian Sea has undergone a larger amount of extension (Turco et al., 2006). Therefore, the Tyrrhenian basin can be subdivided into two different domains: the northern part, characterized by a thinned and rifted continental crust, and the southern domain, which is in parts floored by oceanic crust (Fig. 1.7-C). The boundary of the two domains is marked by a major E-W trending fault system, known as the 41st parallel line (Figs. 1.6, 1.7-C). The central plain (>3,000 m water depth) of the Tyrrhenian Sea, located south of the 41st parallel line can be divided into two sub-basins: the older Vavilov basin in the West, where the oceanic crust formed during the Late Miocene and Early Pliocene (Fig. 1.7-B), and the younger Marsili Basin in the South-

East, where oceanic crust formed during the earliest Pleistocene (Fig. 1.7-C) (Kastens et al., 1988; Casciello et al., 2006).

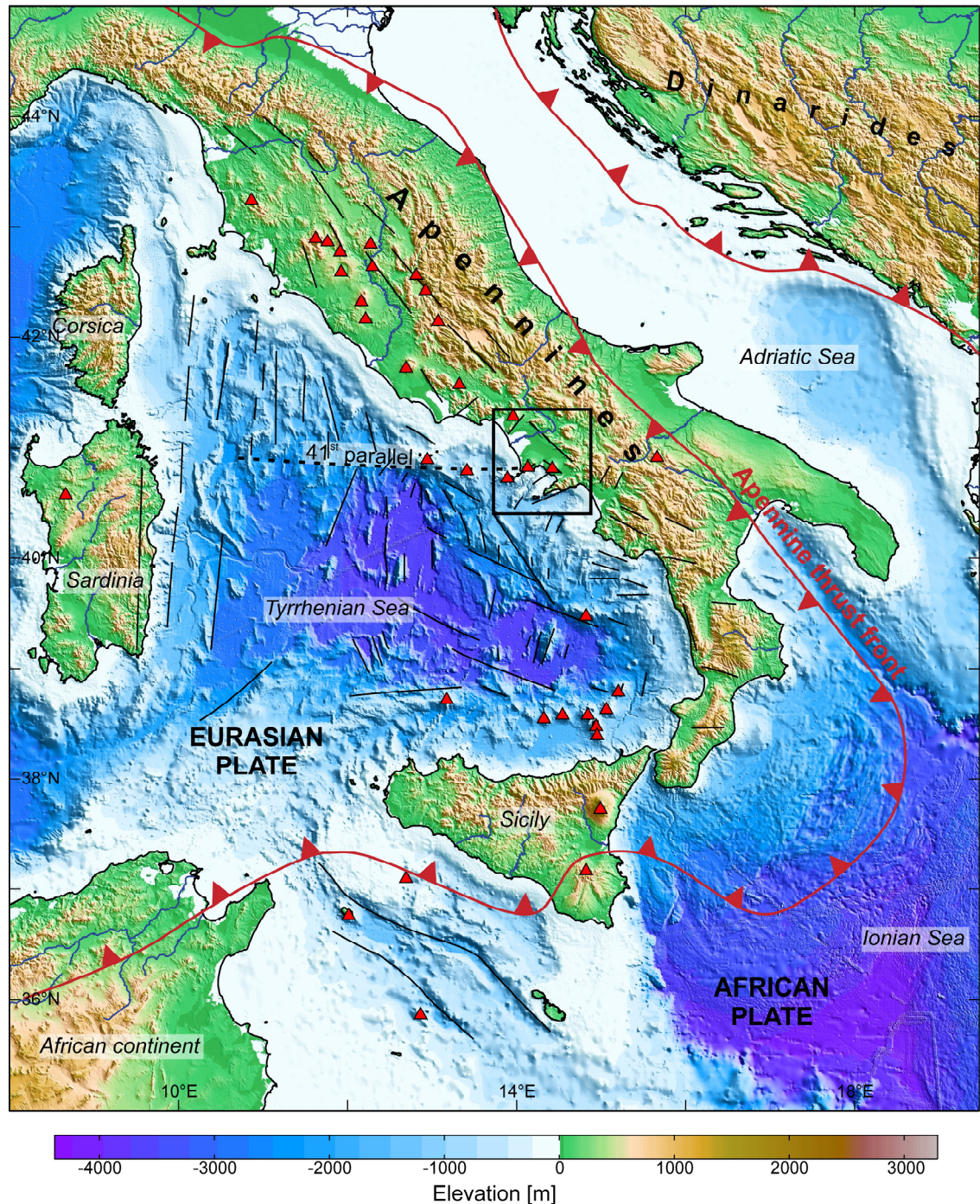


Fig. 1.6: Overview map of the Tyrrhenian Sea and southern Italy with the African-Eurasian subduction zone indicated in dark red. Topography and bathymetry is a 15-arc-seconds grid obtained from the *Shuttle Radar Topographic Mission* © United States Geological Survey (Becker et al., 2009). Red triangles mark major Italian volcanoes (Crosweller et al., 2012). Black solid lines indicate normal faults, simplified and redrawn from Turco et al. (2006) and Boccaletti et al. (1984). Black square indicates the location of Fig. 1.8, which shows a close-up of the Campanian Margin.

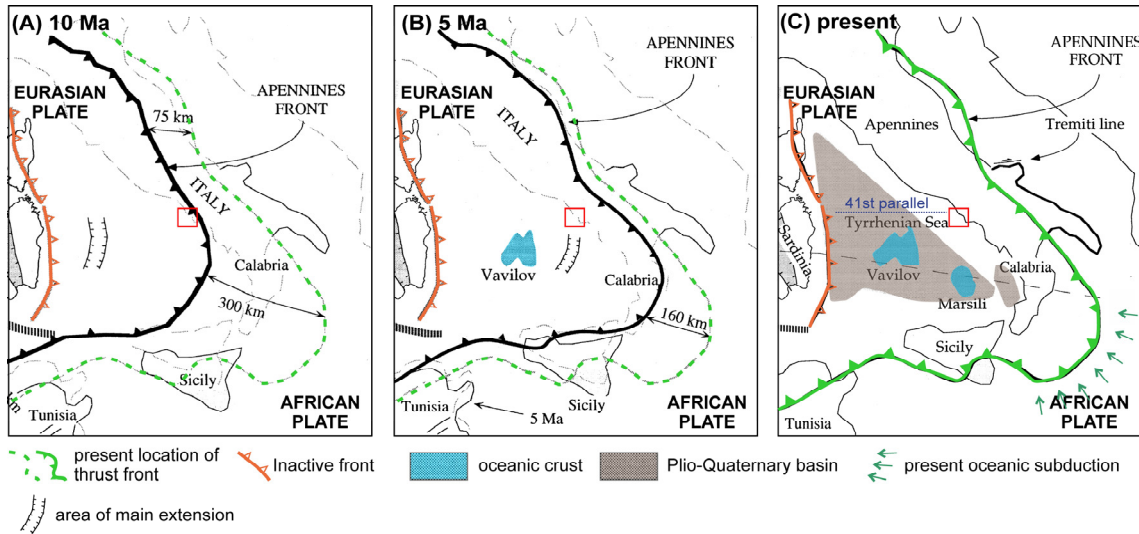


Fig. 1.7: Paleo-tectonic reconstruction of the Tyrrhenian Sea back-arc basin evolution from the Late Miocene to present. Red square indicates the location of the working area (i.e. Gulf of Naples); thick black line indicates location of the African-Eurasian subduction zone at the respective time (modified from Gueguen et al. (1998)).

The early stage (from Late Miocene to Pliocene) of the back-arc extensional tectonism in the Tyrrhenian Sea was characterized by the formation of N-S and NNW-SSE trending normal faults (Trincardi and Zitellini, 1987). During the Pliocene and Quaternary, NW-SE, NE-SW and E-W faults were active along the Tyrrhenian Sea margin (Milia et al., 2013) (Fig. 1.6).

1.3.2 The Campanian Margin

The morphology of the Campanian Margin has primarily been affected by Plio-Quaternary NW-SE and NE-SW trending normal faults displacing the Mesozoic carbonate basement, which was formed around the open Tethys Ocean. The carbonate platform consists mainly of shallow-water limestones and dolomites and is widely exposed in the Apennines and along the Campania Margin (Bernoulli and Jenkyns, 1974). As a consequence of the NW-SE and NE-SW faulting, Plio-Quaternary extensional basins parallel to the Apenninic chain were formed. The Campanian Plain and the Gulf of Naples are representatives of these structural depressions bordered by NW-SE and NE-SW trending normal faults (Fig. 1.8) and filled with a thousands of meters-thick sequence of Plio-Quaternary clastic and volcanoclastic deposits (Piochi et al., 2005; Acocella and Funiciello, 2006; Milia et al., 2013). A detailed overview of the tectonic evolution of the Gulf of Naples is provided in Chapter 3.

Apart from numerous normal faults, the Campanian margin also displays other typical features of a back-arc setting such as a very shallow Moho, high heat flow values, high-amplitude magnetic anomalies and large-volume ignimbritic eruptions (Kastens et al., 1988 and references therein).



Fig. 1.8: Overview map of the Campania Margin, southern Italy (for large-scale map see Figure 1.6). Topography is a 1-arc-seconds grid from the *Shuttle Radar Topographic Mission* © United States Geological Survey. Bathymetry represents a merged grid consisting of (1) a 20x20 m grid in the Gulf of Naples area (D'Argenio et al., 2004a) and (2) a 15-arc-seconds grid in the Bay of Salerno and Gulf of Gaeta areas obtained from the *Shuttle Radar Topographic Mission* © United States Geological Survey (Becker et al., 2009). Solid red lines indicate major normal faults as redrawn from Bruno et al. (2003), Turco et al. (2006), Milia et al. (2013) with MS fault = Magnaghi-Sebeto fault. Black dots indicate location of submerged vents in the CVZ. Blue dashed circle indicates approximate location of the CFC.

1.3.3 Volcanism in the Campanian Plain

Volcanism in the Campanian Plain started at about 0.5 Ma in the northernmost area at the currently extinct Roccamonfina volcano (Fig. 1.8) and migrated further SE to the Neapolitan area during Plio-Pleistocene times (Croweller et al., 2012). Here, volcanic activity has been most severe since ~150 ka (Fig. 1.9). All volcanic centres (i.e. Somma-

Vesuvius, Ischia Island, Campi Flegrei), except Procida Island, show clear evidence of recent activity as indicated by ongoing earthquakes or fumarolic activity (Paoletti et al., 2013).

The Plio-Quaternary volcanism along the Campania margin is strongly controlled by NE-SW and NW-SE trending structural faults (Fig. 1.8) that developed in the course of back-arc extensional tectonism (Bruno et al., 2003; Piochi et al., 2005; Acocella and Funiciello, 2006). The area SE of the Magnaghi-Sebeto fault with the Somma-Vesuvius is mainly characterized by NE-SW trending fractures, whereas the sector NW of the Magnaghi-Sebeto fault, including the CVZ, shows a more complex fault pattern with both NE-SW and NW-SE trending fractures (Fig. 1.8) (Bruno et al., 2003). Please see Chapter 3 for a detailed discussion on the interaction between tectonism and volcanism in the CVZ and at the Somma-Vesuvius. The volcanological history of each of the main volcanic centres is described in detail below.



Fig. 1.9: Summary of the Quaternary eruption history in the Campanian Plain with major caldera-forming events indicated. (Compiled based on ages from Civetta et al., 1991; Di Vito et al., 1999; Brocchini et al., 2001; De Vivo et al., 2001; Santacroce et al., 2003; De Astis et al., 2004; Brown et al., 2008; Cioni et al., 2008; Paoletti et al., 2013).

Campi Flegrei

The Campi Flegrei area has been volcanically active since at least 60 ka (Rosi et al., 1983; Pappalardo et al., 1999). However, in the Campania Plain, older ignimbrite deposits have been recognized, suggesting earlier explosive activity potentially originating from the Campi Flegrei area at ~205, ~184 and ~157 ka (Fig. 1.9) (De Vivo et al., 2001). The majority of volcanism in the Campi Flegrei area was of an explosive nature, depositing complex pyroclastic sequences. Only few effusive units (i.e. lava flows or lava domes) were recognized (Di Vito et al., 1999).

The most pronounced volcanic feature in the Campi Flegrei area is the ~13.5-km wide quasi-circular Campi Flegrei caldera (CFc), located partly onshore, partly offshore (Figs. 1.8, 1.10). This nested-caldera complex was probably formed by two large-scale ignimbritic eruptions: the Campanian Ignimbrite (CI) eruption at ~39 ka, and the Neapolitan Yellow Tuff (NYT) eruption at ~15 (please see Chapter 4 for further

discussion on the formation of the CFc) (e.g. Rosi et al., 1983; Barberi et al., 1991; Orsi et al., 1996; De Vivo et al., 2001; Deino et al., 2004).

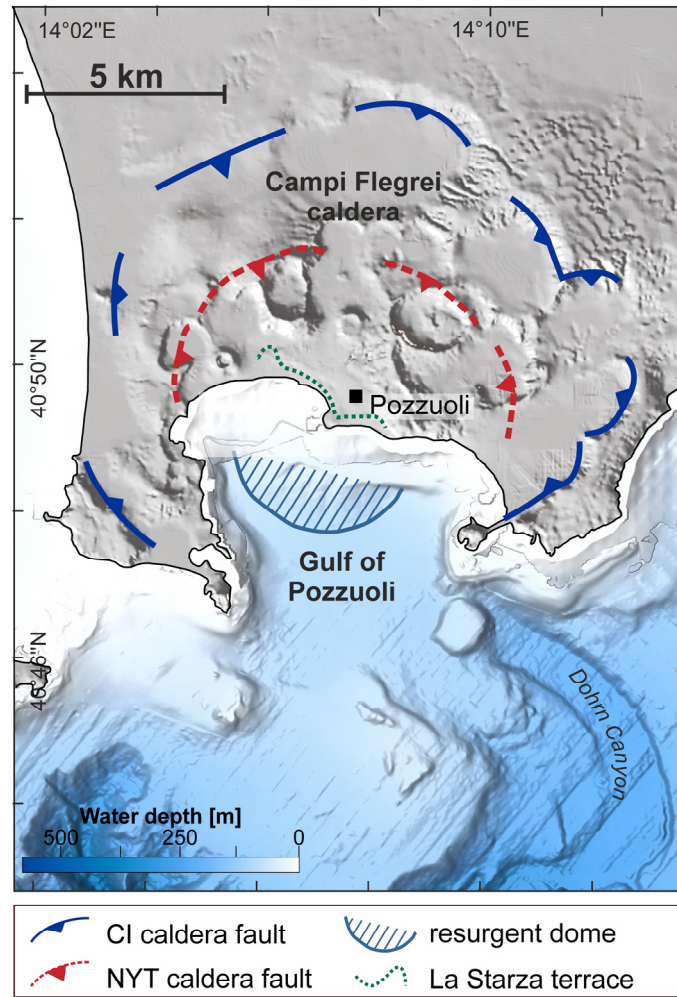


Fig. 1.10: Bathymetric and topographic map of the CFc. Onshore location of the caldera margins, La Starza terrace and the offshore resurgent dome is redrawn from Acocella (2008) and (Sacchi et al., 2014).

Prior to the caldera formation, between 60 and 39 ka, at least eleven explosive and five effusive eruptions occurred. Between the CI and NYT eruption, not less than nine explosive eruptions took place and remnants of ten volcanic edifices were identified (Orsi et al., 2004).

The largest explosive eruption in the whole Neapolitan area was that of the CI at ~39 ka with a total erupted volume of 310 km³ (equivalent to 200 km³ DRE) (Fig. 1.2) (Rolandi et al., 2003). It is regarded as Europe's largest volcanic event of the past 200,000 years. The massive ignimbrite deposits of this eruption cover ~7,000 km² and were also identified offshore (Fusi et al., 1991; Milia et al., 2003). Its ash was dispersed over a distance of more than 2,500 km, extending as far as to the Russian Plain (Pyle et al., 2006). Furthermore, it has been hypothesised that the CI eruption could have caused a volcanic winter, coinciding with the extremely cold Heinrich Event 4 (Pyle et al., 2006;

Costa et al., 2012; Fitzsimmons et al., 2013). This combined environmental forcing might have significantly impacted the ecosystem at that time, potentially even forcing the Late-Pleistocene transition from Neanderthals to “modern” *Homo sapiens* (Fedele et al., 2002, 2013).

The NYT eruption at ~15 ka was the second largest event of the Neapolitan area with ~79 km³ (equivalent to 40 km³ DRE) of emitted volume covering an area of more than 1,000 km² (Scarpati et al., 1993). The climatic effect of the NYT eruption has not been discussed in literature. However, as its erupted volume is approximately equivalent to that of the devastating Tambora eruption (Fig. 1.2), a similar global climatic impact seems probable.

In the post-caldera phase, particularly the onshore topography of the CFc was strongly modified by at least 60 post-collapse eruptions mainly clustered within three volcanic epochs, at 15-9.5 ka (epoch I), 8.6-8.2 ka (epoch II) and 4.8-3.7 ka (epoch III) (please see Chapter 5 for further discussion on the post-caldera phase) (Di Vito et al., 1999; Di Renzo et al., 2011). The most recent eruption occurred at AD 1538, leading to the formation of the 130-m-high cone of Monte Nuovo (Di Vito et al., 1987).

In the course of post-collapse caldera resurgence, a broad resurgent dome has developed in the central part of the Gulf of Pozzuoli (Fig. 1.10) (Sacchi et al., 2014). Onshore, caldera resurgence resulted in the emersion of a previously submarine sector, the so-called *La Starza terrace*, which is presently located at 30 to 55 m above sea level (Fig. 1.10) (Di Vito et al., 1999).

Since the 1960s, the CFc has shown increased post-collapse activity as demonstrated by repeated bradyseism events (i.e., vertical ground movement), generally accompanied by seismicity with shallow earthquakes at max. ~3-4 km depth (De Natale et al., 1991; De Natale et al., 2006; Troise et al., 2008), and increased fumarolic activity (Chiodini et al., 2015). In the town of Pozzuoli, a net uplift of 3.8 ± 0.2 m was generated during two main episodes of rapid short-term uplift between 1969–1972 and 1982–1984 (Del Gaudio et al., 2010). The causes of such uplift phases are still a matter of debate and may be attributed to either hydrothermal (Orsi et al., 1999; Chiodini et al., 2003; Acocella, 2010; Chiodini et al., 2015) or magmatic (Dvorak and Berrino, 1991; D’Auria et al., 2015) processes. For instance, a recent study suggested that the injection of magmatic fluids into a shallow hydrothermal system at ~2 km depth could be a potential trigger (Chiodini et al., 2015). However, another recent publication proposed that the unrest phases may be linked to the emplacement of a magma batch at shallow depth of ~3 km, thereby supporting the theory of a magmatic driving force (D’Auria et al., 2015). Understanding the source of the short-term uplift episodes is of crucial importance and still a missing link in order to reliably assess volcanic hazards and risks. While a magmatic source could be interpreted

as potential eruption precursor, a hydrothermal source would have less severe hazard implications.

Somma-Vesuvius

The Somma-Vesuvius is a central-type volcanic complex consisting of the older Mt. Somma and the Vesuvius volcanic edifices. The formation of the Mt. Somma was mainly related to effusive volcanism (i.e. the generation of lava flows). The oldest lava flows were dated at ~ 0.4 and 0.3 Ma. Between 0.3 Ma and the CI eruption at 39 ka, the Vesuvian area was characterized by volcanic quiescence (Brocchini et al., 2001). The period between 39 and 20 ka was mainly marked by effusive activity at Mt. Somma. At ~ 18 ka, the effusive volcanism changed into explosive activity with the large *Pomici di Base* eruption leading to the first caldera formation at Mt. Somma (Fig. 1.9). Afterwards, at least three additional caldera-forming events related to Plinian eruptions occurred at Mt. Somma, with the *Mercato Pumice* eruption at 8 ka, the *Avellino* eruption at 3.9 ka, and the *Pompeii* eruption at AD 79 (Fig. 1.9) (Santacroce et al., 2003; Cioni et al., 2008). The caldera-forming eruptions were interrupted by smaller, mainly explosive events. The Vesuvius cone began to grow after the AD 79 eruption, characterized by both effusive and explosive eruptions, as well as a minor summit caldera collapse. The last eruption took place in 1944, associated with relatively mild explosive volcanism (Cioni et al., 2008).

Ischia and Procida Islands

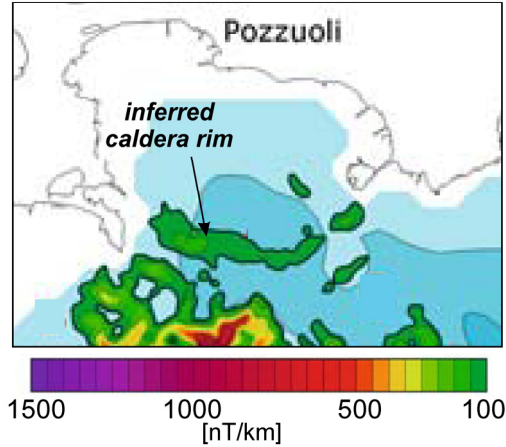
The onset of volcanic activity on Ischia Island is still not precisely known. The oldest dated volcanic deposits revealed an age of ~ 150 ka. However, these dated outcrops are underlain by older (not yet dated) volcanic remnants of a complex volcanic edifice, probably formed by older explosive eruptions (Santacroce et al., 2003). The Ischia volcanic activity can be grouped into four phases: (1) >150 ka; (2) 150 - 33 ka, (3) 28 - 18 ka and (4) 10 ka–AD 1302 (with minor volcanic quiescence between 4.3 and 2.9 ka) (Fig. 1.9) (Civetta et al., 1991; Brown et al., 2008; Paoletti et al., 2013). The Ischia caldera was formed at ~ 55 ka during the *Mount Epomeo Green Tuff* eruption. In the post-caldera phase, between 55 and 33 ka, further major ignimbrites were emplaced (e.g. *Citara Tuff*). The western-central part of the Ischia caldera has been uplifted by ~ 900 m due to block resurgence, which was initiated between 33 and 28 ka (Tibaldi and Vezzoli, 1998; Santacroce et al., 2003).

Procida Island hosts five monogenetic volcanoes (Vivara, Terra Murata, Pozzo Vecchio, Fiumicello and Solchiaro) which have been active between 70 and 14 ka producing pyroclastic deposits and one lava dome (Fig. 1.9) (De Astis et al., 2004).

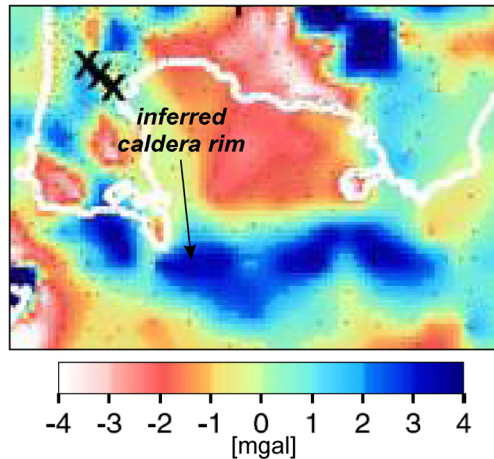
1.3.4 Existing data from the Campi Flegrei caldera

Traditionally, the CFc was investigated based on geological field observations and/or borehole data (e.g. Rosi et al., 1983; Orsi et al., 1996; Di Vito et al., 1999), which allow

(A) horizontal derivative of magnetic data
(modified from: Secomandi et al., 2003)



(B) Residual Bouguer anomaly
(modified from: Capuano and Achauer, 2003)



(C) P-wave velocity at a depth of 1125 m
(modified from: Zollo et al., 2003)

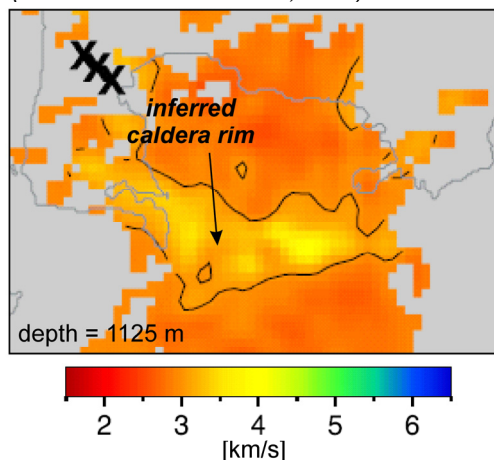


Fig. 1.11: Geophysical evidence for the offshore location of the Campi Flegrei caldera rim in the Gulf of Pozzuoli.

only for selective and, thus, spatially limited insights into the complex caldera system. For instance, Piochi et al. (2013) carried out a systematic reanalysis of four deep onshore exploration wells (80 - 3,050 m deep) drilled by AGIP and SAFEN since the 1940s. Their results showed the complex and inhomogeneous structure of the onshore sector of the CFc and suggested the existence of persistent magma storage at 4-5 km depth, a long-term reservoir at ~8 km depth, shallow intrusions, hydrothermal aquifers and fluid circulation. However, their interpretation left many uncertainties as indicated by the fact that the borehole stratigraphy could not be connected in a reasonable way.

On the basis of geophysical studies such as seismic refraction tomography (e.g. Zollo et al., 2003; Judenherc and Zollo, 2004), gravity (e.g. Florio et al., 1999; Capuano and Achauer, 2003; Capuano et al., 2013) or magnetic (e.g. Florio et al., 1999; Secomandi et al., 2003; Aiello et al., 2005) measurements, the approximate location of the caldera depression and margin could be outlined (Fig. 1.11). For instance, Zollo et al. (2003) reconstructed the offshore caldera structure based on a P-wave velocity model derived from deep tomographic observations. They assumed that the caldera filling is characterized by P-wave velocities of less than 3 km/s, which led them to conclude that the caldera filling has a thickness of ~2 km. In contrast to the caldera filling, the

caldera's morphological edge (caldera margin) is characterized by high P-wave velocities (3.5-4 km/s) probably due to magmatic intrusions (Fig. 1.11-C). Furthermore, the margin can be distinguished by residual Bouguer anomalies (e.g. Capuano and Achauer, 2003) and magnetic anomalies (Secomandi et al., 2003) (Figs. 1.11-A, -B). However, even though such geophysical methods provided good spatial coverage, they were limited by their low resolution.

More recently, several very high-resolution single-channel data were acquired in the Gulf of Pozzuoli (e.g. Milia and Torrente, 2000; D'Argenio et al., 2004; Sacchi et al., 2014) using sparker or uniboom sources with frequencies in the range of kHz. These datasets were limited by their low penetration of a few ten to typically less than 200 m below seafloor. Moreover, many of the previously published single-channel very high-frequency datasets only exist on paper due to analogue recording and, consequently, the imaging quality could not be enhanced by modern processing procedures. Low-frequency and, thus, deeper-penetrating seismic data were mostly acquired in the Gulf of Naples (Fusi, 1996; Milia and Torrente, 1999; Bruno et al., 2003) and are lacking in the offshore sector of the CFc. One deep penetrating multichannel low-resolution seismic line (max. vertical resolution 10 m, signal penetration ~ 1.3 s TWT) crossing over the submerged CFc depression was presented by Milia and Torrente (2007). They interpreted the seismic section in comparison with an onshore geothermal deep borehole as a cyclic sequence of well-layered and chaotic units identified as volcanic deposits. However, the resolution and quality of this seismic line was insufficient to determine details about the internal structure and seismic facies. The lack of high-quality data from the CFc underlines the significance of this thesis.

1.4 Thesis outline

Chapter 1 provides a general introduction into the scientific background and research questions including information on caldera research field, the geological background of the working area, as well as the aims and objectives of this thesis. In Chapter 2, the method of multichannel seismic data acquisition and processing as applied in this thesis is described in detail. Chapters 3 to 5 represent the main body of the thesis in standalone research manuscript format, as outlined in detail below. Chapter 6 provides an overarching conclusion and outlook for further research.

Chapter 3 (*Tectono-sedimentary evolution of the Gulf of Naples half-graben basin (Italy) in interaction with volcanism during the last one million years*) discusses the interaction between regional tectonism, volcanism, and sedimentary deposition in the Gulf of Naples half-graben basin based on a recently acquired multi-frequency multichannel seismic dataset. In particular, the linkage between fault activity and Quaternary volcanism is investigated. The main findings are presented in a novel 3D model outlining the spatial and temporal evolution of the Gulf of Naples half-graben basin during the past one million years.

Chapter 4 (*The Campi Flegrei caldera (Italy): formation and evolution in interplay with sea-level variations since the Campanian Ignimbrite eruption at 39 ka*) addresses the genesis and evolution of the Campi Flegrei caldera during the past 39 ka based on selected high-resolution multichannel seismic profiles from the R/V URANIA research cruise in 2008. This study provides novel evidence for the existence of a nested caldera complex formed by the Campanian Ignimbrite and the Neapolitan Yellow Tuff eruptions at 39 and 15 ka, respectively. The main scientific outcome is a comprehensive conceptual model outlining the formation and evolution of the Campi Flegrei nested-caldera complex in interplay with sea-level fluctuation.

Chapter 5 (*Post-collapse evolution of the Campi Flegrei caldera since the Neapolitan Yellow Tuff eruption at 15 ka: Insights from a 2.5D multichannel seismic survey*) discusses the post-collapse phase of the Campi Flegrei caldera since the NYT eruption at 15 ka. Based on an integrated analysis of a 2.5D grid of high-resolution multichannel seismic data and borehole data from literature, an extensive 3D model illustrating the post-collapse temporal evolution of the Campi Flegrei caldera was developed.

1.5 Declaration of co-author contributions

This cumulative thesis comprises an introductory chapter (Chapter 1) and a methodology chapter (Chapter 2) followed by three joint-authorship manuscripts that shall be published as peer-reviewed articles. The manuscripts were developed in close cooperation with the co-authors. This section provides information on the individual contributions of each co-author to the individual manuscripts and the current manuscript status.

Chapter 3: *Tectono-sedimentary evolution of the Gulf of Naples half-graben basin (Italy) in interaction with volcanism during the last one million years*

Authors: Lena Steinmann, Volkhard Spiess and Marco Sacchi

Status: to be submitted to *Geo-Marine Letters*

The seismic datasets (GeoB08, GeoB16, NAM) utilized in this study originate from in total three research cruises to the Gulf of Naples. The GeoB08 dataset was acquired on the R/V URANIA in 2008, during which the co-author Marco Sacchi was chief scientist and the co-author Volkhard Spiess was mainly responsible for the multichannel seismic data acquisition. The GeoB16 data are from a recent cruise on the R/V MINERVA in 2016. All three authors participated in this cruise: Marco Sacchi was chief scientist, while Volkhard Spiess and I were responsible for the multichannel seismic data acquisition. The processed NAM dataset was provided by Marco Sacchi and initially acquired by the *Institute for Coastal Marine Environment of the National Research Council (IAMC-CNR)* (Naples, Italy) in 1996. I confirm that I processed all utilized GeoB seismic data, carried out the interpretation of all utilized data, developed the scientific concept, created all figures/tables and wrote all sections of the manuscript. The overall scientific concept benefitted greatly from regular discussions with Volkhard Spiess. (*Personal contribution: 90%*)

Chapter 4: *The Campi Flegrei caldera (Italy): formation and evolution in interplay with sea-level variations since the Campanian Ignimbrite eruption at 39 ka*

Authors: Lena Steinmann, Volkhard Spiess and Marco Sacchi

Status: submitted to *Journal of Volcanology and Geothermal Research*

The utilized multichannel seismic data (GeoB08) were acquired during a research cruise on the R/V URANIA in 2008. During this expedition, the co-author Marco Sacchi was chief scientist and the co-author Volkhard Spiess was responsible for the multichannel seismic data acquisition. I confirm that I processed and interpreted all utilized multichannel seismic data, developed the scientific concept, created all figures/tables and wrote all sections of the manuscript. The development of the overall idea was a flowing process, which greatly benefited from practical advice and regular discussions with the

co-authors Volkhard Spiess and Marco Sacchi. Furthermore, they made significant intellectual contributions and reviewed the manuscript before submission. (*Personal contribution: 90%*)

Chapter 5: *Post-collapse evolution of the Campi Flegrei caldera since the Neapolitan Yellow Tuff eruption at 15 ka: Insights from a 2.5D multichannel seismic survey*

Authors: Lena Steinmann, Volkhard Spiess and Marco Sacchi

Status: to be submitted to *Bulletin of Volcanology*

The utilized multichannel seismic data (GeoB08) were acquired during a research cruise on the R/V URANIA in 2008. During this expedition, the co-author Marco Sacchi was chief scientist and the co-author Volkhard Spiess was responsible for the multichannel seismic data acquisition. I confirm that I processed and interpreted all utilized multichannel seismic data, developed the scientific concept, created all figures/tables and wrote all sections of the manuscript. The development of the overall idea was a flowing process, which greatly benefited from regular discussions with the co-authors Volkhard Spiess and Marco Sacchi. (*Personal contribution: 90%*).

Chapter 2

2 Data and Methods

The multichannel seismic data used in this thesis were acquired during two joint Italian-German research expeditions in 2008 (CAFE-7/3 – GeoB08) and 2016 (CAFE_2015 – GeoB16) on the R/V URANIA und R/V MINERVA UNO, respectively (Fig. 2.1). Data acquisition was carried out using the multichannel seismic system of the Department of Geosciences at the University of Bremen (Germany) in different configurations. An additional multichannel seismic dataset (NAM) was utilized for Chapter 3 (Fig. 2.1). This dataset was processed and provided by the *Institute for Coastal Marine Environment of the National Research Council* (IAMC-CNR) (Italy).

2.1 CAFE-7/3 – GeoB08

During the CAFE-7/3 cruise on the R/V URANIA in the Gulf of Naples and Gulf of Pozzuoli in January 2008, 146 multichannel seismic profiles with a total length of ~1,500 km were collected (Fig. 2.1-A). 50 of these are part of a N-S trending semi-3D (i.e. 2.5D) grid crossing over the offshore sector of the Campi Flegrei caldera in the Gulf of Pozzuoli (Fig. 2.1-A). The average lateral profile spacing of the semi-3D grid was 120-150 m.

Two seismic sources were deployed and shot alternatingly: (1) a Soderia GI-Gun with 2x1.7 L chamber volume and a frequency range of approximately 30-500 Hz and (2) a Soderia Mini-GI-Gun with reduced chamber volume of 2x0.1 L producing high frequencies of up to 1000 Hz. Both GI-Guns were towed at ~1.5 m water depth, controlled by small buoys. In order to archive a reasonable shot rate, guns were operated with only ~90 bar air pressure in contrast to typical air pressure of ~150 bar. The general 20 second-long shooting cycle established during the CAFE-7/3 expedition is illustrated in Table 2.1. Typically, the 1.7 L GI-Gun was shot every 20th second, intermitted by 8 shots at every 2nd second of the 0.1 L GI-Gun.

The signal penetration of both sources achieved a maximum of 0.6 s (0.1 L Mini-GI-Gun) and 1.0 s (1.7 L GI-Gun) in the sedimentary succession within the Gulf of Naples half-graben basin. However, in the offshore sector of the Campi Flegrei caldera, where volcanoclastic rocks are abundant, the signal was strongly attenuated and, thus, only a lower penetration of ~0.25 s was achieved for both guns.

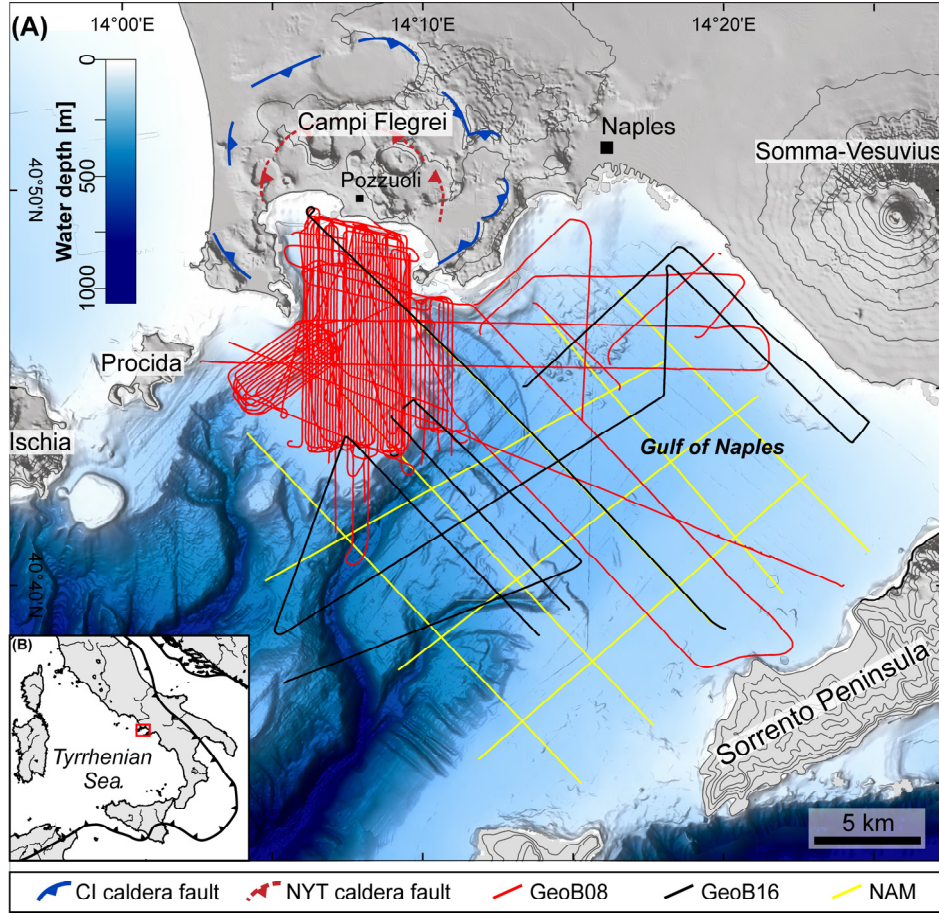


Fig. 2.1: Overview map of the working area in the Gulf of Naples and the acquired multichannel seismic datasets as utilized in this thesis. (A) Topography and bathymetry of the Campi Flegrei volcanic area and the Gulf of Naples with the track chart of the processed and interpreted multichannel seismic data (MCS). Red (GeoB08): MCS from CAFE-7/3; black (GeoB16): MCS from CAFE_2015 (for a map of all acquired lines please refer to Chapter 6, Figure 6.1); yellow (NAM): processed data provided by IAMC-CNR. (B) Red square shows the location of (A) in southern Italy.

In the framework of this thesis, mainly the data from the 0.1 L Mini-GI-Gun were used in order to achieve maximum seismic resolution (vertical resolution ~ 2 m) (Chapter 3-5). Only a few selected profiles acquired with the 1.7 L GI-Gun were utilized to for deeper imaging of the sedimentary fill of the Gulf of Naples half graben (Chapter 3).

Table 2.1: Commonly used trigger scheme during CAFE-7/3 expedition.

	Shot time [s] →														
1.7 L GI	0									0 (20)				0 (40)	
0.1 L GI		4	6	8	10	12	14	16	18		4 (24)	...		4 (44)	...
seismograms	1	2		3		4		5							
	Cycle 1 (20 sec)									Cycle 2			Cycle 3		

During the CAFE-7/3 cruise, two seismic streamers were deployed simultaneously: (1) an especially for shallow water custom-designed streamer of 50 m length, hosting 48 single-

hydrophone channels with a spacing of 1 m and (2) a conventional streamer with an active length of 100 m and 16 hydrophone groups located at 6.25 m intervals, which was intentionally deployed for imaging the deep-seated caldera architecture. In the scope of this thesis, mainly the data recorded with the 48-channel streamer are presented (Chapter 2-5) since it turned out that the proposed deeper imaging of the caldera structure could not be realized with the 16-channel streamer due to high attenuation. However, in the sedimentary succession of the Gulf of Naples half-graben, a high penetration depth was achieved and, thus, the 1.7 L GI gun in combination with the 16-channel streamer were utilized for spatial mapping in Chapter 3.

A custom digital seismograph, the *Marine Multichannel Seismics* (MaMuCS; © Hanno Keil), was used for data recording. The recording length was set to 3 seconds and the sample rate to 125 μ s. Two shots of the 0.1 L GI-Gun were recorded in one seismogram starting at 0 and 2000 ms, respectively. The shots of the 1.7 L GI-Gun were recorded in an individual seismogram starting at 0 ms. Furthermore, both streamers were recorded in the same seismogram. The raw seismic data were stored in the standard SEG-Y format.

2.2 CAFE_2015 – GeoB16

The CAFE_2015 cruise was initially scheduled for November 2015 on the R/V URANIA, hence the choice of name. However, due to a tragic accident of the R/V URANIA, the expedition had to be rescheduled to January/February 2016 and moved to the R/V MINERVA UNO. During the 15-days seismic survey, 278 profiles were acquired with a total length of ~2,400 km. However, only 11 profiles were utilized in the framework of this thesis (Fig. 2.1-A).

During the CAFE_2015 cruise, two seismic sources were deployed: (1) a Sodera GI-Gun with 4.1/1.7 L chamber volume towed at 7-8 m water depth and a frequency range of approximately 5-200 Hz and (2) a Sodera Mini-GI-Gun with reduced chamber volume of 2x0.1 L producing high frequencies of up to 1000 Hz and towed at ~1.5 m water depth.

Within the scope of this thesis, 10 Mini-GI-Gun profiles were used and only one regional profile with the GI-Gun as source. These profiles build the foundation of Chapter 3. The maximum signal penetration in the sedimentary succession within the Gulf of Naples half-graben was ~1.05 s and 1.6 s for the Mini-GI and GI-Gun, respectively. During the acquisition of the 0.1 L Mini-GI-Gun profiles utilized in this thesis, the 4.1 L GI-Gun was not deployed and, hence, a high shot rate of 3 s could be achieved while maintaining high air pressure of ~150 bar. The recording length was set to 2.5 s. The high shot rate provides good data coverage along the profile and, thus, allows for the implementation of a small bin size (1x5 m) during processing (i.e. high horizontal resolution). However, during most profiles, the two sources were shot alternating and recorded in one

seismogram with the 4.1 L GI-Gun starting at 0 s and the Mini-GI-Gun starting at 6 s at a recording length of 8 s. The according shooting cycle is illustrated in Table 2.1.

Table 2.2: Commonly used trigger scheme during CAFE_2015 expedition when both guns were deployed.

	Shot time [s] →											
4.1 L GI	0		15		30		45		0 (60)			0 (120)
0.1 L GI		6		21		36		51		6 (66)	...	4 (126)
seismograms	1		2		3		4					
	Cycle 1 (60 sec)						Cycle 2			Cycle 3		

The seismic signal was recorded using a custom-designed 96-channel streamer (224 m active length) with a broad bandwidth (3-1000 Hz). This streamer has varying channel spacing as illustrated in Figure 2.2. For recording, the MaMuCS software was used. The sample rate was set to 125 μ s and the raw seismic data were stored in the standard SEG-Y format.

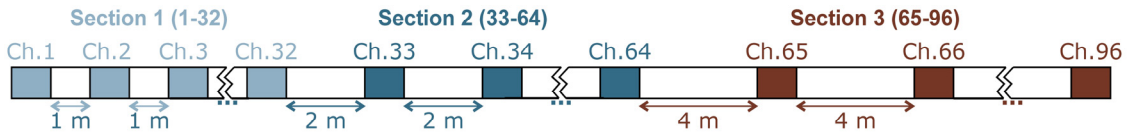


Fig. 2.2: Illustration of the acquisition geometry of the 96-channel streamer during the CAFE_2015 expedition. Channels 1 – 32 have a spacing of 1 m, channels 33-64 have a spacing of 2 m, and channels 65 – 96 have a spacing of 4 m.

2.3 Multichannel seismic data processing

Seismic data processing aims at enhancing the image quality of geological structures in the seismic section in order to facilitate a reliable and convenient interpretation. This is achieved by increasing the signal-to-noise ratio and migrating seismic events to their true subsurface positions. Consequently, the seismic resolution, describable as the ability to distinguish between two closely spaced events, either spatially or temporally, is improved. Acoustic noise can be classified into two different categories: (1) incoherent noise and (2) coherent noise. Incoherent noise comprises noise in the temporal direction and random noise which is uncorrelated from trace to trace. The coherent noise category includes linear noise such as guided waves and ground roll, reverberations and multiples (Yilmaz, 2001). Coherent noise can be treated with trace editing or frequency filtering. In multichannel seismic processing, incoherent noise can significantly be suppressed by stacking all the signals reflected from a mutual point at the seafloor or in the subsurface. This processing step substantially increases the quality of multichannel seismic data compared to single-channel seismic data.

Seismic data processing procedures and results are strongly influenced by acquisition parameters. For instance, data quality is significantly impacted by weather conditions during acquisition, human misconduct during recording, and the condition of the utilized equipment. Furthermore, physical properties of the geological objectives, such as fluid saturation, porosity, permeability, and viscosity, influence the image quality by causing energy scattering and absorption, resulting in signal attenuation.

In this thesis, multichannel seismic data processing was accomplished with the *VISTA 2D/3D Seismic Processing 12* software program, henceforth referred to as VISTA. The geometry set-up was carried out using the custom program *WinGeoapp 0.9.8* (© Hanno Keil) develop in the working group *Marine Technology – Environmental Research* at the Department of Geosciences at the University of Bremen. The processing routine for the profiles from both cruises comprised geometry setup, trace editing, bandpass filtering, residual statics corrections, normal move-out correction, multiple suppression, Common Midpoint (CMP) binning and stacking, noise attenuation and time migration as schematically illustrated in Figure 2.3.

Below, a detailed description of the processing routine of the Mini-GI gun datasets is provided. If not indicated otherwise, the described processing steps were carried out for both, the GeoB08 and GeoB16, datasets. However, it should be noted that the processing of the GeoB08 dataset required several individual steps due to its complicated acquisition set-up and some unusual trigger problems.

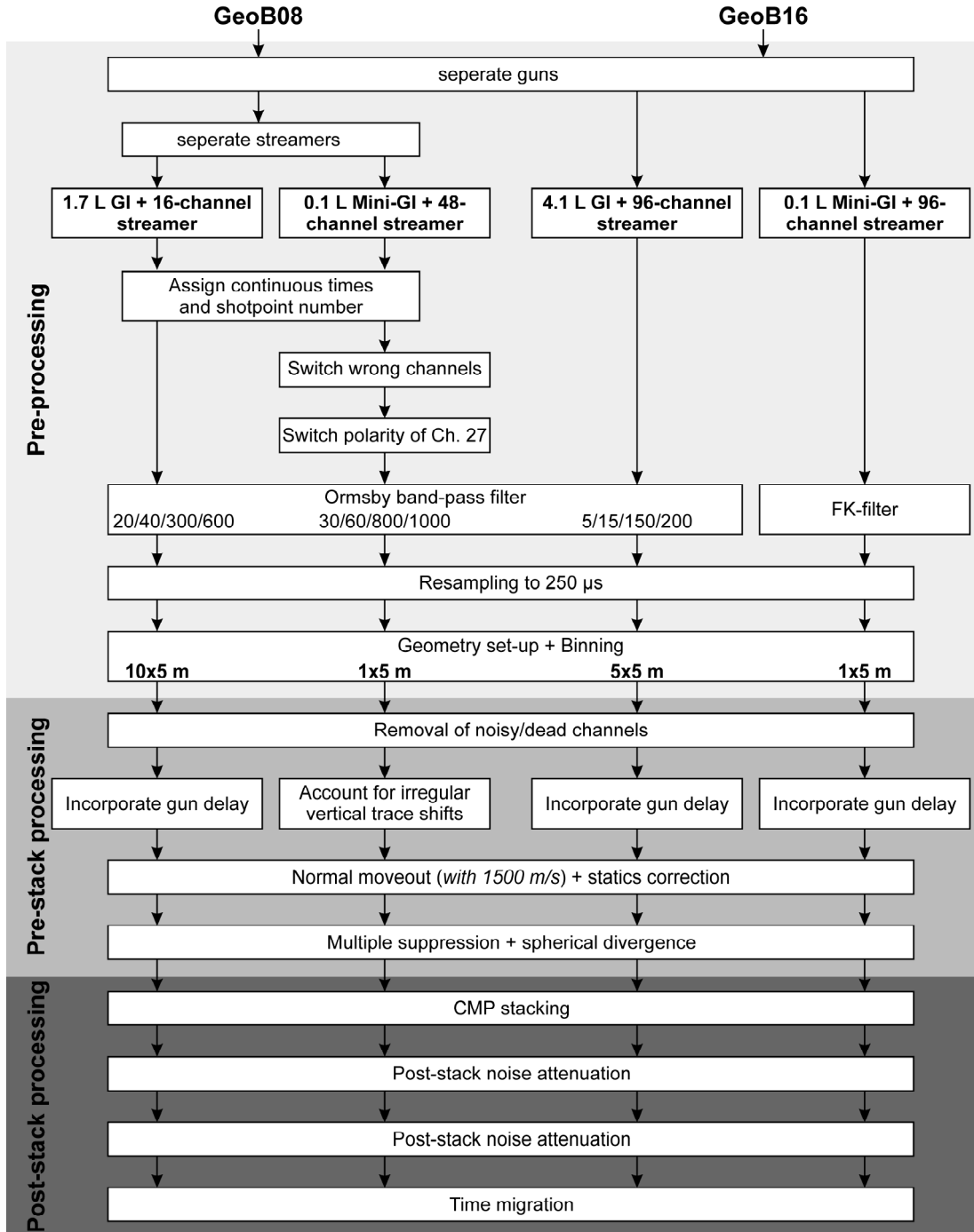


Fig. 2.3: General seismic data processing as applied to the four utilized datasets.

2.3.1 Pre-Processing

Prior geometry set-up, GeoB08 data underwent an elaborate pre-processing due to simultaneous deployment and recording of two streamers and GI-Guns (Fig. 2.4). As consequence, the data had to be split vertically and horizontally to extract datasets each with only one specific gun and streamer. Furthermore, channel 41 of the 48-channel streamer was incorrectly recorded as channel 64, which led to a successive shift of the channels in the seismogram (Fig. 2.5-A). Hence, the wrong channel number assignment

had to be corrected in order to guarantee for a correct geometry set-up and subsequent calculation of source-receiver offsets (Fig. 2.5-B). Finally, four independent datasets were generated during this separation process: (1) 0.1 L GI-Gun + 48 channel streamer, (2) 0.1 L GI-Gun + 16 channel streamer, (3) 1.7 L GI-Gun + 48 channel streamer, and (4) 1.7 L GI-Gun + 16 channel streamer (Fig. 2.3). This thesis focuses on the dataset that was shot with the 0.1 L GI-Gun and recorded with the 48-channel streamer. Thus, the processing of the remaining three datasets will not be discussed further; however, it is summarized in Figure 2.3.

The 0.1 L GI-Gun + 48 channel streamer dataset had to be assigned with new floating shot point numbers and continuous shot times, depending on their trigger scheme. Furthermore, the polarity of channel 27 had to be reversed due to incorrect recording.

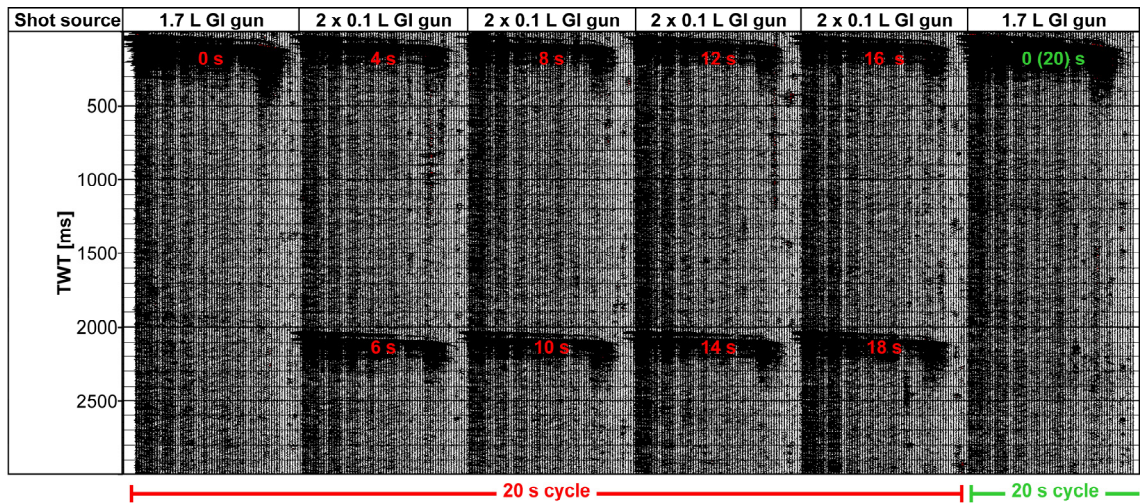


Fig. 2.4: Exemplary illustration of the recording scheme during CAFE-7/3 cruise (GeoB08 data) from profile GeoB08-050. The recorded seismogram has a total length of 3 s. Indicated in red is the timing of one shot cycle consisting of 1 shot of the 1.7 L GI-Gun (at 0 s) followed by 8 shots of the 0.1 L GI-Gun (4 – 18 s). The next cycle (green) starts again with one shot of the 1.7 L GI-Gun (0 (20) s).

Afterwards, a wide Butterworth band-pass filter with filter flanks of 30/60/800/1000 was applied to suppress low and high frequency noise. The GeoB16 Mini-GI-Gun data were filtered with an FK-Filter instead of a Butterworth. After filtering, resampling was conducted to reduce the data volume and to decrease the calculation time of subsequent processing stages. The data were resampled from the original sampling interval of 125 μ s to 250 μ s, which corresponds to a Nyquist frequency of 2,000 Hz. The frequencies produced with the 0.1 L GI-gun are below 1,000 Hz, hence, the Nyquist theorem is satisfied and signal loss due to resampling is prevented.

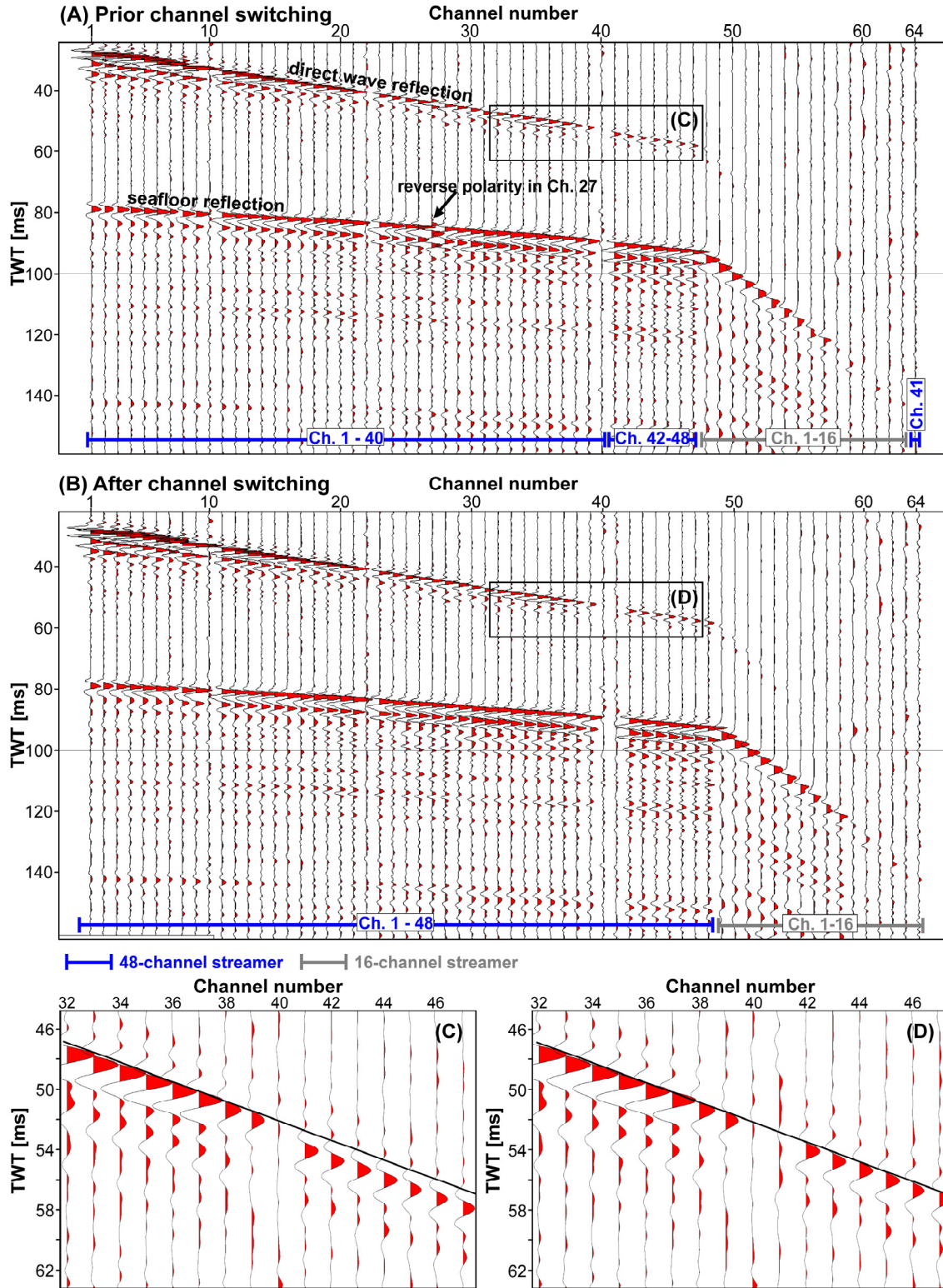


Fig. 2.5: Shot gather of shot 5693 of profile GeoB08-050 (CAFE-7/3), illustrating the incorrect channel recording (A) and the result of the required channel switching (B). An Ormsby band-pass filter (40/80/600/800) was applied for better visualization and the channels are shown equidistant. The close-up (C) shows the vertical displacement of the direct wave reflection due to the missing channel. Close-up (D) shows the result after implementing the channel switching processing step.

2.3.2 Geometry set-up and CMP sorting

The multichannel seismic data were acquired in shot-receiver coordinates commonly referred to as *shot gather* (Fig. 2.6-A). However, multichannel seismic data processing is

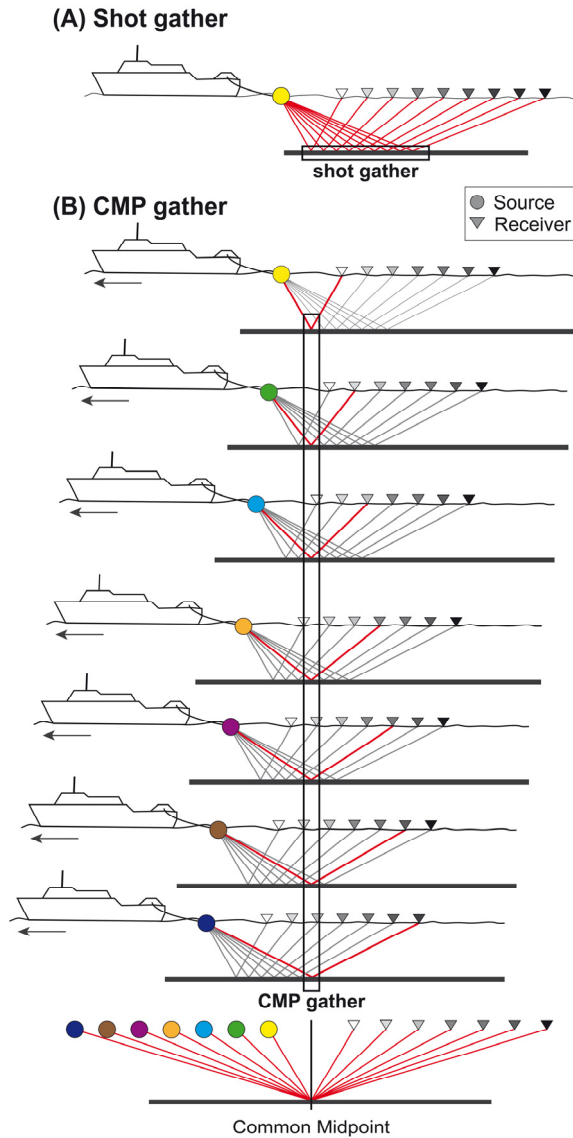


Fig. 2.6: Illustration of (A) shot gather and (B) CMP gather.

conventionally carried out in midpoint-offset coordinates, i.e. *common midpoint (CMP) gather* (Fig. 2.6-B). In order to conduct a CMP gather sorting, shot-receiver midpoints were calculated. The required information about the geographical coordinated of each shot and receiver position were assigned using the software Wingeoapp, which incorporates data from the ship's navigation as well as source and receiver geometry relative to the GPS antenna. The acquisition geometry was obtained from the decks plan that documents the position of the individual equipment relative to each other.

For the subsequent CMP sorting, bins were created. All midpoints located in an individual bin were assigned to the same CMP gather. A bin size of 1 x 5 m in across and along track direction, respectively, was chosen as best compromise between high lateral resolution and sufficient improvement of the signal-to-noise ratio. The average fold of the GeoB08 and GeoB16 datasets is 9 and 14, respectively.

2.3.3 Trace editing

First, noisy channels were removed from the dataset in order to increase the subsequent stacking quality. Then, the gun delay had to be incorporated. Additionally, it turned out that irregular vertical shifts with significant trace displacement of up to 3.5 ms occur from shot to shot in the 0.1 L GI-Gun GeoB08 data (Fig. 2.7-A). As these shifts were not present in the simultaneously acquired 1.7 L GI gun data and also due to their

constantly high amplitude even during fair weather conditions, wave interaction could be ruled out as possible source. Instead, these shifts might be the result of electronic failures of the trigger system, or they are present due to the fact that the gun was operated at low level of air pressure.

These irregular vertical TWT shifts have dramatic influence on the stacking quality and, thus, had to be corrected during processing. To achieve the best possible result, time-consuming interactive processing was applied since the available statics correction modules of the VISTA software did not solve this problem. In detail, the direct wave was picked by using the first break picking algorithm provided by VISTA. Afterwards, the arrival time of the direct wave picks were subtracted from the data using VISTA's *static shift* tool, thereby flattening the dataset. To achieve the best result, this step had to be repeated on the flattened dataset.

Afterwards, the flattening had to be inverted as prerequisite for the subsequent processing steps. Therefore, the individual source-receiver offsets in meters had to be converted to TWT and then they were added to the flattened dataset. The result of this processing step in a receiver gather is exemplarily shown in Figure 2.7. The improvement is clearly visible in the direct wave and seafloor reflection, which lost their artificial irregular character.

2.3.4 Normal moveout (NMO) and statics correction

In a CMP gather, the reflection arrival times as function of the source-receiver offset follow hyperbolic trajectories. The difference between the two-way traveltimes at zero offset and at any other offset is termed normal moveout (NMO) Δt_{NMO} (Fig. 2.8).

For stacking, the normal moveout must be removed, which is achieved with the NMO correction. This is a dynamic correction, meaning that far offsets are shifted more than near offsets, results in a stretching of the data and an artificial increase of the wavelength for larger offsets (i.e., *moveout stretch*) (Fig. 2.8). However, as result of the short streamer, the offsets of the GeoB08 data were relatively small (max. offset of 62 m), thus, the hyperbolic relationship between shot-receiver offset and traveltime delay was not very pronounced. In the GeoB16 dataset, the offsets were larger (max. offset of ~235 m), however, even in this case, the moveout stretch phenomenon had only subordinate effect on the data. Hence, there was no need to account for this effect during processing.

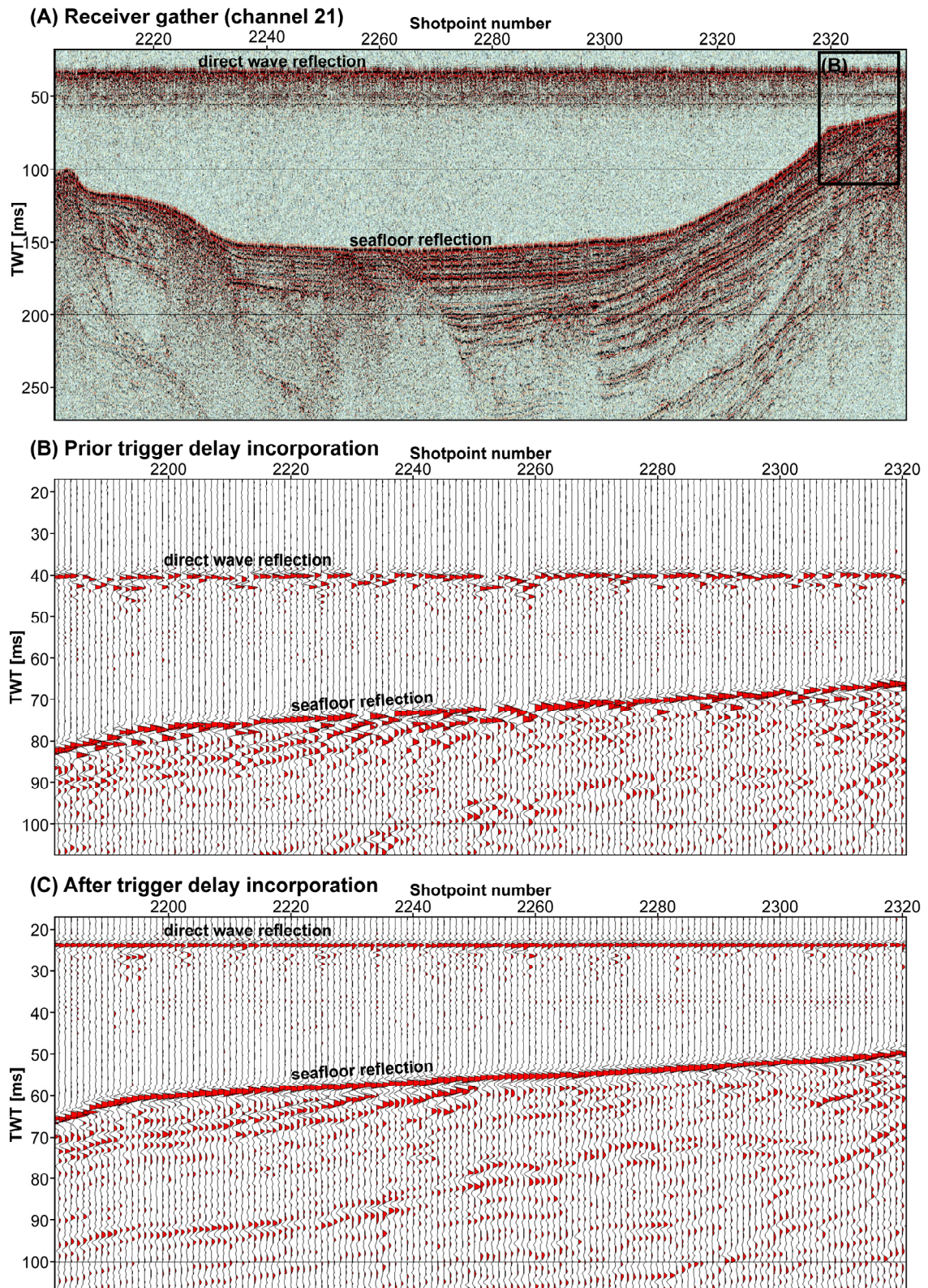


Fig. 2.7: Receiver gather (channel 21) of profile GeoB08-050, illustrating the effect of the irregular vertical shift on the data. (A) shows the uncorrected receiver gather in variable density. (B) shows a close-up of the uncorrected receiver gather and (C) shows the corrected receiver gather.

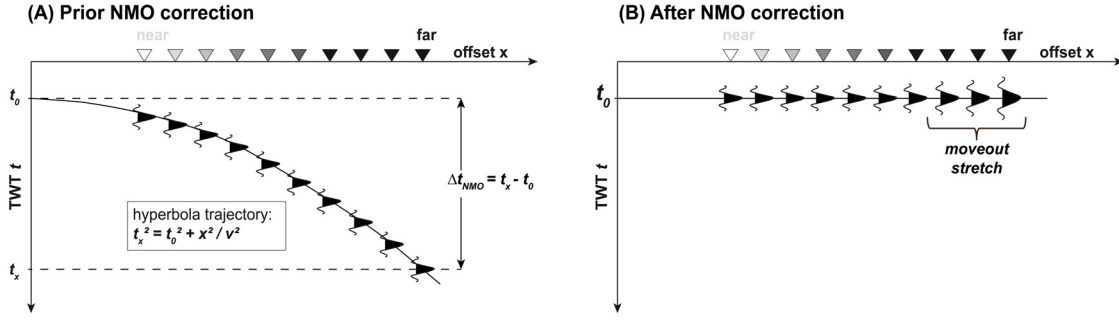


Fig. 2.8: The hyperbolic two-way travelttime (TWT) difference (normal moveout) with increasing offset is shown bottom right. TWT is a function of the source-receiver offset as with $t = \text{TWT}$; $t_0 = \text{zero offset two-way travelttime}$; $x = \text{source-receiver offset}$ and $v = \text{velocity of medium above the reflection}$.

Typically, an interactive velocity analysis would be carried out prior NMO correction in order to determine the vertical and horizontal variability of the acoustic wave velocities in the seismic section. However, it turned out that – due to the acquisition geometry – an NMO correction with a constant velocity of 1500 m/s provided excellent results. Therefore, the time-consuming velocity analysis was made superfluous, allowing for the processing of a large number of seismic profiles in reasonable time.

On the NMO-corrected CMP gather, a residual statics correction was applied using the VISTA tool *MCorrel*. This processing step compensates for vertical streamer movement in the water column due to waves, thus, improving the stacking quality.

2.3.5 Multiple suppression and spherical divergence

Generally, it is assumed that primary reflections are unpredictable while multiples are regarded as predictable or periodic component of a seismic trace. The predictive deconvolution was utilized to predict and suppress a significant part of this periodic multiple energy from the seismogram, which masked primary reflections (Fig. 2.9-A). The operator length was typically set to a value between 20 and 60 ms and the operator taper was set to half of the operator length. 1 % was the commonly used value for pre-whitening. As prediction lag, the first-break of the seafloor reflection was picked and used as input. The predictive deconvolution was applied to an unstacked, NMO-corrected dataset. The result of the multiple attenuation using the predictive deconvolution is shown in Figure 2.9.

Afterwards, the data underwent an inverse NMO correction in order to apply a spherical divergence correction. This is essentially a gain correction to enhance the signal of deeper-lying primary and weaker far-offset reflections by compensating for amplitude decays as function of time due to square law spherical spreading. This step was applied subsequent to multiple suppression in order to increase the signal of the reflections that were previously masked by multiples. Following that, the dataset was once more NMO corrected using a constant velocity of 1500 m/s.

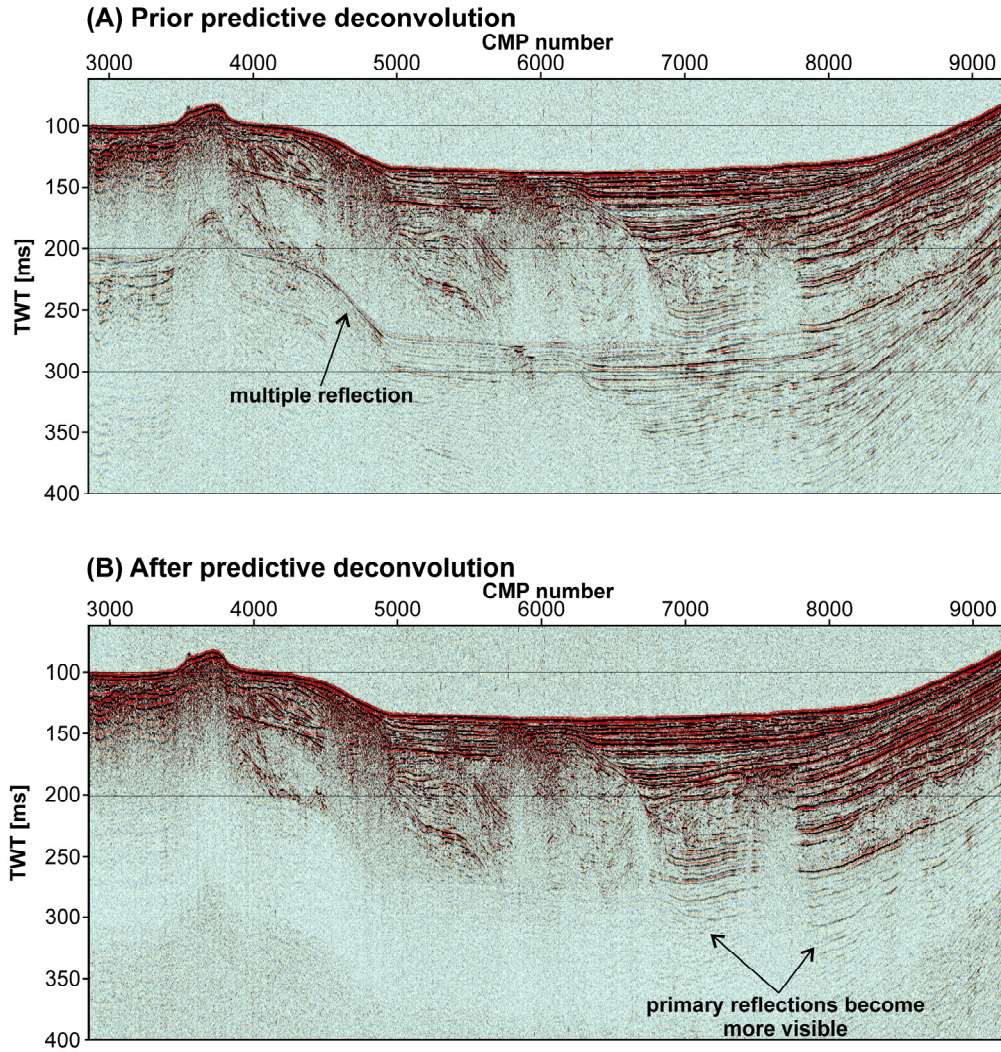


Fig. 2.9: CMP stack of profile GeB08-050 (CAFE-7/3). (A) CMP stack without predictive deconvolution, containing multiples. (B) CMP stack after predictive deconvolution, when a significant amount of multiple energy was removed.

2.3.6 CMP stacking

Finally, all traces in each CMP gather of the NMO-corrected dataset were summed up (i.e., *stacked*) over the offset axis, creating a CMP stack. The main goal of the CMP stacking is to summate the acoustic energy in order to enhance seismic events and suppress random noise, thereby improving the signal-to-noise ratio. Moreover, the stacking process substantially reduces data volume by creating a compressed zero-offset seismic section.

2.3.7 Post-stack noise attenuation

In order to further attenuate random noise and enhance signal quality in the stacked section, the so-called *4D-DEC* and *ThresAB VISTA* tools were applied. The 4D-DEC

algorithm removes random noise from the seismic section by cross-correlating energy peaks in adjacent traces within small overlapping windows of time and space. If an energy peak does not correspond to a continuous reflection, it is being suppressed. The final product is a noise attenuated model dataset. However, since random noise preserves amplitude in noisy patches, wherever noise is being removed, the remaining seismic signal is weak.

The ThresAB algorithm compares the enhanced model dataset created with the 4D-DEC tool and to the original seismic section. In this process, a noise-to-signal ratio is being computed assuming that the model represents the main signal. If this ratio exceeds a manually set threshold, then the signal component of the original trace is increased and the noise signal is decreased. Otherwise, the trace is left untouched. The main advantage of this procedure is that the seismic signal can be enhanced wherever needed and only to a desired level. Overall, this processing step considerably enhanced the signal-to-noise ratio of the seismic data (Fig. 2.10) and was, thus, applied to all seismic profiles, despite the fact that it was rather time-consuming due to long computation time. However, it should also be noted that as accompanying effect this processing step slightly enhanced the multiple reflection.

2.3.8 Time migration

During the processing step CMP sorting, it is assumed that all traces within one CMP gather resemble the midpoint between source and receiver. Since this assumption would only apply to an unrealistic geological setting with exclusively horizontal bedding, dipping reflections appear displaced into up-dip direction. In particular, a complex geology with for instance anticlines and synclines appear as so-called *bow ties* (i.e., concave-upward reflections). Furthermore, diffraction hyperbolas may occur along edges of abruptly ending or discontinuous reflection (e.g. along faults).

The objective of seismic data migration is to correct these displacements and make the stacked section resemble the actual geological cross-section in order to guarantee for a reliable interpretation. This is achieved by moving dipping events from their apparent location into their true subsurface position and collapsing diffraction hyperbolas, thereby increasing the spatial resolution.

Here, a finite-difference (FD) migration was applied (Fig. 2.11). This 2D post-stack time migration algorithm uses the principles of downward continuation of the wavefield at finite depth intervals, based on a steep-dip approximation to the wave equation (Yilmaz, 2001). The FD migration was applied using a constant velocity model of 1500 m/s, a finite depth interval (i.e., *tau step*) of 1 ms, a taper pad value of 50 traces and a filtered 45-65 degrees solution.

The advantage of the FD migration compared to other time migration algorithms is the fact that it is very robust to errors in the velocity model. This makes it particularly suitable for the here presented application since only a constant velocity model was used.

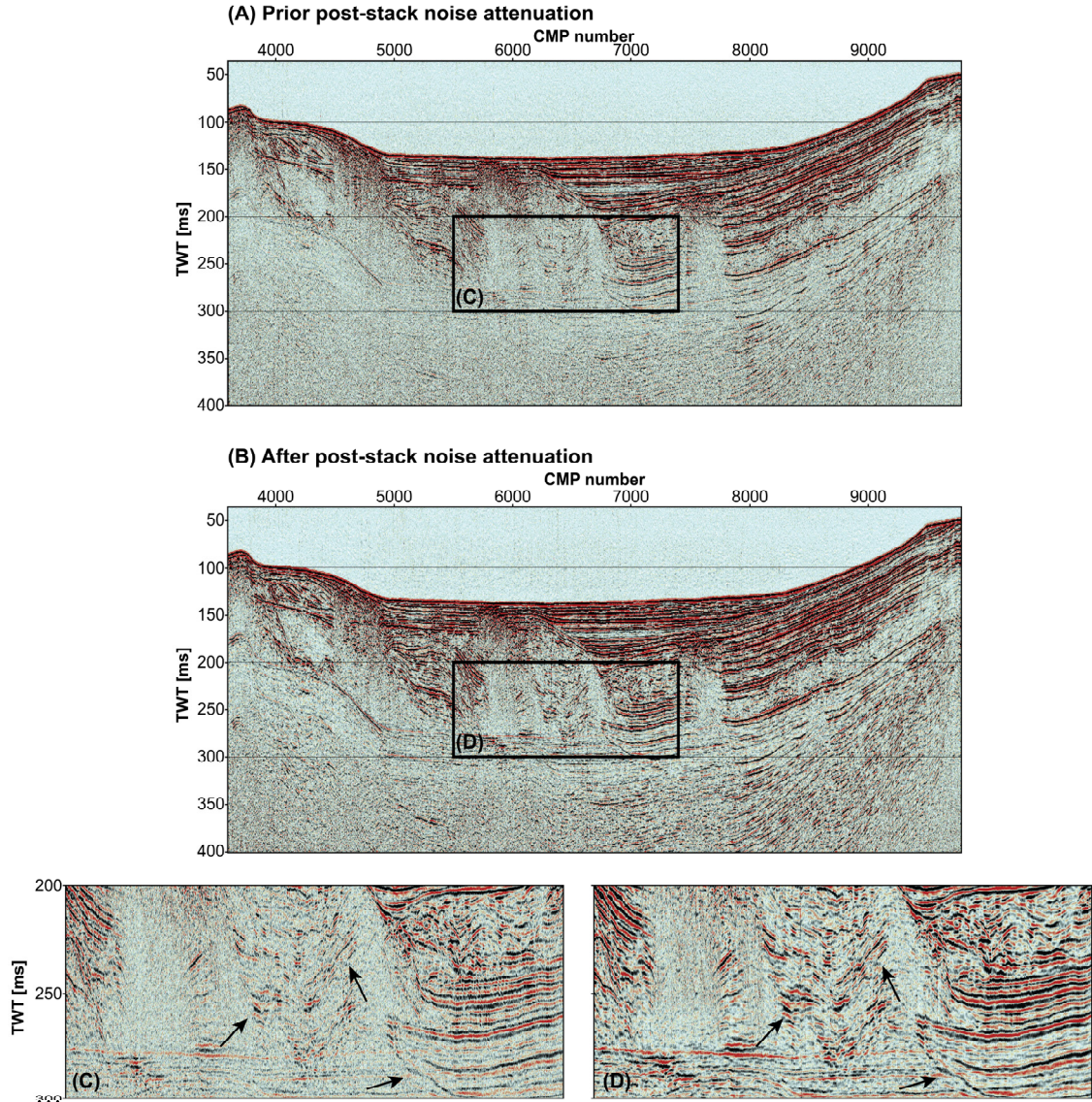


Fig. 2.10: Stack of profile GeoB08-050 (CAFE-7/3), illustrating the effect of post-stack noise attenuation using the VISTA 4D-Dec and ThresAb modules on the dataset. (A) and (C) Prior post-stack noise attenuation. (B) and (D) After post-stack noise attenuation. Arrows highlight areas where the effect of the noise attenuation is particularly visible.

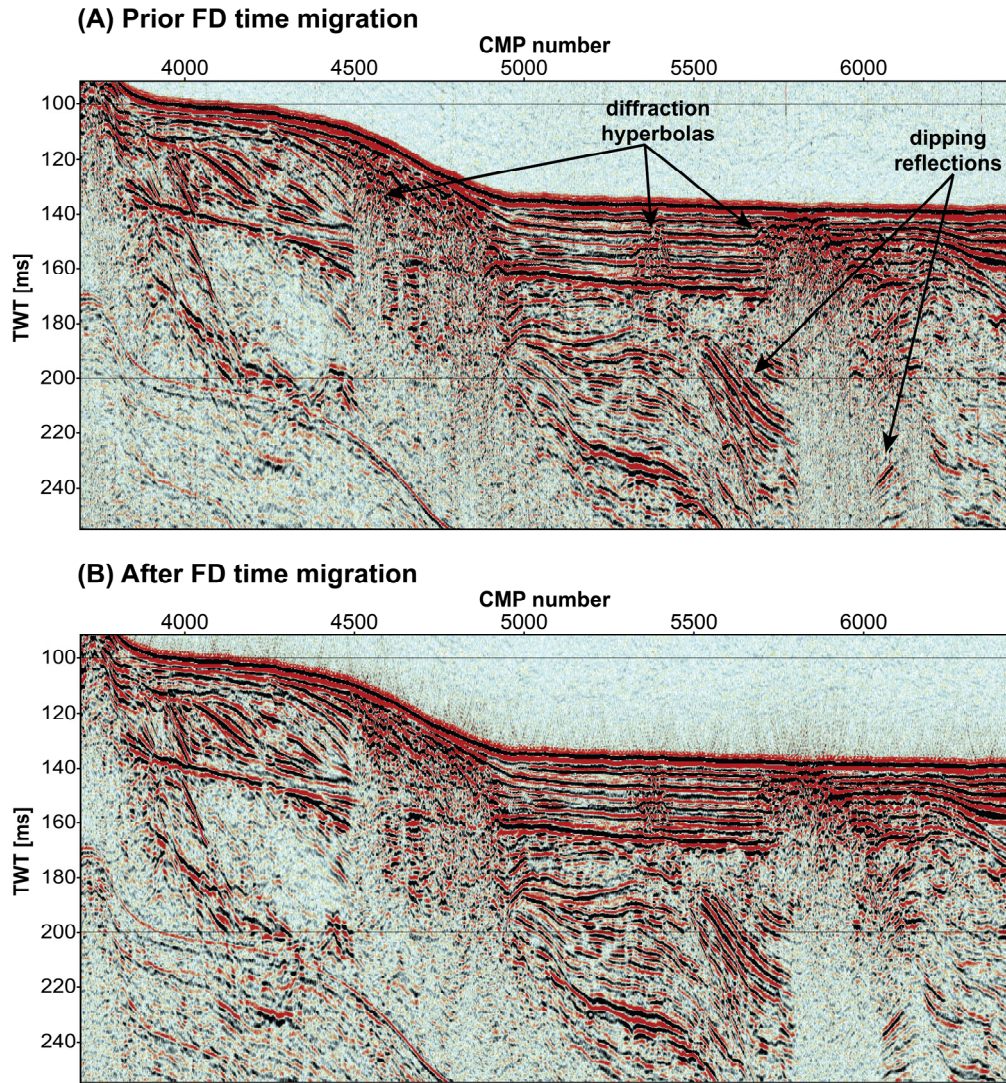


Fig. 2.11: Close-up of the stacked (A) and migrated (B) profile GeoB08-050 (CAFE-7/3), illustrating the effect of the FD migration on the dataset. Diffraction hyperbolas are removed and dipping reflectors are moved to their true subsurface position.

Chapter 3

Tectono-sedimentary evolution of the Gulf of Naples half-graben basin (Italy) in interaction with volcanism during the last one million years

Lena Steinmann^{1,2}, Volkhard Spiess¹, Marco Sacchi³

¹Faculty of Geosciences, University of Bremen, 28359 Klagenfurter Str., Bremen, Germany

²MARUM – Center for Marine Environmental Sciences, University of Bremen, Leobener Str., 28359 Bremen, Germany

³Istituto per l'Ambiente Marino Costiero (IAMC), Consiglio Nazionale delle Ricerche (CNR), Calata Porta di Massa, 80133 Napoli, Italy

3 Abstract

The Gulf of Naples represents a Plio-Quaternary half-graben basin that was formed in the course of the Tyrrhenian Sea opening by NE-SW and NW-SE-striking faults. The related regional faults are assumed to be strongly linked to the adjacent Quaternary volcanism.

In this study, we investigate the stratigraphic sequences deposited within the Gulf of Naples half-graben utilizing multi-frequency multichannel seismic data. The objectives are to provide new insights on the interaction between fault activity and volcanism as well as to refine and extend the understanding of the tectono-sedimentary evolution of the Gulf of Naples half graben during the past one million years. The main findings are presented in a novel and comprehensive 3D model outlining the spatial and temporal evolution of the Gulf of Naples half-graben basin during the past one million years.

Two tectonically active periods leading to the subsidence of the half-graben were recognized (1) between 1 and 0.40 Ma and (2) between 0.14 to 0.02 Ma. During these intervals, the Gulf of Naples has subsided by a minimum of 1.3 km, which is equivalent to an average subsidence rate of at least 2.6 m/kyr. In contrast, the timespans between 0.40 and 0.14 Ma and since 0.02 Ma seem to have been tectonically stable. The Gulf of Naples is filled with a minimum of 1.2-km Plio-Quaternary sediments. Most of these sequences deposited between 1 and 0.04 Ma.

The onset of increased tectonic activity at 0.14 Ma is approximately coeval with the initiation of intense volcanism. We suggest that both processes were related to the reactivation of major NE-SW and NW-SE-trending normal faults, which potentially also triggered the large-scale Campanian Ignimbrite eruption at 39 ka. On the other hand, a tectonic control on the Neapolitan Yellow Tuff (NYT) eruption at 15 ka could not be confirmed.

3.1 Introduction

Half grabens are fault-bounded, asymmetric sedimentary basins that progressively form in the course of extensional tectonism (McKenzie, 1978; Barr, 1987; Leeder and Gawthorpe, 1987). They are common features in continental and oceanic environments observed for instance at the East African Rift System (Chorowicz, 2005), the Galicia Bank (Llave et al., 2008), the Rhine Graben (Derer et al., 2005), the Gulf of Corinth (Moretti et al., 2003), and the Tyrrhenian Sea margin (Milia and Torrente, 1999; Casciello et al., 2006). Such basins provide significant accommodation space, which allows for the long-term and continuous preservation of sedimentary strata. The formation of stratigraphic sequences within sedimentary basins is generally controlled by (1) glacio-eustatic sea-level variations, (2) tectonics and (3) sediment flux (Frostick and Steel, 1993; Catuneanu, 2002). Investigating the stacking pattern and geometry of such sequences permits the reconstruction of the basin formation and evolution in interplay with changes in the depositional system.

Furthermore, in volcanically active regions, sedimentary basins represent a unique record of the volcanological history. Submarine basins in particular preserve and incorporate volcanic deposits in the sedimentary strata as they are less prone to erosion than their subaerial counterparts. Moreover, large-scale volcanic eruption can provide significant sediment influx by, for instance, the rapid emplacement of thick ignimbrite sheets (Brown and Andrews, 2015; Neri et al., 2015b). In fact, the volcanoclastic contribution to the total volume of the sedimentary fill may be up to 25% (Einsele, 2000).

In areas of crustal thinning, regional faults, including the bounding faults of half-graben basins, are assumed to have strong control on the ascent of magma and, thus, on the occurrence of volcanic activity. Such a link was for instance suggested for the Taupo Volcanic Zone (New Zealand) (Spinks et al., 2005), the Toba caldera (Indonesia) (Bellier and Sébrier, 1994), the Mayon Volcano (Philippines) (Lagmay et al., 2005), as well as the Campi Flegrei Volcanic Zone (CVZ) and the Somma-Vesuvius (Italy) (Acocella and Funicello, 2006; Bellucci et al., 2006; Turco et al., 2006).

In this study, we investigate the tectonic setting around the CVZ and Somma-Vesuvius in order to provide new insights on a potential mutual linkage of tectonism and volcanism. More specifically, we examine the sedimentary sequences deposited in the

adjacent Gulf of Naples half-graben basin with respect to volcano-tectonic activity, as a close linkage between the NE-SW and NW-SE half-graben fault system and the intense volcanism has been suggested (Acocella and Funiciello, 2006; Bellucci et al., 2006; Turco et al., 2006). For the same reason, the Gulf of Naples half-graben structure and fill has been subject to several studies based on the same low-frequency single-channel reflection seismic surveys during the last decades (e.g. Fusi et al., 1991; Milia and Torrente, 1999; Milia et al., 2003; Milia et al., 2006; Milia and Torrente, 2007). These investigations provided important stratigraphic information by imaging (1) a tilted Mesozoic carbonate basement cropping out at the Sorrento Peninsula, (2) an overlying succession of thick Plio-Quaternary sediments and (3) major ignimbritic units related to the Campanian Ignimbrite and Neapolitan Yellow Tuff eruptions at 39 and 15 ka, respectively. However, the utilized seismic data were of low vertical resolution (~ 10 m), thereby restricting the assessment of stratigraphic sequences. Furthermore, the seismic data were recorded graphically in analogue format and, thus, the data quality was limited and could not be enhanced by modern processing procedures.

Here, we present a set of recently acquired multi-frequency multichannel seismic data, which provide the ideal combination of resolution and penetration and are thus suitable for refining and complementing the previously proposed stratigraphic framework based on the low-frequency single-channel reflection seismic data (e.g. Fusi et al., 1991; Milia and Torrente, 1999; Milia et al., 2003; Milia et al., 2006; Milia and Torrente, 2007). This study shall contribute to the overall understanding of the interaction between tectonism, volcanism and sedimentary deposition in the Gulf of Naples. The main findings of this work are presented in a comprehensive 3D tectono-sedimentary model outlining the evolution of the Gulf of Naples half-graben basin during the past 1 Ma is presented.

3.2 Regional setting

The Gulf of Naples represents a Plio-Quaternary half-graben basin, bordered by NE-SW and NW-SE-striking normal faults formed at a late stage of the Tyrrhenian Sea opening (Malinverno and Ryan, 1986; Kastens et al., 1988). It is located on the Campania continental margin in southern Italy and extends over an area of $\sim 1,000$ km², including the small embayment of the Gulf of Pozzuoli (Fig. 3.1). The half-graben basement consists of NW-tilted Mesozoic carbonates (Fusi, 1996), cropping out at the Sorrento Peninsula (Bernoulli and Jenkyns, 1974; Brocchini et al., 2001) and forming the NE-SW-elongated submerged structural high of the Banco di Fuori (Fusi, 1996) (Fig. 3.1). To the North, the Gulf of Naples is bordered by the NE-trending CVZ (including the Campi Flegrei area as well as Ischia and Procida Islands). Another prominent volcano is the Somma-Vesuvius located in the NE (Fig. 3.1).

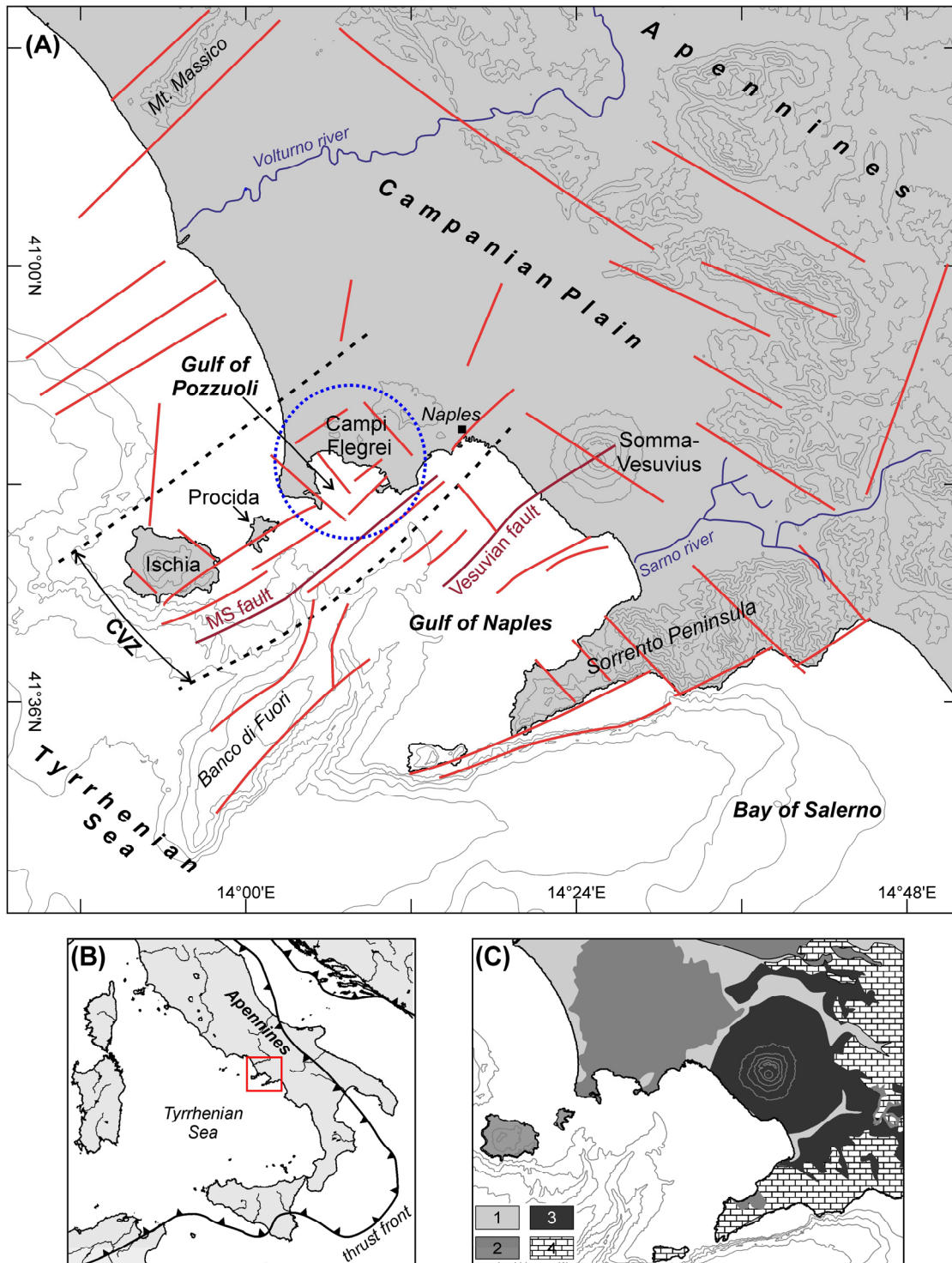


Fig. 3.1:(A) Close-up map of the Campania Margin for location see red rectangle in (B). (B) Overview map of the Italian Peninsula and the Tyrrhenian Sea with the African-Eurasian subduction zone indicated as thrust front. (C) geological sketch map of the working area with 1=Quaternary continental and marine sediments, 2=CVZ volcanic deposits, 3=Somma-Vesuvius volcanic deposits, and 4=Mesozoic carbonates (modified after Di Renzo et al., 2007). Contour lines in (A) and (C) have a spacing of 200 m.

The onset of severe volcanic activity in the Campania area was at ~150 ka at Ischia Island (Santacroce et al., 2003; Acocella and Funiciello, 2006). Two major ignimbritic

eruptions namely the Campanian Ignimbrite (CI) and the Neapolitan Yellow Tuff (NYT) occurred at 39 and 15 ka, respectively, and are assumed to have formed the nested Campi Flegrei caldera (e.g. Rosi et al., 1983; Barberi et al., 1991; Orsi et al., 1996; Deino et al., 2004; Acocella, 2008). The related ignimbrite deposits occur widespread onshore as well as offshore and have also been identified in previous low-frequency seismoacoustic studies in the Gulf of Naples (e.g. Fusi et al., 1991; Milia and Torrente, 1999; Milia et al., 2003; Milia et al., 2006; Milia and Torrente, 2007). The volcanic activity occurring along the Campania Margin is assumed to be strongly controlled by regional extensional NE-SW and NW-SE fault systems that formed in the course of the Tyrrhenian Sea opening (Milia et al., 2003; Acocella and Funiciello, 2006; Bellucci et al., 2006; Turco et al., 2006). For instance, Turco et al. (2006) investigated the whole Tyrrhenian Sea margin and generally proposed that volcanic activity at the Campania Margin is linked to a change in extensional direction of the Tyrrhenian Sea opening from E-W to NE-SW that occurred in the Early Pleistocene; Acocella and Funiciello (2006) suggested that the CVZ and Somma-Vesuvius are located at the intersection of the NE-SW and NW-SE trending fault systems, where the permeability of the crust is increased and the rise and emplacement of the magma is focused; and Bellucci et al. (2006) argued that regional NW-SE-trending acted as eruption fissures for the emplacement of Quaternary ignimbrites, thereby excluding the existence of a collapse caldera in the Campi Flegrei area. The formation of the prevailing NE-SW and NW-SE-oriented fault systems in the Gulf of Naples is described in detail below.

In the Late Pliocene to Early Pleistocene (3.5-0.75 Ma), NW-SE faults developed along the Campania Margin, displacing the Mesozoic carbonate platform and producing NE-oriented horst and graben structures (Turco et al., 2006; Milia et al., 2013). Borehole observations suggest that these faults led to the initial submersion of the Gulf of Naples and the Campania Plain at ~1 Ma (Brocchini et al., 2001). Due to its relatively young age, no deposits related to the Messinian Salinity Crisis are present in the Gulf of Naples area (Fusi et al., 1991).

Since the Middle Pleistocene (<0.75 Ma), the NW-oriented faults were replaced by NE-trending faults due to a change in the extension direction from NE-SW to NW-SE. This marks the beginning of the NW-oriented Gulf of Naples half-graben formation (Turco et al., 2006; Milia et al., 2013). Furthermore, structural carbonatic highs (Mount Massico, Sorrento Peninsula, Banco di Fuori) and additional lows (the Gulf of Gaeta and the Bay of Salerno) transversal to the Apennine chain were produced (Hippolyte et al., 1994; Milia et al., 2003; Turco et al., 2006; Milia et al., 2013).

The tectonic development of the Gulf of Naples since the Middle Pleistocene is still a matter of debate. According to low-frequency reflection seismic studies, tectonic activity ceased at 0.4 Ma, leading to a tectonically stable phase since 0.4 Ma (Milia et al., 2003).

On the contrary, Milia et al. (2013) propose that the Campania Margin underwent an E-W extensional phase since 0.4 Ma, which supposedly led to the formation of NNE-SSW faults and the reactivation of older NW-SE and NE-SW faults. Others even proposed that highest rates of subsidence were reached during the Holocene (since ~ 5 ka) (Brancaccio et al., 1991).

The full vertical extent of the Gulf of Naples half-graben is still subject of discussions. For instance, the Mesozoic carbonates were identified at a depth of 1,670 m in the Trecase borehole close the Somma Vesuvius (Brocchini et al., 2001), low-frequency seismic studies suggested a depth of at least 1,100 m in the Gulf of Naples (Fusi, 1996), and in the Campi Flegrei area, the carbonatic basement was not recovered even in 3,000-m deep boreholes (Rosi et al., 1983; Piochi et al., 2013). In that respect, also the rate of subsidence is still uncertain. As average subsidence rate 0.23 m/kyr has been suggested (Brancaccio et al., 1991). However, considering that the Gulf of Naples half graben is a relatively young tectonic feature formed during the past 1 Ma and that its vertical extent likely exceeds 1,000 m, 0.23 m/kyr represents an unrealistically low value.

3.3 Materials and methods

In this study, we utilized five multi-frequency multichannel seismic datasets acquired in the Gulf of Naples during three different research expeditions (Fig. 3.2). Their specifications are summarized in Table 3.1.

The seismic dataset labelled with “GeoB” were acquired using the multichannel seismic equipment of the University of Bremen in different configurations (Fig. 3.2). The GeoB16 datasets was acquired during a recent research cruise on the R/V MINERVA in January/February 2016. During this expedition, two seismic sources were deployed and shot alternatingly: (1) a Mini-GI-Gun with reduced chamber volume of 2x0.1 L (GeoB16-x(1)) and (2) a GI-Gun with 4.1/1.7 L chamber volume (GeoB16-x(2)). The seismic signal was recorded using a custom-designed 96-channel streamer (224 m active length) with a broad bandwidth (3-1000 Hz).

The GeoB08 datasets were recorded during a research cruise on the R/V URANIA in January 2008 (Fig. 3.2). Again, two seismic sources were deployed simultaneously: (2) a Mini-GI-Gun with reduced chamber volume of 2x0.1 L (GeoB08-x(1)) and (1) a GI-Gun with 2x1.7 L (GeoB08-x(2)). The seismic signal of the 0.1 L Mini-GI-Gun was recorded using a shallow water custom-designed streamer of 50 m length, hosting 48 single-hydrophone channels with a spacing of 1 m. The 1.7 L GI-Gun shots were recorded with a conventional 100-m long, 16-channel streamer.

The GeoB data underwent a full processing routine including geometry setup, trace editing, bandpass filtering (30/60-800/1000 Hz), residual statics corrections, normal move-out correction, multiple suppression, common mid-point (CMP) binning and

stacking, noise attenuation and time migration. The vertical and horizontal resolution of each dataset is presented in Table 3.1.

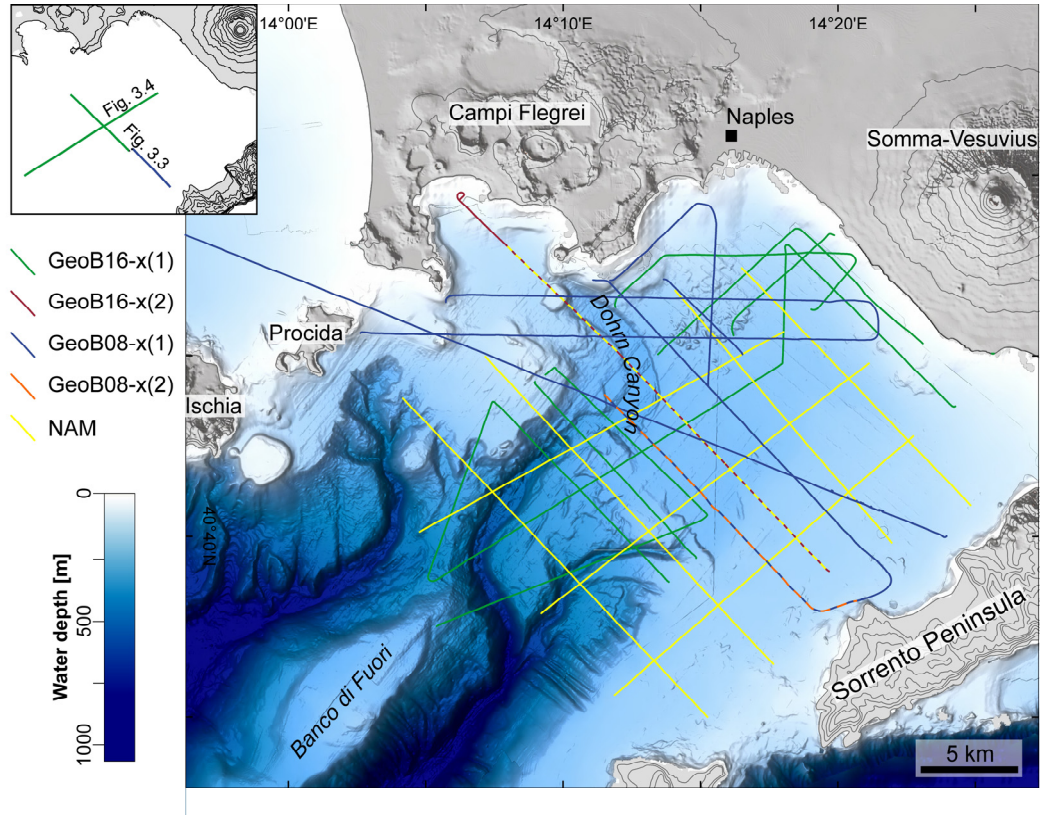


Fig. 3.2: Overview map of the Gulf of Naples. Utilized seismic datasets as described in Table 3.1 are illustrated in different colours. Multicolour, dashed lines indicate that both multiple seismic dataset were used. Onshore contour lines have a spacing of 100 m.

The so-called “NAM” multichannel seismic dataset was acquired in 1996 by the *Institute for Coastal Marine Environment of the National Research Council* (IAMC-CNR) using an air-gun as seismic source, no further information on the acquisition configuration is available (Fig. 3.2).

Table 3.1: Summary of the specifications of the utilized multichannel seismic datasets.

Seismic datasets	Frequency range [Hz]	Central frequency [Hz]	Max. signal penetration [s]	Max. vertical resolution [m]	Horizontal resolution [m]
GeoB08-x(1) (2x0.1 L Mini-GI)	30-1000	250	0.60	2	1
GeoB16-x(1) (2x0.1 L Mini-GI)	30-1000	200	1.05	2	1
GeoB08-x(2) (2x1.7 L GI)	30-500	70	1.00	5	10
NAM	50-300	70	1.60	6	6
GeoB16-x(2) (4.1/1.7 L GI)	5-200	50	1.60	10	5

The seismostratigraphic context from previous studies was based on low-frequency seismic data with an average vertical resolution of 10 m and a maximum signal penetration of 1 s TWT (e.g. Fusi et al., 1991; Milia and Torrente, 1999; Milia et al., 2003; Milia et al., 2006; Milia and Torrente, 2007). With the multi-frequency seismic dataset utilized in this study, we will be able to carry out a more detailed seismostratigraphic analysis resolving features as small as 2 m as well as to extend the stratigraphy to greater depth of up to 1.6 s TWT.

3.4 Results

We present two representative high-resolution seismic profiles from the Gulf of Naples. Figure 3.3 shows a composed line of two parallel seismic profiles, which are separated by a ~500 m NE-SW shift, covering the Gulf of Naples in NW-SE direction, perpendicular to the Sorrento Peninsula. It extends over the continental shelf and the Dohrn Canyon covering a water-depth range from ~100 to 255 m. Figure 3.4 shows the NE-SW-trending seismic profile GeoB16-259, which runs perpendicular to the coastline offshore Vesuvius and crosses over the Dohrn Canyon at its SW end. The water depth on this profile ranges from ~150 to 580 m.

3.4.1 Seismic analysis

In total, six main seismic units (MC, SU1 - 5) with associated subunits were determined based on a seismic facies and seismic sequence analysis (Mitchum et al., 1977; Embry, 1995; Catuneanu, 2002). Four key unconformities (U1-U4) were defined and spatially mapped as shown in Figure 4.5. Using these key horizons, thickness maps were produced to illustrate the spatial distribution of the main seismic units (Figs. 4.6, 4.7). The facies description of all units is summarized in Table 3.2 and described in detail below.

Seismic Unit MC

Seismic Unit MC represents the reflection-free acoustic basement that dips steeply towards the NW and NE (Figs. 3.3, 3.4). Its top presents a widespread unconformity (U1) (Fig. 3.5-A). At shallow depths (<0.23 s TWT) close to the Sorrento Peninsula, U1 is marked by a high-amplitude, relatively flat (~1°) reflection (Fig. 3.1). This shallow-water platform (Fig. 3.5-A) coincides with a thickness minimum in the overlying strata (Fig. 3.6-A). In the vicinity of the Banco di Fuori, Seismic Unit MC shows another topographic high that also coincides with a minimum thickness of the overlying strata (Figs. 3.5-A, 3.6-A). These elevated areas are surrounded by a steep (~7°) NW and NE dipping slope (Fig. 3.5-A). U1 could be traced up to a maximum depth of ~1.6 s TWT (i.e. maximum seismic signal penetration) (Fig. 3.5-A). Hence, the thickness estimates for SU1+2 (Fig. 3.6-A) beyond the point at which U1 lies below the seismic penetration

limit represent only minimum values calculated using a minimum depth of 1.6 s TWT for U1.

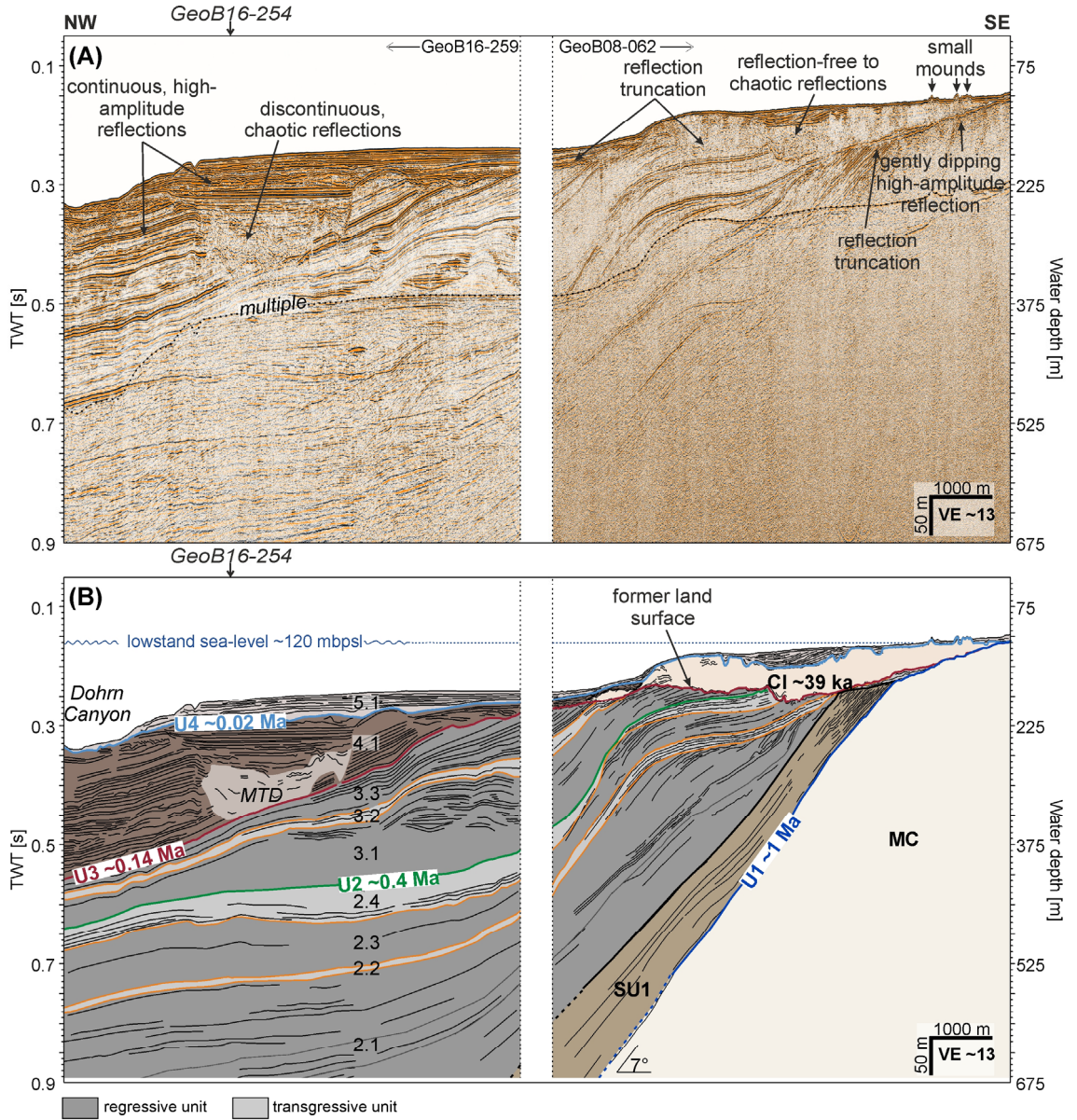


Fig. 3.3: Composed NE-SW-trending multichannel seismic line consisting of profile GeoB16-259 and GeoB08-062 acquired during the cruises in 2016 and 2008, respectively. The 0.1 L Mini-GI-Gun served as source for both profiles. The white gap indicates a ~500-m NE-SW shift. (A) shows the uninterpreted and (B) shows the interpreted seismic section illustrating the main stratigraphic units (MC, SU1-5) and associated unconformities (U1-U4). For the profile location see Figure 3.2.

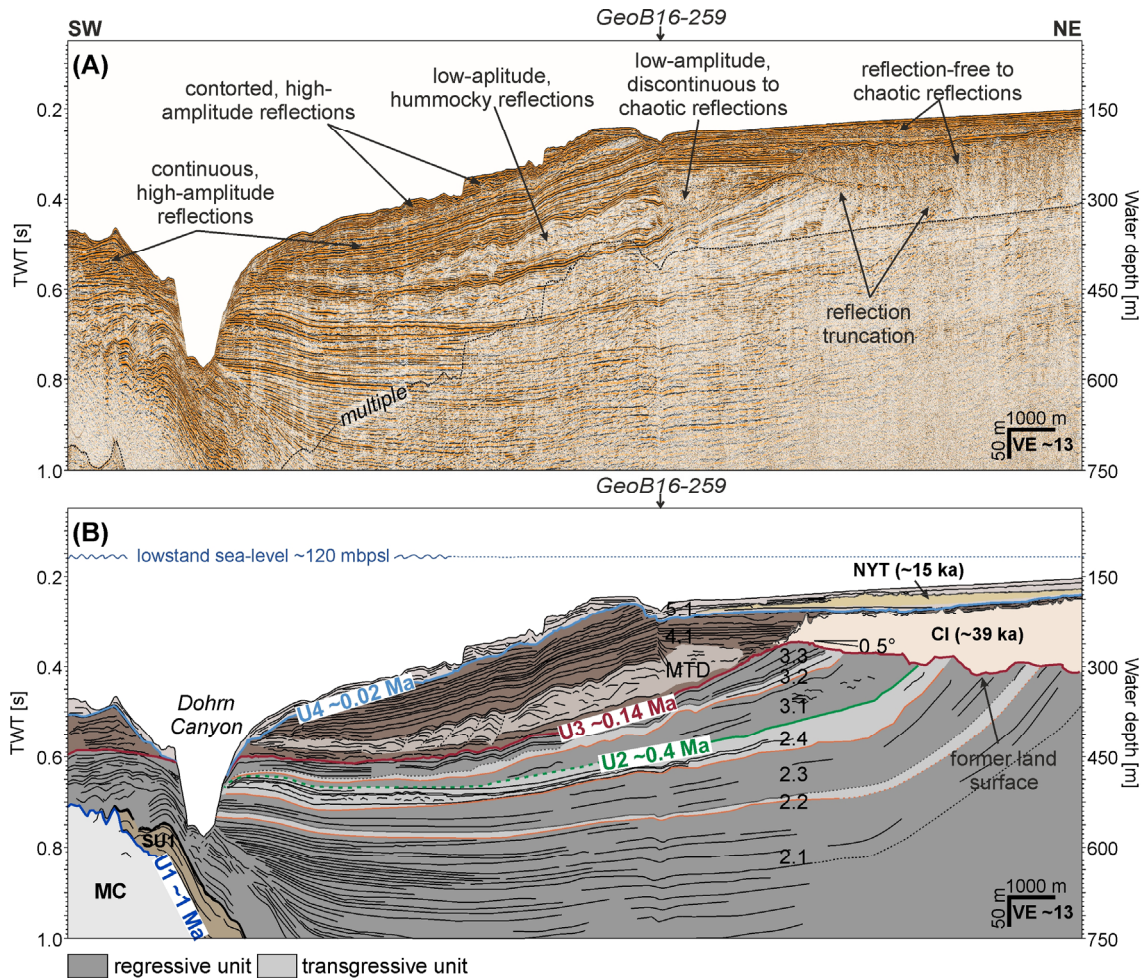


Fig. 3.4: Multichannel reflection seismic profile GeoB16-254 acquired with the 0.1 L-Mini-GI-gun as source acquired during the CAFE_2015 cruise. (A) shows the uninterpreted and (B) shows the interpreted section illustrating the main stratigraphic units (MC, SU1-5) and associated unconformities (U1-U4). For the profile location see Figure 3.2.

Seismic Unit 1 (SU1)

SU1 lies conformably on top of Seismic Unit MC (Figs. 3.3, 3.4). It comprises continuous, moderate to high amplitude reflections of parallel to subparallel configuration. Its reflections are mainly parallel to subparallel to the underlying unconformity U1, showing a dip of $\sim 7^\circ$ towards the NW (Fig. 3.3). However, the reflections diverge increasingly with depth leading to a slight thickness increase and wedge shape (Fig. 3.3). At shallow depth (< 0.24 s TWT), clear reflection truncation is visible along a flat surface, which represents the extension of the high-amplitude, relatively flat reflection U1 (Fig. 3.3). Due to a lack of reflectivity and distinguishing character, the top of SU1 could not be traced over all profiles. Hence, the thickness of SU1 could not be considered individually but instead is combined with the thickness of SU2 (see below).

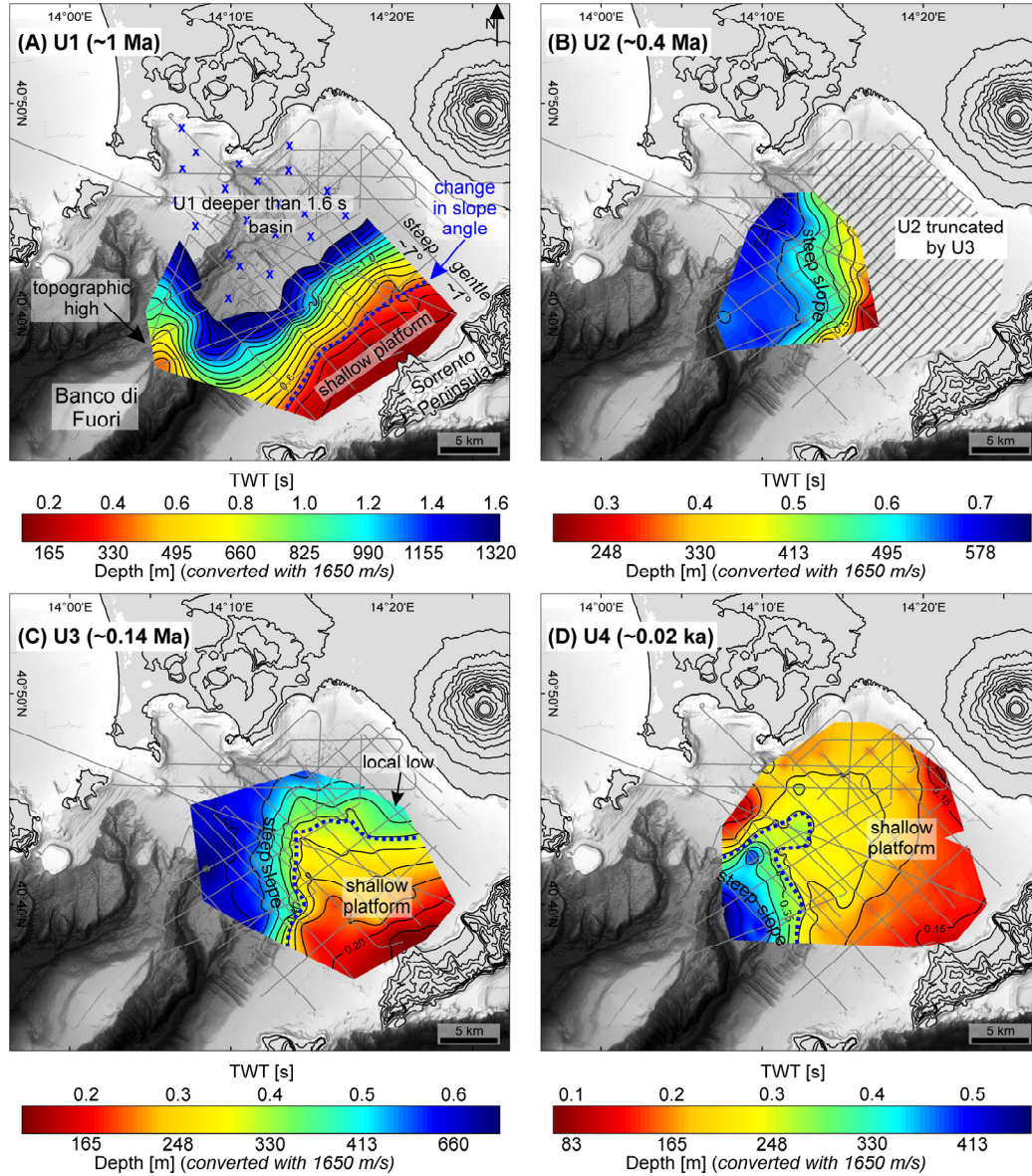


Fig. 3.5: Gridded horizon maps of the four main unconformities U1-U4 (A-D) illustrating their depth distribution. A constant velocity of 1650 m/s representing the mean velocity of the marine sediments was applied for an approximate depth conversion (Sacchi et al., 2014). The onshore contour lines have spacing of 100 m.

Seismic Unit 2 (SU2)

SU2 features continuous, low to moderate amplitude reflections with parallel to subparallel configuration (Figs. 3.3, 3.4). It consists of in total four subunits (SU2.1-2.4). SU2.1 and 2.3 represent oblique prograding clinoforms with toplap reflection termination against the overlying internal unconformity (Fig. 3.3). In contrast, SU2.2 and 2.4 correspond to retrogradational sequences with onlap terminations on the underlying internal unconformities (Fig. 3.3). At its top, SU2 is confined by the unconformity U2. Towards the South, the topsets of SU2 are well preserved (Fig. 3.3). Here, only at shallow depth (<250 s TWT) the reflections of SU2.3 and 2.4 as well as unconformity U2 are truncated by the overlying unconformity U3 (Figs. 3.3, 3.5-B). Towards the NW, all

subunits of SU2 are truncated along U2 (Fig. 3.4, 3.5-B). Generally, U2 is characterized by a steep N-S-trending and westward dipping slope between 0.2 and 0.55 s TWT followed by a gently dipping area at higher depths (>0.55 s TWT) (Fig. 3.5-B). The compiled thickness maximum of the SU1 and SU2 of at least 1.35 s TWT coincides with the topographic low (i.e. basin) of the underlying unconformity U1 (Figs. 3.5-A, 3.6-A). The overall thickness of SU1+SU2 is generally relatively high, ranging from ~ 0.3 to 1.35 s TWT (Fig. 3.6-A).

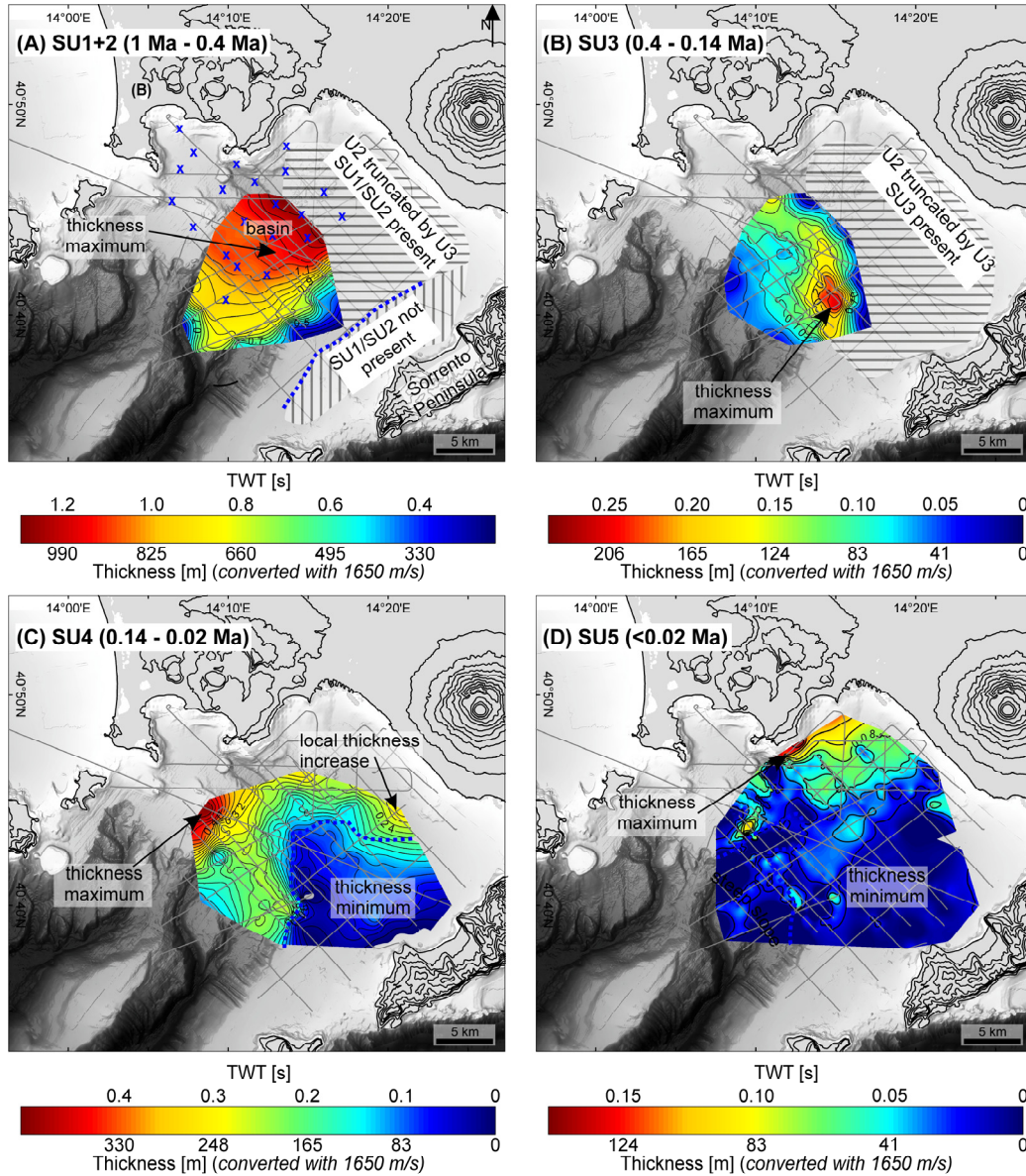


Fig. 3.6: Thickness maps illustrating the spatial distribution of the individual seismic units SU1-5 (A-D). Blue “x” in (A) indicates the area, where U1 is located beneath the seismic penetration limit of ~ 1.6 s TWT (Fig. 3.5). Blue dashed line in (A) and (C) corresponds to the shallow platform identified in Figure 3.5. A constant velocity of 1650 m/s representing the mean velocity of the marine sediments was applied for an approximate depth conversion (Sacchi et al., 2014). The onshore contour lines have spacing of 100 m.

Seismic Unit 3 (SU3)

SU3 comprises continuous, low to moderate amplitude reflections with parallel to subparallel configuration and locally wavy patches (Figs. 3.3, 3.4). It consists of three subunits (SU3.1-3.3) confined by the unconformities U2 and U3 at its base and top, respectively. SU3.1 and 3.3 represent oblique prograding clinoforms and SU3.2 represents a retrogradational unit. The topsets of SU3 are not present; instead their reflections are clearly truncated by the overlying unconformity U3 in shallow depth between 0.25 and 0.5 s TWT (Figs. 3.3, 3.4, 3.6-B). The thickness maximum (~ 0.29 s TWT) of SU3 shows an N-S-trending elongated shape and coincides with the steep slope of the underlying unconformity U2 (Figs. 3.5-B, 3.6-B).

Seismic Unit 4 (SU4)

SU4 comprises three subunits (SU4.1, MTD, CI) of distinct seismoacoustic character (Figs. 3.3, 3.4). It is bounded by unconformity U3 at its base and by unconformity U4 at its top. SU4.1 is characterized by mainly high-amplitude, continuous reflections with parallel to subparallel configuration. It shows a progradational to aggradational trend and is present mostly on the steep-dipping slope of the underlying unconformity U3 (Figs. 3.5-C, 3.6-C). At shallow depth, the reflections of SU4.1 are truncated by the overlying unconformity U4 (Fig. 3.3).

The Seismic Unit MTD is interbedded in SU4.1 and occurs only locally on the steep-dipping slope of U3. It features discontinuous, low-amplitude, chaotic to contorted reflections (Figs. 3.3, 3.4).

The prominent Seismic Unit CI shows reflection-free to chaotic seismic facies (Figs. 3.3, 3.4). In the Gulf of Naples, it is located directly on top of the truncational, shallow platform of U3. At shallow depth (~ 0.16 s TWT), the CI is characterized by a relatively flat top (Fig. 3.3). Its overall shape may be described as mounded wedge.

Overall, SU4 shows a thickness maximum of ~ 0.5 s TWT in the offshore sector of the Campi Flegrei area (Fig. 3.6-C). Generally, the thickness of SU4 shows an increase towards the steep slope of the underlying unconformity U3 (Fig. 3.5-C). Another prominent thickness increase can be observed at shallow depth offshore Vesuvius and coincides with a local topographic low of the underlying unconformity U3 (Figs. 3.5-C, 3.6-C). This increase is mainly attributed to the presence and thickness maximum of the Seismic Unit CI (Fig. 3.7-A). SU4 shows a thickness minimum coinciding with the shallow platform of the underlying unconformity U3 (Fig. 3.5-C). On this platform, mainly the CI is present with a thickness of ~ 0.12 s TWT (Fig. 3.7-A). The maximum thickness of the CI is ~ 0.23 s TWT (Fig. 3.7-A). However, in large areas, the bottom of the CI could not be imaged due to limited signal penetration. Hence, in those places, the CI might be significantly thicker.

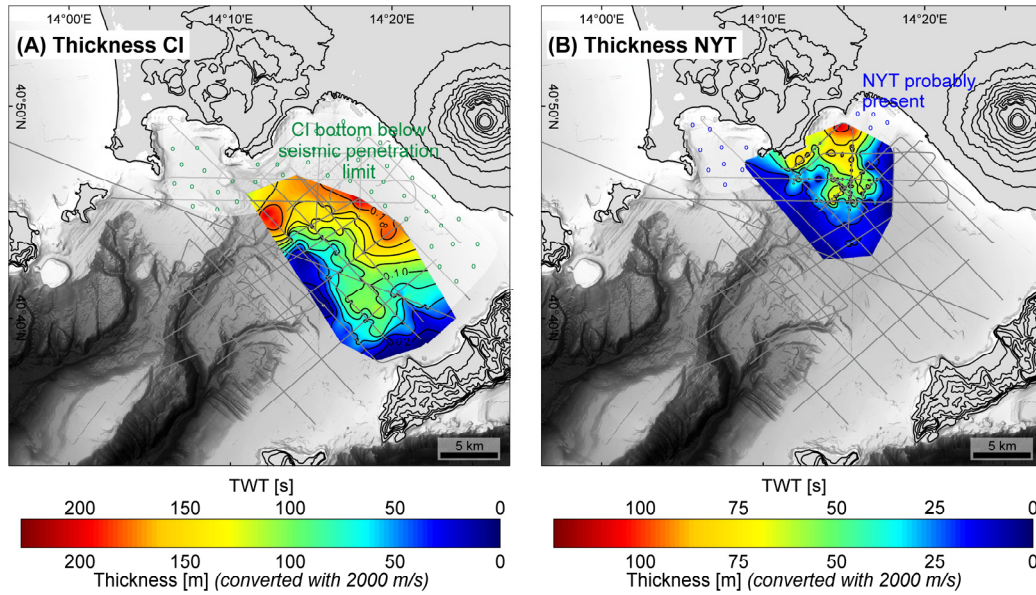


Fig. 3.7: Thickness maps of the CI (A) and the NYT (B) deposits. A constant velocity of 2,000 m/s as representative velocity for pyroclastic rocks was applied for an approximate depth conversion (Vanorio et al., 2002).

Seismic Unit 5 (SU5)

The uppermost identified unit, SU5, comprises two subunits (SU5.1, NYT), which are distinctively different in their seismoacoustic nature. SU5 is bounded at its base and top by unconformity U4 and the seafloor, respectively (Figs. 3.3, 3.4). U4 is characterized by a relatively flat shallow-water platform followed by a steep SW-dipping slope (Fig. 3.5-D). SU5.1 consists of continuous, high-amplitude reflections with mainly parallel to subparallel configuration. On the steep slope of the underlying unconformity U4, locally contorted reflection can be observed (Fig. 3.3). Its reflection pattern is mainly aggradational. Seismic Unit NYT is interbedded in SU5.1 and shows a discontinuous, chaotic seismic facies (Fig. 3.4). It was identified mainly offshore Naples and the Campi Flegrei area, where it shows a maximum thickness of ~0.12 s TWT (Fig. 3.7-B). The overall morphology of the NYT is mounded to wedge-shaped with local small-scale highs. SU5 is the thinnest of all identified units with a maximum thickness of ~0.17 s TWT offshore Naples, coinciding with the maximum thickness of the NYT (Figs. 3.6-D, 3.7-B). Apart from that, the thickness of SU5 is relatively uniform and mainly made up of SU5.1.

Table 3.2: Summary of the seismic facies description and associated geological interpretation.

Seismic Unit	Continuity	Amplitude	Reflection configuration	Reflection pattern/ external shape	Geological interpretation	Age range [Ma]
SU5	NYT	Low	Chaotic	Mounded wedge	Pyroclastic density current deposit related to the Neapolitan Yellow Tuff eruption	~0.015
	5.1	High	Parallel to subparallel, locally hummocky	Aggradational	Lowstand, transgressive and highstand deposits	<0.02
SU4	CI	Low to reflection-free	Chaotic to reflection-free	Mounded wedge	Pyroclastic density current deposit related to the Campanian Ignimbrite eruption	~0.039
	MTD	Low	Chaotic	Slump	Mass-wasting deposit potentially triggered by CI eruption	~0.14 – 0.02
SU3	4.1	High	Parallel to subparallel	Progradational to aggradational	Transgressive-regressive sequence with interbedded MTD (see above)	~0.14 – 0.02
	3.3	Low to moderate	Parallel to subparallel, locally slightly convergent/wavy	Oblique progradational	Eroded transgressive-regressive sequence	~0.33 – 0.14
SU2	3.2	Low to moderate	Parallel to subparallel, locally wavy	Retrogradational (?)	Eroded transgressive sequence	~0.34 – 0.33
	3.1	Low to moderate	Parallel to subparallel	Oblique progradational	Eroded regressive sequence	~0.40 – 0.34
SU2	2.4	Low to moderate	Parallel to subparallel, convergent, local MTD	Retrogradational	Well-preserved transgressive sequence	~0.43 – 0.40
	2.3	Low to moderate	Parallel to subparallel, locally slightly convergent	Oblique progradational	Well-preserved regressive sequence	~0.60 – 0.43
	2.2	Low to moderate	Parallel to subparallel	Retrogradational	Well-preserved transgressive sequence	~0.63 – 0.60
	2.1	Low to moderate	Parallel to subparallel	Oblique progradational	Well-preserved regressive sequence	~0.77 – 0.63
SU1	Continuous	Moderate to high	Parallel to subparallel, slightly divergent	Tilted wedge	Mainly aggradational marine sediments (siltstone) deposited in the early stage of flooding due to NW-SE faulting (small NE-SW component present)	~1 – 0.77
U1	-	Reflection-free	-	Tilted basement	Apennine carbonate platform	Mesozoic

3.5 Discussion

3.5.1 Stratigraphic framework

Seismic Unit MC was interpreted as Mesozoic carbonate platform cropping out at the Sorrento Peninsula and forming the basement of the Plio-Quaternary half graben. It consists mainly of limestones and dolomites and was formed in shallow water areas around the open Tethys Ocean (Bernoulli and Jenkyns, 1974; Brocchini et al., 2001). Our interpretation of this unit is in accordance with findings from previous, low-frequency seismoacoustic studies carried out in the Gulf of Naples (Fusi et al., 1991; Milia and Torrente, 1999).

SU1 lies directly on top of Seismic Unit MC and was interpreted as a marine sedimentary unit corresponding to the first marine sequence overlying the Mesozoic carbonates in the Trecase borehole (Brocchini et al., 2001). Based on nannofossil biostratigraphy at the base of the marine unit from the Trecase well, an approximate maximum age of ~1 Ma could be ascribed to this unit (Brocchini et al., 2001). SU1 was probably deposited during an early phase of flooding mainly related to subsidence due to NW-SE faulting during the Early Pleistocene (1-0.75 Ma) (Fig. 3.8) (Brocchini et al., 2001; Turco et al., 2006; Milia et al., 2013). This is in agreement with the interpretation from Milia and Torrente (1999). However, our data show a thickness increase towards the NE (i.e. the half-graben basin), which implies that subsidence related to NE-SW faulting was probably already active during the time of deposition.

At ~0.75 Ma, the NW-SE faults were entirely replaced by NE-SE faults, leading to the formation of the NW-trending half-graben system along the Campania Margin (Turco et al., 2006; Milia et al., 2013). The top of SU1 corresponds to this major change in the tectonic regime (Fig. 3.8). Hence, SU2 represents the first unit that has deposited during the main phase of NE-SW faulting and related half-graben formation. Overall, SU2 shows a clear NE-progradational trend building out the shelf mainly towards the NW. Also it fills up the accommodation space in the half-graben basin. In detail, SU2 consists of two regressive (SU2.1, 2.3) and two transgressive (SU2.2, 2.4) sequences. SU2.1, the first unit that deposited after the onset of predominant NW-SE faulting, was interpreted as regressive because of its oblique progradational reflection pattern. Hence, we assume that SU2.1 deposited during a phase of sea-level fall between 0.75 and 0.63 Ma (Fig. 3.8). SU2.1 is overlain by a transgressive sequence due to its retrogradational reflection pattern and onlap reflection termination. It was probably formed during sea-level rise between 0.63 and 0.6 Ma (Fig. 3.8). SU2.3 and SU2.4 represent a similar sea-level cycle with a regressive and transgressive sequence, respectively. SU2.3 was interpreted as being deposited between 0.60 and 0.43 Ma and SU2.4 as being deposited between 0.43 and 0.40 Ma (Fig. 3.8). These regressive-transgressive sequences are well-preserved in the SW

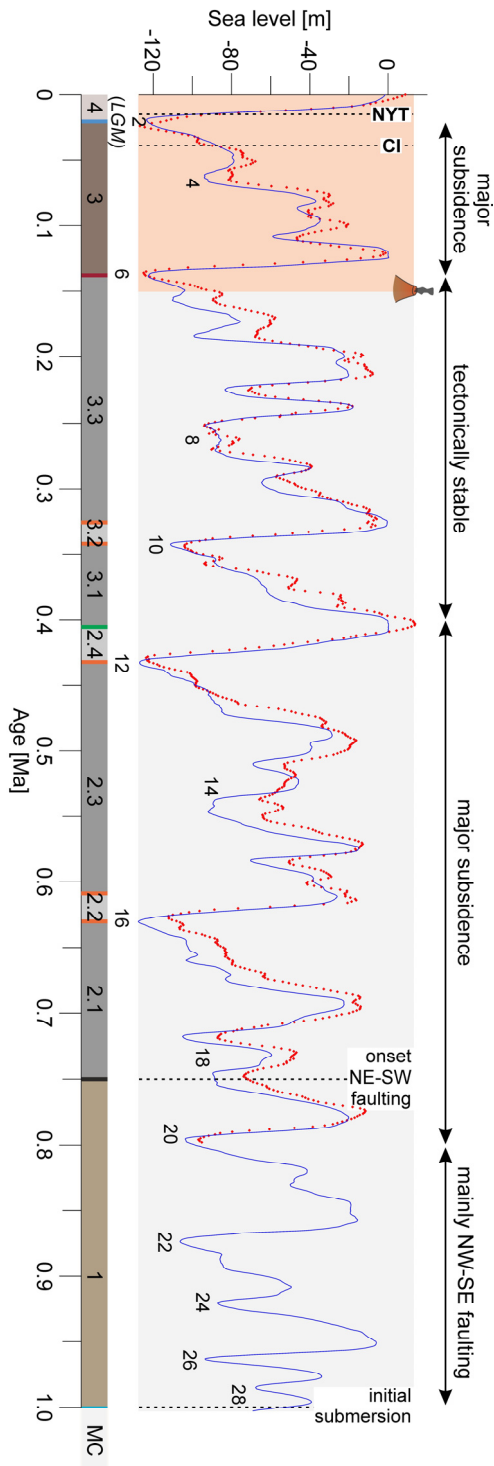


Fig. 3.8: Stratigraphic column (left) in correlation to sea-level variations during the past 1 Ma. Major tectonic events as well as the onset of volcanism (light red area) are indicated. Blue solid line: sea-level curve from Bintanja and van de Wal (2008); red dots: sea-level curve from Spratt and Lisiecki (2016).

part of the Gulf, where they show only minor erosion along the overlying unconformity U3 (Fig. 3.3).

SU3 represents a strongly eroded set of regressive and transgressive sequences with a SW-progradational trend (Figs. 3.3, 3.4). SU3.1 was interpreted as a regressive sequence formed during sea-level fall between 0.40 and 0.34 Ma. SU3.2 is assumed to be a transgressive sequence, deposited during sea-level rise between 0.34 and 0.33 Ma. SU3.3 was probably formed during another phase of sea-level fall between 0.33 and 0.14 Ma and, thus, interpreted as regressive (Fig. 3.8). The shallow-water portion of the top of SU3, unconformity U3, represents a widespread strongly erosive unconformity interpreted as a former land surface (Figs. 3.3, 3.4) formed mainly during the MIS 6 lowstand around ~0.14 Ma. This surface loses its erosive character towards higher depth, where it represents the paleo continental slope (Fig. 3.5-C). Due to severe erosion along this surface, the topsets of SU3 are not preserved.

Furthermore, U3 marks a significant change in seismic amplitude from low to moderate amplitudes in SU3 to high amplitudes on top in SU4.1 and SU5 (Figs. 3.3, 3.4). This prominent amplitude increase was interpreted as being related to the onset of severe volcanic activity at the CVZ and the Somma-Vesuvius at ~150 ka (Fig. 3.8). Consequently, volcanic material such as ash was highly abundant and, intercalated between marine sediments, led to strong impedance contrasts (i.e. high amplitudes).

SU4 is located between unconformity U3 and U4 and was interpreted as being deposited between 0.14 (MIS 6) and 0.02 Ma (MIS2, i.e. LGM) (Fig. 3.8). It consists of a transgressive-regressive

sequence (SU4.1) with a prominent interbedded mass-waste deposit (MTD), both of which are mainly located on the steep slope of U3 interpreted as the former continental slope (Figs. 3.3, 3.4). Furthermore, SU4 also comprises the CI unit, which was interpreted as pyroclastic density current deposit related to the Campanian Ignimbrite eruption at 39 ka. This unit is mainly present on the erosive shallow-water portion of U3 (i.e. former land surface) (Figs. 3.5-C, 3.7-A). The thickness maximum of SU4 is located in the offshore sector of the CVZ and is probably related to increased deposition due to severe volcanic activity in that area (Fig. 3.6-C). Furthermore, the CI deposit fills up the accommodation space provided on the shallow-water platform by the post-MIS 6 tilting (Fig. 3.4). The thickness of the CI is highest in topographic depressions of U3 (Fig. 3.5-C, Fig. 3.7-A). Consequently, the geometry of the shelf is significantly changed, for instance in Figure 3.4 the previously landward-dipping surface (U3) shows a seaward dip after the CI emplacement. Due to its coeval timing and in accordance with findings from Fusi et al. (1991), the MTD deposit located on the continental slope was interpreted as secondary event related to the CI eruption caused by for instance earthquakes, tsunami wave, or instability of the slope after the rapid CI emplacement.

SU5, the uppermost seismic unit, was interpreted as lowstand, transgressive and highstand deposits that accumulated since ~ 0.02 Ma (i.e. LGM) (Fig. 3.8). Subunit SU5.1 represents marine deposits probably intercalated with thin volcanic layers. This unit shows a mainly aggradational trend. The NYT, which is interbedded in SU5.1, was interpreted as pyroclastic density current deposit related to the Neapolitan Yellow Tuff eruption in the Campi Flegrei area at ~ 15 ka. This deposit was confidently identified offshore Naples (Fig. 3.7-B) and is probably also present in the Gulf of Pozzuoli.

3.5.2 Volcano-tectonic implications

During the timespan from 1 to 0.4 Ma, the rate of tectonic subsidence related to NW-SE and NE-SW faulting seems to have been relatively high, which is indicated by (1) the preservation of the topsets within SU2 and (2) the significant thickness of the sedimentary succession within the most subsided part of the half-graben basin. The transition from dominantly NW-SE to NE-SW faulting at ~ 0.75 Ma and the associated change in accommodation space is clearly marked by a shift from aggradational (SU1) to progradational (SU2) depositional sequences. In the time interval from 1 to 0.4 Ma, a sedimentary package of at least 1.1-km thickness (i.e. 1.35 s TWT) deposited within the half-graben (Fig. 3.6-A). This is equivalent to an accumulation rate of 1.8 m/kyr. In comparison, the timespan from 0.4 to 0.14 Ma was characterized by significantly lower rate of deposition with a maximum of ~ 240 m (i.e. 0.29 s TWT) (Fig. 3.6-B), which represents an accumulation rate of ~ 0.9 m/kyr. Also, during this interval, severe erosion occurred during lowstand as indicated by the fact that the topsets of SU3 are not

preserved (Figs. 3.3, 3.4). Hence, we inferred that significant tectonic subsidence occurred in the time period from 1 to 0.4 Ma, while the timespan from 0.4 to 0.14 Ma was comparatively tectonically stable. This supports findings from previous low-frequency seismoacoustic studies from the Gulf of Naples (Milia et al., 2003) and the adjacent Gulf of Gaeta (Milia et al., 2013), stating that the NE-SW faults, producing the Gulf of Naples half graben, were mainly active between 0.7 and 0.4 Ma.

The fact that the shallow, erosive platform of U3 represents a former land surface implies that it used to be located as shallow as 120 meter below present sea-level (*mbpsl*) during MIS 6. However, presently the erosive portion of U3 is located at higher depths of up to 375 mbpsl (0.5 s TWT) (Fig. 3.5-C). Accordingly, we infer that this surface subsided by at least 255 m since the MIS 6 sea-level lowstand. Furthermore, U3 shows an unusual landward tilt towards the Somma-Vesuvius (Fig. 3.4). As the LGM unconformity seems to not be affected by major subsidence, we suppose that the vast amount of vertical displacement occurred in the timespan from 0.14 to 0.02 Ma (Fig. 3.8). This subsidence phase was interpreted as being related to the reactivation of major normal faults. The landward tilting of the MIS 6 unconformity (U3) towards the Somma-Vesuvius was probably caused by renewed vertical displacement along a NW-SE-trending fault at the Somma-Vesuvius (Fig. 3.9-C) (Brocchini et al., 2001; Milia et al., 2013). Furthermore, we hypothesize that a major NE-SW fault in the CVZ may also have been reactivated and potentially initiated subsidence (Fig.3.9-C).

Milia et al. (2013) have already proposed that a deepening of the adjacent Southern Gaeta Basin occurred since 0.4 Ma due to the reactivation of NW-SE and NE-SW faults as well as the formation of NNE-SSW normal faults. Based on our findings, we can extend their conclusion by stating that the Gulf of Naples half-graben basin probably underwent deepening between 0.4 and 0.02 Ma as well.

It is striking that this phase of increased tectonic subsidence approximately coincides with the onset of intense volcanic activity in the area, including the large-scale CI eruption (Fig. 3.8). Previous studies have suggested that volcanism in the CVZ and at the Somma-Vesuvius are strongly controlled by the adjacent NE-SW and NW-SE fault system (Acocella and Funiciello, 2006). Our findings support this hypothesis by suggesting a link between subsidence in the Gulf of Naples and adjacent volcanism. For instance, caldera forming events during which large amounts of magma are ejected within only a short timespan may lead to significant subsidence (Cole et al., 2005), which may also affect the surrounding area. In return, it may also be possible that a stress change due to active tectonism triggered volcanic activity (Acocella and Funiciello, 2006; Allan et al., 2012).

Since 0.02 Ma, the Gulf of Naples seems to have been tectonically relatively stable (Fig. 3.8). Nonetheless, this timespan is still characterized by significant volcanism in the CVZ

and at the Somma-Vesuvius. Therefore, we conclude that either the tectonic control on eruptions played only a minor role from 0.02 Ma onwards, or that the presented seismic data were not able to resolve subsidence during this relative short time span.

Using the maximum present-day depth of unconformity U1 (the top of the Mesozoic carbonate platform) we were able to approximate the overall subsidence rate related to the half-graben formation. Considering that most of the NE-SW fault-controlled subsidence probably occurred during the timespan from 0.77 to 0.4 Ma and from 0.14 to 0.02 Ma and using ~1.3 km (1.6 s TWT, Fig. 3.5-A) as maximum identified displacement, we inferred an average subsidence rate of ~2.6 m/kyr. However, as the Mesozoic platform may be located significantly deeper than 1.3 km in parts, this value should be regarded as a conservative estimate.

3.5.3 Tectono-sedimentary evolution

Based on the above described stratigraphic context, we developed a 3D tectono-sedimentary model outlining evolution of the Gulf of Naples during the past 1 Ma in four stages (Fig. 3.9).

Stage 1 (1 Ma – 0.40 Ma)

At the beginning of Stage 1 (Fig. 3.9-A), between 1 Ma and 0.75 Ma, the Gulf of Naples underwent a first phase of flooding mainly due to NW-SE faulting. However, at least a slight NE-SW component was already present. At 0.75 Ma, the NW-SE faults were ultimately replaced by NE-SW faults, leading to the formation of the half-graben basin of the Gulf of Naples. Between 0.75 and 0.40 Ma, the Mesozoic basement was uplifted along the Sorrento Peninsula and the Banco di Fuori and subsided towards the Campi Flegrei and Naples area. Hence, significant accommodation space was created and rapidly filled by marine deposits. During that time the shelf prograded towards the NW, where the amount of subsidence was highest. A minimum accumulation rate of 1.86 m/kyr was inferred within the half-graben basin. Due to the significant subsidence, the regressive-transgressive sequences deposited between 0.75 and 0.40 Ma are well preserved.

Stage 2 (0.40 – 0.14 Ma)

Stage 2 (Fig. 3.9-B) is characterized by tectonic stability. The shelf prograded mainly towards the SW and was subaerially exposed during lowstand, thereby undergoing severe erosion. Hence, the topsets of the regressive-transgressive sequences are not preserved. At the end of this stage, during the MIS 6 lowstand at ~0.14 Ma, the continental shelf was subaerially exposed.

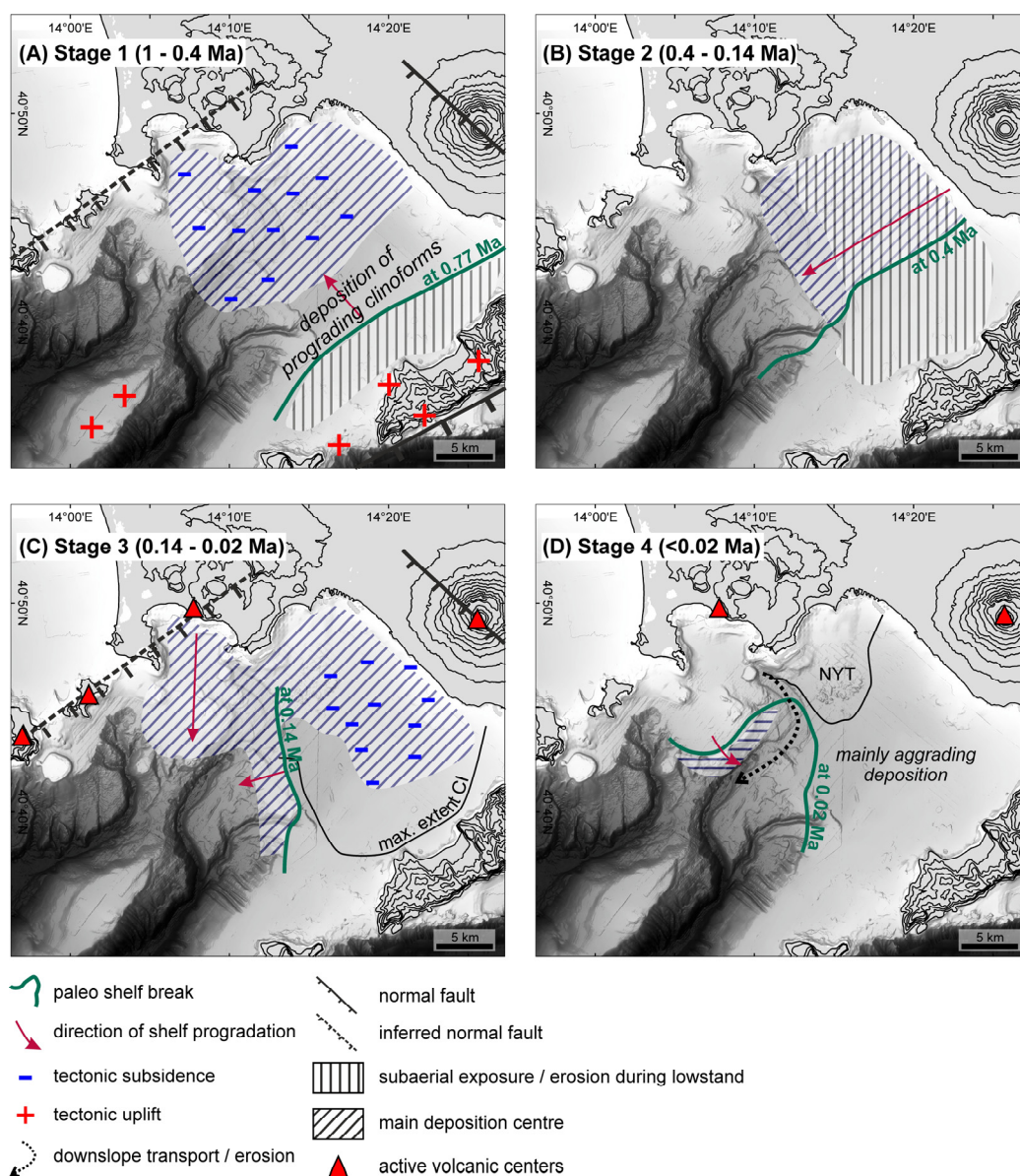


Fig. 3.9: 3D tectono-sedimentary model outlining the evolution of the Gulf of Naples over the past 1 Ma. The onshore contour lines have a spacing of 100 m. For detailed description of the four stages see section 3.5.3.

Stage 3 (0.14 – 0.02 Ma)

Stage 3 (Fig. 3-9-C) is marked by intense volcanic activity in the CVZ and at the Somma-Vesuvius as well as reoccurring tectonic subsidence. The coeval onset of active tectonism and volcanism is indicative of a mutual mechanism or linkage and may be triggered by the reactivation of major NE-SW and NW-SE faults in the CVZ and at the Somma-Vesuvius, respectively.

Due to severe volcanic activity during Stage 3, significant amounts of volcanic material were probably deposited offshore. A large-scale volcanic, potentially caldera-forming eruption namely the CI eruption occurred at ~39 ka in the Campi Flegrei area. An associated massive pyroclastic density current was emplaced in the Gulf of Naples with

maximum thickness of at least 230 m. Probably due to significant volcanoclastic input from the Campi Flegrei, the shelf prograded significantly towards the South in the Campi Flegrei area. Reactivation of a NW-SE fault at the Somma-Vesuvius and potentially also the reactivation of a NE-SW fault in the CVZ may be responsible for a maximum subsidence of the continental shelf of 255 m.

Stage 4 (0.02 Ma – present)

During Stage 4 (Fig. 3.9-D), sea-level rose from the LGM lowstand of 120 mbpsl to its present location. This phase seem to be tectonically relatively stable. Compared to Stage 1-3, only minor marine deposition occurred during this stage. The shelf edge has approximately reached its present day location. Downslope transport occurs along the Dohrn Canyon. The most significant event to affect the Gulf of Naples depositional environment was the NYT eruption at 15 ka, during which a massive pyroclastic density current was emplaced in the Gulf of Naples with a maximum thickness of at least 120 m.

3.6 Conclusions

On the foundation of a multi-frequency multichannel seismic dataset, we investigated the tectono-sedimentary evolution of the Gulf of Naples in interplay with volcanic activity. Our main findings are presented in a comprehensive 3D depositional model outlining the interaction between deposition, tectonism and volcanism during the past one million years. As this is the first spatial and temporal model of its kind, it represents an important complement to previously established conceptual 2D tectono-stratigraphic models (Milia and Torrente, 1999; Milia et al., 2003) as well as a significant contribution towards comprehending the tectonic development of the area as well as its linkage to adjacent volcanism. The here presented findings further underline the previously proposed close connection between tectonism and Quaternary volcanism along the Campania Margin.

More specifically, our findings suggest that tectonism in the Gulf of Naples, associated with NW-SE and NE-SW faults, was mainly active during two time intervals: (1) from 1 to 0.4 Ma and (2) from 0.14 to 0.02 Ma. During these periods, the Gulf of Naples has subsided by at least 1.3 km, which yields an average subsidence rate of ~2.6 m/kyr. The onset of tectonic activity at 0.14 Ma, is approximately coeval with the initiation of intense volcanism in the CVZ as well as at the Somma-Vesuvius and was interpreted as being related to the reactivation of major normal faults. In the CVZ, the reactivation of a NE-SW-trending fault probably led to further tectonic subsidence of the half graben, thereby facilitating the ascent of magma and, thus, eruptions. This suggests that the large-scale CI eruption at 39 ka was triggered by regional tectonism. At the Somma-Vesuvius, the reactivation of a NW-SE trending fault seems to have caused additional subsidence as well as eruptions. However, since 0.02 Ma, and thus including the NYT

eruption at 15 ka, there is no evidence of major subsidence in the Gulf of Naples, which may either indicate that the tectonic control on eruption mechanisms merely played a minor role during that time span, or that the seismic data were not able to resolve subsidence during this relatively short time interval.

Overall, the half-graben basin is filled with a minimum of 1.2-km Plio-Quaternary sediments. Most of the sedimentary fill was deposited during the timespan from 1 to 0.4 Ma with a high accumulation rate of 1.8 m/kyr. In contrast, during the tectonically stable timespan between 0.4 and 0.14 Ma, significantly lower sedimentation rates of maximally ~ 0.9 m/kyr were observed. The continental shelf underwent severe subaerial erosion during the MIS 6 lowstand at ~ 0.14 Ma, producing a prominent erosive unconformity (U3).

3.7 Acknowledgements

The GeoB08 seismic dataset was acquired during the CAFE-7/3 expedition funded by the Italian Research Council through the CNR Shiptime Programme (Oceanographic Cruise_CAFE_07), seismic acquisition was supported by German Research Foundation (DFG) within the ICDP priority programme (Grant No. SP296/30-1). The GeoB16 seismic dataset was acquired during the CAFE_2015 cruise funded by the Italian Research Council through the CNR Shiptime Programme (Oceanographic Cruise_CAFE_07), seismic acquisition was supported by German Research Foundation (DFG) within the IODP priority programme (Grant No. SP293/37-1). Data processing and analysis was funded through the DFG's ICDP priority programme (Grant No. SP296/34-1; SP296/34-2). The NAM seismic dataset was provided by the Institute for Coastal Marine Environment of the National Research Council (IAMC-CNR). Additional support was provided by the Bremen International Graduate School for Marine Sciences (GLOMAR). We are grateful to Schlumberger for providing the VISTA 2D/3D Seismic Data Processing software package and to IHS for providing the KINGDOM seismic interpretation software.

This page is intentionally left blank

Chapter 4

The Campi Flegrei caldera (Italy): formation and evolution in interplay with sea-level variations since the Campanian Ignimbrite eruption at 39 ka

Lena Steinmann^{1,2}, Volkhard Spiess¹, Marco Sacchi³

¹Faculty of Geosciences, University of Bremen, 28359 Klagfurter Str., Bremen, Germany

²MARUM – Center for Marine Environmental Sciences, University of Bremen, Leobener Str., 28359 Bremen, Germany

³Istituto per l'Ambiente Marino Costiero (IAMC), Consiglio Nazionale delle Ricerche (CNR), Calata Porta di Massa, 80133 Napoli, Italy

4 Abstract

To date, the origin of the Campi Flegrei caldera is still under debate and may be related to (1) a single caldera collapse associated with the Neapolitan Yellow Tuff (NYT) eruption, (2) two subsequent caldera collapses associated with the NYT and the preceding Campanian Ignimbrite (CI) eruptions forming a nested-caldera complex, or (3) not related to a caldera collapse after all. Here, we study the submerged portion of the caldera, which has favoured a marine depositional setting and, thus, represents an ideal location for the reconstruction of its formation history, utilizing multichannel seismic data. Volcanic deposits and edifices were seismically distinguished from sedimentary successions, and the stratigraphy could be refined and extended back to the Campanian Ignimbrite eruption at ~39 ka.

For the first time, high-resolution reflection seismic data revealed the existence of a nested-caldera complex formed during the CI eruption at ~39 ka and the more recent NYT eruption at ~15 ka. A ring-fault bounding an inner caldera collapse structure was clearly imaged. It appears that this inner ring-fault was initially activated during the CI caldera collapse and later reactivated during the NYT caldera collapse with different amounts of subsidence. The NYT caldera probably formed during an asymmetrical, piecemeal-like collapse with a maximum subsidence of ~75 m in the offshore portion. The vertical displacement related to the CI caldera collapse may be significantly larger.

The submerged caldera depression accommodates post-eruption sediments. Within this high-resolution archive, two major unconformities developed at ~ 8.6 ka and 5 ka, when resurgence-related uplift exceeded the rate of sea-level rise concurrent with the emersion of the La Starza terrace. A previously unknown post-collapse submarine volcanic mound located between Nisida Island and Nisida Bank probably formed between 4.8 and 3.7 ka. Also, the Penta Palummo Bank appears to be constructed of at least two monogenetic volcanic edifices, the Penta Palummo volcano formed at ~ 100 ka and a younger mushroom-shaped unit formed between 39 and 15 ka. The formation and evolution of the Campi Flegrei caldera in interplay with sea-level fluctuations over the past ~ 39 ka is presented in a comprehensive conceptual model. As the genesis of the Campi Flegrei caldera is still a hotly debated topic in literature, our discoveries can be regarded as a substantial advancement in the understanding of the Campi Flegrei volcanic area.

4.1 Introduction

Comprehending past volcanic eruptions is the key to improve our understanding of present-day volcanic activity and to assess potential hazards and risks of future eruptions. Since collapse calderas are typically formed by extremely destructive explosive eruptions, they have attracted particular attention in scientific communities and governmental institutions worldwide. Apart from devastatingly impacting environment and population, massive caldera-forming eruptions have the potential to trigger a global catastrophe second only to that from a large meteorite impact (Self, 2015).

In general, calderas are defined as subcircular topographic depressions originating from a collapse or subsidence into the top of a partly drained magma chamber during or immediately after an explosive volcanic eruption (Cole et al., 2005). Highly hazardous volcanic products from caldera-forming eruptions are pyroclastic density currents, often depositing large-volume ignimbrites. Understanding their dynamics and dispersal is essential in order to effectively mitigate risks to local populations (Neri et al., 2015a and references therein).

In the post-collapse phase, many calderas are characterized by resurgence (i.e., renewed inflation of the magma chamber), resulting in long-term uplift of the intra-caldera area (Smith and Bailey, 1968; Acocella et al., 2000; Cole et al., 2005). One prime example of a resurgent collapse caldera is the partly submerged Campi Flegrei caldera (CFc) located in southern Italy at the western border of the densely populated city of Naples. This caldera has been regarded as one of the world's most active calderas, demonstrated by recent unrest episodes accompanied by seismicity and increased fumarolic activity. A future eruption could expose nearly 2.5 million people to volcanic hazards. Thus, the CFc is considered as being one of the maximum risk volcanic areas on Earth.

Despite ample research, the formation history of the CFc is still controversial. Traditionally, the CFc has been regarded as a nested-caldera system, formed by two major ignimbritic eruptions namely the Campanian Ignimbrite (CI) eruption at ~ 39 ka and the Neapolitan Yellow Tuff (NYT) eruption at ~ 15 ka (e.g. Rosi et al., 1983; Barberi et al., 1991; Orsi et al., 1996; Deino et al., 2004; Acocella, 2008). On the other hand, it has been suggested that the caldera formation was related only to the NYT eruption, while the CI eruption was assumed to have occurred along fissure-type vents without leading to a collapse (e.g. Di Girolamo et al., 1984; Florio et al., 1999; De Vivo et al., 2001). Some authors have questioned the existence of a caldera in Campi Flegrei entirely (Bellucci et al., 2006; Milia et al., 2006; Milia and Torrente, 2007). Comprehending the genesis of the CFc is still a missing link in the understanding of the overall volcanic system and its dynamics. Investigations of the caldera subsurface structures therefore should shed light on its origin. Geophysical studies have provided important structural information of calderas in general and the CFc in particular. In the case of the CFc, the approximate location of the caldera depression and margin was determined based on gravimetric (Florio et al., 1999; Capuano and Achauer, 2003), magnetic (Secomandi et al., 2003) and refraction seismic data (Zollo et al., 2003). A more detailed image of the offshore sector of the CFc is provided by marine reflection seismic studies. However, most of these investigations were based on very high-resolution single-channel data using sparker and uniboom sources with frequencies above 1000 Hz, thus achieving only limited penetration from a few tens to hundred meter below the seafloor (e.g. Milia and Torrente, 2000; D’Argenio et al., 2004b; Sacchi et al., 2014). Moreover, many of the previously published very high-frequency single-channel datasets only exist as paper recordings (e.g. Fusi et al., 1991; Milia and Torrente, 2000; D’Argenio et al., 2004b), thus hampering the enhancement of data quality by modern processing procedures.

Here we present high-resolution multichannel seismic data, which use lower signal frequencies < 1000 Hz and provide a significantly better signal-to-noise ratio utilizing advanced processing techniques. The objective of the present study is to refine the stratigraphic and tectonic understanding of the offshore sector of the CFc. We investigate the interplay between sea-level variations and volcanic processes including caldera collapses and post-collapse deformation over the past ~ 39 ka. A comprehensive conceptual evolutionary model is presented, which may be regarded as a substantial step towards the understanding of the CFc formation and evolution.

4.2 Regional setting

The active Campi Flegrei volcanic field (also known as *Phlegrean Fields*) is situated between the Apennine Mountain range and the Tyrrhenian Sea in the graben-like structure of the Campanian Plain in Italy (Fig. 4.1). The most distinct volcanic feature is

the CFc, covering an area of ~ 130 km² defined by a quasi-circular depression, located both onshore and offshore. The submerged, southern caldera part reaches into the Gulf of Pozzuoli, a smaller embayment of the Gulf of Naples (Fig. 4.1). To the South, the CFc is bordered by the submarine Penta Palummo (PPB) and Misenò (MB) Banks as well as the Nisida Volcanic Complex, consisting of the submarine Nisida Bank (NB) and the subaerial Nisida Island (Fig. 4.1). The onshore caldera topography, in particular, has been intensively modified by post-caldera volcanism. Major morphological features in the Gulf of Naples are the incising *Dohrn Canyon* and the rugged seafloor area associated with the *Banco della Montagna* (Fig. 4.1).

Generally, it has been assumed that a large caldera depression bounded by an outer ring-fault was formed during the CI eruption at ~ 39 ka, while a smaller caldera depression bordered by an inner ring-fault was formed during the more recent NYT eruption at ~ 15 ka (Fig. 4.1) (e.g. Rosi et al., 1983; Barberi et al., 1991; Orsi et al., 1996; Deino et al., 2004; Acocella, 2008). In the post-collapse phase, volcanic activity continued with more than 60 intra-caldera eruptions, mostly occurring within three volcanic epochs, at 15-9.5 ka (epoch I), 8.6-8.2 ka (epoch II) and 4.8-3.7 ka (epoch III) (Di Vito et al., 1999; Di Renzo et al., 2011). The most recent eruption in 1538 AD followed a rapid episode of uplift and led to the formation of the Monte Nuovo tuff cone (Fig. 4.1). While the volcano-tectonic activity imposed a strong influence on the depositional environment in the Campi Flegrei volcanic area, also sea-level variations significantly affected the depositional regime. In fact, a physical link between Quaternary sea-level changes and intensified explosive volcanic activity in the Mediterranean has frequently been suggested (e.g. McGuire et al., 1997).

Since the 1960s, Campi Flegrei volcanic activity intensified as indicated by repeated bradyseism events (i.e., vertical ground movement), generally accompanied by seismicity with earthquakes as shallow as ~ 3 -4 km depth (De Natale et al., 1991; Troise et al., 2008) and increased fumarolic activity (Chiodini et al., 2015). Two main episodes of rapid uplift occurred in the central part of the CFc (town of Pozzuoli) between 1969–1972 and 1982–1984, generating a net uplift of 3.8 ± 0.2 m (Troise et al., 2008). These relatively recent short-term uplift phases were inferred to be triggered by the injection of magmatic fluids into a shallow hydrothermal system at ~ 2 km depth (Chiodini et al., 2015).

On the other hand, long-term uplift has occurred in the intra-caldera area with rates of several tens of meters within a few thousand years, being attributed to caldera resurgence (Orsi et al., 1996; Di Vito et al., 1999; Acocella, 2010; Sacchi et al., 2014). At the beginning of volcanic Epochs I and II at ~ 8.6 ka and ~ 5 ka, respectively (Cinque et al., 1985; Di Vito et al., 1999), resurgence-related uplift even exceeded the rate of sea-level rise, leading to the emersion of the previously submarine portion of the Gulf of Pozzuoli, the so-called *La Starza terrace* (Fig. 4.1). While at ~ 8.6 ka, the La Starza terrace was

only temporarily emerged, at ~ 5 ka, the final emersion of the La Starza terrace occurred. Presently, it is located at 30 to 55 m above sea-level. Offshore, a 5-km broad dome associated with a summit depression related to apical extension has developed in the course of resurgence-related uplift (Fig. 4.1) (Sacchi et al., 2014).

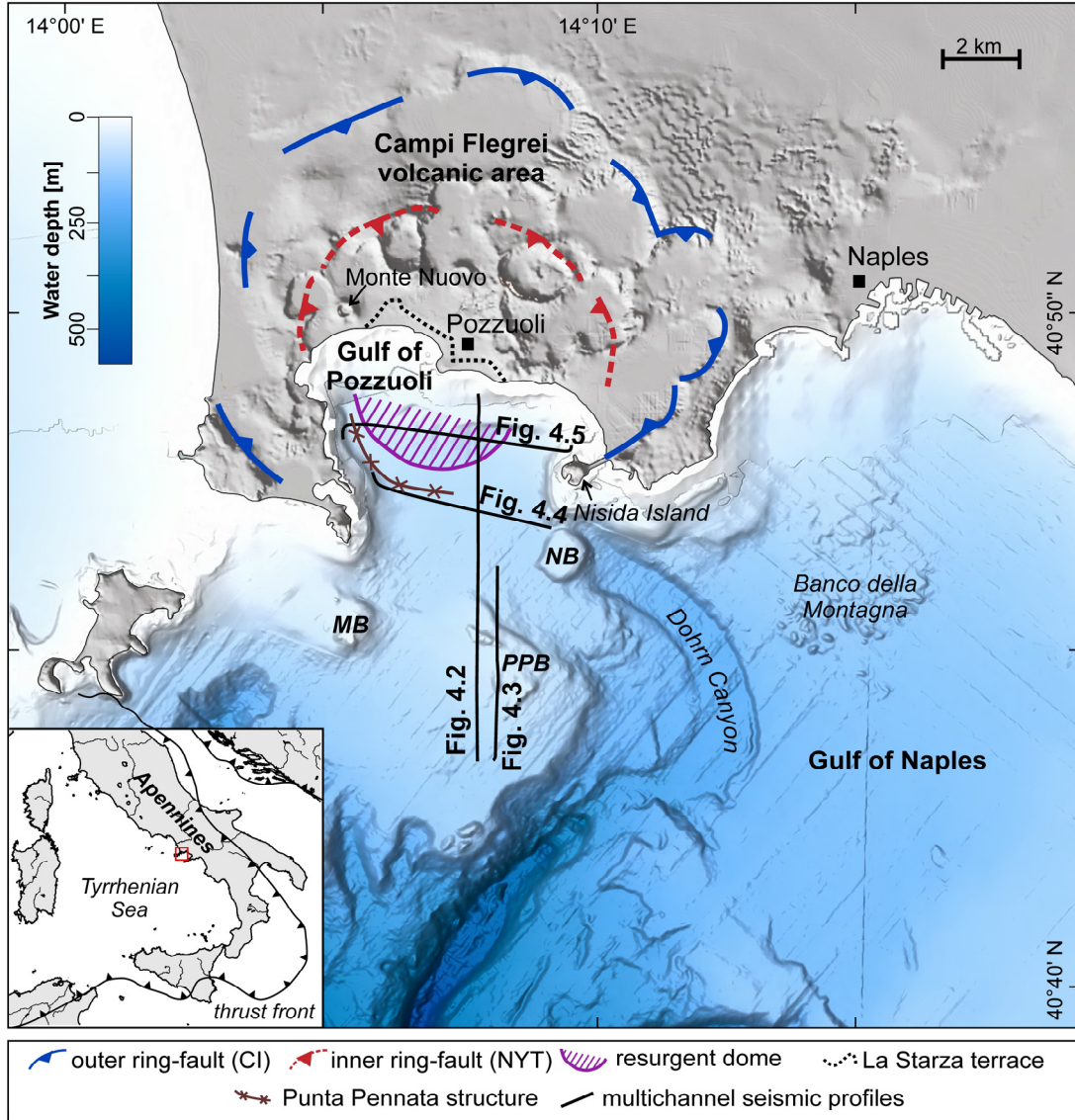


Fig. 4.1: Topography and bathymetry of the Campi Flegrei volcanic area and the Gulf of Naples with location of the presented multichannel seismic profiles. The locations of the onshore caldera rim and offshore resurgent dome were adapted from Acocella (2008) and Sacchi et al., (2014), respectively. MB = Miseno Bank, PPB = Penta Palummo Bank, NB = Nisida Bank.

4.3 Materials and methods

The high-resolution multichannel seismic profiles (Fig. 4.1) presented in this study, were collected during a research cruise in the Gulf of Naples and the Gulf of Pozzuoli in 2008. A mini GI-gun seismic source with 0.1 L chamber volumes produced frequencies up to 1000 Hz with the central frequency at ~ 250 Hz. The seismic signal was recorded with a

50-m long, 48-channel single hydrophone streamer. The multichannel processing routine included geometry setup, trace editing, bandpass filtering (30/60-800/1000 Hz), residual statics corrections, normal move-out correction, multiple suppression, common mid-point (CMP) binning and stacking, noise attenuation and time migration. Compared to single-channel data, multichannel processing allowed enhancing signal-to-noise ratio significantly by suppressing ambient noise and multiples, thereby increasing the overall imaging depth. In this respect, presented data are superior to previously published single-channel studies (e.g. Milia and Torrente, 2000; D'Argenio et al., 2004b; Sacchi et al., 2014).

The vertical resolution limit of the seismic dataset, which mostly depends on the source signal frequency, is ~ 2 m. The horizontal resolution is defined by the CMP bin size, which was set ~ 1 m (with an average fold of 9) in order to achieve maximum horizontal resolution. The seismic signal penetration is strongly influenced by high signal attenuation in volcanoclastic rocks and typically reaches ~ 250 ms TWT (~ 190 m).

4.4 Results

In this study, four selected high-resolution multichannel seismic profiles, crossing in different orientations the Gulf of Pozzuoli and the offshore structure of the CFc are presented (Fig. 4.1). The ~ 9.7 -km long Line GeoB08-050 (Fig. 4.2) extends from the inner shelf in the North to the outer shelf in the South. It passes over the resurgent dome, the margin of the CFc and the PPB. In order to illustrate the stacking pattern of the PPB, the 5.5-km long, N-S trending Line GeoB08-032 is presented (Fig. 4.3). The E-W oriented Lines GeoB08-070 and GeoB-08-065 intersect Line GeoB-08-050. Line GeoB08-070 (Fig. 4.4) has a length of ~ 5.3 km and covers the southern margin of the CFc. It ranges from the Punta Pennata structure in the East to the Nisida Complex in the West. Line GeoB08-065 (Fig. 4.5) has a length of ~ 6.6 km and images the resurgent dome as well as the eastern and western caldera margins.

4.4.1 Seismic analysis

The seismostratigraphic concept was based on the approach of Mitchum et al. (1977) involving seismic sequence and seismic facies analysis. In total, nine major seismic units were identified based on their seismic reflection pattern, reflection attributes, internal reflection configuration, external shape and reflection termination. Table 4.1 summarizes the main seismic unit characteristics. Along the caldera margin, all units are interrupted by reflection-free zones associated with overlying high-amplitude, reverse polarity reflections (Figs. 4.2, 4.4). Additionally, major structural features were identified and described in detail below. For conservative displacement and thickness estimations, two-way traveltimes (TWT) were converted to meters using a constant velocity of 1500 m/s.

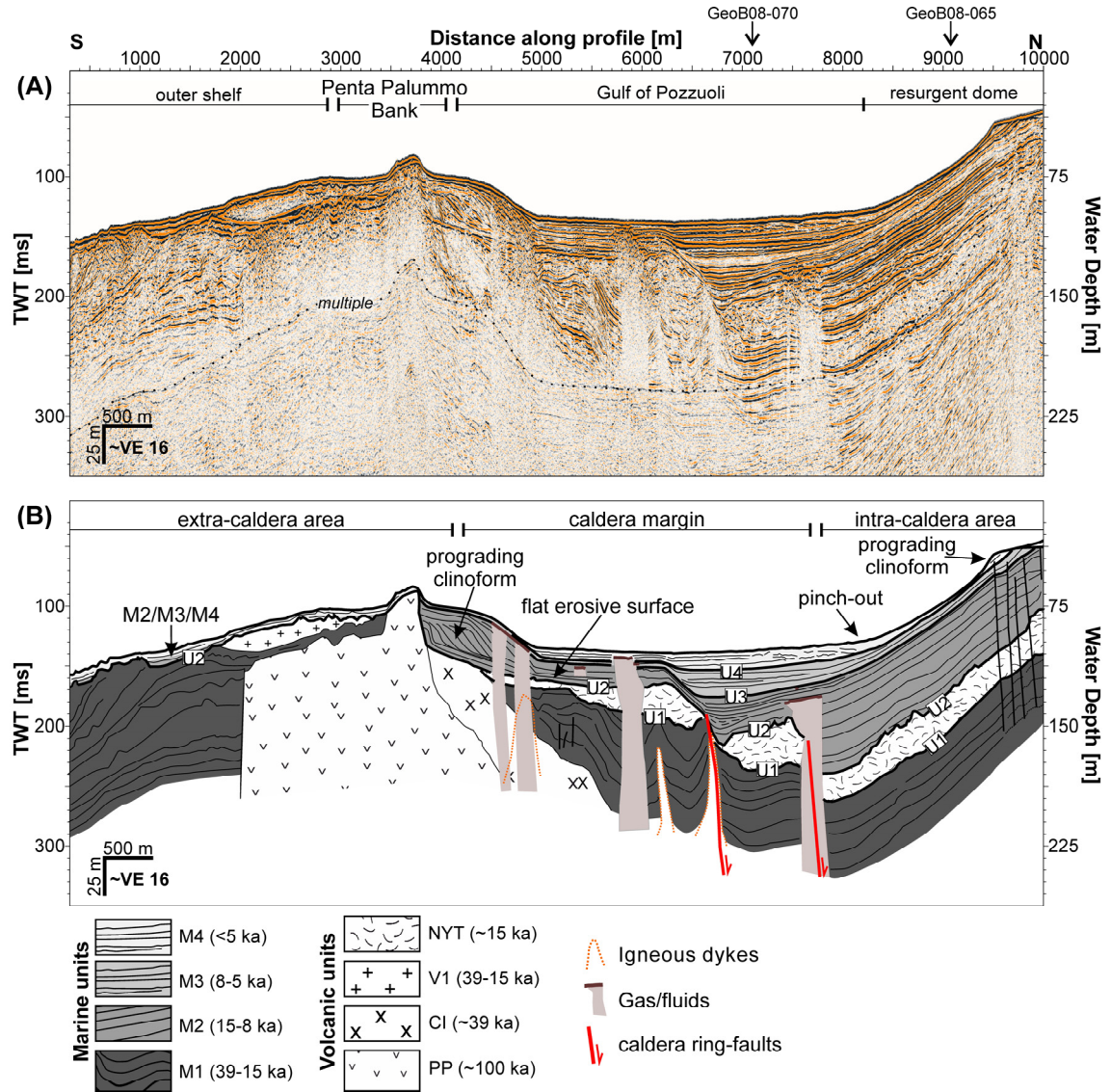


Fig. 4.2: N-S trending multichannel seismic profile GeoB08-050, showing the caldera ring-fault as well as different marine and volcanic Seismic Units in the offshore sector of the CFC (for location see Fig. 1). (A) shows the uninterpreted section and (B) shows the interpreted section.

Seismic Unit PP (*Penta Palummo volcano*)

Seismic Unit PP is associated with the bathymetric high of the PPB (Fig. 4.1). The base of this unit could not be recognized in the seismic data. It has an overall mounded shape characterized by a gently dipping flank ($\sim 5^\circ$) towards the Gulf of Pozzuoli and a steep scarp ($\sim 45^\circ$) on the outer shelf side (Figs. 4.2, 4.3).

Seismic Unit CI (*Campanian Ignimbrite*)

Seismic Unit CI covers Seismic Unit PP, as shown in Figure 4.2. However, in the other profiles the base of the CI lies beneath seismic signal penetration. Towards the centre of the Gulf of Pozzuoli, the top of CI descends beneath seismic signal penetration limit and, thus, could not be mapped (Fig. 4.2). The unit appears to be absent on the outer shelf.

In water depth of <120 m, the top of the CI represents a flat, erosive unconformity (U2) (Figs. 4.2, 4.3).

Seismic Unit V1 (*Volcanic 1*)

Seismic Unit V1 is located south of Seismic Unit PP and forms a pronounced bathymetric high at the seafloor, which is also related to the PPB (Figs. 4.1, 4.2, 4.3). It covers Seismic Units PP and M1 and is confined at its top by Unconformity U2 (Figs. 4.2, 4.3).

Seismic Unit NYT (*Neapolitan Yellow Tuff*)

Seismic Unit NYT was only identified in the Gulf of Pozzuoli and appears to be absent on the outer shelf (Fig. 4.2). In the vicinity of the PP, the top of the NYT is characterized by a relatively flat, high-amplitude reflection located in a water depth between 110 to 120 m (Fig. 4.2). This surface correlates with the erosive Unconformity U2, which loses its erosive character towards deeper water (Fig. 4.2). The base of the NYT corresponds to an irregular and erosional Unconformity (U1), cutting into the underlying strata (M1) (Fig. 4.4). The NYT unit is characterized by an irregular top with local, small-scale bathymetric highs (lumps, mound-like features) associated with the maximum unit thickness of ~52 ms TWT (~40 m) (Fig. 4.4).

Seismic Unit V2 (*Volcanic 2*)

Seismic Unit V2 is interbedded in Seismic Unit M4 (Fig. 4.4). It only occurs locally in the eastern sector of the Gulf of Pozzuoli between Nisida Island and Nisida Bank. It shows a mounded shape forming a distinct bathymetric high at the seafloor, which can also be recognized in the bathymetry (Fig. 4.1).

Seismic Unit M1 (*Marine 1*)

Seismic Unit M1 can be found on the outer shelf as well as in the Gulf of Pozzuoli (Figs. 4.2-4.4). In the vicinity of the PPB on the Gulf of Pozzuoli side, the well-layered, continuous reflections pass into discontinuous, strongly deformed strata disrupted by reflection-free zones often accompanied by upward-bending reflections (Fig. 4.2). In this area, the reflections are being truncated by the erosional Unconformity U1 (Figs. 4.2, 4.4). On the outer shelf, the reflections of M1 show a complex prograding stacking pattern and are being truncated by an irregular, high-amplitude angular unconformity U2 (Fig. 4.2). Along the eastern and western caldera margin, M1 seems to be absent (Fig. 4.5).

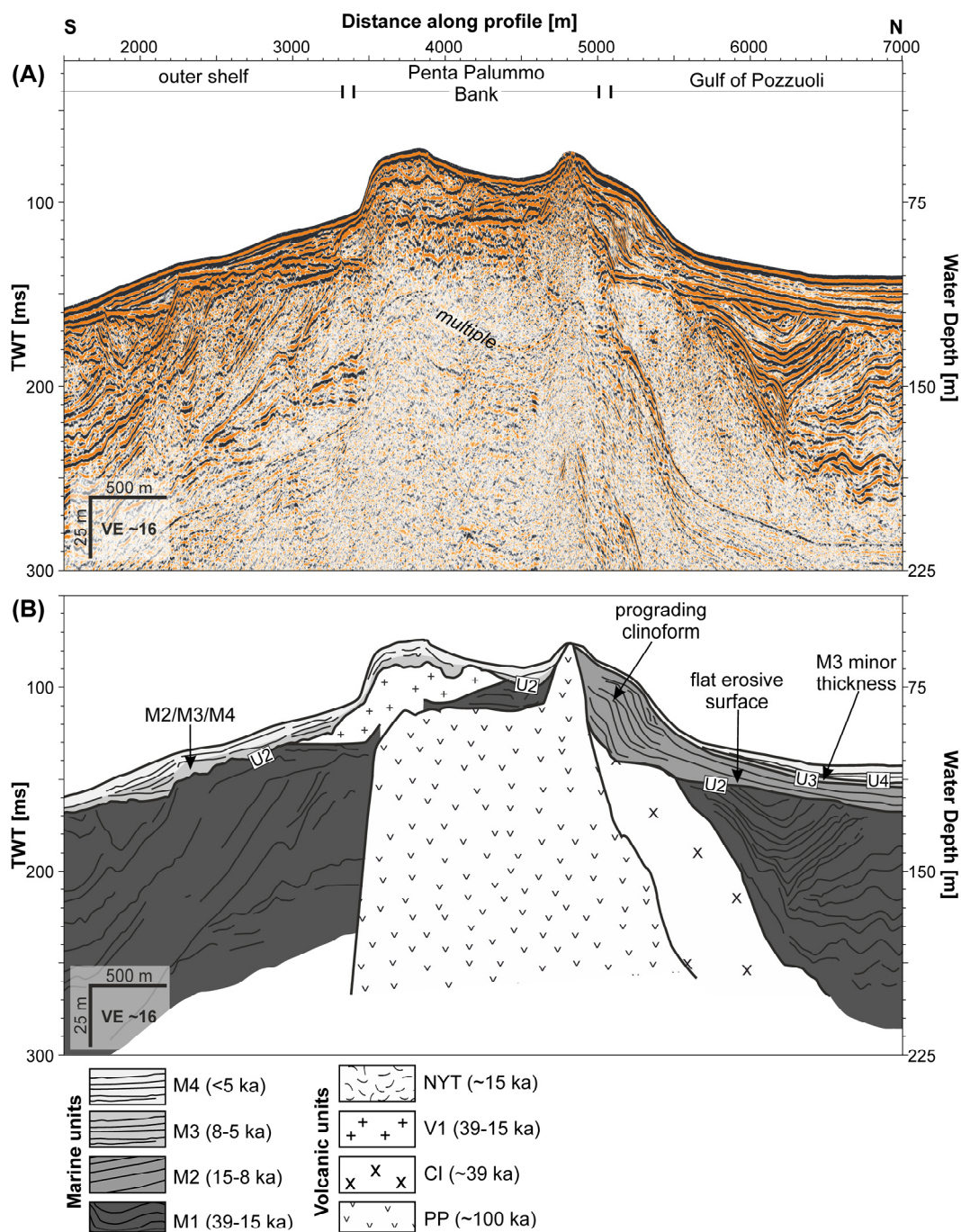


Fig. 4.3: N-S trending multichannel seismic profile GeoB08-032, crossing the PPB and illustrating the different marine and volcanic Seismic Units (for location see Fig. 4.1). (A) shows the uninterpreted section and (B) shows the interpreted section.

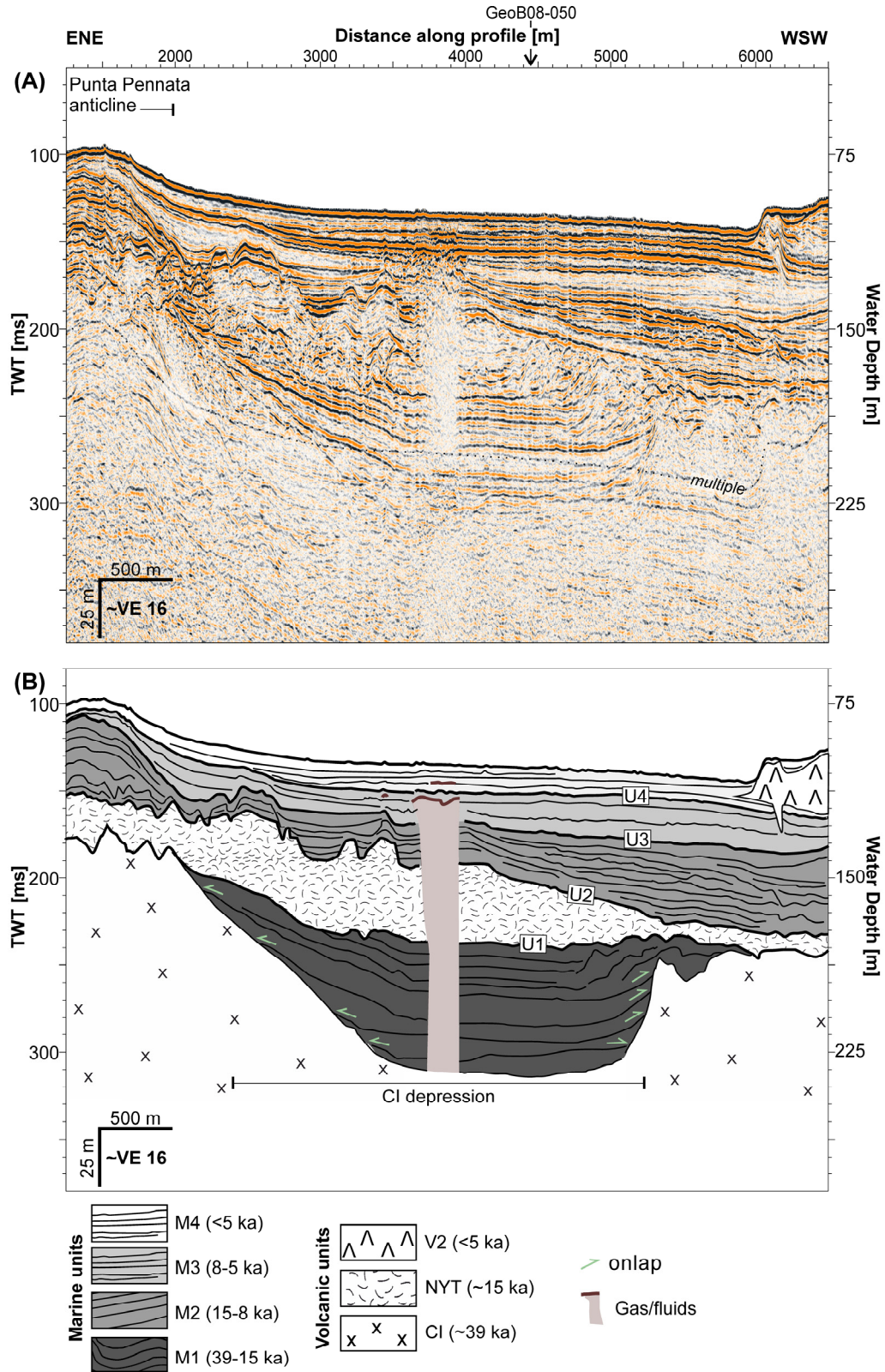


Fig. 4.4: ENE-WSW trending multichannel seismic profile GeoB08-070, showing depression in the CI deposit, which probably represents the caldera depression, as well as different marine and volcanic Seismic Units in the offshore sector of the CFc (for location see Fig. 4.1). (A) shows the uninterpreted section and (B) shows the interpreted section.

Seismic Unit M2 (*Marine 2*)

Seismic Unit M2 lies on top of Unconformity U2 and shows an overall aggradational stacking pattern. In the vicinity of the PP, it exhibits a sigmoidal prograding clinoform (Fig. 4.2). Unit M2 has a maximum thickness of ~90 ms TWT (~68 m) in the intra-calddera area (Figs. 4.2, 4.5). It is not possible to discriminate between M2, M3 and M4 on the outer shelf due to the reduced stratigraphic thickness (Figs. 4.2, 4.3).

Seismic Unit M3 (*Marine 3*)

Reflections of Seismic Unit M3 onlap on the underlying unconformity (U3) and, thus, pinch out towards the center of the resurgent dome leading to a minimum thickness of ~8 ms TWT (~6 m) (Fig. 4.5). While M3 is clearly visible in the Gulf of Pozzuoli, Units M2, M3 and M4 on the outer shelf comprise a thin veneer not possible to resolve (Figs. 4.2, 4.3).

Seismic Unit M4 (*Marine 4*)

Similar to M3, the reflections of the uppermost Seismic Unit M4 terminate as onlap on an underlying unconformity (U4) and pinch out towards the top of the resurgent dome, creating a thickness minimum (Figs. 4.2, 4.5). In shallow water depth, a minor oblique-tangential prograding clinoform can be observed (Fig. 4.2). While M3 is clearly visible in the Gulf of Pozzuoli, it is not possible to resolve M2, M3 and M4 on the outer shelf for reasons mentioned above (Figs. 4.2, 4.3).

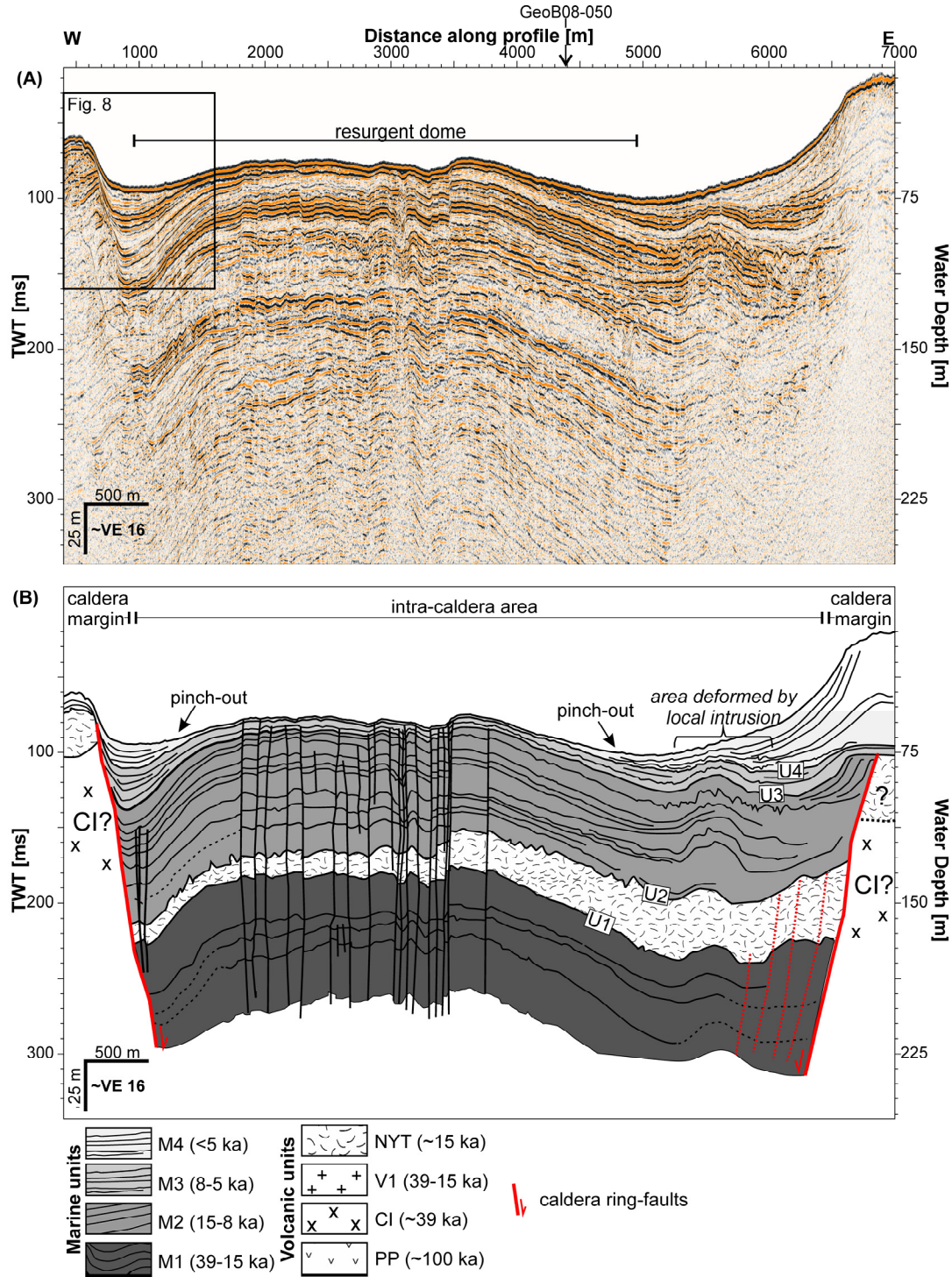


Fig. 4.5: E-W trending multichannel seismic profile GeoB08-065, showing the resurgent dome and associated fault swarm, main caldera ring-fault as well as different marine and volcanic Seismic Units located in the offshore sector of the CFc (for location see Fig. 4.1). (A) shows the uninterpreted section and (B) shows the interpreted section.

Structures

The most striking structural feature observed in the multichannel seismic dataset is a distinct normal fault located along the caldera margin, labelled *caldera ring-fault* (Figs. 4.2, 4.5). In the South, this ring-fault occurs as ring-fault zone with two vertical offsets

(Fig. 4.2). The ring-fault is characterized by variable amounts of displacement of the NYT (Fig. 4.2, 4.5) and the underlying Unit M1 (Fig. 4.2). A maximum offset of ~ 130 ms TWT (~ 98 m) of the NYT at the ring-fault can be observed along the western caldera margin (Fig. 4.5), while the displacement in the East and South is less with ~ 100 ms TWT (~ 75 m) (Fig. 4.5) and 70 ms TWT (~ 53 m) (Fig. 4.2), respectively. Furthermore, in Line GeoB08-065 it appears that the CI is also displaced along this ring-fault (Fig. 4.5). However, in the caldera depression, the top of the CI deposits could not be identified (Fig. 4.5) which is probably due to its location below the seismic penetration limit. On this assumption, we inferred that the CI is probably located below 300 ms TWT, suggesting an offset of at least 200 ms TWT (~ 150 m) along the ring-fault. Furthermore, in Line GeoB08-070, the CI clearly exhibits a distinct depression filled with ~ 90 ms TWT (~ 68 m) thick deposit of Unit M1 (Fig. 4.4), which also suggests a vertical displacement prior to M1 deposition.








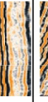
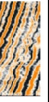
In addition to this main normal fault with large offsets, a swarm of high-angle normal faults with a maximum displacement of 10 ms TWT (~ 8 m) and an associated small-scale depression can be observed at the crest of the resurgent dome (Fig. 4.5). These faults displace all identified seismic units down to a subsurface depth of ~ 250 ms TWT (~ 190 m).

4.5 Discussion

4.5.1 Stratigraphic context

Based on the above described seismic characteristics, deposits of volcanic origin and volcanic edifices could be distinguished from marine sediments. While the volcanic units (PP, CI, NYT, V1 and V2) exhibit reflection-free facies, chaotic reflection pattern, irregular bounding surfaces and a mounded external shape, the marine units (M1-M4) are stratified with continuous reflections and parallel to subparallel reflection configuration. The reflection-free zones associated with overlying high-amplitude, reversed polarity reflections were interpreted as trapped gases and/or fluids (Figs 4.2, 4.4). A detailed interpretation of each seismic unit with respect to their origin and age is provided in the following sections and summarized in Table 4.1. Figure 4.6 illustrates the volcanic events and sea-level fluctuations in stratigraphic context.

Table 4.1: Seismic facies description and related geological interpretation.

Seismic Unit	Seismic reflection pattern	Continuity	Amplitude	Reflection configuration	External shape	Geological interpretation	Age range
V2		Discontinuous	Low with interbedded high-amplitude reflections	Contorted to chaotic	Mound	Mounded volcanic edifice	4.8 – 3.8 ka
NYT		Discontinuous	Low with interbedded high-amplitude reflections	Chaotic	Irregular	Pyroclastic density current deposit related to the NYT eruption	~15 ka
V1		Discontinuous	High	Contorted to chaotic	Mound (mushroom-shaped)	Mounded volcanic edifice	15 – 39 ka
CI		Reflection-free	Reflection-free with few interbedded high-amplitude reflections	Reflection-free	Irregular	Pyroclastic density current deposit related to the CI eruption	~39 ka
PP		Discontinuous	Reflection-free facies with high-amplitude reflections at upper boundary	Reflection-free	Mound	Volcanic edifice corresponding to the Penta Palummo volcano	~100 ka
M4		Continuous	Low to high	Parallel to subparallel	Wedge	Highstand marine deposits deposited during caldera resurgence	<5 ka
M3		Continuous	Gradually increasing from bottom to top	Parallel to subparallel	Wedge	Transgressive marine deposits deposited during caldera resurgence	5 – 8.6 ka
M2		Continuous	Moderate to high	Parallel to subparallel Local sigmoidal prograding clinoform	Fill	Transgressive marine deposits rapidly filling the caldera depression after the NYT collapse	8.6 – 15 ka
M1		Variable	Moderate to high	Variable	Fill	Transgressive and lowstand marine deposits deposited between the CI and NYT eruptions and filling the CI caldera depression	15 – 39 ka
Volcanic deposits							
Marine deposits							

Volcanic deposition, edifices and related features

The acoustically transparent Seismic Unit PP corresponds to the Penta Palummo volcano (Milia, 2010), which outcrops at the PPB (Figs. 4.1-4.3). Previous seismostratigraphic studies suggest that it was formed ~100 ka ago (Milia and Torrente, 2000; Milia, 2010). Another volcanic unit (V1) is also associated with a bathymetric high at PPB and appears to be younger than the PP volcano, as it is stratigraphically located above it (Figs. 4.2, 4.3). These two monogenetic volcanoes are separated by an inter-ruptive sedimentary unit (M1). Based on its stratigraphic location between M1 and Unconformity U2 the age of V1 was determined to be between 39 and 15 ka (see section *Marine deposition* for age determination of U2 and M1).

Towards the Gulf of Pozzuoli, the PP volcano is overlain by Seismic Unit CI, which was interpreted as pyroclastic density current deposit related to the CI eruption at ~39 ka (De Vivo et al., 2001). The lack of reflectivity suggests a rapid emplacement and high porosity as similarly described for the Taupo ignimbrite in New Zealand (Davy and Caldwell, 1998). Other seismostratigraphic studies documented the widespread occurrence of the CI in the Gulf of Naples and reported a similar reflection-free seismic signature (e.g. Fusi et al., 1991; D'Argenio et al., 2004b).

Seismic Unit NYT shows a clear flow-like depositional character indicated by a chaotic seismic facies, an irregular top and local erosion of the underlying strata M1 (Figs. 4.2-4.4). Based on its stratigraphic position and considering the strongly volcanically influenced depositional regime, these observations suggest that Seismic Unit NYT represents a pyroclastic density current deposit associated with the NYT eruption at ~15 ka (Deino et al., 2004). The interpretation is in accordance with findings from other seismoacoustic studies, which identified the top of the NYT at similar depths without being able to reliably image the lower limit and underlying strata (Milia and Torrente, 2000; D'Argenio et al., 2004b; Aiello et al., 2012; Sacchi et al., 2014). Similar seismic characteristics associated with pyroclastic density current deposits including reflection-free facies, chaotic reflection pattern and irregular bounding surfaces have also been observed in other submarine caldera settings such as the Tonga Arc (Kim et al., 2013). Further distinguishing features of the NYT are local bathymetric highs deforming the overlying strata (Fig. 4.4), thereby implying a diapiric, post-emplacement nature. Similar mounds were described further at the *Banco della Montagna* (Fig. 4.1) and interpreted as diapiric structures involving volcanoclastic deposits from the NYT eruption (D'Argenio et al., 2004a; Passaro et al., 2014; Passaro et al., 2016). The NYT deposits could not be identified on the outer shelf south of the PPB (Fig. 4.2), which indicates that the PPB likely acted as barrier for the pyroclastic density current.

Seismic Unit V2 occurs only locally between Nisida Island and Nisida Bank and was interpreted as previously unidentified volcanic mound (Fig. 4.4). V2 is interbedded in M4

and, thus, its inferred age is <5 ka (see section *Marine deposition* for age determination of M4). V2 was probably formed during Volcanic Epoch III between 4.8 and 3.8 ka.

Further noteworthy local volcanic features, occurring along the southern caldera margin, are conduit-like reflection-free zones associated with surrounding upward-bending reflections of M1 (Fig. 4.2). Caldera margins are typically regarded as tectonically weak, favoring the emplacement of post-collapse magmatic intrusions (Walter, 2008). Hence, these zones were interpreted as igneous dykes. As they appear to deform the reflections of M1, suggesting post-depositional emplacement, their inferred age is <39 ka.

Furthermore, deformation of Units M1, NYT, M2 and M3 probably related to a small-scale intrusion in the vicinity of the caldera fault dated at ~ 3.9 ka (Sacchi et al., 2014) can be observed on Line GeoB08-065 at distance 5500 m (Fig. 4.5). Previously, this intrusion was interpreted as being situated at

shallow subsurface depth of ~ 130 m (Sacchi et al., 2014). However, the multichannel seismic data show that the deeper lying units (NYT, M1) are also deformed by this intrusion (Fig. 4.5), thus, suggesting that the intrusion is actually located beneath the seismic penetration limit.

Marine deposition

In the Gulf of Pozzuoli, M1 is overlain by the NYT and bounded at its bottom by the CI, implying deposition between 39 ka and 15 ka. Here, the top of M1, Unconformity U1, is characterized by local erosion interpreted as being related to the rapid, flow-like

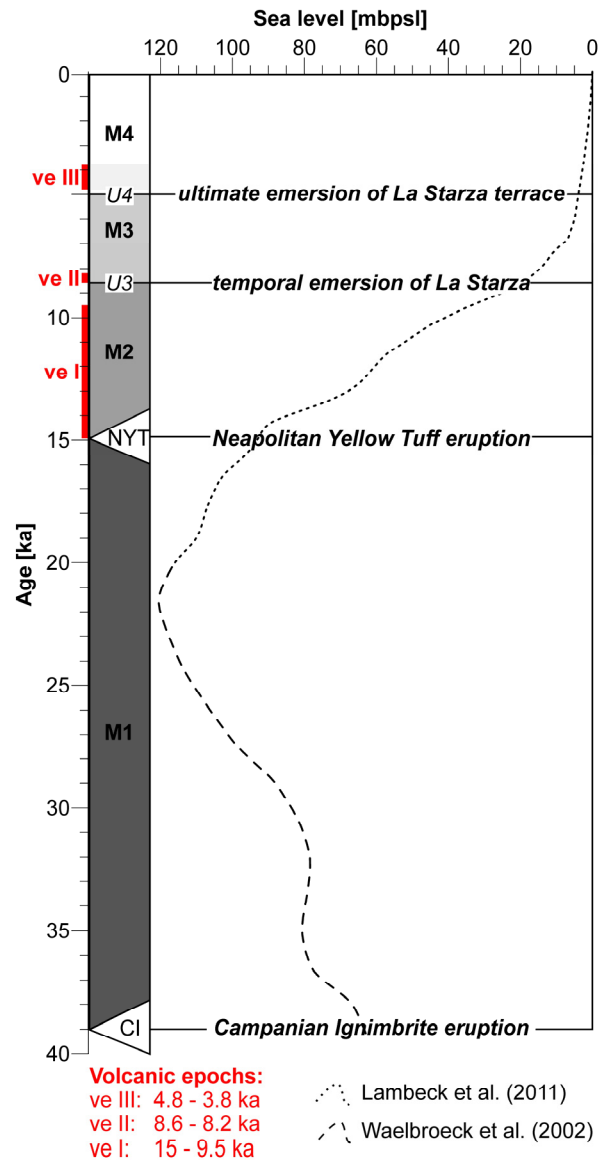


Fig. 4.6: Stratigraphic column and volcanic activity in correlation with sea level variations. The three volcanic epochs (ve) are indicated in red. Sea level curve from 0 -20 ka adapted from Lambeck et al. (2011) and from 20-40 ka adapted from Waelbroeck et al. (2002).

emplacement of the NYT (Fig. 4.2, 4.4). On the outer shelf, where the NYT is absent and the CI is either absent or located beneath the limits of seismic resolution, M1 is eroded at its top by Unconformity U2. This surface was likely formed by a succession of erosional phases including (1) shoreline erosion during sea-level fall, (2) erosion under subaerial conditions during LGM lowstand, and (3) reworking by coastal marine processes during sea-level rise. It represents a transgressive surface developed between 18 and 15 ka ago.

The NYT is overlain by marine Unit M2. Based on its stratigraphic position between the NYT and M3, it can be assumed that M2 deposited during sea-level rise between 15 ka and 8 ka (see below for age determination of M3).

M2 is overlain by the significantly thinner marine Unit M3, which is bounded at its base by Unconformity U3. U3 probably formed at the beginning of Volcanic Epoch II, at ~8.6 ka, when uplift related to resurgence exceeded sea-level rise, leading to the temporal emersion of the La Starza terrace (Fig. 4.6). Consequently, the accommodation space on the resurgent dome was limited, creating onlap termination of the reflections of M3 onto U3 and a hiatus and associated thickness minimum in the most uplifted area (Figs. 4.2, 4.5). The top of M3, Unconformity U4, probably formed as result of another phase of resurgence-related uplift exceeding the rate of sea-level rise at the beginning of Volcanic Epoch III, at ~5 ka, which led to the final emersion of the La Starza terrace (Fig. 4.6). Thus, it can be inferred that M3 deposited between 8.6 and 5 ka. Therefore, the uppermost marine Unit M4, which lies above U4, has been deposited since ~5 ka. U4 also marks the limitation of accommodation space on the resurgent dome, which again can be seen as distinct onlap reflection terminations and associated thickness minimum of the overlying Unit M4 (Figs. 4.2, 4.5).

During the deposition of marine Units M2-M4, particularly the onshore sector of the Campi Flegrei volcanic area was dominated by intense volcanic activity associated with volcanic Epochs I (14.9-9.5 ka), II (8.6-8.2 ka) and III (4.8-3.8 ka). Therefore, it can be inferred that these units consist to some extent of reworked volcanoclastic material and possibly also some small-scale (below seismic resolution limit) interlayered debris flows and/or minor pyroclastic density currents.

4.5.2 Caldera formation and evolution

On the basis of the multichannel seismic dataset, we investigated the interplay between volcano-tectonic processes and sea-level variations in the offshore sector of the CFc since ~39 ka. Based on the stratigraphic location of the main pyroclastic units (i.e., NYT and CI), inferences were drawn about the depositional environment during and after the respective eruptions, providing insights into the caldera formation history. The seismic data show indication for two separate caldera collapses related to the CI eruption at ~39 ka and the NYT eruption at ~15 ka. Thus, the findings suggest the existence of a

nested-caldera system. The ring-fault we identified in the seismic data probably represents the inner caldera ring-fault (Fig. 4.1), which seems to have already been activated during the CI collapse and later reactivated during the NYT collapse. On the basis of the E-W oriented multichannel seismic profile GeoB08-065 (Fig. 4.5), a 7-stage model for the CFc formation and evolution in interplay with sea-level variations since 39 ka (Fig. 4.7) was developed and is further described below.

CI eruption and caldera collapse (~39 ka)

According to global mean sea-level reconstructions, sea-level was at ~60 meters below present sea-level (=mbpsl) at time of the CI eruption (Waelbroeck et al., 2002) (Fig. 4.6). We identified the CI deposit in water as shallow as 75 m, suggesting that the CI pyroclastic density current entered the sea and deposited under shallow marine conditions. Traditionally, it has been assumed that pyroclastic density currents are disrupted and transformed into water-supported mass-flows when entering the ocean (Cas and Wright, 1991). However, according to analogue models, pyroclastic density currents with volumes exceeding 10 km³ are capable of temporarily pushing back the shoreline in a shallow marine setting, allowing for the contemporaneous emplacement of hot ignimbrite on the seabed (Legros and Druitt, 2000). Thus, it is likely that the CI pyroclastic density current, which had an estimated volume of ~130 km³ (Pyle et al., 2006), caused a temporal retreat of the shoreline, implying that the deposit identified as CI in the seismic data represents a primary pyroclastic density current deposit (i.e., ignimbrite).

Line GeoB08-070 clearly shows the occurrence of a depression in the CI deposit (Fig. 4.4), probably formed by a caldera collapse associated with the CI eruption. This hypothesis is further strengthened by observations from Line GeoB08-065, where we found the top of the CI deposit in water depth between 75 and 110 m at the eastern and western margins, respectively, but not in the (with the seismic data imaged) uppermost 200 ms TWT (~150 m) of the intra-caldera depression (Fig. 4.5). Also, Line GeoB08-050 shows that the CI unit descends below the seismic signal penetration limit towards the intra-caldera area (Fig. 4.2). Thus, we assume that the top of CI is significantly deeper within the intra-caldera depression, which is only explained by subsidence related to the caldera collapse that occurred as consequence of the CI eruption (see *Stage 1* of our caldera-evolutionary model (Fig. 4.7-A)). The cumulative vertical displacement of the CI along the caldera ring-fault is at least 150 m. However, as 75 m of subsidence must be attributed to the subsequent NYT caldera collapse (see section *NYT eruption and caldera collapse*), the CI caldera collapse accounts for a minimum of 75 m. As we were not able to image the depth of the CI caldera floor in the seismic data, the total displacement could be significantly higher. For instance, an average downthrow of ~700-800 m was previously suggested based on onshore borehole observations (Barberi et al.,

1991) while tomographic studies indicate a collapse in the range of 1-2 km (Zollo et al., 2003; Judenherc and Zollo, 2004).

Inter-eruptive phase (39 - 15 ka)

The timespan between the two caldera-forming events, the CI and NYT eruptions, was characterized by sea-level variations towards the LGM (~20 ka), which we illustrated in two stages (Stages 2, 3) (Figs. 4.7-B/-C). The CI caldera depression created significant accommodation space and was probably submerged during the LGM when sea-level was at ~120 mbpsl (Fig. 4.6), facilitating the deposition of marine sediments (Fig. 4.7-B). It is filled with at least 93 ms TWT (~70 m) thick marine sediments (M1), deposited between the CI and NYT eruption. In contrast, these deposits cannot be found at the eastern and western caldera margin (Fig. 4.5). In fact, the flat top of the CI along the caldera margin (Fig. 4.2) likely indicates erosion during sea-level fall and under subaerial conditions during the LGM lowstand (Fig. 4.7-B). Between LGM and NYT eruption (20 – 15 ka), sea-level rose at moderate rates from ~120 to ~93 mbpsl (~5.4 m/ka) (Fig. 4.6), further increasing the accommodation space in the caldera depression and facilitating the deposition of marine sediment (M1) (Fig. 4.7-C).

NYT eruption and caldera collapse (~15 ka)

At the time of the NYT eruption and subsequent caldera collapse, sea-level was positioned at ~93 mbpsl (Lambeck et al., 2011) (Fig. 4.6). In the East, the base of the NYT outside of the caldera depression is found at ~145 ms TWT (~110 m) (Fig. 4.5), while in the South it is located at ~186 ms TWT (~140 m) (Fig. 4.2). Considering the fact that sea-level was at ~93 mbpsl at the time of the NYT eruption (Fig. 4.6), it can be deduced that the Gulf of Pozzuoli was already (at least partially) submerged and, thus, that the NYT pyroclastic density current deposited in a shoreline or shallow marine setting similar as during the CI eruption. In the East, the top of the NYT is located at ~100 ms TWT (~75 m) (Fig. 4.5), implying that its rapid emplacement caused a local displacement of the shoreline, leading to subaerial conditions. The estimated volume of the NYT ignimbrite deposit is ~15 km³ (Scarpati et al., 1993), thus, the NYT pyroclastic density current meets the requirements for being capable of displacing the shoreline in a shallow marine setting (Legros and Druitt, 2000).

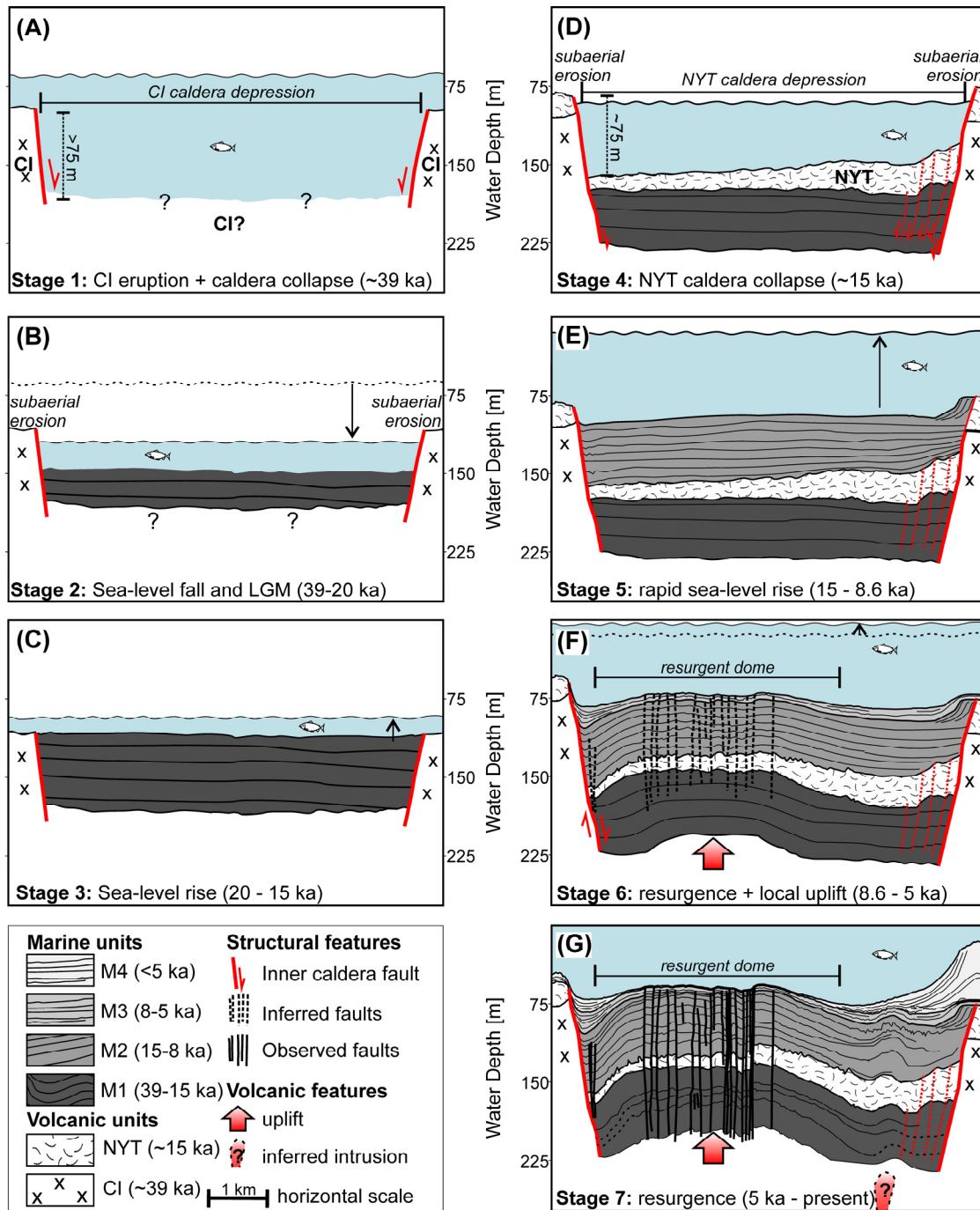


Fig. 4.7: Conceptual 2-dimensional reconstruction of the caldera formation and evolution since ~39 ka based on GeoB08-065 (Fig. 4.5). The model shows the caldera formation in the course of the CI and NYT eruption as well as subsequent deformation and deposition in interplay with sea-level variations. For detailed explanation see text in section 4.5.2.

In the course of the caldera collapse, seawater entered the caldera depression re-establishing submarine conditions, while the margin underwent subaerial erosion as shown in evolutionary *Stage 4* (Fig. 4.7-D). In the southern Gulf of Pozzuoli, the NYT pyroclastic density current probably entered the sea and deposited under marine

conditions. The PPB was subaerially exposed, separating the outer shelf from the Gulf of Pozzuoli and acting as a barrier for the NYT dispersal (Fig. 4.2).

Along the western caldera margin, the base of the NYT can be found in a depth as shallow as 100 ms TWT (~ 75 m) (Fig. 4.5). This area, however, experienced ~ 46 ms TWT (~ 35 m) post-caldera tectonic uplift associated with the Punta Pennata structure (see section *Post-collapse deformation and deposition*). Thus, the present position of the NYT along the western caldera margin does not represent the original elevation (i.e., paleo-surface) at the time of emplacement. Instead, if corrected for this uplift, the base of the NYT lies at similar depth as observed along the eastern caldera margin (~ 145 ms TWT; ~ 110 m) (Fig. 4.5). Taking the post-collapse uplift of the western caldera margin into account, we estimated a subsidence amount of ~ 100 ms TWT (~ 75 m) along the eastern and western caldera margin related to the NYT caldera collapse. Comparing this value to the southern sector of the caldera, it becomes obvious that the displacement is less pronounced with only ~ 70 ms TWT (~ 53 m) offset (Fig. 4.2). These variable displacement values suggest a non-uniform subsidence style, thereby indicating an asymmetrical caldera collapse such as a piecemeal or trap-door collapse style rather than a symmetrical caldera collapse (Cole et al., 2005). An asymmetrical caldera collapse might be related to a relatively small-volume eruption, an asymmetrical magma chamber, or regional tectonic influence (Lipman, 1997).

Post-collapse deformation and deposition (15 ka – present)

The post-collapse phase was characterized by sea-level rise, resurgence, post-collapse eruptions and local uplift events, summarized in *Stages 5 to 7* (Figs. 4.7-E to -G).

Between 15 and 8.6 ka (*Stage 5*), sea-level rose considerably from ~ 93 to ~ 19 mbpsl (11.5 m/ka) (Fig. 4.6). This rapid transgression in combination with the previous NYT caldera collapse created significant accommodation space in the intra-caldera depression, which had rapidly been filled by marine Unit M2 (Fig. 4.7-E). This period was characterized by intense activity related to Volcanic Epoch I (14.9 - 9.5 ka).

Between 8.6 and 5 ka (*Stage 6*) sea-level rose at a moderate rate from ~ 19 to ~ 4 mbpsl (~ 4 m/ka) (Fig. 4.6) and volcanic activity related to Volcanic Epoch II (8.6 – 8.2 ka). At the beginning of this stage, uplift rates related to resurgence exceeded sea-level rise, resulting in the formation of a wide dome probably already accompanied by extensional fractures at its crest and the formation of Unconformity U3. Seismic Unit M3 deposited during this time (Fig. 4.7-F). Its thickness is relatively small compared to marine Unit M2, which is a result of reduced accommodation space due to resurgence-related uplift in the centre of the caldera and decreased rate of sea-level rise.

Furthermore, since 8.6 ka, the western caldera margin underwent local post-collapse, synsedimentary uplift. This is indicated by local thickness variations of M3 and M4 in combination with upward bending, onlapping reflections across the western caldera

margin (Fig. 4.8). As consequence of this local uplift, accommodation space was limited on the uplifted block as evident by the absence (or minor thickness of <1 m) of M3 (Figs. 4.5, 4.8). During that time, sedimentation was focused along the hanging wall side as indicated by a relative thickness increase of M3 (Fig. 4.8). Furthermore, our seismic data suggest that the activity of this uplift has decreased since ~5 ka as indicated by a drape-like shape of M4 on top of the uplifted block (Fig. 4.8). This uplifted area likely corresponds to the westward continuation of the arc-shaped Punta Pennata structure, previously interpreted as detachment fold of tectonic origin related to simple shear regimes (Milia and Torrente, 2000).

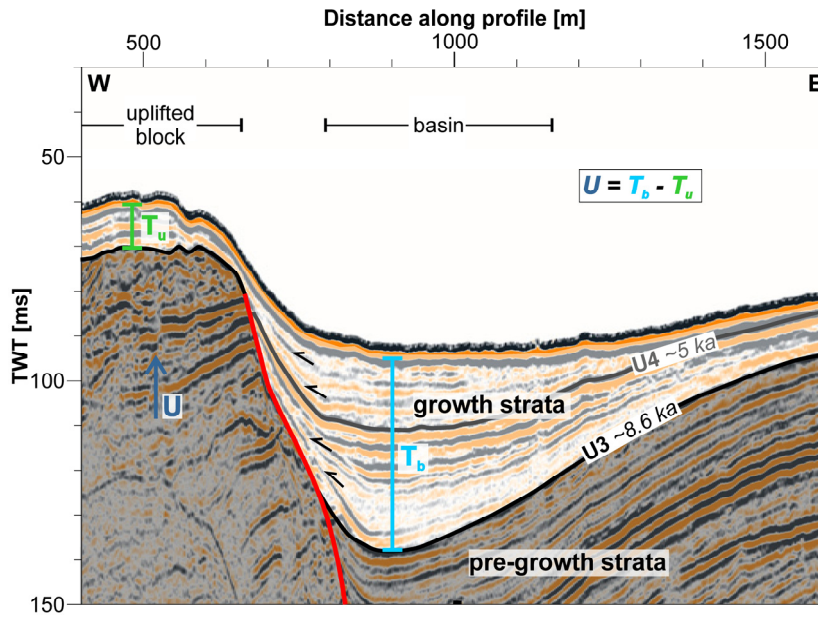


Fig. 4.8: Close-up of GeoB08-065 to illustrate the mathematical relationship between total uplift of the western margin (U), sediment thickness on the uplifted block (T_u) and sediment thickness in the basin (T_b). Black arrows indicate onlap reflection termination.

Thickness variations of growth strata (in this case M3 and M4) across synsedimentary structures are directly related to variations in displacement rates along faults and folds and, thus, may be used to estimate their kinematics (Pochat et al., 2009 and references therein). According to Suppe et al. (1992), the total amount of uplift U is equal to the growth strata thickness along the basin T_b minus the growth strata thickness on the uplifted block T_u (Fig. 4.7). Hence, we estimated the total amount of uplift that has occurred since ~8.6 ka to be ~46 ms TWT (~35 m) (using $T_b=56$ ms, $T_u=10$ ms). Since 5 ka (*Stage 7*), sea-level rose at a minor rate from 4 mbpsl to present day conditions (0.8 m/ka) (Fig. 4.6). Similar to *Stage 6*, the beginning of Stage 7 is characterized by a phase of resurgence-related uplift exceeding the rate of sea-level rise and the associated formation of Unconformity U4 (Fig. 4.7-G). During this timespan, marine Unit M4 was deposited. The resurgent dome reaches its present-day appearance with the associated

normal faults and crestral depression. The seafloor is clearly affected by the apical normal faults, indicating relatively recent activity. A small intrusion is emplaced at ~ 3.8 ka (Sacchi et al., 2014) below the seismic penetration limit.

4.6 Conclusions

Utilizing a high-resolution multichannel seismic data set, we investigated the formation and evolution of the Campi Flegrei nested-caldera complex. The submerged portion of the caldera depression acts as local depocenter and offers a unique opportunity to study caldera formation and post-caldera processes avoiding limitations due to urbanization or strong subaerial erosion. A conceptual model outlines the interplay between volcano-tectonic processes and sea-level fluctuations over the past ~ 39 ka, providing novel insights into the genesis and evolution of the CFc.

For the first time, high-resolution reflection seismic data showed evidence for the existence of a nested caldera formed by two ignimbritic eruptions and caldera collapses related to the more recent NYT eruption at ~ 15 ka and the preceding CI eruption at ~ 39 ka. Our results suggest that the inner caldera-fault was already (partially) activated during the CI collapse and then reactivated during the NYT collapse, however, with different amounts of subsidence, supporting findings from (Acocella, 2008). Regarding the NYT caldera collapse, we infer a maximum vertical displacement of ~ 75 m along the eastern and western submerged margins. Along the southern margin, the NYT caldera collapse occurred along a ring-fault zone with a total displacement of ~ 53 m. Compared to onshore boreholes, suggesting a collapse of ~ 600 m related to the NYT eruption (Orsi et al., 1996), these offshore observed amounts of collapse are relatively small. This discrepancy may be explained by an asymmetrical, piecemeal-like collapse with variable amounts of subsidence within the collapsed area (Lipman, 1997) and highlights the complexity and variability of collapse calderas. In general, it appears that the CI caldera collapse was associated with a significantly larger amount of subsidence than the NYT caldera collapse.

The post-collapse depositional environment in the offshore sector of the CFc was mainly influenced by sea-level rise, caldera resurgence, small-scale volcanic eruptions and local uplift of the western caldera margin related to the Punta Pennata structure. The multichannel seismic data provide a superb image of the resurgent dome supporting findings from analogue models of the formation of an apical depression and high-angle normal faults in the course of resurgence (Acocella et al., 2001).

Moreover, we were able to contribute to the regional volcanic stratigraphy by identifying a previously unknown post-collapse submarine volcanic mound (V2) located between Nisida Island and Nisida Bank, probably formed during Volcanic Epoch III between 4.8 and 3.7 ka. Also, our data suggest that the PPB consists of at least two monogenetic

volcanic edifices including the PP volcano probably formed at ~ 100 ka and a younger mushroom-shaped unit probably formed between 39 and 15 ka.

This study highlights the suitability of multichannel reflection seismics to investigate subsurface structure of a submerged caldera, allowing for a spatial assessment and for a quantification of deformation and for budgeting volcanic, lacustrine and marine deposition.

4.7 Acknowledgements

The seismic dataset was acquired during the CAFE-7/3 expedition funded by the Italian Research Council through the CNR Shiptime Programme (Oceanographic Cruise_CAFE_07), seismic acquisition was supported by German Research Foundation (DFG) within the ICDP priority programme (Grant No. SP296/30-1). Data processing and analysis was funded through the DFG's ICDP priority programme (Grant No. SP296/34-1; SP296/34-2). Additional support was provided by the Bremen International Graduate School for Marine Sciences (GLOMAR). We are grateful to Schlumberger for providing the VISTA 2D/3D Seismic Data Processing software package and to IHS for providing the KINGDOM seismic interpretation software.

Chapter 5

Post-collapse evolution of the Campi Flegrei caldera since the Neapolitan Yellow Tuff eruption at 15 ka: Insights from a 2.5D multichannel seismic survey

Lena Steinmann^{1,2}, Volkhard Spiess¹, Marco Sacchi³

¹Faculty of Geosciences, University of Bremen, 28359 Klagfurter Str., Bremen, Germany

²MARUM – Center for Marine Environmental Sciences, University of Bremen, Leobener Str., 28359 Bremen, Germany

³Istituto per l'Ambiente Marino Costiero (IAMC), Consiglio Nazionale delle Ricerche (CNR), Calata Porta di Massa, 80133 Napoli, Italy

5 Abstract

In the post-collapse phase, the majority of caldera systems remain active, posing a potential threat to the nearby population and environment. Comprehending post-collapse processes at active calderas is of major importance to understand the overall caldera-system, its evolution and state. The Campi Flegrei caldera is regarded as most active caldera on Earth and, thus, provides an ideal natural laboratory to study such processes. In this study, we present a semi-3D grid of high-resolution multichannel seismic profiles, providing novel insights on the evolution of the Campi Flegrei caldera since the last caldera-forming eruption, namely the Neapolitan Yellow Tuff (NYT) eruption, at ~15 ka. The high spatial data coverage in combination with high-vertical resolution allows for a comprehensive spatial and temporal investigation of the post-collapse depositional regime in interplay with volcanic activity and sea-level rise.

Based on the seismic data, the offshore location of major structural features such as the NYT-caldera ring-fault, the Punta Pennata anticline and the resurgent dome could be mapped in detail. Our results suggest that the NYT caldera is filled with on average ~61 m marine sediment deposited between 15 and 8.6 ka. Furthermore, we found that the NYT caldera ring-fault acted as pathways for the post-collapse ascent of deeper seated gases and/or fluids possibly related to the hypothesised existence of a shallow hydrothermal system. The presence of shallow gas/fluid-rich patches southward of the NYT caldera ring-fault points towards the existence of a deeper fracture zone probably

related to the Campanian Ignimbrite caldera collapse at ~ 39 ka. Based on the stratigraphic location of the gas/fluid-rich patches, we inferred that the ascent has occurred relatively recently (< 3.7 ka). Moreover, we identified two volcanoclastic units related to the Capo Miseno and Nisida cone eruptions at ~ 3.7 and ~ 3.98 ka, respectively. Our results suggest that these pyroclastic flows entered the sea and deposited under marine conditions. The estimated DRE volume of the Capo Miseno and Nisida cone pyroclastic flow deposits is at least 0.08 km^3 and 0.1 km^3 , respectively. An additional volcanoclastic unit related to the Nisida Bank probably formed between 10.3 and 9.5 ka has a DRE volume of 0.14 km^3 , thereby indicating a large-scale eruption.

Based on an integrated interpretation of the seismic profiles and borehole data from literature, we developed a novel 3D model illustrating the temporal post-collapse evolution of the Campi Flegrei caldera in five stages. In the model we outline the shift of the shoreline as well as major depositional and structural features in interplay with sea-level variations and volcano-tectonic activity over the past ~ 15 ka.

5.1 Introduction

Caldera-forming explosive eruptions are considered as one of the most catastrophic natural events to affect the Earth's surface and human society (Rampino, 2002; Self, 2015). Even in the post-collapse stage, the majority of caldera systems remain active as illustrated by seismicity, ground deformation, thermal activity and eruptions, thereby posing a potential threat to the nearby population and environment. Resurgent calderas in particular are often accompanied by vent eruptions along the ring-fracture zone (Smith and Bailey, 1968; Lipman, 1984). Understanding post-collapse processes at active calderas provides crucial insights into the overall caldera evolution and state, which is necessary in order to assess potential hazards and risk for future eruptions.

The Campi Flegrei caldera (CFc) located in southern Italy at the western border of the densely populated city of Naples has been regarded as one of the world's most active calderas and, thus, provides an ideal natural laboratory to investigate post-collapse evolutionary processes. Its activity has recently been proven by episodes of unrest involving ground deformation, seismicity and increased temperature at the fumaroles. The CFc was characterized by more than 60 post-collapse eruptions, mostly clustered within three volcanic epochs, at 15-9.5 ka (epoch I), 8.6-8.2 ka (epoch II) and 4.8-3.7 ka (epoch III) (Di Vito et al., 1999; Di Renzo et al., 2011). Furthermore, the CFc has undergone intensified caldera resurgence during its post-collapse phase (Cinque et al., 1985; Di Vito et al., 1999).

During the last decades, the CFc has been extensively studied due to its history of catastrophic volcanic eruptions and ongoing unrest. Traditionally, the CFc was investigated based on geological field observations and/or borehole data (e.g. Rosi et al.,

1983; Orsi et al., 1996; Di Vito et al., 1999), which allow only for selective and, thus, spatially limited insights into the complex caldera system. More recently, on the basis of geophysical studies such as seismic refraction tomography (e.g. Zollo et al., 2003; Judenherc and Zollo, 2004), gravity (e.g. Florio et al., 1999; Capuano and Achauer, 2003; Capuano et al., 2013) or magnetic (e.g. Florio et al., 1999; Secomandi et al., 2003; Aiello et al., 2005) measurements, the approximate location of the caldera depression and margin could be outlined. However, even though such geophysical methods provide good spatial coverage, they are limited by their low resolution. More detailed insights into the shallow structures of the submerged CFc were provided by high-frequency 2D marine reflection seismic investigations (D’Argenio et al., 2004b; Milia, 2010; Aiello et al., 2012; Sacchi et al., 2014, Chapter 4). Despite their high-resolution, these reflection seismic studies were lacking spatial coverage, which is crucial in order to fully understand a complex caldera system. Ideally, a combination of high-resolution and high-spatial coverage would be necessary to reliably assess the post-collapse state and evolution of the CFc. The high spatial and vertical resolution provided by 3D reflection seismic data has the capacity to fill this gap and advance our understanding of collapse-caldera systems in general and the CFc in particular.

In this study, we present the first semi-3D grid of high-resolution multichannel seismic from a submerged caldera setting in order to investigate the post-collapse evolution of the CFc in spatial and temporal detail. Such a marine investigation provides the opportunity to study the complete stratigraphic record without the challenges posed on land by subsequent destruction or burial of earlier features. Eventually, we integrate our interpretation from the semi-3D seismic data with onshore stratigraphic columns from boreholes in literature and develop an extensive evolutionary model outlining the development of the CFc during the past 15 ka since the last caldera collapse related to the Neapolitan Yellow Tuff (NYT) eruption.

5.2 Regional setting

The CFc is a Quaternary nested caldera within the graben-like structure of the Campanian Plain (southern Italy), which was formed in the course of the Plio-Quaternary Tyrrhenian Sea opening. With the city of Naples at its eastern margin and the town of Pozzuoli in its centre (Fig. 5.1), the CFc is located in a densely populated area.

The CFc is a quasi-circular depression with a diameter of ~13 km, located half onshore, half offshore (Fig. 5.1). The nested caldera was formed by two large-scale ignimbritic eruptions at ~15 and ~39 ka namely the NYT and Campanian Ignimbrite (CI) eruptions, respectively (e.g. Rosi et al., 1983; Barberi et al., 1991; Orsi et al., 1996; De Vivo et al., 2001; Deino et al., 2004).

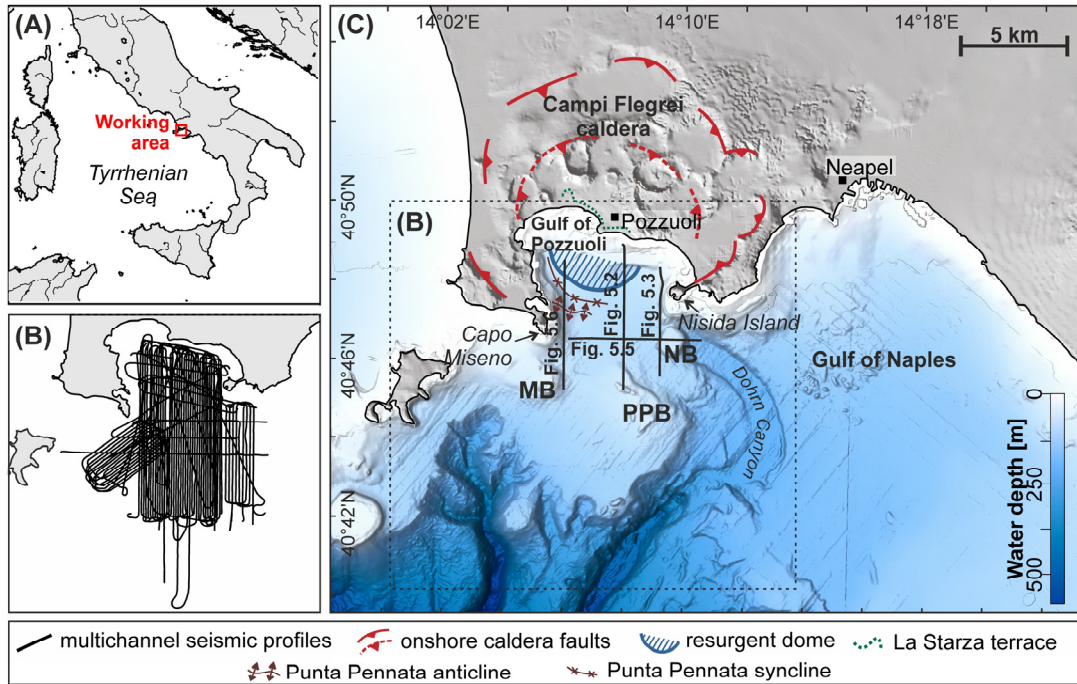


Fig. 5.1: (A) Location of the working area in southern Italy between the Apennines and the Tyrrhenian Sea. (B) Location of the semi-3D high-resolution multichannel seismic profiles acquired during the CAFE7-3 cruise in 2008. (C) Bathymetric and topographic map of the CFc area with location of the seismic profiles presented in this study. The onshore locations of the main Campi Flegrei caldera faults and resurgent dome are redrawn after Acocella (2008) and Sacchi et al. (2014), respectively.

The offshore sector of the CFc is situated in the Gulf of Pozzuoli, a small embayment at the north-western side of the Gulf of Naples. To the South, the CFc is bordered by a belt of submarine vents consisting of the Penta Palummo, Miseno and Nisida Banks (Fig. 5.1). While the Penta Palummo and Miseno banks are of Late Pleistocene origin, the Nisida Bank was formed in the post-collapse phase probably between 10.3 and 9.5 ka (Di Vito et al., 1999). Since ~8 ka, the eastern part of the Gulf of Pozzuoli has undergone synsedimentary folding along the curved Punta Pennata fold, leading to the uplift of the Punta Pennata anticline and syncline (Fig. 5.1). This fold features limb rotation kinematics and is probably of tectonic origin (Milia and Torrente, 2000).

Particularly, the onshore topography of the CFc was strongly modified by at least 60 post-collapse eruptions mainly clustered within three volcanic epochs, at 15-9.5 ka (epoch I), 8.6-8.2 ka (epoch II) and 4.8-3.8 ka (epoch III) (Di Vito et al., 1999). During the last decades, different age determination techniques were applied in order to establish a reliable chronostratigraphic record of the post-collapse eruption history. However, the application of various methods resulted in a heterogeneous timescales. For instance, the chronostratigraphic position of the Capo Miseno eruption is still controversial as it was dated at several different ages (3.7 ± 0.5 ka, Di Renzo et al. (2011); 3.9 ± 0.06 ka, Sacchi et al. (2014); 4 ka, Di Girolamo et al. (1984); 5.1 ± 0.1 ka, Insinga et al. (2006)). Based on the stratigraphic position of the Capo Miseno deposit, Di Vito et al. (1999) went even

further back in time and attributed the Capo Miseno eruption to volcanic epoch I. Similar age discrepancies can be observed for the Nisida volcano (Nisida island) eruption. While Di Vito et al. (1999) ascribed the Nisida tuff cone activity to volcanic epoch I, Di Renzo et al. (2011) and (Fedele et al., 2011) dated its activity at 3.98 ± 0.53 ka and 3.92 ± 0.09 ka (volcanic epoch III), respectively. Since volcanic epoch III, the CFc area has been characterized by volcanic quiescence, interrupted only by the most recent eruption at 1538 AD, which followed a rapid episode of uplift and led to the formation of the Monte Nuovo tuff cone (Di Vito et al., 1987).

In the course of post-collapse caldera resurgence, a broad resurgent dome accompanied by a summit depression related to apical extension has developed in central part of the Gulf of Pozzuoli (Fig. 5.1) (Sacchi et al., 2014, Chapter 4). Onshore, caldera resurgence resulted in the emersion of a previously submarine sector, the so-called *La Starza terrace* (Fig. 5.1). At the beginning of volcanic epoch I and II at ~ 8.6 ka and ~ 5 ka, respectively, resurgence-related uplift exceeded sea-level rise, thereby leading to the development of marine unconformities offshore (Milia and Torrente, 2000; Sacchi et al., 2014, Chapter 4) and palaeosols onshore (Di Vito et al., 1999). While the La Starza terrace was only temporarily emerged during the first phase at ~ 8.6 ka, the second phase at ~ 5 ka led to the final emersion. Presently, the La Starza terrace is located at 30 to 55 m above sea-level (Fig. 5.1).

During post-Roman times (< 2 ka), the coastal area of the Gulf of Pozzuoli probably subsided by 5 to 25 m as indicated by the presence of submerged Roman archaeological sites (Passaro et al., 2013) and the occurrence of a drowned infralittoral prograding wedge located below their substantial hydrostatic equilibrium (Sacchi et al., 2014).

Even more recently, since the 1960s, the CFc has shown increased post-collapse activity as demonstrated by repeated bradyseism events (i.e., vertical ground movement), generally accompanied by seismicity with shallow earthquakes at max. ~ 3 -4 km depth (De Natale et al., 1991; De Natale et al., 2006; Troise et al., 2008) and increased fumarolic activity (Chiodini et al., 2015). In the town of Pozzuoli, a net uplift of 3.8 ± 0.2 m was generated during two main episodes of rapid short-term uplift between 1969–1972 and 1982–1984 (Del Gaudio et al., 2010). While long-term caldera resurgence is likely related to the inflation of a deeper underlying magma system, such relatively short-term uplift phases are probably triggered by the injection of magmatic fluids into a shallow hydrothermal system at ~ 2 km depth (Orsi et al., 1999; Chiodini et al., 2003; Acocella, 2010; Chiodini et al., 2015).

5.3 Materials and methods

Here we present high-resolution multichannel seismic data collected during an oceanographic cruise (CAFE-7/3) on the *R/V URANIA* in the Gulf of Naples and the

Gulf of Pozzuoli in 2008 (Fig.5.1-B). This study is based on in total 88 seismic profiles of which 48 are part of a densely spaced (75 - 150 m spacing) N-S oriented semi-3D grid crossing over the offshore sector of the Campi Flegrei caldera. During the expedition, data acquisition was carried out using the high-resolution multichannel seismic system of the Department of Geosciences at the University of Bremen, Germany. A mini GI-gun with chamber volumes of 0.1 L, sensitive in a frequency range of up to 1000 Hz, served as source. The seismic signal was recorded with a 50-m long, 48-channel streamer.

Seismic data processing was carried out with the software package ‘VISTA Seismic Processing 2D/3D’ (Schlumberger). The processing routine included geometry setup, trace editing, bandpass filtering (30/60-800/1000 Hz), residual statics corrections, normal move-out correction, multiple suppression, common mid-point (CMP) binning and stacking, noise attenuation and time migration. The seismic data were resampled to 4 kHz sample frequency. As result of such elaborate multichannel processing, the signal-to-noise ratio was significantly enhanced and disturbing multiples were considerably reduced, which facilitates a reliable seismic interpretation. The superior data quality in combination with the dense semi-3D coverage allows for a comprehensive, high-resolution investigation of the depositional environment in the submerged part of the CFc and distinguishes this study from previously published hydroacoustic studies (e.g. Milia and Torrente, 2000; D’Argenio et al., 2004b; Sacchi et al., 2014).

The vertical resolution limit of the seismic dataset, depending mostly on the source signal frequency, is ~1 m. The horizontal resolution is defined by the CMP bin size, which was set to 1 m in order to achieve maximum horizontal resolution on most profiles. The seismic signal penetration is strongly influenced by high signal attenuation in volcanic rocks and lies at typically ~250 ms TWT (~190 m). Seismic data interpretation was accomplished using the IHS Kingdom Software package.

5.4 Results

In order to exemplify the main seismic units, we present four representative high-resolution multichannel seismic sections. Seismic line GeoB08-040 (Fig. 5.2) has a length of ~7.1 km and extends from the coastal shallow water in the North to the Penta Palummo Bank in the South, covering the resurgent dome and the southern caldera margin. The ~5.2 km long N-S trending seismic profile GeoB08-036 (Fig. 5.3) is located offshore Nisida Island and crosses over the Nisida Bank. GeoB08-040 and GeoB08-036 are intersected by the ~6.3 km long E-W oriented seismic profile GeoB08-026, which crosses over the Dohrn Canyon and Nisida Bank (Fig. 5.5). The N-S trending profile GeoB08-029 (Fig. 5.6) with a length of ~6.1 km is located offshore Capo Miseno, intersecting the Miseno Bank in the South and crossing over the Punta Pennata anticline/syncline structure as well as the resurgent dome in the North.

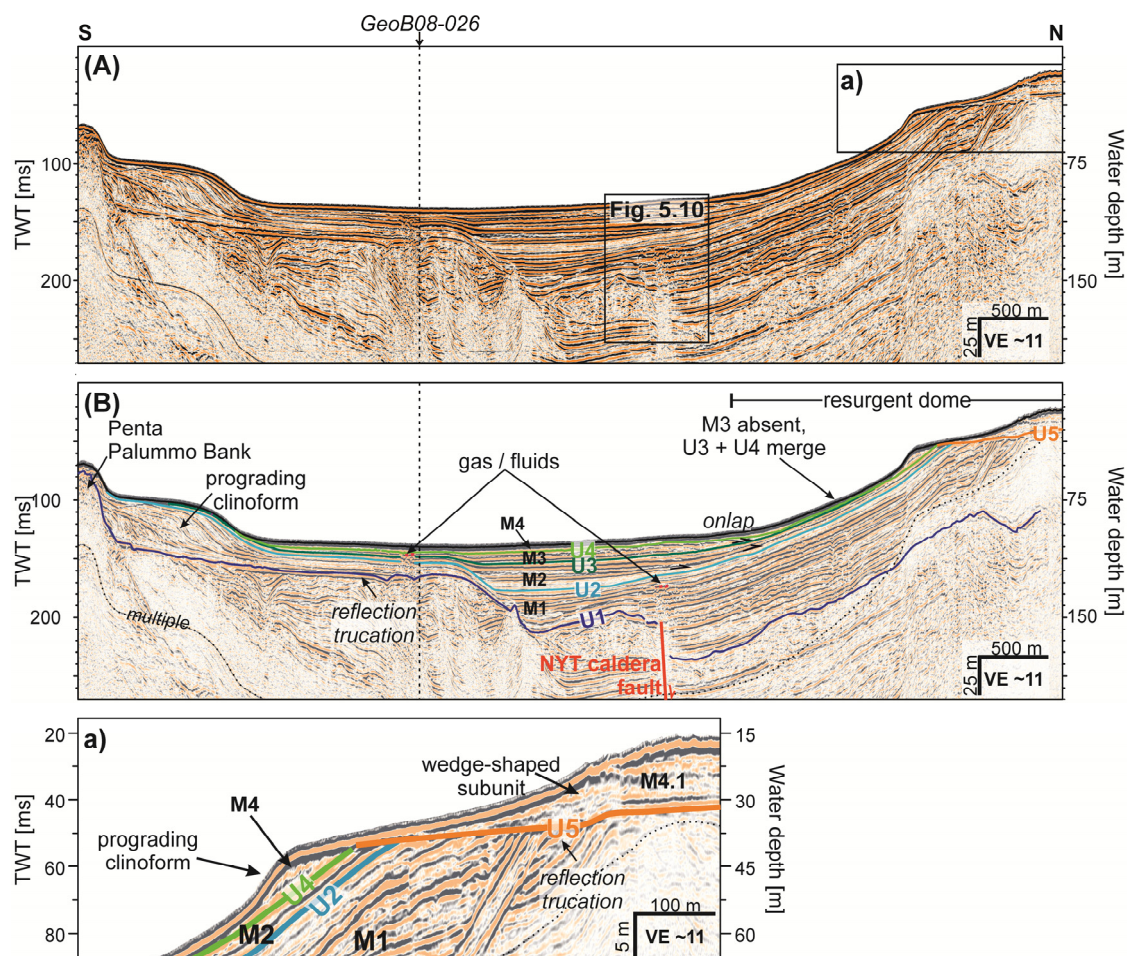


Fig. 5.2: N-S trending multichannel seismic profile GeoB08-044, showing the main marine units (M1-M4) with subunit M4.1, associated unconformities (U1-U5), ascending gases/fluids (dotted dark red line) and a shallow CFc fault (solid red line). Dotted black line indicates intersection with profile GeoB08-026. (A) shows the uninterpreted section; (B) shows the interpreted section; (a) shows a close-up of the prograding coastal wedge (M4.1). For profile location see Figure 5.1.

5.4.1 Seismic analysis

Based on a seismostratigraphic approach after Mitchum et al. (1977) and Vail et al. (1977), four main seismic units, labelled from bottom to top as M1-M4, were identified in the Gulf of Pozzuoli. These units are characterized by mainly parallel to subparallel reflections with good to moderate lateral continuity and variable internal reflection amplitudes from low to high. Hence, these deposits were interpreted as marine sediments. They are bounded at their base by major discontinuities named U1-U5 from bottom to top.

Locally, three additional units (V1-V3) are interbedded within M2 and M4¹. These interbedded units show reflection-free seismic facies with interbedded high-amplitude

¹ With respect to Chapter 4, I would like to mention that there are some overlaps in the seismic analysis. The here defined Seismic Unit M1 and M2 corresponds to Seismic Unit M2 and M3 from Chapter 4, respectively. Therefore, the here defined unconformities U1, U2, U3 also correspond to

reflections, low lateral continuity and/or contorted reflection configurations. Furthermore, they show a distinct morphology often characterized by a local increase in thickness, irregular bounding surfaces and/or a mounded topography. Based on these seismoacoustic characteristics, unit V1-V3 were interpreted as being of volcanic origin, such as pyroclastic flow deposits, or volcanic edifices. In patches along the southern border of the Gulf of Pozzuoli, the units M1-M4 are disturbed by reflections with high-amplitude and/or reversed polarity in association with acoustic turbidity and blanking (Figs. 5.2, 5.5, 5.6). Such seismoacoustic signatures indicate the presence of gas and/or fluids. These shallow zones occur down to a maximum seafloor depth of ~60 m (Fig. 5.5-a).

The topography of the widespread unconformity U1 is presented in a 3D image in order to illustrate major structural, volcanological and erosive features (Fig. 5.4).

Isochore maps illustrate the spatial distribution of the true vertical thickness of the defined units M1-M4, thereby highlighting depositional centres (Fig. 5.7). For time-to-depth conversion, we used a constant velocity of 1,650 m/s, representing the mean velocity of the uppermost ~200 m (Sacchi et al., 2014). The volumes of the volcanic units were estimated using a constant velocity of 2,000 m/s (Vanorio et al., 2002).

Seismic Unit M1 (Marine 1)

M1 is bounded at its base by the widespread major unconformity U1, which is overall characterized by an irregular morphology with locally erosive character visible in the seismic section as truncation of the underlying reflections (Fig. 5.2). U1 is characterized by a channel-like topographic low (Fig. 5.4) associated with reflection truncation in the seismic section (Fig. 5.5) and corresponding to the present-day location of the Dohrn Canyon (Fig. 5.1). At its top, M1 is mainly confined by unconformity U2. Locally, in the northern coastal area of the Gulf of Pozzuoli, the reflections of M1 are being truncated by the flat unconformity U5 located in between 53 and 42 ms TWT (Fig. 5.2). Unit V1 (*Volcanic 1*), a local cone-shaped feature characterized by a mainly reflection-free seismic facies with interbedded high-amplitude patches and upward bending reflections at its flanks, is intercalated in M1 (Figs. 5.3, 5.5). V1 forms a topographic high in unconformity U2, associated with a local thickness maximum of M1 of 147 m (Fig. 5.7-A). This topographic high can also be recognized in the bathymetry and corresponds to the Nisida Bank (Fig. 5.1). V1 has a total volume of 0.24 km³ and covers an area of 4.3 km². Towards the central part of the Gulf of Pozzuoli, M1 shows a distinct and relatively

the in Chapter 4 mentioned unconformities U2, U3, U4, respectively. Furthermore, V2 in this Chapter corresponds to V2 in Chapter 4. However, the seismostratigraphic analysis presented in this Chapter provides a higher resolution (i.e. more units) in the uppermost interval (M3, M4, M4.1 from this Chapter represent Seismic Unit M4 from Chapter 4) as well as some additional volcanic units (V1, V3).

abrupt arc-shaped increase in thickness to an average of ~61 m (Fig. 5.7-A), which coincides with a distinct vertical displacement of U1 (ranging from 140 to 30 ms TWT) (Figs. 5.2, 5.5). In comparison, beyond the arc-shaped border and excluding V1, the mean thickness of M1 is only ~19 m (Fig. 5.7-A). Another local increase in thickness can be found offshore Porto Miseno (Fig. 5.7-A). Furthermore, an elongated, relatively thicker structure is located along the border of the Penta Palummo and Miseno Bank, corresponding to a sigmoidal prograding clinoform in the seismic section (Fig. 5.2).

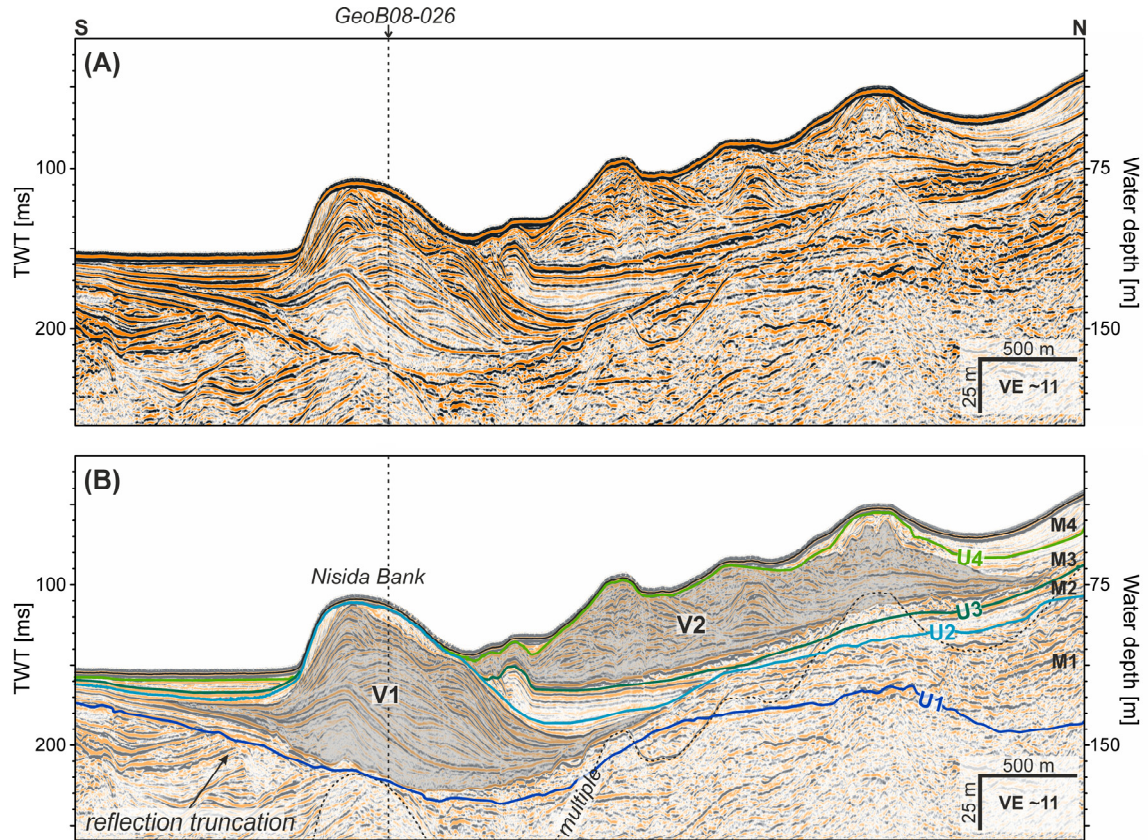


Fig. 5.3: N-S trending multichannel seismic profile GeoB08-036, showing the main marine units (M1-M4) and volcanic units V1 and V2 (shaded grey). Dotted black line indicates intersection with profile GeoB08-026. (A) shows the uninterpreted section and (B) shows the interpreted section. For profile location see Figure 5.1.

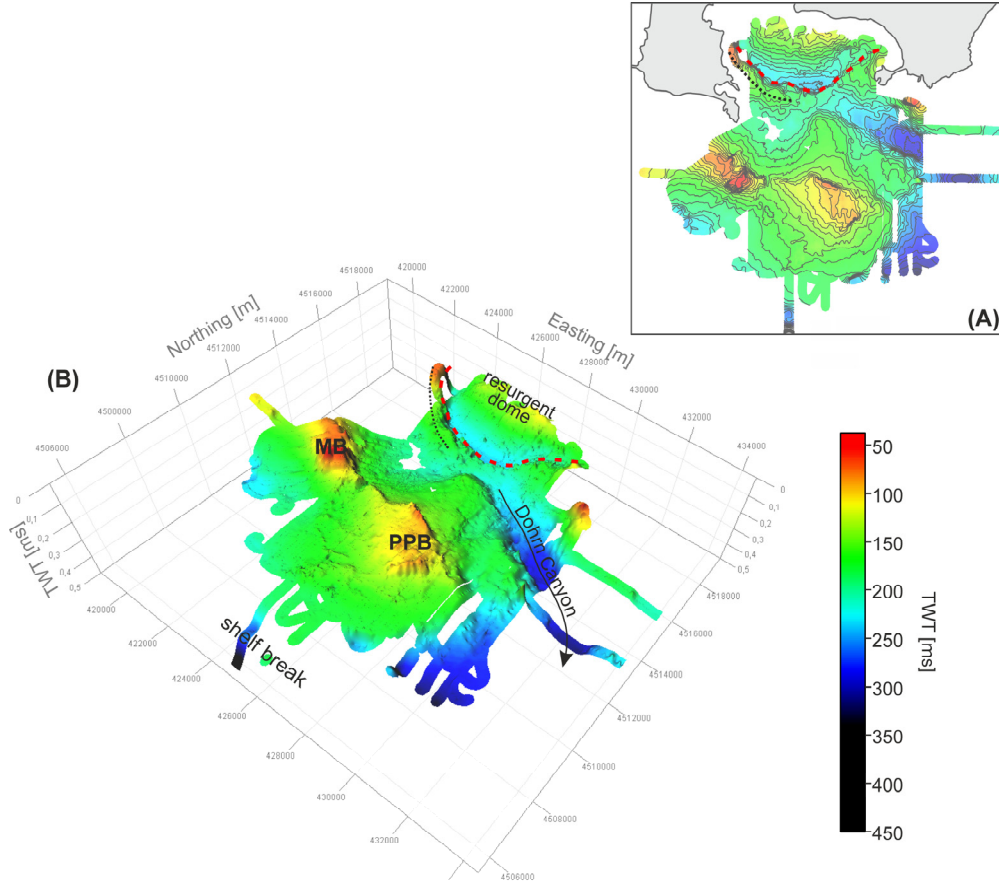


Fig. 5.4: Topography of unconformity U1 with major structural, volcanological and erosive features being indicated. (A) Plane map view; (B) 3D of same map section. Black dotted line = Punta Pennata fold; red dashed line = NYT caldera fault; MB = Miseno Bank, PPB = Penta Palummo Bank.

Seismic Unit M2 (*Marine 2*)

M2 is confined at its base by unconformity U2 and at its top by unconformity U3 (Figs. 5.2, 5.3, 5.5). This unit is characterized by a relatively minor mean thickness of only ~9 m. Between Capo Miseno and Nisida Island, M2 shows increased thickness with a maximum value of ~28 m (Fig. 5.7-B). A curved thickness minimum can be observed offshore Bacoli (Fig. 5.7-B), corresponding to the Punta Pennata anticline (Figs. 5.1, 5.6). In the seismic section, this minimum correlates with onlap reflection termination and upward-bending reflections (Fig. 5.6), which is also visible in the topography of unconformity U1 (Fig. 5.4). This topographic high corresponds to the resurgent dome (Fig. 5.1). Offshore the town of Pozzuoli, the internal reflections of M2 onlap on the underlying unconformity U2 and closer to the shore they are being truncated by the flat unconformity U5 (Fig. 5.2), leading to the absence / distinct thickness minimum of M2 (Fig. 5.7-B).

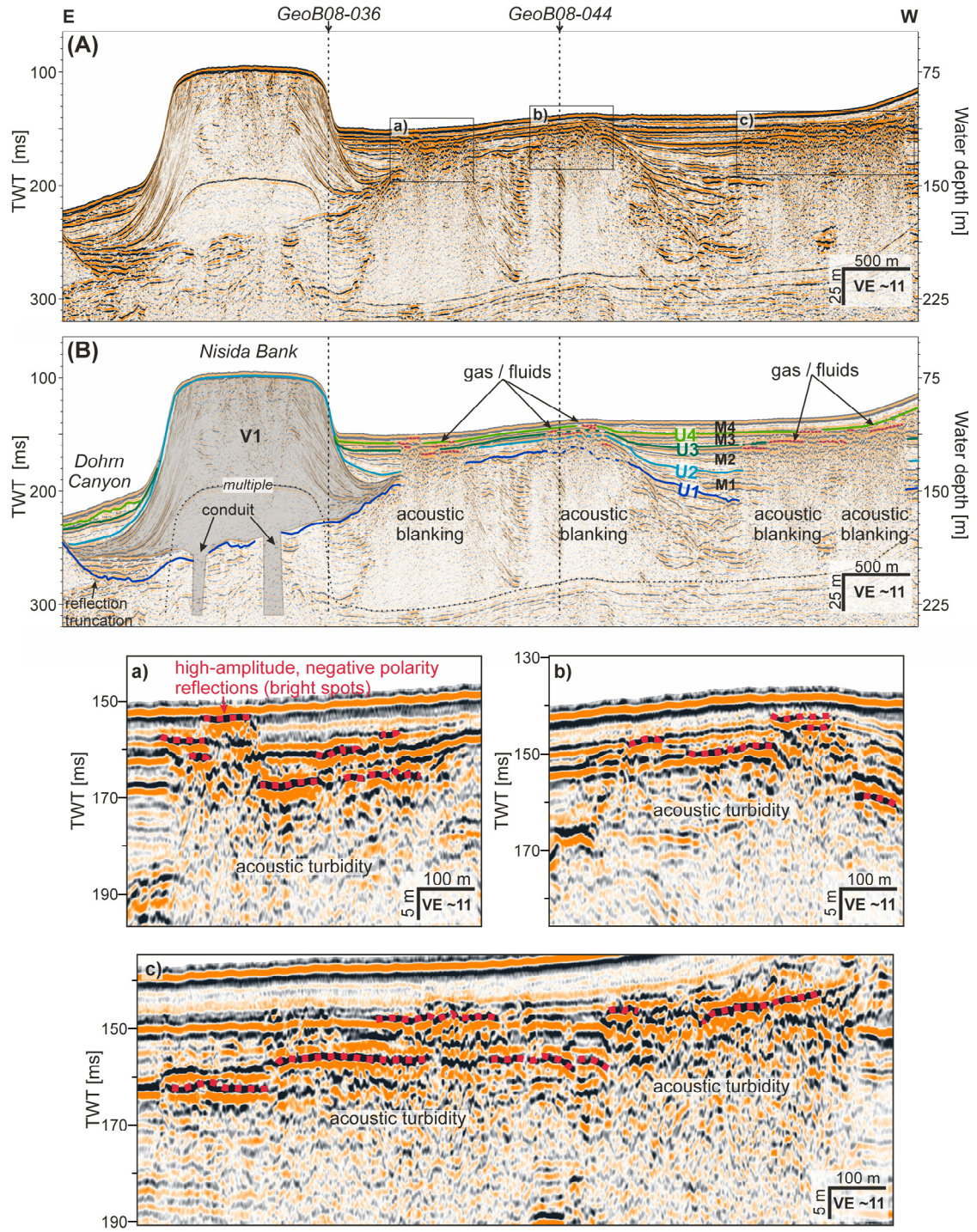


Fig. 5.5: E-W trending multichannel seismic profile GeoB08-026, showing the main marine units (M1-M4), volcanic unit V1 (shaded grey) and ascending gases/fluids (dotted dark red line). Dotted black lines indicate intersections with profiles GeoB08-044 and GeoB08-036. (A) shows the uninterpreted section and (B) shows the interpreted section. (a), (b) and (c) show close-ups of the shallow gas/fluid-enriched zones. For profile location see Figure 5.1.

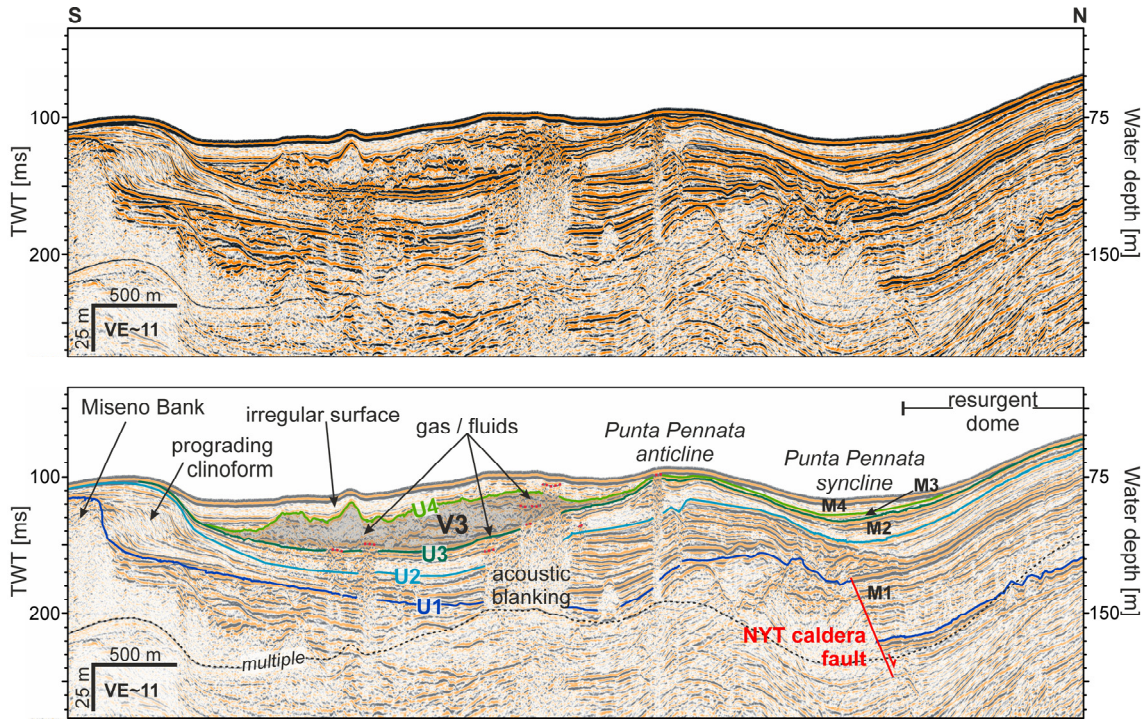


Fig. 5.6: N-S trending profile GeoB08-029, showing the main seismic units (M1-M4), volcanic unit V3 (shaded grey), ascending gases/fluids (dotted dark red line) and NYT caldera fault (solid red line). For profile location see Figure 5.1.

Seismic unit M3 (*Marine 3*)

M3 is located between unconformity U3 at its base and U4 at its top. The units V2 and V3 are interbedded in M3 and associated with two pronounced thickness maxima of ~106 m and ~77 m located offshore Nisida Island and Capo Miseno, respectively (Fig. 5.7-C). V2 and V3 are characterized by low amplitude reflections with interbedded high-amplitude patches, low lateral continuity and contorted configuration (Figs. 5.3, 5.6). Both units show an overall mounded morphology. On top of V2 and V3, unconformity U4 is irregular with local topographic highs (Figs. 5.3, 5.6). V2 and V3 were interpreted as pyroclastic flow related to the Nisida Island and Capo Miseno eruptions, respectively. The estimated volume of V2 is 0.15 km³ and this unit extends over a total area of 3.7 km². V3 has a total volume of 0.1 km³ and covers an area of ~5.1 km². Excluding V2 and V3, the mean thickness of M3 is relatively minor with ~5 m. In the central part of the Gulf of Pozzuoli, the reflection of M3 onlap on the underlying unconformity U3 (Fig. 5.2), thereby leading to the absence of unit M3 and the merging of U3 and U4 (Fig. 5.7-C). As previously described for unit M2, this area corresponds to upward-bending reflections in the seismic and a dome-shaped high of unconformity U1 (Fig. 5.4), correlating with the location of the resurgent dome (Fig. 5.1). Another minor thickness decrease (Fig. 5.7-C), associated with onlap reflection termination and upward-bending reflections, can be seen offshore Bacoli, which again corresponds to the Punta Pennata anticline (Figs. 5.1, 5.4, 5.6).

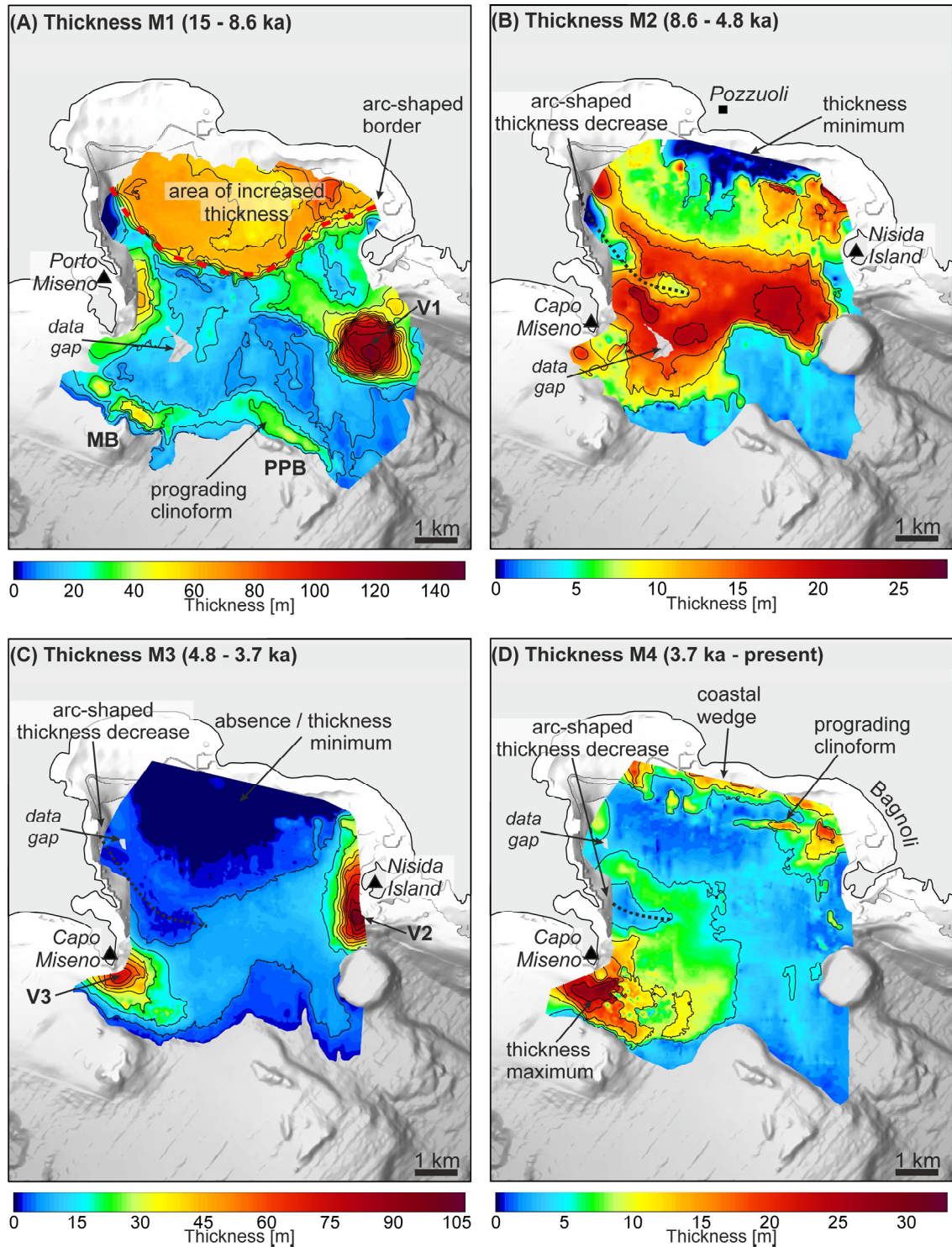


Fig. 5.7: Isochore maps of the main seismic units (M1-M4) illustrating centres of deposition (dark red) and non-deposition (dark blue).

Seismic unit M4 (*Marine 4*)

The uppermost unit M4 lies between the unconformity U4 at its base and the seafloor. A wedge-shaped subunit (M4.1), confined by unconformity U5 at its base, is present locally in the northern coastal part of the Gulf of Pozzuoli (Fig. 5.2). The mean thickness of M4 is ~5 m, while maximum values of ~32 m can be observed offshore Capo Miseno (Fig.

5.7-D). In that place, M4 lies above the irregular upper boundary of V3 (U4) (Fig. 5.6), filling up topographic depression in unconformity U4 and leading to a smoothed seafloor morphology. Offshore Bagnoli, we can observe an elongated structure with increased sediment thickness, corresponding to a sigmoidal prograding clinoform in the seismic section (Fig. 5.7-D). Similar as observed for M2 and M3, a minor curved thickness decrease can be observed offshore Bacoli (Fig. 5.7-D), corresponding in the seismic section to onlapping reflections associated with the Punta Pennata anticline (Fig. 5.1, 5.6).

5.5 Discussion

We propose that the marine unit M1 deposited in the in the course of rapid sea-level rise (11.5 m/ka) between 15 to 8.6 ka, which includes volcanic epoch I (15-9.5 ka). Marine unit M2 likely deposited in the time-span from ~8.6 to 5 ka, comprising volcanic epoch II (8.6 – 8.2 ka). This time was characterized by moderate sea-level rise (~4 m/ka) and intensified resurgence-related uplift, which resulted in the formation of an intra-caldera resurgent dome. Between ~5 and 3.7 ka, when sea-level rise was minor (~1 m/ka) and uplift related to caldera resurgence exceeded the rate of sea-level rise once more, marine unit M3 deposited. The uppermost unit M4 probably deposited since 3.7 ka, a time-span characterized by volcanic quiescence and post-Roman subsidence (<2 ka). A detailed stratigraphic analysis and the main age-defining markers are outlined in section 5.5.1 and summarized in Fig. 5.8.

5.5.1 Seismostratigraphic framework

The marine unconformity U1 represents an erosional surface probably formed by a succession of erosive processes occurring (1) in a shoreline setting during sea-level fall, (2) under subaerial conditions during the Last Glacial Maximum (LGM) lowstand, and (3) in a coastal environment during the early phase of sea-level rise. Hence, U1 was probably formed between 18 and 15 ka, thereby marking the onset of rapid sea-level rise and of the deposition of marine unit M1 (Fig. 5.8). U1 shows a clear erosive character along the present-day location of the Dohrn Canyon, indicating its activity at the time of the formation of U1. U1 corresponds to unconformity U2 as described by Steinmann et al. (Chapter 4) and, thus, also forms the top of the NYT, which erupted at 15 ka. U1 is significantly displaced towards the centre of the Gulf of Pozzuoli along an arc-shaped boundary (Figs. 5.2, 5.4, 5.7). This vertical offset correlates with a thickness maximum of the overlying marine unit M1 and was interpreted as the NYT caldera fault, which downthrows the central part of the Gulf of Pozzuoli, thereby creating significant accommodation space in the caldera depression. In the course of transgression after the NYT caldera collapse, the available accommodation space is rapidly filled up with on

average ~61 m thick marine sediments (M1). Another local thickness increase of M1 can be found offshore Porto Miseno (Fig. 5.7-A). This could possibly be related to enhanced sediment input after the Porto Miseno eruption at 11.8 ± 0.9 ka (Di Renzo et al., 2011), which occurred in close vicinity. However, no seismoacoustic evidence (i.e. reflection-free facies, chaotic reflection configuration) for the submarine deposition of a pyroclastic flow deposit related to that eruption could be found.

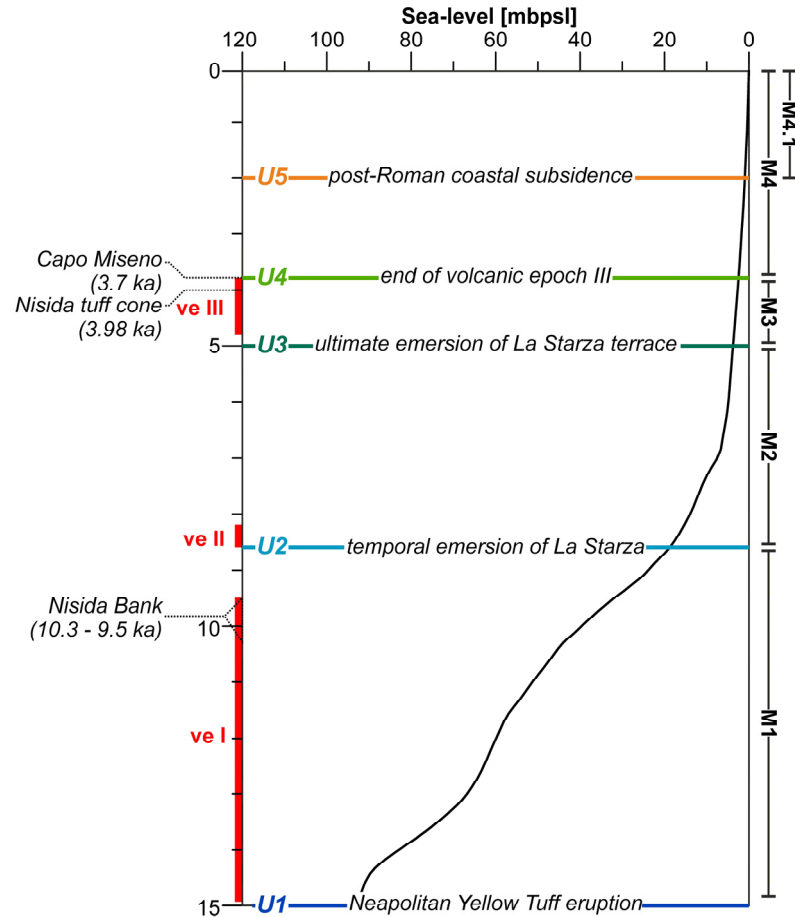


Fig. 5.8: Graphical summary of main stratigraphic markers (unconformities U1-U5) and depositional units (seismic units M1-M4) in correlation with sea-level rise. In red, we indicated the three main volcanic epochs: ve I=volcanic epoch I (15-9.5 ka), ve II=volcanic epoch II (8.6-8.2 ka), ve III=volcanic epoch III (4.8-3.7 ka). The relative sea-level curve was adapted from Lambeck et al. (2011).

The marine unconformity U2 separates marine unit M1 from M2 and likely developed at the beginning of volcanic epoch II at ~8.6 ka when uplift related to caldera resurgence exceeded the rate of sea-level rise, thereby forming a broad resurgent dome in the intra-caldera area (Figs. 5.1, 5.4, 5.8) (Sacchi et al., 2014, Chapter 4). Consequently, the accommodation space on the most uplifted part was limited, which led to the formation of the observed onlap reflection termination and thickness minimum of the overlying unit M2 (Figs. 5.2, 5.7-B). Furthermore, a curved thickness minimum can be observed offshore Bacoli (Fig. 5.7-B, -C), which corresponds to onlapping reflection termination in

the seismic section and was attributed to limitation of accommodation space due to the onset of uplift at the Punta Pennata fold. Seismic unit V1, which corresponds to the volcanic cone of the Nisida Bank, is stratigraphically located between U1 and U2 (Fig. 5.3, 5.5). Based on an investigation of the relative stratigraphic position of tephra layers, the age of Nisida bank was previously estimated between 10.3 and 9.5 ka (volcanic epoch I) (Di Vito et al., 1999), which is in agreement with our age constraint from the seismic data (15 – 8.6 ka). The downslope transport through the Dohrn Canyon was probably limited by the formation of the Nisida tuff cone in its head. This is also evident in the seismics, as the overlying unconformities U2-U4 do not show a distinct erosive character in the vicinity of the Dohrn Canyon (Fig. 5.5). Using an average magma density of 2.3 kg/m³ (Wohletz et al., 1999) and tuff density of 1.3 kg/m³ (Heap et al., 2014), we estimated the Dense-Rock Equivalent (DRE) volume for seismic unit V1 (0.14 km³) (Table 5.1). According to the Volcanic Explosivity Index (VEI), the Nisida Bank eruption may be categorized as large-scale eruption (VEI = 4) (Newhall and Self, 1982). Prior to volcanic epoch II at ~5 ka, when the La Starza terrace was ultimately emerged as consequence of a second phase of resurgence-related uplift exceeding sea-level, the marine unconformity U3 was formed (Fig. 5.8). Hence, the accommodation space on top of the resurgent dome was once more significantly reduced, leading to the development of onlap reflection termination and thickness minimum of the overlying unit M2 (Fig. 5.2, 5.7-B).

The marine unconformity U4 marks the top of volcanic deposits V2 and V3, which were interpreted as pyroclastic flow deposits related to the Nisida Island and the Capo Miseno eruptions, respectively. Based on our seismostratigraphic approach, we can already infer that V2 and V3 probably deposited in the course of volcanic epoch III (4.8 – 3.7 ka). This finding supports the proposed age from Di Renzo et al. (2011) (3.7 ± 0.5 ka for Capo Miseno, 3.98 ± 0.53 ka for Nisida Island), Fedele et al. (2011) (3.92 ± 0.09 ka for Nisida Island), Sacchi et al. (2014) (3.9 ± 0.06 ka for Capo Miseno) and Di Girolamo et al. (1984) (~4 ka for Capo Miseno), while excluding the ages from Insinga et al. (2006) (5.1 ± 0.1 ka for Capo Miseno) and Di Vito et al. (1999) (volcanic epoch I for Capo Miseno and Nisida Island). With respect to the proposed ages from literature, we assigned unconformity U4 an age of 3.7 ka, thereby marking the termination of volcanic epoch III (Fig. 5.8). At the time of the Capo Miseno and Nisida cone eruption, sea level was located between 2.5 and 2.7 mbpsl (Fig. 5.8). As the pyroclastic flow deposit of both eruptions (V2, V3) were found in water depth of up to 100 m, we assume that the pyroclastic flow entered the sea and, thus, depositing under marine conditions. The total DRE volume of both eruptions was estimated using the calculated offshore DRE volume and published estimations of the onshore DRE volume (Table 5.1). The Nisida Island eruption has a total DRE volume of ~0.1 km³ and, thus, may also be categorized as

large-scale eruption (VEI = 4). The Capo Miseno eruption, with a total DRE volume of $\sim 0.08 \text{ km}^3$, may be classified as moderate-large scale eruption (VEI = 3).

Table 5.1: Volume calculations for identified volcanic units. *: $DRE = \text{submarine volume [km}^3] \times \text{tuff density [kg/m}^3] / \text{magma density [kg/m}^3]$ using magma density = 2.3 kg/m^3 and tuff density = 1.3 kg/m^3 ; #: from Di Renzo et al. (2011).

Eruption	Nisida Bank	Nisida Island	Capo Miseno
Seismic Unit	V1	V2	V3
Age [ka]	10.3- 9.5	3.98	3.7
Submarine area [km ²]	4.3	3.7	5.1
Submarine volume [km ³]	0.24	0.15	0.10
Submarine volume (DRE) [km ³]*	0.14	0.08	0.06
Onshore volume (DRE) [km ³] [#]	-	0.02	0.02
Total volume (DRE) [km ³]	0.14	0.1	0.08

Unconformity U5 was found exclusively in the coastal area in the northern sector of the Gulf of Pozzuoli (Fig. 5.2). This unconformity shows a distinct erosive character as evident by reflection truncation and, thus probably formed in shallow water setting at 20 m water depth. However, presently, this erosive unconformity can be found in water depth ranging from 45 to 23 m, thereby indicating subsidence of 25 – 3 m, which is in agreement with Sacchi et al. (2014). Hence, U5 probably marks the onset of post-Roman coastal subsidence ($\sim 2 \text{ ka}$), which created accommodation space, thereby leading to the deposition of the coastal wedge (M4.1) since 2 ka (Fig. 5.8).

Seismic unit M2, M3 and M4 show onlap reflection termination, upward bending reflections and a thickness minimum associated with the Punta Pennata fold (Fig. 5.6). Hence, we inferred that uplift at the Punta Pennata fold has already begun when seismic unit M2 deposited (between 8.6 and 5 ka) and continued during the deposition of unit M3 (5- 3.7 ka) and M5 (3.7 ka – present), thereby supporting findings from Milia and Torrente (2000).

5.5.2 Shallow hydrothermal gases and/or fluids

Figure 5.9 illustrates the distribution of gas/fluid-enriched patches in the southern part of the Gulf of Pozzuoli. It is striking that some of these patches occur in close vicinity of the NYT caldera fault. Numerical models have already indicated that major faults may act as conduit for the ascent of high-temperature fluids (Jasim et al., 2015). These modelling results can be verified by our seismic data, which evidently show shallow gas/fluid accumulation above the NYT caldera fault (Fig. 5.10). Hence, we propose that the NYT caldera fault acts as pathway for the ascent of hydrothermal gases and/or fluids probably originating from a shallow ($< 2 \text{ km}$ depth) hydrothermal aquifer (Chiodini et al., 2015).

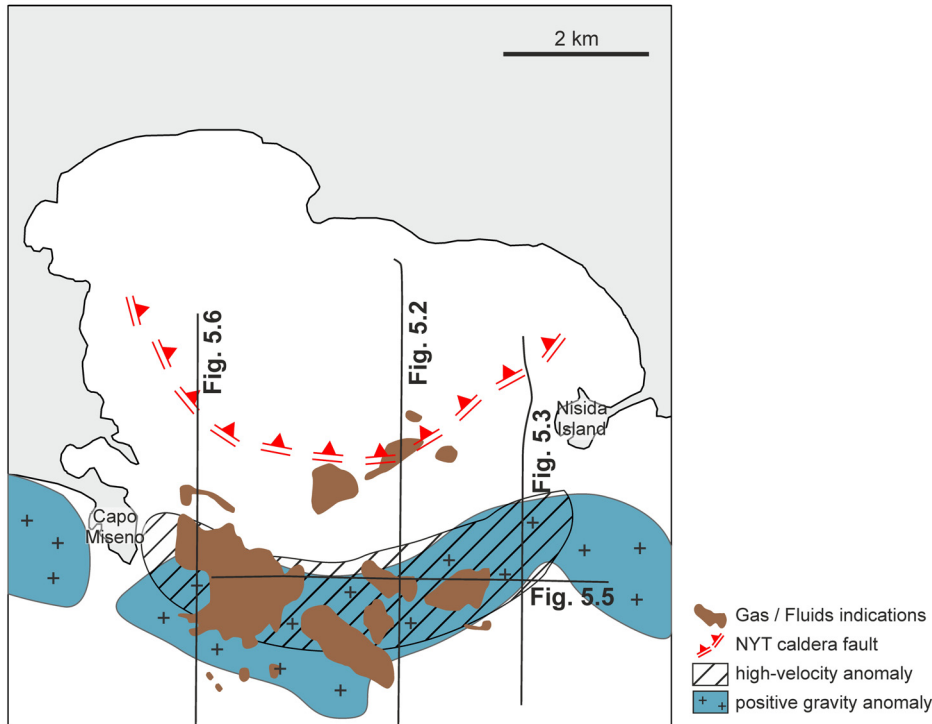


Fig. 5.9: Location of gas and NYT caldera fault as inferred from multichannel seismic data. High-velocity anomaly and positive gravity anomaly were modified after Dello Iacono et al. (2009), Capuano and Achauer (2003) and (Zollo et al., 2003).

Nonetheless, the main portion of the observed gas/fluids is located south of the NYT caldera fault, stretching from Capo Miseno almost to Nisida Island (Fig. 5.9). In this area, we did not observe any major fractures in our seismic data, which could possibly act as pathways. However, these gas/fluid-enriched zones coincide with the presence of a deeper (0.75-1.0 km depth) high-velocity anomaly (Dello Iacono et al., 2009) and positive gravity Bouguer gravity anomaly (Capuano and Achauer, 2003; Zollo et al., 2003). These arc-shaped anomalies were previously attributed to the hypothesized presence of deeper caldera rim, probably associated with intense fracturing and intrusions. The occurrence of trapped gases/fluids in sediments at shallow depth can be regarded as further evidence for the existence of a deep fractured zone probably related to the CI caldera rim. Thus, our findings support the presence of a nested-caldera system formed by the NYT and CI eruptions, with two fractured caldera rims, both facilitating the ascent of hydrothermal gases/fluids originating from an underlying hydrothermal system. As we can observe the gases/fluids in very shallow depth below the seafloor, it can be assumed that the ascent is still occurring in recent times.

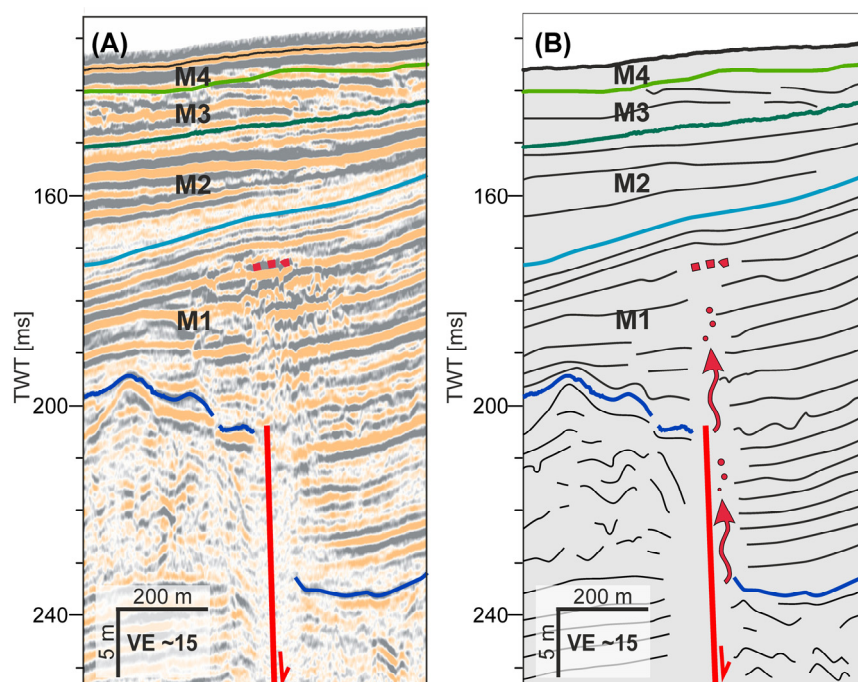


Fig. 5.10: (A) Close-up of multichannel seismic profile GeoB08-044 (for entire profile see Figure 5.2). (B) Sketch of close-up illustrating how the NYT caldera fault acts as pathway for the ascent of deeper-seated hydrothermal gases/fluids.

5.5.3 3D evolutionary model

Based on integrated observations from the high-resolution multichannel seismic data grid and onshore stratigraphic columns from borehole data, a spatial evolutionary model of the Campi Flegrei area, covering the past ~15 ka, was developed (Fig. 5.11). It illustrates the shift of the shoreline as well as main depositional and structural features in interplay with sea-level variations and volcano-tectonic activity in 5 Stages.

Stage 1 (~15 ka, after NYT caldera collapse) (Fig. 5.11-A)

During this time, when sea-level was located at ~93 mbpsl (Fig. 5.8), the NYT caldera collapsed, resulting in a subsidence of the intra-caldera depression along an arch-shaped caldera fault in the South, which likely continues in the northern sector, thereby forming the caldera depression. Consequently, the subsided central part was likely submerged as indicated by the unconformity U1 being located below the sea-level at that time (~93 m). Outside of the depression, south of Posillipo, U1 is located above the sea-level at that time, thereby indicating that the emplacement of the massive NYT pyroclastic flow led to a shoreline retreat. The Miseno Bank was connected to the mainland, forming a peninsula, while the Penta Palummo Bank formed an isolated island. A shallow marine terrace was located around the emerged Miseno and Penta Palummo Banks. The Dohrn Canyon eroded the U1 and, thus, was evidently active, probably transporting large amounts of sediment to the deeper sea.

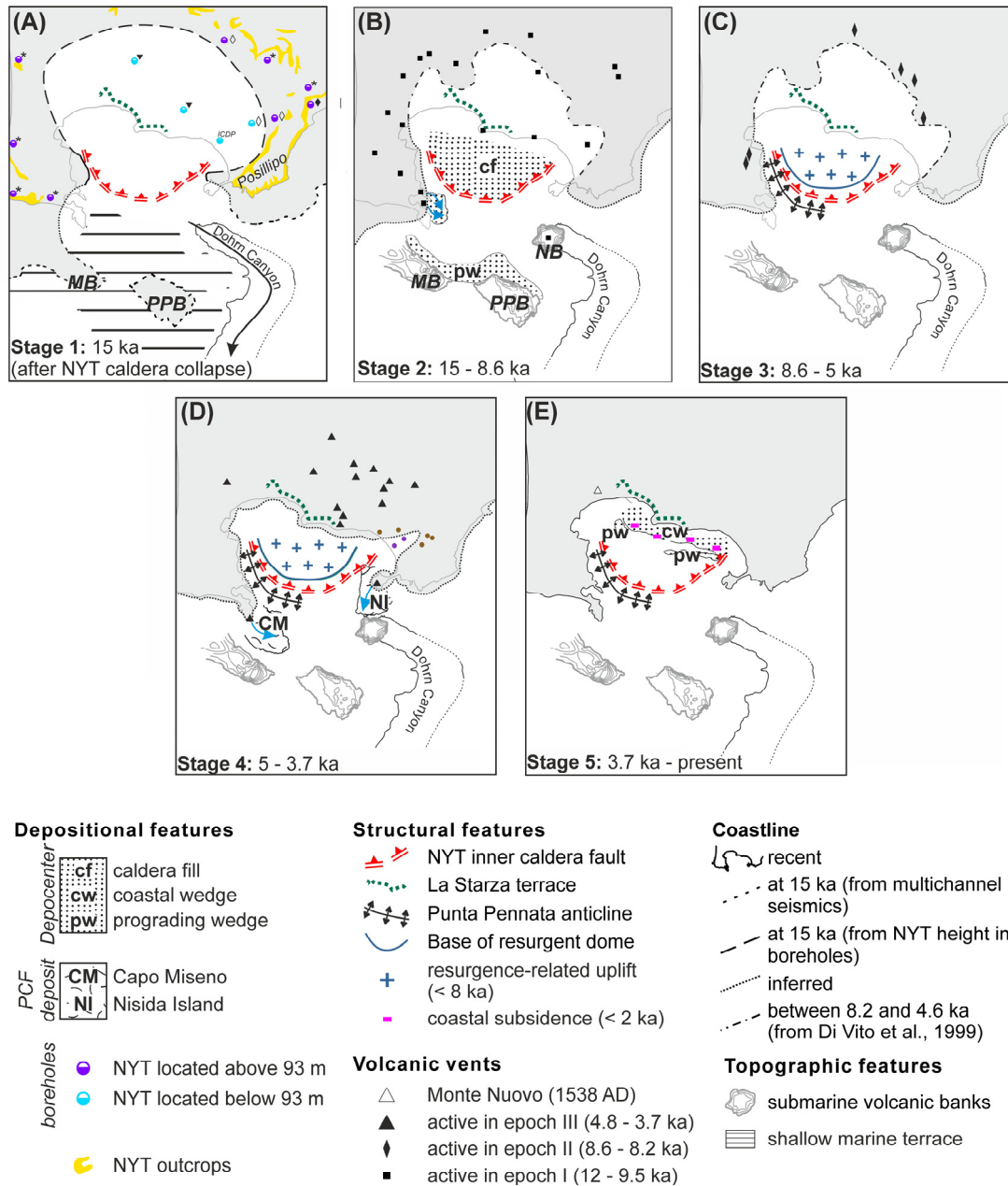


Fig. 5.11: Campi Flegrei caldera spatial evolutionary model illustrating deposition centres, structural features and the shift of the coastline in interplay with sea-level rise. Borehole stratigraphy from *Rolandi et al. (2003), ▼Milia and Torrente (2011), ◇Orsi et al., 1996, ◆Bellucci et al. (2006).

Stage 2 (~15 – 8.6 ka) (Fig. 5.11-B)

During the timespan from ~15 to 8.6 ka, sea-level rose rapidly from 93 mbpsl to 19 mbpsl (~12 m/ka) (Fig. 5.8), leading to a landward movement of the shoreline outside of the caldera depression and the submersion of the Miseno and Punta Palummo Banks. Furthermore, along the Campi Flegrei caldera margin, the shoreline shape was significantly influenced by volcanic eruptions occurring in the course of volcanic epoch I (15 – 9.5 ka). The eruption of Bacoli (12.8 ka) and Porto Miseno (11.8 ka) likely led to an increased input of sediments into the sea (e.g. due to landslides), thereby leading to

the formation of a depocenter offshore. The formation of Nisida Bank (~10 ka) in the head of the Dohrn Canyon inhibits down-canyon transport. The interplay of sea-level rise and previous subsidence of the caldera depression created significant accommodation space in the depression, which was rapidly filled by the deposition of marine Unit M2 (cf). Furthermore, a prograding wedge developed along the bathymetric highs of the submarine Miseno and Penta Palummo Bank.

Stage 3 (8.6 – 5 ka) (Fig. 5.11-C)

During Stage 3, sea-level rose less significantly from 19 mbpsl to 4 mbpsl (4 m/ka) (Fig. 5.8), leading to a landward retreat of the shoreline outside of the caldera structure. The onshore domain was dominated by six magmatic to phreatomagmatic eruptions. At the beginning of Stage 3 between 8.6 and 8.2 ka (Di Vito et al., 1999), the La Starza terrace was temporarily emerged due to resurgence-related uplift rates increasing the rate of sea-level rise. Consequently, the accommodation space on the resurgence dome was limited, leading to only minor sedimentation and the development of marine unconformity U3. Moreover, the Punta Pennata fold was activated leading to the formation of the arch-shaped Punta Pennata anticline along the submerged south-eastern caldera margin.

Stage 4 (5 – 3.7 ka) (Fig. 5.11-D)

This timespan was characterized by minor sea-level rise from 4 mbpsl to 2.7 mbpsl (Fig. 5.8) accompanied by a minor landward displacement of the shoreline in the extra-caldera area. The intra-caldera area underwent ongoing uplift due to resurgence, resulting in the ultimate emersion of the La Starza terrace at the beginning of volcanic epoch III (~ 5 ka) and the development of unconformity U4. The Bagnoli Plain was still submerged as evident by marine deposition overlying the volcanic deposits of epoch III in borehole observations (Di Vito et al., 1999). In the course of the nearshore Capo Miseno eruption at ~3.7 ka and the Nisida Island eruption at ~3.98 ka, thick pyroclastic flows entered the sea and deposited on the seafloor, covering an area of 5.1 km² and 3.7 km², respectively. During Stage 4, the Punta Pennata fold was still active.

Stage 5 (3.7 ka – present) (Fig. 5.11-E)

During Stage 5, sea-level rose insignificantly from 2.7 mbpsl to present day conditions (Fig. 5.8). Probably between 3.7 and 2 ka, an infralittoral prograding wedge (pw) developed, which has subsided by 5-25 m as consequence of coastal subsidence during the past ~2 kyrs. Post-Roman coastal subsidence led to the creation of accommodation space, which was filled by a coastal prograding wedge (cw, i.e. M4.1) during the past ~2 ka. The Punta Pennata fold was still active during Stage 5.

5.6 Conclusions

A semi-3D grid of high-resolution multichannel seismic data provided comprehensive insights into the post-collapse evolution of the Campi Flegrei caldera since the NYT eruption at ~ 15 ka. Based on an integrated analysis of the here presented seismic data and previously published borehole data, a novel 3D model, illustrating post-collapse deposition in response to sea-level variations and volcano-tectonic activity, was established.

Four major sedimentary units (M1-M4) deposited in the course of sea-level rise and three main volcanoclastic units, related to the Nisida Bank (V1), the Nisida Island (V2) and the Capo Miseno (V3) eruptions, could be identified in the seismic data. The ages of the volcanic units could be constrained based on a seismostratigraphic approach, thereby supporting previously proposed values from Di Vito et al. (1999) for the Nisida Bank (10.3-9.5 ka) and from Di Renzo et al. (2011) for the Capo Miseno (3.7 ka) and Nisida Island (3.98 ka) eruptions. The Nisida Bank, which is entirely submarine, has a total DRE volume of 0.14 km^3 , indicating a large-scale eruption. The Nisida Island and Capo Miseno units represent pyroclastic flow deposits that entered the sea and deposited under marine condition. Hence, they only represent a portion of the overall erupted material. The estimated total DRE volume of the Nisida Island and Capo Miseno eruptions yields values of 0.10 km^3 and 0.08 km^3 , respectively. This indicates that the Nisida Island eruption was of (at least) large scale, while the Capo Miseno eruption was of (at least) moderate scale.

Based on the seismic data, major structural features such as an arc-shaped shallow NYT caldera fault, the Punta Pennata anticline and a resurgent dome in the intra-caldera area could be mapped in detail. Our results suggest that the NYT caldera depression is filled with on average ~ 61 m thick marine sediments, deposited between 15 and 8.6 ka. Moreover, we found evidence that the NYT caldera fault acts as pathway for the post-collapse ascent of gases/fluids, probably originating from a previously hypothesized shallow hydrothermal system. The presence of shallow gas/fluid-rich patches south of the NYT caldera fault indicates the existence of a deeper fracture zone probably related to the Campanian Ignimbrite caldera collapse at ~ 39 ka. As these gas/fluid-rich zones are located in the uppermost marine unit (M4), we inferred that the ascent has occurred relatively recent (< 3.7 ka).

In the timespan from 8.6 to 3.7 ka, the depositional environment in the offshore sector of the Campi Flegrei caldera was mainly influenced by the development of a post-collapse resurgent dome in the intra-caldera area. As result of resurgence-related uplift exceeding the rate of sea-level rise, major unconformities developed and the accommodation space on top of the resurgent dome was significantly limited. Furthermore, the Punta Pennata fold has been active since 8.6 ka, leading to local uplift and limitation of accommodation

space. Between 3.7 and 2 ka, an infralittoral prograding wedge developed in the coastal shallow water. Furthermore, coastal erosion took place in water depth of ≤ 20 m, leading to the formation of a local erosional unconformity. Since 2 ka, the coastal area of the Gulf of Pozzuoli has undergone post-Roman subsidence of 3-25 m. Consequently, accommodation space was created and a coastal prograding wedge has deposited.

5.7 Acknowledgements

The seismic dataset was acquired during the CAFE-7/3 expedition funded by the Italian Research Council through the CNR Shiptime Programme (Oceanographic Cruise_CAFE_07), seismic acquisition was supported by German Research Foundation (DFG) within the ICDP priority programme (Grant No. SP296/30-1). Data processing and analysis was funded through the DFG's ICDP priority programme (Grant No. SP296/34-1; SP296/34-2). Additional support was provided by the Bremen International Graduate School for Marine Sciences (GLOMAR). We are grateful to Schlumberger for providing the VISTA 2D/3D Seismic Data Processing software package and to IHS for providing the KINGDOM seismic interpretation software.

This page is intentionally left blank

Chapter 6

6 Conclusions and Outlook

Within this thesis, multichannel reflection seismic data from the Campi Flegrei caldera (southern Italy) were utilized as a unique example to investigate the formation and evolution of large collapse calderas. Such calderas are associated with the most destructive and violent type of volcanic activity, and are capable of triggering catastrophes in the same order of magnitude as giant meteorite impacts. Consequently, caldera-forming eruptions can have – and have had – devastating socioeconomic impacts and also severe effects on the global climate (Self, 2015). Comprehending past caldera-forming events constitutes a first step towards improving our understanding of present-day volcanism and towards assessing the full hazard potential of future eruptions.

This main aim of this thesis was to significantly improve the overall knowledge of caldera volcanism by investigating (1) the link between regional tectonism and volcanic activity, (2) caldera-formation mechanisms, and (3) post-caldera volcano-tectonic processes at the world’s most active caldera, the Campi Flegrei caldera located in southern Italy (De Natale et al., 2006). The Campi Flegrei caldera is among the highest volcanic risk areas on Earth due to its history of large-scale explosive eruptions, its ongoing episodes of unrest, and the population density of its direct surroundings, with nearly 2.5 million people living in its close vicinity (De Natale et al., 2006; Ricci et al., 2013). These characteristics highlight a strong need for understanding the Campi Flegrei caldera’s genesis and evolution.

The database of this thesis is a hitherto novel set of multichannel reflection seismic data, which were utilized to examine the offshore portion of the Campi Flegrei caldera as well as the greater vicinity of the Gulf of Naples. Within the framework of this thesis, the first semi-3D multichannel seismic investigation of a large-collapse caldera was presented, providing novel insights on the origin and post-caldera evolution of the Campi Flegrei caldera. In this respect, the current thesis underlined the excellent suitability of multichannel reflection seismics in exploring subsurface structures of (partly) submerged calderas across the planet, such as the Santorini caldera (Greece), the Toba caldera (Indonesia), and the Kikai caldera (Japan). Additionally, the dataset was acquired as pre-site survey for a joint IODP/ICDP campaign.

The main findings of this work were presented in three standalone research manuscripts (Chapters 3 – 5). Chapter 3 focused on the tectono-sedimentary development of the Gulf of Naples over a long time span of one million years. In Chapter 4 and 5 the focus was shifted towards the Campi Flegrei caldera, with Chapter 4 mainly dealing with the

caldera genesis, and Chapter 5 outlining the post-caldera evolution. The main outcomes of these three manuscripts are synthesised in the following sections.

6.1 Tectono-sedimentary processes in the Gulf of Naples

Chapter 3 discussed the regional tectonic setting and explored the interaction between fault activity and volcanism at the Campi Flegrei Volcanic Zone (CVZ) and the Somma-Vesuvius. More specifically, it investigated the tectono-sedimentary evolution of the Gulf of Naples half-graben during the last million years in new detail. The chapter revealed two tectonically active periods leading to the main subsidence of the half-graben (1) between 1 and 0.40 Ma and (2) between 0.14 to 0.02 Ma. In contrast, the timespans between 0.40 and 0.14 Ma and from 0.02 Ma onwards have been periods of tectonic stability. The onset of increased tectonic activity at 0.14 Ma is approximately coincident with the initiation of intense volcanism in the CVZ and at the Somma-Vesuvius. This observation strongly suggests a close linkage between tectonism and volcanism. Therefore, tectonic and volcanic activities since 0.14 Ma were interpreted as being related to the reactivation of major normal faults. In the CVZ, the reactivation of a NE-SW-trending fault probably led to tectonic subsidence of the half graben, thereby facilitating the ascent of magma and, thus, eruptions. This suggests that the large-scale CI eruption at 39 ka was triggered by regional tectonism. At the Somma-Vesuvius, the reactivation of a NW-SE trending fault probably led to additional subsidence as well as eruptions. However, since 0.02 Ma, and thus including the NYT eruption at 15 ka, there is no evidence of major subsidence in the Gulf of Naples, which may either indicate that the tectonic control on eruption mechanisms merely played a minor role during that time span, or that the seismic data were not able to resolve subsidence during this relatively short time interval.

This above described interaction between deposition, tectonism and volcanism was presented in a comprehensive 3D model outlining the spatial and temporal evolution of the Gulf of Naples half-graben basin during the past one million years (Fig. 3.9). This new model represents an important contribution towards understanding the tectonic development of the area as well as its link to local volcanism.

6.2 The origin of the Campi Flegrei caldera

In Chapter 4, the strongly debated origin of the Campi Flegrei caldera (nested vs. single caldera) was investigated utilizing selected high-resolution multichannel seismic profiles. For the first time, high-resolution reflection seismic data were able to reveal the presence of a nested-caldera complex formed during two collapses related to the CI eruption at ~39 ka and the more recent NYT eruption at ~15 ka. An inner-caldera ring-fault separating the caldera margin from the caldera depression was clearly imaged. In the Eastern and Western sections of the caldera margin, this fault was already activated

during the CI eruption. However, at the Southern caldera margin, the fault was only associated with the smaller NYT collapse, with the CI fracture zone being assumed to lie further South and at greater depths (Chapter 5). The NYT caldera seems to have been formed in the course of an asymmetrical, piecemeal-like collapse with variable amounts of subsidence with a maximum subsidence of ~ 75 m in the offshore portion. In contrast, the CI caldera collapse was probably in the range from several hundreds of meters to a few kilometres.

The genesis and evolution of the Campi Flegrei caldera with respect to the above described collapse history and post-collapse caldera resurgence was presented in a novel conceptual model (Fig. 4.7). This model outlines the formation of a nested-caldera system and should be applicable to other caldera settings. Hence, the findings presented in Chapter 4 may be regarded as a significant advancement towards a better understanding of the Campi Flegrei caldera in particular, as well as the formation of nested calderas in general.

6.3 Post-collapse processes and deposition at the Campi Flegrei caldera

In Chapter 5, the caldera evolution since the NYT eruption at 15 ka was investigated utilizing a semi-3D high-resolution multichannel seismic dataset. This study represents the first 3D analysis of a submerged caldera setting, its structure and infill deposits. The high spatial data coverage in combination with high-vertical resolution allowed for a comprehensive examination of the depositional environment, as well as the assessment of the volume of post-collapse eruptions. As main outcome, a novel 3D model (Fig. 5.11), illustrating post-collapse deposition in response to sea-level variations and volcano-tectonic activity, was established based on an integrated analysis of the presented multichannel seismic data and previously published borehole data.

The 3D-investigative effort enabled the imaging of the NYT caldera structure, which was strongly modified in the post-collapse phase by caldera resurgence, post-caldera volcanism, local tectonic uplift, and sea-level variations. It indicated that the NYT caldera is bounded by an arc-shaped ring-fault, which correspond to the same ring-fault as described in Chapter 4. The caldera depression acted as significant accommodation space in the post-collapse phase and is filled with an on average 61-m thick sequence of marine and reworked volcanoclastic sediments that was deposited between 15 and 8.6 ka. Since ~ 8.6 ka, the depositional environment was mainly influenced by caldera resurgence, thereby limiting the accommodation space on the uplifted resurgent dome. At ~ 5 ka, resurgence-related uplift ultimately led to the emersion of the northern part of the caldera depression. Before that time, the majority of the caldera depression was submerged.

The 3D aspect of the dataset allowed for a new assessment of post-caldera eruption volumes of major volcanoclastic units identified in the offshore sector of the caldera. The erupted volume of the submarine Nisida Bank was estimated to be $\sim 0.14 \text{ km}^3$ (DRE), leading to the conclusion that the Nisida Bank eruption represents a large-scale eruption according to the Volcanic Explosivity Index (VEI=4). The estimated total DRE volumes (onshore and offshore) of the Nisida Island and Capo Miseno eruptions yielded values of 0.10 km^3 and 0.08 km^3 , respectively. This indicates that the Nisida Island eruption was also of (at least) large scale (VEI=4), while the Capo Miseno eruption was of (at least) moderate scale (VEI=3). These values substantially outnumber estimations of previous studies, which only considered the onshore deposits of these eruptions (Di Renzo et al., 2011) and thereby underestimated the overall amount of erupted material and the explosive magnitude of the eruptions. Therefore, the findings of Chapter 5 significantly improve the understanding of the post-caldera volcanic activity by showing that some eruptions might have been considerably larger and more devastating than previously estimated. Moreover, the combination of a seismostratigraphic approach and previously published data, allowed for advanced constraining the eruption chronology.

6.4 Hydrothermalism at the Campi Flegrei caldera

Previous studies proposed that the source of the recent short-term episodes of unrest at the Campi Flegrei caldera may be associated with fluid migration related to a hypothesized shallow ($<2 \text{ km}$) hydrothermal system (Lima et al., 2009; Chiodini et al., 2015). In Chapter 5, the influence of hydrothermalism on the offshore sector of the Campi Flegrei caldera was investigated in order to test this hypothesis.

Based on a spatial mapping of shallow amplitude anomalies interpreted as gas/fluid-enriched patches, it could be inferred that the NYT caldera fault acts as a pathway for the ascent of hydrothermal gases/fluids likely originating from the hypothesized hydrothermal aquifer. Therefore, these gases/fluids can be regarded as shallow expression of a deeper hydrothermal aquifer ($<2 \text{ km}$). However, given that the majority of gases/fluid-rich zones are located further south of the NYT caldera fault, these zones were interpreted as being indicative of a deep-seated fracture zone probably related to the CI caldera collapse at 39 ka. Additionally, as these gases and/or fluids are located at very shallow depths below the seafloor, it was concluded that the fluid migration has occurred relatively recently ($<3.7 \text{ ka}$) and may still be ongoing.

These findings verified modelling results, which indicated that major faults may act as conduits for the ascent of high-temperature fluids (Jasim et al., 2015). Furthermore, they support and update the hypotheses of the existence of a shallow hydrothermal system by showing clear evidence for recent hydrothermal activity in the offshore sector of the

Campi Flegrei caldera, which in return indirectly strengthens the theory of hydrothermalism be the driving force for the phases of recent unrest.

6.5 Outlook

This thesis may be regarded as a significant advancement in the overall understanding of the genesis and evolution of the Campi Flegrei caldera as well as the tectonic formation of the Gulf of Naples half-graben basin.

Nevertheless, further research is still required to be able to answer the following questions:

- What is the maximum vertical extent of the CI caldera? And what is the appearance of its deep-seated architecture and the volcanic roots?
- Did any other large-scale ignimbritic eruption occur in the Campi Flegrei area prior the CI eruption?
- What is the appearance of the hydrothermal system at greater depths?
- What is the link between the hydrothermal and magmatic systems in generating unrest episodes? And do the ongoing episodes of unrest represent eruption precursors?

In order to investigate these questions, a joint IODP/ICDP approach was initiated and new seismic data were acquired. In particular, the interaction between shallow hydrothermalism and deeper magmatic activity shall be examined in order to understand their contribution to the ongoing unrest episodes. In that respect, it is of high priority to find out whether the unrest episodes may be related to changes in the magmatic system, which could be interpreted as eruption precursors. Understanding the ongoing unrest episodes is of paramount importance for the reliable assessment of the hazard potential of the Campi Flegrei area. While the ICDP drilling (*Campi Flegrei Deep Drilling Project, CFDDP*) successfully finished the 500-m long pilot hole drilling in December 2012, an associated IODP drilling is still in the pre-proposal stage (671-pre/-pre2).

The high-resolution seismic data presented in this thesis, in combination with a new 3D grid (25-50 m spacing) of low-frequency data (central frequency 50 Hz) that was acquired in January/February 2016 (Fig. 6.1), acts as pre-site survey for the combined IODP/ICDP drilling campaign. The signal penetration of the low-frequency seismic data achieved the IODP target depth of maximally 2 km. Hence, they are suitable to reactivate the IODP proposal as well as to guide a diverted ICDP drilling into the centre of the Gulf of Pozzuoli. The objectives, drilling strategies as well as the positioning of new IODP drill sites will also be further discussed and refined during a Magellan workshop planned for early 2017.

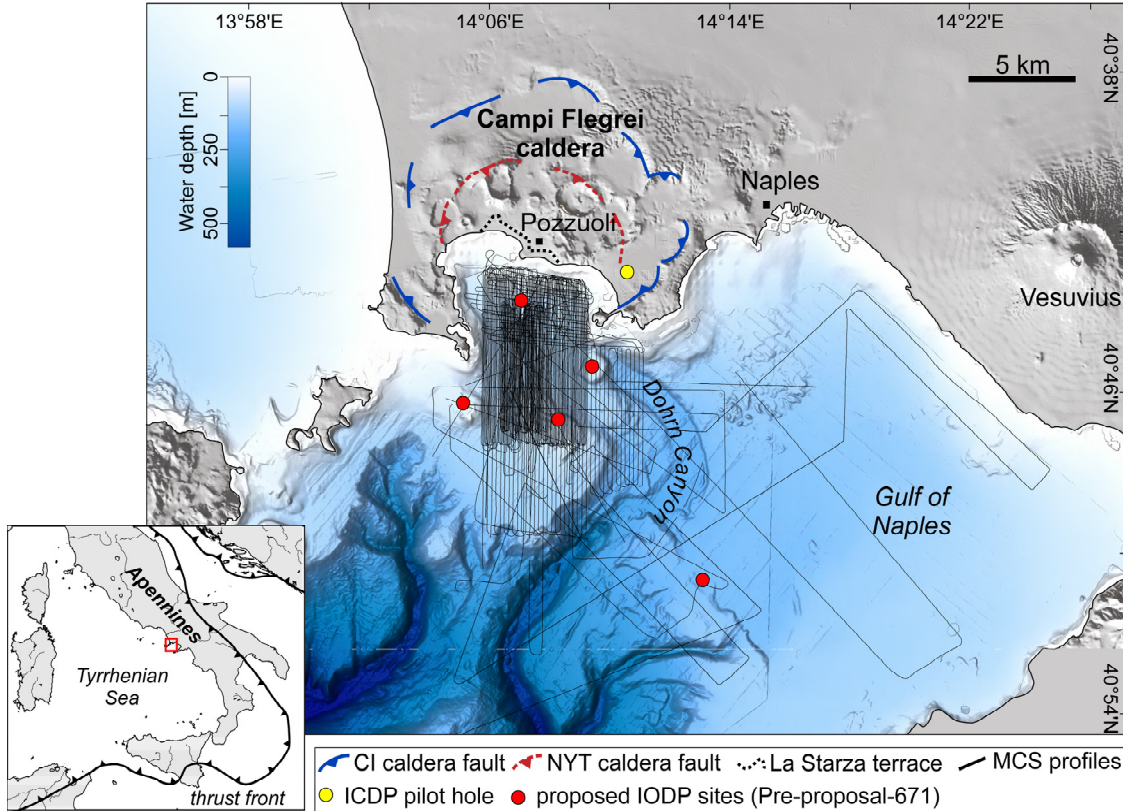


Fig. 6.1: Overview map of all the GeoB16 profiles acquired in the Gulf of Naples and the Gulf of Pozzuoli. The semi-3D grid has a profile spacing of 25 to 50 m.

In detail, the low-frequency seismic data allow for an imaging of hydrothermally altered zones (visible as amplitude anomalies) and deep-seated fluid pathways (fault mapping), thereby providing crucial information on the existence and location of a hypothesised hydrothermal system. Moreover, they allow for the identification of volcanic feeder-dikes (zones of acoustic blanking below volcanic features). Furthermore, the data permit an extension of the stratigraphic concept into greater depths, which would significantly contribute to the understanding of the volcanological history prior the CI event at 39 ka. In addition to being recorded with a seismic streamer, the GI-gun shots were also recorded by onshore and offshore earthquake monitoring seismometers of the *Osservatorio Vesuviano* (part of INGV) and OBS systems deployed on the floor of the Gulf of Pozzuoli. This offers the opportunity to integrate a velocity profile with the reflection seismic data, thereby providing crucial insights on the lithology of adjacent deposits. For instance, based on this approach, additional validity could be added to the seismic data interpretation, high-velocity features such as intrusions could be distinguished from volcanoclastic or marine sediments, and it would be possible to gain information on the nature of zones of acoustic blanking.

Acknowledgements

First, I would like to thank my supervisor, Volkhard Spiess, for providing me the opportunity to combine my favourite research topic with my preferred research method in my doctoral project. Thank you for the guidance, trust, and support, which greatly helped me developing my own ideas and advancing the thesis. Also thanks for all the provided opportunities, be it expedition/conference participations or gathering teaching experience.

Moreover, I would like to thank Sebastian Krastel, who has not just spontaneously agreed to review my thesis but who has also provided me my first “HiWi” job in 2008 and thereby my first real insights into geophysics. So, thanks a lot for this very early support, which probably to some extent lay the ground for this doctoral thesis.

Tante grazie to Marco Sacchi, who, with his patience, kindness and Italian easygoingness, made my visits to beautiful Napoli as well the time on board an amazing experience. Thank you for the delicious Italian food, the many teeny-tiny espressos, the cruise with your sail boat as well as all the scientific discussions and advice.

Furthermore, I would like to thank Wolfgang Bach for being part of my thesis committee and giving helpful advice.

Special thanks go to my friends and colleagues from the MTU working group: Fenna Bergmann, Noémi Fekete, Julia Haberkern, Hanno Keil, Florian Meier, Aisgo Oguro, Asli Özmaral, Luisa Palamenghi, Carlos Ramos, Anna Reusch, Tilmann Schwenk, Zsuzsanna Tóth, and Stefan Wenau. Thanks for all the fun moments that we shared during our innumerable coffee breaks, lunches and our very unique *seismic events* as well as on-board and during conferences. In this sense, many thanks also to my PhD and postdoc fellows from MARUM/GLOMAR, FB5 and AWI, in particular, Grit Warratz, Andreas Türke and Tanja Hörner. It has been a great and unique experience with you guys.

Many thanks also to the student assistants who supported this project namely Rouven Brune, Gino Frielingshaus, and Henning Marinkovic.

Last but definitely not least, I would like to thank the people who have already been there before the PhD and who will hopefully stick around much longer. Thanks for all the positive distraction and open ears. In particular, I would like to thank my family including my parents, my grandparents, my brothers and their small families, as well as Wout for their never-ending support and encouragement. Without you guys I would have never even started writing this thesis, you are the best.

References

- Acocella, V., 2007. Understanding caldera structure and development: An overview of analogue models compared to natural calderas. *Earth-Science Reviews* 85, 125-160.
- Acocella, V., 2008. Activating and reactivating pairs of nested collapses during caldera-forming eruptions: Campi Flegrei (Italy). *Geophysical Research Letters* 35, L17304.
- Acocella, V., 2010. Evaluating fracture patterns within a resurgent caldera: Campi Flegrei, Italy. *Bulletin of Volcanology* 72, 623-638.
- Acocella, V., Cifelli, F., Funiciello, R., 2000. Analogue models of collapse calderas and resurgent domes. *Journal of Volcanology and Geothermal Research* 104, 81-96.
- Acocella, V., Cifelli, F., Funiciello, R., 2001. The control of overburden thickness on resurgent domes: insights from analogue models. *Journal of Volcanology and Geothermal Research* 111, 137-153.
- Acocella, V., Funiciello, R., 1999. The interaction between regional and local tectonics during resurgent doming: the case of the island of Ischia, Italy. *Journal of Volcanology and Geothermal Research* 88, 109-123.
- Acocella, V., Funiciello, R., 2006. Transverse systems along the extensional Tyrrhenian margin of central Italy and their influence on volcanism. *Tectonics* 25, TC2003.
- Aiello, G., Angelino, A., Argenio, B., Marsella, E., Pelosi, N., Ruggieri, S., Siniscalchi, A., 2005. Buried volcanic structures in the Gulf of Naples (Southern Tyrrhenian Sea, Italy) resulting from high resolution magnetic survey and seismic profiling.
- Aiello, G., Marsella, E., Fiore, V., 2012. New seismo-stratigraphic and marine magnetic data of the Gulf of Pozzuoli (Naples Bay, Tyrrhenian Sea, Italy): inferences for the tectonic and magmatic events of the Phlegrean Fields volcanic complex (Campania). *Mar Geophys Res* 33, 97-125.
- Aizawa, K., Acocella, V., Yoshida, T., 2006. How the development of magma chambers affects collapse calderas: insights from an overview, in: Troise, C., De Natale, G., Kilburn, C.R.J. (Eds.), *Mechanisms of Activity and Unrest at Large Calderas*. Geological Society, London, pp. 65-81.
- Albino, F., Pinel, V., Sigmundsson, F., 2010. Influence of surface load variations on eruption likelihood: application to two Icelandic subglacial volcanoes, Grímsvötn and Katla. *Geophysical Journal International* 181, 1510-1524.
- Allan, A.S.R., Wilson, C.J.N., Millet, M.-A., Wysoczanski, R.J., 2012. The invisible hand: Tectonic triggering and modulation of a rhyolitic supereruption. *Geology*.

- Bailey, R.A., Dalrymple, G.B., Lanphere, M.A., 1976. Volcanism, structure, and geochronology of Long Valley Caldera, Mono County, California. *Journal of Geophysical Research* 81, 725-744.
- Barberi, F., Cassano, E., La Torre, P., Sbrana, A., 1991. Structural evolution of Campi Flegrei caldera in light of volcanological and geophysical data. *Journal of Volcanology and Geothermal Research* 48, 33-49.
- Barr, D., 1987. Structural/stratigraphic models for extensional basins of half-graben type. *Journal of Structural Geology* 9, 491-500.
- Becker, J.J., Sandwell, D.T., Smith, W.H.F., Braud, J., Binder, B., Depner, J., Fabre, D., Factor, J., Ingalls, S., Kim, S.-H., Ladner, R., Marks, K., Nelson, S., Pharaoh, A., Sharman, G., Trimmer, R., von Rosenberg, R., Wallace, G., Weatherall, P., 2009. Global Bathymetry and Elevation Data at 30 Arc Seconds Resolution: SRTM30_PLUS. *Marine Geodesy* 32, 355-371.
- Bellier, O., Sébrier, M., 1994. Relationship between tectonism and volcanism along the Great Sumatran Fault Zone deduced by spot image analyses. *Tectonophysics* 233, 215-231.
- Bellucci, F., Milia, A., Rolandi, G., Torrente, M.M., 2006. Chapter 8 Structural control on the Upper Pleistocene ignimbrite eruptions in the Neapolitan area (Italy): volcano tectonic faults versus caldera faults, in: Vivo, B.D. (Ed.), *Developments in Volcanology*. Elsevier, pp. 163-180.
- Bernoulli, D., Jenkyns, H.C., 1974. Alpine, Mediterranean, and Central Atlantic Mesozoic Facies in Relation to the Early Evolution of the Tethys, Modern and Ancient Geosynclinal Sedimentation. *Society of Economic Paleontologists and Mineralogists*, pp. 129-160.
- Boccaletti, M., Nicolich, R., Tortorici, L., 1984. Geological and Geodynamical Aspects on the Mediterranean The Calabrian Arc and the Ionian Sea in the dynamic evolution of the Central Mediterranean. *Marine Geology* 55, 219-245.
- Brancaccio, L., Cinque, A., Romano, P., Roskopf, C., Russo, F., Santangelo, N., Santo, A., 1991. Geomorphology and neotectonic evolution of a sector of the Tyrrhenian flank of the southern Apennines (Region of Naples, Italy). *Z. Geomorph. N.F.* 82, 47-58.
- Branney, M., Acocella, V., 2015. Calderas, in: Sigurdsson, H. (Ed.), *The Encyclopedia of Volcanoes (Second Edition)*. Academic Press, Amsterdam, pp. 299-315.
- Branney, M.J., Kokelaar, P., 2001. *Pyroclastic Density Currents and the Sedimentation of Ignimbrites*. Geological Society of London.
- Bray, J.R., 1977. Pleistocene Volcanism and Glacial Initiation. *Science* 197, 251-254.

- Brocchini, D., Principe, C., Castradori, D., Laurenzi, A.M., Gorla, L., 2001. Quaternary evolution of the southern sector of the Campanian Plain and early Somma-Vesuvius activity: insights from the Trecase 1 well. *Mineralogy and Petrology* 73, 67-91.
- Brown, R.J., Andrews, G.D.M., 2015. Deposits of Pyroclastic Density Currents The Encyclopedia of Volcanoes (Second Edition). Academic Press, Amsterdam, pp. 631-648.
- Brown, R.J., Orsi, G., de Vita, S., 2008. New insights into Late Pleistocene explosive volcanic activity and caldera formation on Ischia (southern Italy). *Bulletin of Volcanology* 70, 583-603.
- Bruno, P.P.G., Rapolla, A., Di Fiore, V., 2003. Structural setting of the Bay of Naples (Italy) seismic reflection data: implications for Campanian volcanism. *Tectonophysics* 372, 193-213.
- Burgisser, A., Bergantz, G.W., 2002. Reconciling pyroclastic flow and surge: the multiphase physics of pyroclastic density currents. *Earth and Planetary Science Letters* 202, 405-418.
- Capuano, P., Achauer, U., 2003. Gravity field modeling in the Vesuvius and Campanian area, in: Zollo, A., Bobbio, A., Gasparini, P., Casale, R., Yeroyanni, M. (Eds.), *TomoVes Seismic Project: Looking Inside Mt. Vesuvius*. CUEN, Naples, Italy.
- Capuano, P., Russo, G., Civetta, L., Orsi, G., D'Antonio, M., Moretti, R., 2013. The active portion of the Campi Flegrei caldera structure imaged by 3-D inversion of gravity data. *Geochemistry, Geophysics, Geosystems* 14, 4681-4697.
- Cas, R., Wright, J., 1991. Subaqueous pyroclastic flows and ignimbrites: an assessment. *Bulletin of Volcanology* 53, 357-380.
- Casciello, E., Cesarano, M., Pappone, G., 2006. Extensional detachment faulting on the Tyrrhenian margin of the southern Apennines contractional belt (Italy). *Journal of the Geological Society* 163, 617-629.
- Catuneanu, O., 2002. Sequence stratigraphy of clastic systems: concepts, merits, and pitfalls. *Journal of African Earth Sciences* 35, 1-43.
- Chiodini, G., Todesco, M., Caliro, S., Del Gaudio, C., Macedonio, G., Russo, M., 2003. Magma degassing as a trigger of bradyseismic events: The case of Phlegrean Fields (Italy). *Geophysical Research Letters* 30, n/a-n/a.
- Chiodini, G., Vandemeulebrouck, J., Caliro, S., D'Auria, L., De Martino, P., Mangiacapra, A., Petrillo, Z., 2015. Evidence of thermal-driven processes triggering the 2005–2014 unrest at Campi Flegrei caldera. *Earth and Planetary Science Letters* 414, 58-67.

- Chorowicz, J., 2005. The East African rift system. *Journal of African Earth Sciences* 43, 379-410.
- Cinque, A., Rolandi, G., Zamperelli, V., 1985. L'estensione dei depositi marini Olocenici nei Campi Flegrei in relazione alla vulcano-tettonica. *Boll. Soc. Geol. Ital.* 104, 327-348.
- Cioni, R., Bertagnini, A., Santacroce, R., Andronico, D., 2008. Explosive activity and eruption scenarios at Somma-Vesuvius (Italy): Towards a new classification scheme. *Journal of Volcanology and Geothermal Research* 178, 331-346.
- Cioni, R., Pistolesi, M., Rosi, M., 2015. Plinian and Subplinian Eruptions in: Sigurdsson, H. (Ed.), *The Encyclopedia of Volcanoes (Second Edition)*. Academic Press, Amsterdam, pp. 519-535.
- Cioni, R., Santacroce, R., Sbrana, A., 1999. Pyroclastic deposits as a guide for reconstructing the multi-stage evolution of the Somma-Vesuvius Caldera. *Bulletin of Volcanology* 61, 207-222.
- Civetta, L., Gallo, G., Orsi, G., 1991. Sr- and Nd-isotope and trace-element constraints on the chemical evolution of the magmatic system of Ischia (Italy) in the last 55 ka. *Journal of Volcanology and Geothermal Research* 46, 213-230.
- Cole, J.W., Milner, D.M., Spinks, K.D., 2005. Calderas and caldera structures: a review. *Earth-Science Reviews* 69, 1-26.
- Costa, A., Folch, A., Macedonio, G., Giaccio, B., Isaia, R., Smith, V.C., 2012. Quantifying volcanic ash dispersal and impact of the Campanian Ignimbrite super-eruption. *Geophysical Research Letters* 39.
- Crosweller, H.S., Arora, B., Brown, S.K., Cottrell, E., Deligne, N.I., Guerrero, N.O., Hobbs, L., Kiyosugi, K., Loughlin, S.C., Lowndes, J., Nayembil, M., Siebert, L., Sparks, R.S.J., Takarada, S., Venzke, E., 2012. Global database on large magnitude explosive volcanic eruptions (LaMEVE). *Journal of Applied Volcanology* 1, 1-13.
- D'Argenio, A., Aiello, G., de Alteriis, G., Milia, A., Sacchi, M., Tonielli, R., Angelino, A., Budillon, F., Chiocci, F., Conforti, A., de Lauro, M., di Martino, G., D'Isanto, C., Esposito, E., Ferraro, L., Innangi, S., Insinga, D.D., Iorio, M., Marsella, E., Molisso, F., Morra, V., Passaro, S., Pelosi, N., Porfido, S., Raspini, A., Ruggieri, S., Sarnacchiaro, G., Terranova, C., Vilardo, G., Violante, C., 2004a. Digital elevation model of the Bay of Naples and adjacent areas, eastern Tyrrhenian Sea, in: Pasquarè, G., Venturini, C., Groppelli, G. (Eds.), *Mapping Geology in Italy*. APAT Dipartimento Difesa del Suolo-Servizio Geologico d'Italia, Rome, pp. 21-28.
- D'Argenio, A., Pescatore, T., Senatore, M.R., 2004b. Sea-level change and volcano-tectonic interplay. The Gulf of Pozzuoli (Campi Flegrei, Eastern Tyrrhenian Sea) during the last 39 ka. *Journal of Volcanology and Geothermal Research* 133, 105-121.

- D'Auria, L., Pepe, S., Castaldo, R., Giudicepietro, F., Macedonio, G., Ricciolino, P., Tizzani, P., Casu, F., Lanari, R., Manzo, M., Martini, M., Sansosti, E., Zinno, I., 2015. Magma injection beneath the urban area of Naples: a new mechanism for the 2012–2013 volcanic unrest at Campi Flegrei caldera. *Scientific Reports* 5, 13100.
- Davy, B.W., Caldwell, T.G., 1998. Gravity, magnetic and seismic surveys of the caldera complex, Lake Taupo, North Island, New Zealand. *Journal of Volcanology and Geothermal Research* 81, 69–89.
- De Astis, G., Pappalardo, L., Piochi, M., 2004. Procida volcanic history: new insights into the evolution of the Phlegraean Volcanic District (Campania region, Italy). *Bulletin of Volcanology* 66, 622–641.
- De Natale, G., Pingue, F., Allard, P., Zollo, A., 1991. Geophysical and geochemical modelling of the 1982–1984 unrest phenomena at Campi Flegrei caldera (southern Italy). *Journal of Volcanology and Geothermal Research* 48, 199–222.
- De Natale, G., Troise, C., Pingue, F., Mastrolorenzo, G., Pappalardo, L., Battaglia, M., Boschi, E., 2006. The Campi Flegrei caldera: Unrest mechanisms and hazards, in: Troise, C., De Natale, G., Kilburn, C.R.J. (Eds.), *Mechanisms of Activity and Unrest at Large Calderas*. Geological Society, London, pp. 25–45.
- de Silva, S., Lindsay, J.M., 2015. Primary Volcanic Landforms in: Sigurdsson, H. (Ed.), *The Encyclopedia of Volcanoes (Second Edition)*. Academic Press, Amsterdam, pp. 273–297.
- De Vivo, B., Rolandi, G., Gans, P.B., Calvert, A., Bohrson, W.A., Spera, F.J., Belkin, H.E., 2001. New constraints on the pyroclastic eruptive history of the Campanian volcanic Plain (Italy). *Mineralogy and Petrology* 73, 47–65.
- Deino, A.L., Orsi, G., de Vita, S., Piochi, M., 2004. The age of the Neapolitan Yellow Tuff caldera-forming eruption (Campi Flegrei caldera – Italy) assessed by $^{40}\text{Ar}/^{39}\text{Ar}$ dating method. *Journal of Volcanology and Geothermal Research* 133, 157–170.
- Del Gaudio, C., Aquino, I., Ricciardi, G.P., Ricco, C., Scandone, R., 2010. Unrest episodes at Campi Flegrei: A reconstruction of vertical ground movements during 1905–2009. *Journal of Volcanology and Geothermal Research* 195, 48–56.
- Dello Iacono, D., Zollo, A., Vassallo, M., Vanorio, T., Judenherc, S., 2009. Seismic images and rock properties of the very shallow structure of Campi Flegrei caldera (southern Italy). *Bulletin of Volcanology* 71, 275–284.
- Derer, C.E., Schumacher, M.E., Schäfer, A., 2005. The northern Upper Rhine Graben: basin geometry and early syn-rift tectono-sedimentary evolution. *International Journal of Earth Sciences* 94, 640–656.

- Dewey, J.F., Helman, M.L., Turco, E., Hutton, D.H.W., Knott, S.D., 1989. Kinematics of the western Mediterranean, in: Coward, M.P., Dietrich, D., Park, R.G. (Eds.), *Alpine Tectonics*, Geological Society Special Publication, pp. 265-283.
- Di Girolamo, P., Ghiara, M.R., Lirer, L., Munno, R., Rolandi, G., Stanzione, D., 1984. Vulcanologia e petrologia dei Campi Flegrei. *Boll. Soc. Geol. It.* 103, 349-413.
- Di Renzo, V., Arienzo, I., Civetta, L., D'Antonio, M., Tonarini, S., Di Vito, M.A., Orsi, G., 2011. The magmatic feeding system of the Campi Flegrei caldera: Architecture and temporal evolution. *Chemical Geology* 281, 227-241.
- Di Vito, M., Lirer, L., Mastrolorenzo, G., Rolandi, G., 1987. The 1538 Monte Nuovo eruption (Campi Flegrei, Italy). *Bulletin of Volcanology* 49, 608-615.
- Di Vito, M.A., Isaia, R., Orsi, G., Southon, J., de Vita, S., D'Antonio, M., Pappalardo, L., Piochi, M., 1999. Volcanism and deformation since 12,000 years at the Campi Flegrei caldera (Italy). *Journal of Volcanology and Geothermal Research* 91, 221-246.
- Druitt, T.H., 1998. Pyroclastic density currents. Geological Society, London, Special Publications 145, 145-182.
- Druitt, T.H., Sparks, R.S.J., 1984. On the formation of calderas during ignimbrite eruptions. *Nature* 310, 679-681.
- Dufek, J., Esposti Ongaro, T., Roche, O., 2015. Pyroclastic Density Currents: Processes and Models A2 - Sigurdsson, Haraldur, *The Encyclopedia of Volcanoes* (Second Edition). Academic Press, Amsterdam, pp. 617-629.
- Dvorak, J.J., Berrino, G., 1991. Recent ground movement and seismic activity in Campi Flegrei, southern Italy: Episodic growth of a resurgent dome. *Journal of Geophysical Research: Solid Earth* 96, 2309-2323.
- Einsele, G., 2000. *Sedimentary basins: evolution, facies, and sediment budget*, 2nd, completely rev. and enl. ed. Springer Verlag, Berlin.
- Embry, A.F., 1995. Sequence boundaries and sequence hierarchies: problems and proposals, in: R.J. Steel, V.L.F.E.P.J., Mathieu, C. (Eds.), *Norwegian Petroleum Society Special Publications*. Elsevier, pp. 1-11.
- Fedele, F.G., Giaccio, B., Isaia, R., Orsi, G., 2002. Ecosystem Impact of the Campanian Ignimbrite Eruption in Late Pleistocene Europe. *Quaternary Research* 57, 420-424.
- Fedele, F.G., Giaccio, B., Isaia, R., Orsi, G., 2013. The Campanian Ignimbrite Eruption, Heinrich Event 4, and Palaeolithic Change in Europe: A High-Resolution Investigation, *Volcanism and the Earth's Atmosphere*. American Geophysical Union, pp. 301-325.

- Fedele, L., Insinga, D.D., Calvert, A.T., Morra, V., Perrotta, A., Scarpati, C., 2011. $^{40}\text{Ar}/^{39}\text{Ar}$ dating of tuff vents in the Campi Flegrei caldera (southern Italy): toward a new chronostratigraphic reconstruction of the Holocene volcanic activity. *Bulletin of Volcanology* 73, 1323-1336.
- Fitzsimmons, K.E., Hambach, U., Veres, D., Iovita, R., 2013. The Campanian Ignimbrite Eruption: New Data on Volcanic Ash Dispersal and Its Potential Impact on Human Evolution. *PLoS ONE* 8.
- Florio, G., Fedi, M., Cella, F., Rapolla, A., 1999. The Campanian Plain and Phlegrean Fields: structural setting from potential field data. *Journal of Volcanology and Geothermal Research* 91, 361-379.
- Frostick, L.E., Steel, R.J., 1993. Tectonic Signatures in Sedimentary Basin Fills: An Overview, Tectonic Controls and Signatures in Sedimentary Successions. Blackwell Publishing Ltd., pp. 1-9.
- Fusi, N., 1996. Structural settings of the carbonatic basement and its relationship with magma uprising in the Gulf of Naples (Southern Italy). *Annals of Geophysics* 39, 493-509.
- Fusi, N., Mirabile, L., Camerlenghi, A., Ranieri, G., 1991. Marine geophysical survey of the Gulf of Naples (Italy): Relationship between submarine volcanic activity and sedimentation. *Mem. Soc. Geol. It.* 47, 95-114.
- Geyer, A., Martí, J., 2008. The new worldwide collapse caldera database (CCDB): A tool for studying and understanding caldera processes. *Journal of Volcanology and Geothermal Research* 175, 334-354.
- Gueguen, E., Doglioni, C., Fernandez, M., 1998. On the post-25 Ma geodynamic evolution of the western Mediterranean. *Tectonophysics* 298, 259-269.
- Hall, K., 1982. Rapid deglaciation as an initiator of volcanic activity: An hypothesis. *Earth Surface Processes and Landforms* 7, 45-51.
- Heap, M.J., Baud, P., Meredith, P.G., Vinciguerra, S., Reuschlé, T., 2014. The permeability and elastic moduli of tuff from Campi Flegrei, Italy: implications for ground deformation modelling. *Solid Earth* 5, 25-44.
- Hippolyte, J.C., Angelier, J., Roure, F., 1994. A major geodynamic change revealed by Quaternary stress patterns in the southern Apennines (Italy). *Tectonophysics* 230, 199-210.
- Insinga, D., Calvert, A.T., Lanphere, M.A., Morra, V., Perrotta, A., Sacchi, M., Scarpati, C., Saburomaru, J., Fedele, L., 2006. Chapter 6 The Late-Holocene evolution of the Miseno area (south-western Campi Flegrei) as inferred by stratigraphy, petrochemistry

- and $^{40}\text{Ar}/^{39}\text{Ar}$ geochronology, in: Vivo, B.D. (Ed.), *Developments in Volcanology*. Elsevier, pp. 97-124.
- Jasim, A., Whitaker, F.F., Rust, A.C., 2015. Impact of channelized flow on temperature distribution and fluid flow in restless calderas: Insight from Campi Flegrei caldera, Italy. *Journal of Volcanology and Geothermal Research* 303, 157-174.
- Judenherc, S., Zollo, A., 2004. The Bay of Naples (southern Italy): Constraints on the volcanic structures inferred from a dense seismic survey. *Journal of Geophysical Research: Solid Earth* 109.
- Kastens, K., Mascle, J., Auroux, C., Bonatti, E., Broglia, C., Channell, J., Curzi, P., Emeis, K.-C., Glaçon, G., Hasegawa, S., Hieke, W., Mascle, G., McCoy, F., McKenzie, J., Mendelson, J., Müller, C., Réhault, J.-P., Robertson, A., Sartori, R., Sprovieri, R., Torrii, M., 1988. ODP Leg 107 in the Tyrrhenian Sea: Insights into passive margin and back-arc basin evolution. *Geological Society of America Bulletin* 100, 1140-1156.
- Kennedy, B., Wilcock, J., Stix, J., 2012. Caldera resurgence during magma replenishment and rejuvenation at Valles and Lake City calderas. *Bulletin of Volcanology* 74, 1833-1847.
- Kim, H.-J., Jou, H.-T., Lee, G.-H., Na, J.-H., Kim, H.-S., Jang, U., Lee, K.-Y., Kim, C.-H., Lee, S.H., Park, C.-H., Jung, S.-K., Suk, B.-C., 2013. Caldera structure of submarine Volcano #1 on the Tonga Arc at $21^{\circ}09'S$, southwestern Pacific: Analysis of multichannel seismic profiling. *Earth Planet Sp* 65, 893-900.
- Lagmay, A.M.F., Tengonciang, A.M.P., Uy, H.S., 2005. Structural setting of the Bicol Basin and kinematic analysis of fractures on Mayon Volcano, Philippines. *Journal of Volcanology and Geothermal Research* 144, 23-36.
- Lambeck, K., Antonioli, F., Anzidei, M., Ferranti, L., Leoni, G., Scicchitano, G., Silenzi, S., 2011. Sea level change along the Italian coast during the Holocene and projections for the future. *Quaternary International* 232, 250-257.
- Lavecchia, G., 1988. The tyrrhenian-apennines system: structural setting and seismotectogenesis. *Tectonophysics* 147, 263-296.
- Leeder, M.R., Gawthorpe, R.L., 1987. Sedimentary models for extensional tilt-block/half-graben basins. *Geological Society, London, Special Publications* 28, 139-152.
- Legros, F., Druitt, T.H., 2000. On the emplacement of ignimbrite in shallow-marine environments. *Journal of Volcanology and Geothermal Research* 95, 9-22.
- Lima, A., De Vivo, B., Spera, F.J., Bodnar, R.J., Milia, A., Nunziata, C., Belkin, H.E., Cannatelli, C., 2009. Thermodynamic model for uplift and deflation episodes

(bradyseism) associated with magmatic–hydrothermal activity at the Campi Flegrei (Italy). *Earth-Science Reviews* 97, 44-58.

Lipman, P.W., 1984. The roots of ash flow calderas in western North America: Windows into the tops of granitic batholiths. *Journal of Geophysical Research: Solid Earth* 89, 8801-8841.

Lipman, P.W., 1997. Subsidence of ash-flow calderas: relation to caldera size and magma-chamber geometry. *Bulletin of Volcanology* 59, 198-218.

Llave, E., García, M., Pérez, C., Sayago, M., Farrán, M., Ercilla, G., Somoza, L., León, R., Maestro, A., Medialdea, T., Hernández-Molina, F.J., Álvarez, R., Durán, R., Mohamed, K., 2008. Morphological feature analyses of the Prestige half-graben on the SW Galicia Bank. *Marine Geology* 249, 7-20.

Malinverno, A., 2012. Evolution of the Tyrrhenian Sea-Calabrian Arc system: the past and the present. *Rend. Online Soc. Geol. It.* 12, 11-15.

Malinverno, A., Ryan, W.B.F., 1986. Extension in the Tyrrhenian Sea and shortening in the Apennines as result of arc migration driven by sinking of the lithosphere. *Tectonics* 5, 227-245.

Mason, B.G., Pyle, D.M., Dade, W.B., Jupp, T., 2004. Seasonality of volcanic eruptions. *Journal of Geophysical Research: Solid Earth* 109, B04206.

Mastin, L.G., Van Eaton, A.R., Lowenstern, J.B., 2014. Modeling ash fall distribution from a Yellowstone supereruption. *Geochemistry, Geophysics, Geosystems* 15, 3459-3475.

McGuire, W.J., Howarth, R.J., Firth, C.R., Solow, A.R., Pullen, A.D., Saunders, S.J., Stewart, I.S., Vita-Finzi, C., 1997. Correlation between rate of sea-level change and frequency of explosive volcanism in the Mediterranean. *Nature* 389, 473-476.

McKenzie, D., 1978. Some remarks on the development of sedimentary basins. *Earth and Planetary Science Letters* 40, 25-32.

Milia, A., 2010. The stratigraphic signature of volcanism off Campi Flegrei (Bay of Naples, Italy). *Geological Society of America Special Papers* 464, 155-170.

Milia, A., Mirabile, L., Torrente, M.M., Dvorak, J.J., 1998. Volcanism offshore of Vesuvius Volcano in Naples Bay. *Bulletin of Volcanology* 59, 404-413.

Milia, A., Torrente, M.M., 1999. Tectonics and stratigraphic architecture of a peri-Tyrrhenian half-graben (Bay of Naples, Italy). *Tectonophysics* 315, 301-318.

Milia, A., Torrente, M.M., 2000. Fold uplift and synkinematic stratal architectures in a region of active transtensional tectonics and volcanism, eastern Tyrrhenian Sea. *Geological Society of America Bulletin* 112, 1531-1542.

- Milia, A., Torrente, M.M., 2007. The influence of paleogeographic setting and crustal subsidence on the architecture of ignimbrites in the Bay of Naples (Italy). *Earth and Planetary Science Letters* 263, 192-206.
- Milia, A., Torrente, M.M., 2011. The possible role of extensional faults in localizing magmatic activity: a crustal model for the Campanian Volcanic Zone (eastern Tyrrhenian Sea, Italy). *Journal of the Geological Society* 168, 471-484.
- Milia, A., Torrente, M.M., Giordano, F., Mirabile, L., 2006. Rapid changes of the accommodation space in the Late Quaternary succession of Naples Bay, Italy: the influence of volcanism and tectonics, in: Vivo, B.D. (Ed.), *Developments in Volcanology*. Elsevier, pp. 53-68.
- Milia, A., Torrente, M.M., Massa, B., Iannace, P., 2013. Progressive changes in rifting directions in the Campania margin (Italy): New constraints for the Tyrrhenian Sea opening. *Global and Planetary Change* 109, 3-17.
- Milia, A., Torrente, M.M., Russo, M., Zuppetta, A., 2003. Tectonics and crustal structure of the Campania continental margin: relationships with volcanism. *Mineralogy and Petrology* 79, 33-47.
- Mitchum, R.M., Vail, P.R., Sangree, J.B., 1977. Seismic Stratigraphy and Global Changes of Sea Level, Part 6: Stratigraphic Interpretation of Seismic Reflection Patterns in Depositional Sequences, in: Payton, C.E. (Ed.), *Seismic Stratigraphy -Applications to Hydrocarbon Exploration*. AAPG Memoir, pp. 117-133.
- Moretti, I., Sakellariou, D., Lykousis, V., Micarelli, L., 2003. The Gulf of Corinth: an active half graben? *Journal of Geodynamics* 36, 323-340.
- Neri, A., Esposti Ongaro, T., Voight, B., Widiwijayanti, C., 2015a. Chapter 5 - Pyroclastic Density Current Hazards and Risk A2 - Papale, John F. ShroderPaolo, Volcanic Hazards, Risks and Disasters. Elsevier, Boston, pp. 109-140.
- Neri, A., Esposti Ongaro, T., Voight, B., Widiwijayanti, C., 2015b. Pyroclastic Density Current Hazards and Risk, in: Papale, P. (Ed.), *Volcanic Hazards, Risks and Disasters*. Elsevier, Boston, pp. 109-140.
- Newhall, C.G., Self, S., 1982. The volcanic explosivity index (VEI) an estimate of explosive magnitude for historical volcanism. *Journal of Geophysical Research: Oceans* 87, 1231-1238.
- Orsi, G., Civetta, L., Del Gaudio, C., de Vita, S., Di Vito, M.A., Isaia, R., Petrazzuoli, S.M., Ricciardi, G.P., Ricco, C., 1999. Short-term ground deformations and seismicity in the resurgent Campi Flegrei caldera (Italy): an example of active block-resurgence in a densely populated area. *Journal of Volcanology and Geothermal Research* 91, 415-451.

- Orsi, G., De Vita, S., di Vito, M., 1996. The restless, resurgent Campi Flegrei nested caldera (Italy): constraints on its evolution and configuration. *Journal of Volcanology and Geothermal Research* 74, 179-214.
- Orsi, G., Vito, M., Isaia, R., 2004. Volcanic hazard assessment at the restless Campi Flegrei caldera. *Bulletin of Volcanology* 66.
- Paoletti, V., D'Antonio, M., Rapolla, A., 2013. The structural setting of the Ischia Island (Phlegrean Volcanic District, Southern Italy): Inferences from geophysics and geochemistry. *Journal of Volcanology and Geothermal Research* 249, 155-173.
- Pappalardo, L., Civetta, L., D'Antonio, M., Deino, A., Di Vito, M., Orsi, G., Carandente, A., de Vita, S., Isaia, R., Piochi, M., 1999. Chemical and Sr-isotopical evolution of the Phlegraean magmatic system before the Campanian Ignimbrite and the Neapolitan Yellow Tuff eruptions. *Journal of Volcanology and Geothermal Research* 91, 141-166.
- Passaro, S., Barra, M., Saggiomo, R., Di Giacomo, S., Leotta, A., Uhlen, H., Mazzola, S., 2013. Multi-resolution morpho-bathymetric survey results at the Pozzuoli–Baia underwater archaeological site (Naples, Italy). *Journal of Archaeological Science* 40, 1268-1278.
- Passaro, S., Genovese, S., Sacchi, M., Barra, M., Rumolo, P., Tamburrino, S., Mazzola, S., Basilone, G., Placenti, F., Aronica, S., Bonanno, A., 2014. First hydroacoustic evidence of marine, active fluid vents in the Naples Bay continental shelf (Southern Italy). *Journal of Volcanology and Geothermal Research* 285, 29-35.
- Passaro, S., Tamburrino, S., Vallefucio, M., Tassi, F., Vaselli, O., Giannini, L., Chiodini, G., Caliro, S., Sacchi, M., Rizzo, A.L., Ventura, G., 2016. Seafloor doming driven by degassing processes unveils sprouting volcanism in coastal areas. *Scientific Reports* 6, 22448.
- Piochi, M., Bruno, P.P., De Astis, G., 2005. Relative roles of rifting tectonics and magma ascent processes: Inferences from geophysical, structural, volcanological, and geochemical data for the Neapolitan volcanic region (southern Italy). *Geochemistry, Geophysics, Geosystems* 6.
- Piochi, M., Kilburn, C.R.J., Di Vito, M., Mormone, A., Tramelli, A., Troise, C., de Natale, G., 2013. The volcanic and geothermally active Campi Flegrei caldera: an integrated multidisciplinary image of its buried structure. *International Journal of Earth Sciences - GR Geologische Rundschau* 103, 401-421.
- Pochat, S., Castelltort, S., Choblet, G., Van Den Driessche, J., 2009. High-resolution record of tectonic and sedimentary processes in growth strata. *Marine and Petroleum Geology* 26, 1350-1364.

- Pyle, D.M., Ricketts, G.D., Margari, V., van Andel, T.H., Sinitsyn, A.A., Praslov, N.D., Lisitsyn, S., 2006. Wide dispersal and deposition of distal tephra during the Pleistocene 'Campanian Ignimbrite/Y5' eruption, Italy. *Quaternary Science Reviews* 25, 2713-2728.
- Rampino, M.R., 2002. Supereruptions as a Threat to Civilizations on Earth-like Planets. *Icarus* 156, 562-569.
- Rampino, M.R., Self, S., 1982. Historic eruptions of Tambora (1815), Krakatau (1883), and Agung (1963), their stratospheric aerosols, and climatic impact. *Quaternary Research* 18, 127-143.
- Rampino, M.R., Self, S., Fairbridge, R.W., 1979. Can Rapid Climatic Change Cause Volcanic Eruptions? *Science* 206, 826-829.
- Ricci, T., Barberi, F., Davis, M.S., Isaia, R., Nave, R., 2013. Volcanic risk perception in the Campi Flegrei area. *Journal of Volcanology and Geothermal Research* 254, 118-130.
- Robock, A., 2000. Volcanic eruptions and climate. *Reviews of Geophysics* 38, 191-219.
- Rolandi, G., Bellucci, F., Heizler, M.T., Belkin, H.E., De Vivo, B., 2003. Tectonic controls on the genesis of ignimbrites from the Campanian Volcanic Zone, southern Italy. *Mineralogy and Petrology* 79, 3-31.
- Rosi, M., Sbrana, A., Principe, C., 1983. The phlegraean fields: Structural evolution, volcanic history and eruptive mechanisms. *Journal of Volcanology and Geothermal Research* 17, 273-288.
- Sacchi, M., Pepe, F., Corradino, M., Insinga, D.D., Molisso, F., Lubritto, C., 2014. The Neapolitan Yellow Tuff caldera offshore the Campi Flegrei: Stratal architecture and kinematic reconstruction during the last 15 ky. *Marine Geology* 354, 15-33.
- Santacroce, R., Cristofolini, R., La Volpe, L., Orsi, G., Rosi, M., 2003. Italian active volcanoes. *Episodes* 26, 227-234.
- Scarpati, C., Cole, P., Perrotta, A., 1993. The Neapolitan Yellow Tuff — A large volume multiphase eruption from Campi Flegrei, Southern Italy. *Bulletin of Volcanology* 55, 343-356.
- Secomandi, M., Paoletti, V., Aiello, G., Fedi, M., Marsella, E., Ruggieri, S., D'Argenio, B., Rapolla, A., 2003. Analysis of the magnetic anomaly field of the volcanic district of the Bay of Naples, Italy. *Marine Geophysical Researches* 24, 207-221.
- Self, S., 2015. Explosive Super-Eruptions and Potential Global Impacts, in: Papale, J.F.S. (Ed.), *Volcanic Hazards, Risks and Disasters*. Elsevier, Boston, pp. 399-418.
- Self, S., Rampino, M.R., Newton, M.S., Wolff, J.A., 1984. Volcanological study of the great Tambora eruption of 1815. *Geology* 12, 659-663.

- Sigurdsson, H., Carey, S., Mandeville, C., Bronto, S., 1991. Pyroclastic flows of the 1883 Krakatau eruption. *Eos, Transactions American Geophysical Union* 72, 377-381.
- Smith, R.L., Bailey, R.A., 1968. Resurgent Cauldrons. *Geological Society of America Memoirs* 116, 613-662.
- Spinks, K.D., Acocella, V., Cole, J.W., Bassett, K.N., 2005. Structural control of volcanism and caldera development in the transtensional Taupo Volcanic Zone, New Zealand. *Journal of Volcanology and Geothermal Research* 144, 7-22.
- Suppe, J., Chou, G., Hook, S., 1992. Rates of folding and faulting determined from growth strata, in: McClay, K.R. (Ed.), *Thrust Tectonics*. Springer Netherlands, pp. 105-121.
- Tibaldi, A., Vezzoli, L., 1998. The space problem of caldera resurgence: an example from Ischia Island, Italy. *Geologische Rundschau* 87, 53-66.
- Trincardi, F., Zitellini, N., 1987. The Rifting of the Tyrrhenian Sea. *Geo-Marine Letters* 7, 1-6.
- Troise, C., De Natale, G., Pingue, F., Tammaro, U., De Martino, P., Obrizzo, F., Boschi, E., 2008. A New Uplift Episode at Campi Flegrei Caldera (Southern Italy): Implications for Unrest Interpretation and Eruption Hazard Evaluation. 10, 375-392.
- Turco, E., Schettino, A., Pierantoni, P.P., Santarelli, G., 2006. The Pleistocene extension of the Campania Plain in the framework of the southern Tyrrhenian tectonic evolution: morphotectonic analysis, kinematic model and implications for volcanism, in: Vivo, B.D. (Ed.), *Developments in Volcanology*. Elsevier, pp. 27-51.
- Vail, P.R., Mitchum, R.M., Thompson, S., 1977. Seismic Stratigraphy and Global Changes of Sea Level, Part 3: Relative Changes of Sea Level from Coastal Onlap, in: Payton, C.E. (Ed.), *Seismic Stratigraphy - Applications to Hydrocarbon Exploration*. AAPG Memoir, pp. 63-81.
- Vanorio, T., Prasad, M., Patella, D., Nur, A., 2002. Ultrasonic velocity measurements in volcanic rocks: correlation with microtexture. *Geophysical Journal International* 149, 22-36.
- Waelbroeck, C., Labeyrie, L., Michel, E., Duplessy, J.C., McManus, J.F., Lambeck, K., Balbon, E., Labracherie, M., 2002. Sea-level and deep water temperature changes derived from benthic foraminifera isotopic records. *Quaternary Science Reviews* 21, 295-305.
- Walter, T.R., 2008. Chapter 9 Facilitating Dike Intrusions into Ring-Faults, in: Joachim, G., Joan, M., iacute (Eds.), *Developments in Volcanology*. Elsevier, pp. 351-374.

- Williams, M.A.J., Ambrose, S.H., van der Kaars, S., Ruehlemann, C., Chattopadhyaya, U., Pal, J., Chauhan, P.R., 2009. Environmental impact of the 73 ka Toba super-eruption in South Asia. *Palaeogeography, Palaeoclimatology, Palaeoecology* 284, 295-314.
- Wilson, C.J.N., 2001. The 26.5 ka Oruanui eruption, New Zealand: an introduction and overview. *Journal of Volcanology and Geothermal Research* 112, 133-174.
- Wohletz, K., Civetta, L., Orsi, G., 1999. Thermal evolution of the Phlegraean magmatic system. *Journal of Volcanology and Geothermal Research* 91, 381-414.
- Yilmaz, Ö., 2001. *Seismic Data Analysis - Processing, Inversion and Interpretation of Seismic Data*. Society of Exploration Geoph, Tulsa.
- Zollo, A., Judenherc, S., Auger, E., D'Auria, L., Virieux, J., Capuano, P., Chiarabba, C., de Franco, R., Makris, J., Michelini, A., Musacchio, G., 2003. Evidence for the buried rim of Campi Flegrei caldera from 3-d active seismic imaging. *Geophysical Research Letters* 30, 2002.

Versicherung an Eides Statt
gem. § 5 Abs. 5 der Promotionsordnung vom 15.07.2015

Ich, Lena Steinmann, Humboldtstraße 159, 28203 Bremen, 2127644

(Vorname, Name, Anschrift, ggf. Matr.-Nr.)

versichere an Eides Statt durch meine Unterschrift, dass ich die vorstehende Arbeit selbständig und ohne fremde Hilfe angefertigt und alle Stellen, die ich wörtlich dem Sinne nach aus Veröffentlichungen entnommen habe, als solche kenntlich gemacht habe, mich auch keiner anderen

als der angegebenen Literatur oder sonstiger Hilfsmittel bedient habe, und die zu Prüfungszwecken beigelegte elektronische Version der Dissertation mit der abgegebenen gedruckten Version identisch ist.

Ich versichere an Eides Statt, dass ich die vorgenannten Angaben nach bestem Wissen und Gewissen gemacht habe und dass die Angaben der Wahrheit entsprechen und ich nichts verschwiegen habe.

Die Strafbarkeit einer falschen eidesstattlichen Versicherung ist mir bekannt, namentlich die Strafandrohung gemäß § 156 StGB bis zu drei Jahren Freiheitsstrafe oder Geldstrafe bei vorsätzlicher Begehung der Tat bzw. gemäß § 161 Abs. 1 StGB bis zu einem Jahr Freiheitsstrafe oder Geldstrafe bei fahrlässiger Begehung.

Ort, Datum

Unterschrift